UNIVERSITY OF SOUTHAMPTON

FACULTY OF ENGINEERING, SCIENCE & MATHEMATICS

School of Earth and Ocean Sciences

An Investigation into Hf and Fe Isotopes in Ferromanganese Deposits and Their Applications to Paleoceanography

By

Nan-Chin Chu

Thesis for the degree of Doctor of Philosophy

November 2003

Graduate School of the Southampton Oceanography Centre

This PhD dissertation by

Nan-Chin Chu

has been produced under the supervision of the following persons

Supervisors

Prof. Robert W. Nesbitt

Prof. Christopher R. German

Chair of Advisory Panel

Prof. Carl L. Amos

UNIVERSITY OF SOUTHAMPTON

ABSTRACT

FACULTY OF SCIENCE
SCHOOL OF OCEAN AND EARTH SCIENCES

Doctor of Philosophy

AN INVESTIGATION INTO Hf AND Fe ISOTOPES IN FERROMANGANESE DEPOSITS AND THEIR APPLICATIONS TO PALEOCEANOGRAPHY

by Nan-Chin Chu

The past decade has seen major advances in palaeoceanography and an important factor in the accumulating database has been geochemical studies of ferromanganese crusts. The use of these crusts as proxies for palaeoceanography owes much to isotope geochemistry; in particular, recent advances in mass spectrometry have opened up major opportunities to exploit the information contained within Fe-Mn crusts. Although a wide range of isotopic systems can now be measured with sufficient precision, their potentials as environmental tracers still need to be fully assessed. The prime foci of this study have been to investigate two of these *new* potential tracers, the Hf and Fe isotopic systems, and their applications to marine environmental studies. My work has focussed on a suite of ferromanganese crusts from the Pacific Ocean (Central Pacific and Izu-Bonin back-arc basin), encompassed different geographic and geologic settings, to obtain new insights into the *present* and *past* sources of Hf and Fe in seawater.

First, a Hf isotope analytical method has been established for multi-collection Inductively Coupled Plasma Mass Spectrometry (MC-ICP-MS, Chu *et al.*, 2002). This refined method has led to the determination of a new set of ytterbium (Yb) isotopic ratios benefitting from improved isobaric interference corrections and offering a promising future application: *in situ* Laser ablation analyses.

The present-day profile of $^{176}Hf/^{177}Hf$ ratios in the Pacific Ocean has been inferred by analysing surface scrapings of Fe-Mn crusts collected at various water-depths in the Central Pacific. In these samples, Nd isotope and rare earth element distributions correlate well with hydrological properties inferred from WOCE data, demonstrating the applicability of this approach. The Hf isotopic composition does not display any significant variations with depth, throughout the water column, confirming that its oceanic residence time (τ_{Hf}) is most probably longer than that of Nd and similar to that of the thermohaline circulation (~1500 yr). Estimated Hf isotopic compositions for Pacific Intermediate Water and Pacific Deep Water masses are suggested, based upon this vertical distribution.

Isotopic depth-profiles for Hf, Nd and Pb drilled into three Fe-Mn crusts have been measured to help decipher the radiogenic isotope budget of the Central Pacific and Izu-Bonin back-arc basin throughout the Late Neogene. Isotopic records for Central Pacific crusts match those from the literature, showing no significant variations over the last 10 Myr. For the Izu-Bonin area, by contrast, Pb-isotope variations suggest mixing between dissolved inputs from aeolian loess and volcanic island arcs. A decoupling of the Hf and Nd isotope records is observed in both Izu-Bonin crusts at ~4Ma. This could be a direct consequence of either localised hydrothermal activity or a variation in the input of weathered arc material that preferentially impacts upon Hf.

Finally, the first high-resolution Fe isotopic measurements for the Pacific Ocean were carried out in the same depth profiles. The varying Fe isotopic compositions demonstrate that ocean basins are heterogeneous with respect to Fe isotopes (i.e., dissolved Fe exhibits a short ocean residence time) and the source of Fe is different in the Izu-Bonin Basin from that in the Central Pacific Ocean. In the Izu-Bonin area, negative $\delta^{56}Fe$ values point clearly toward a hydrothermal influence associated with the back-arc volcanic setting. Differences between Fe isotopic records for the two Izu-Bonin crusts, only *ca.* 80 km apart from each other, can be attributed to the differing sample depths and crustal growth rate of these two samples. Both a deeper location and a faster growth rate would provide mechanisms to prevent hydrothermal signals being diluted or overprinted by seawater signatures. The good correlation observed between basin-wide volcanic activity pulses and temporal Fe isotope variations suggests that Fe isotopes could be used as tracers of past hydrothermal activity because terrestrial sources of iron are all characterised by homogeneous Fe isotopic compositions. Despite the potentials for Fe and to a lesser extent Hf isotopes, as demonstrated in this work, the absence of several end members still restricts their applications and requires further constraints.

Contents

Acknowledgements

From the beginning of my graduate training to the completion of this thesis, my achievements, if any, were built on the help of many others. Foremost among them are my supervisors, Robert Nesbitt and Christopher German; they have made the most effort and deserve the highest credit. It was the most enjoyable moment when discussing results with them. Through their sharp questions and comments, I, besides being stimulated, learned how to construct my ideas and logics. Thanks to their open minds and relaxed attitudes, I had much freedom to decide where my project should go, be able to attend many international conferences and have interactions with the whole community. They have given me the most profound influences both in science and in life.

My gratitude must then go to Rose Boella, who has inspired me with her enthusiasm for chemistry. Her good spirit got never defeated even after many of our numerous experiments ended in failures. I am equally grateful to Rex Taylor who patiently led me from basics of how the instruments work to a close collaboration during the later stage of my work. My precious hands-on experiences have accumulated from their endless time with me. I am undoubtedly indebted to them.

I thank Peter Halbach and Akira Usui, who provided me with valuable samples; Martin Frank and Peter Kubik, who welcome me to visit ETH and in assistance with the age determination of the samples, and Darryl Green and Andy Milton for assisting in ICP-AES and ICP-MS measurements. Thanks as well to Germain Bayon, Osamu Ishizuka, Der-Chuen Lee, Ros Rickaby, Shen-Su Sun, Tina van de Flierdt and many other colleagues inside or outside SOC for discussions throughout the formation of my thesis.

I must address here my many thanks to Gideon Henderson. Because of his understanding and patience, I can have access to the facilities in the Department of Earth Sciences, University of Oxford, and finally be able to complete the writings before the long-waiting new project.

The National Oceanography Library is thanked for their wonderful resources from which I have benefited greatly. This work is funded by University of Southampton Taiwanese Postgraduate Scholarships and the Micromass, UK. I also thank the World University Network (WUN) Exchange Scheme who gave me the funding to carry out an exciting Fe project in the UW-Madison.

Clark Johnson and Brian Beard are thanked for their host during the exchange, discussions and efforts in maintaining the lab at its top performance allowing me to acquire data most efficiently while in Madison. This experience has certainly opened a new page in my research area.

My acknowledgements also go to my teachers and mentors from National Taiwan University: Ping-Mei Liew, Sun-Lin Chung, and Cheng-Hong Chen. They showed me how fascinating isotope geochemistry can be, encouraged me, and finally lead me to England, the land of mass spectrometry, for further exploration.

Thanks to my NTU B83 grade classmates and friends at the other end of the internet line, who constantly shared jokes with me to keep me motivated or listen to my complains when things went wrong. I want to thank especially Carolyn and the Nesbitt family, who welcomed and included me as part of them the first day I arrived in this foreign world and gave me the warmest home one could ever dream of. And special thanks to Germain whose encouragements and support have helped me through many difficulties...

Finally, my wholehearted thanks go to my parents, who completely support their daughter to do whatever she liked. Without them I would never have had the courage to come all this way to pursue my dream.

I must say, these years were really enjoyable, probably the best part of my student life. Thank you!

...(the revolution) came instead from the deep-sea...; and from mass spectrometry, which obviously has nothing to do with the trusted geological hammer.

C. Emiliani (1995), Terra Nova, 7 (6), 587.

Chapter 1. Introduction

1-1 Preface

Nature has provided a powerful form of tracers that allows us to investigate a range of geological and biogeochemical processes on Earth: 'radiogenic isotopes' which decay with time from one isotope to another through radioactive decay and 'stable isotopes' in which the relative abundances of the naturally occurring isotopes of any given element are varied by a combination of physical, chemical and biological processes (cf Faure, 1986; Dickin, 1997). Following the pioneering studies of Harold Urey and Alfred Nier (e.g. Urey, 1947; Reynolds, 1998), isotope geochemistry progressed rapidly throughout the second half of the last century, coupled directly to continuous innovations in mass spectrometer technology. This close relationship between technological progress and rapid developments in the science has been demonstrated most recently in the case of multi-collector plasma source mass spectrometer, originating in the early 1990's (Walder and Freedman, 1992; Walder *et al.*, 1993). This new technology overcomes analytical difficulties associated with a number of elements and, thus, has allowed rapid progress in our understanding and application of a number of novel isotope systems.

It has long been realised that deep-sea records can provide a great deal of information about Earth System processes, e.g. concerning climate change and planetary orbit forcing (see, e.g., Emiliani, 1995 and references therein). Thus, the search for suitable materials that can yield proxies of past ocean composition and behaviour is a prime focus of modern marine geochemical research. Isotopes, in particular, have played an important role in improving our views on paleoclimate, ocean circulation and biology productivity. Nevertheless, we still face challenges ahead, both in terms of generating high-quality analytical data and in refining the use of our chosen proxies for more reliable and accurate applications - most tracers respond to more than one variable and so their data do not necessarily allow completely unequivocal interpretations. Table 1.1 provides a summary of isotopic tracers which have been analysed in marine materials and that are of (potential) utility as proxies in the modern and/or paleo-ocean. Among these, some isotope systems have only begun to be investigated within the past 10 years. The 'unknowns' of the capabilities and limits associated with these isotopic tracers, therefore, require perhaps

most urgent investigation. That, therefore, has been the prime motivation behind this study in which two key isotope systems in particular are investigated: Lu-Hf and Fe-isotopes.

Table 1.1 Review of isotopic tracers in marine materials. (Isotopes marked in bold are investigated in this study)

Isotopic system	Marine Materials	Proxies	Principles	Selected References
$\delta^{6}Li$	Sediments	Continental weathering	Kinetic fractionation cause ^{6}Li preferentially being weathered than ^{7}Li.	Huh *et al*. (2001)
$^{10}Be/^{9}Be$	Fe-Mn Crusts	Atmospheric fallout (^{10}Be) vs erosion of continental crust (^{9}Be)	^{10}Be increases with age of the water messes by remineralisation process, whereas ^{9}Be is homogenous in deep water. A dating tool for Fe-Mn Crusts.	Von Blanckenburg and O'Nions (1999)
$\delta^{11}B$	Planktonic forams	paleo-pH, $p\,CO_2$	Isotopic fractionation between boron species that are pH-dependent.	Pearson and Palmer (2000), Lemarchand *et al* (2000), Palmer and Pearson (2003).
$\delta^{13}C$	Benthic forams	Ocean circulation- a non-conservative tracer/ atmospheric CO_2	$\delta^{13}C$ anticorrelates to nutrient by organic uptakes causing high-nutrient 'aged' signatures.	Curry and Lohmann (1983), Ravelo and Anderson (2000), Pagani *et al*. (1999)
$\Delta^{14}C$	Benthic-planktonic forams	Deepwater formation rate	The radiocarbon age difference between the water formed by benthic or planktonic forams.	Broecker (1982), Adkins and Boyle (1997)
$\delta^{18}O$	Biogenic skeleton / ice core	Paleotemperature. Paleosalinity.	Isotopic 'vital effect' and mass dependent fractionation.	Emiliani (1955), Shackelton and Opdyke (1973), Duplessy *et al*. (1993), Rohling (2000)
$\delta^{30}Si$	Diatoms/ marine sponges	Opal production, nutrient utilisation	Isotopic fractionation during opal biomineralization.	DeLaRocha *et al* (1998), DeLaRocha (2003)
$\delta^{44}Ca$	Carbonates/ phosphates	Paleotemparature, continental weathering	Biomineralisation process, temperature influences certain foram species, and continental weathering release high Ca flux and compensate the biological fractionation effect.	Zhu and Macdougall (1998), Nagler *et al*. (2000), DeLeRocha and DePaolo (2000), Schmitt *et al*. (2003)
$\delta^{56}Fe$	Fe-Mn Crusts	Hydrothermal input/ biological effect	Low values of hydrothermal signatures. Kinetic or equilibrium fractionations.	Zhu *et al*. (2000)
$\delta^{65}Cu$	Sediments	Potential for redox and biological process.	Fractionation caused by organism uptakes and hydrothermal process.	Zhu *et al*. (2000), Marechal and Albarede (2002), Zhu *et al*. (2002)

Table 1.1 (cont.)

Isotopic system	Marine Materials	Proxies	Principles	Selected References
$\delta^{66}Zn$	Sediments (Fe-Mn nodule)/ carbonate	Ocean productivity	Biological fractionation.	Marechal *et al*. (2000) Pichat *et al.* (2003)
$^{87}Sr/^{86}Sr$	Forams/ authigenic sediments/ Fe-Mn crust	Continental weathering	High (radiogenic) values for old continent. This proxy will nevertheless be affected by the dissolution of marine carbonates, hydrothermal inputs and young volcanics weathering.	Henderson *et al.* (1994), Derry *et al.* (1996)
$\delta^{98/95}Mo$	Sediments/ Fe-Mn crust	Atmospheric oxygen level (paleo-redox)	Chemical behaviours under different oxidation state cause equilibrium or kinetic fractionations.	Barling *et al*. (2001), Siebert *et al*. (2003)
$^{143}Nd/^{144}Nd$	sediments/ Fe-Mn crusts	Continental weathering/ ocean circulation	Radiogenic values from weathering of young volcanic materials with moderate ocean residence time.	Burton *et al*. (1999), Rutberg *et al*. (2000), Frank *et al*. (2002), Bayon *et al*. (2003).
$^{176}Hf/^{177}Hf$	Fe-Mn Crusts	Erosion of continental crust/ hydrothermal input	Zircon effect identifies physical congruent weathering. Hydeothermal input with radiogenic signatures.	Lee *et al*. (1998), Piotrowski *et al*. (2000), David *et al*. (2001), van de Flierdt *et al*. (2002).
$^{187}Os/^{186}Os$	Forams/ sediments/ Fe-Mn crusts	Impact events / continental weathering	Old continents have high (radiogenic) values but could be masked by organic-rich sediment (high Re/Os) weathering. Low values by hydrothermal alterations, weathering of ultramafic/ volcanic rocks or large impact events by cosmogenic input.	Oxburgh (1998), Ravizza (2000), Ravizza and Peucker-Ehrenbrink (2003), Cave *et al*. (2003)
$^{203}Tl/^{205}Tl$	Fe-Mn crusts	hydrothermal input/ volcanic activity or oceanic crust alteration balance	Enriched in hydrothermal fluids, volcanic gasses and altered MORB.	Rehkamper *et al*. (2002); Rehkamper and Nielsen (2004)
Pb isotopes	sediments/ Fe-Mn crusts	Weathering fluxes/ minor hydrothermal input/ circulation	Radiogenic values from loess and old continental weathering. Shorter (~100 yr) residence time reflect local circulations. Less scavenging properties than Nd traces minor hydrothermal input.	Christensen *et al*. (1997), Reynold *et al.* (1999), Abouchami *et al*. (1999), Claude-Ivanaj *et al.* (2001), Vlastélic *et al.* (2001), van de Flierdt *et al*. (2003).
$^{231}Pa/^{230}Th$	Sediments	Deep water flow rate/ paleoproductivity	^{230}Th is more reactive than ^{231}Pa therefore less advecting distance in deep water flow (N Atlantic). Their removal from seawater depends on productivity and particle composition (Southern Ocean).	Kumar *et al*. (1995), Yu *et al.* (1996), Walter *et al.* (1997)

In the next section of this chapter (section 1-2), I describe the basic principles of mass spectrometry and isotopic analysis, leading on to a discussion of the particular merits of modern instrumentation including both a) multi-collector analysis and b) plasma-source mass spectrometry. Next (section 1-3) I provide a brief synthesis of

the current state of the art in marine isotope geochemistry for both radiogenic isotopes (concentrating on the Lu-Hf system) and stable transition metal isotopes (notably Fe). In the following section (1-4) I describe the different kinds of Fe-Mn material recovered from the seafloor which can be utilised for marine geochemical studies. I conclude (section 1-5) with a synopsis of the remaining chapters of the thesis and their contents.

1-2 Principles of Mass Spectrometry

Isotopes are atoms whose nuclei contain the same number of protons but a different number of neutrons. Isotopes are denoted as $^{A}_{Z}E$, where A denotes the mass number (i.e., sum of the number of protons and neutrons in its nucleus) and Z denotes the atomic number (i.e., proton, which is equally charged and opposite in polarity to the surrounding electrons that determines the chemical properties of that atom) of an element E. Atomic weight of each naturally occurring element is therefore the weighed average of its various isotopes. Isotopes can be divided into two fundamental kinds, stable and unstable (radioactive) species. The stability of the nuclides depends on the ratio of their neutrons and protons (i.e., when N/Z is nearly equal, the nuclide is more stable) and with even numbers of protons and neutrons. Examples of stable isotopes are $^{12}_{6}C$-$^{13}_{6}C$, $^{16}_{8}O$-$^{18}_{8}O$, which stay within the stability field (N/Z~1) and $^{56}_{26}Fe$-$^{54}_{26}Fe$, which has even numbers for neutrons and protons. However, most known nuclides are not stable and decompose (decay) spontaneously until they achieve a stable nuclear configuration. Decay processes involve the emission of radiation and, in some; electrons are captured by the nucleus. For example, ^{147}Sm decays to ^{143}Nd with an α-emission and ^{176}Lu decays to ^{177}Hf with a β-emission. The decay constant (λ) is the probability of a decay among some number of nuclides (N) within some infinitely small time interval (dt). The mean life (τ, i.e., the average life expectancy of a radioactive atom) of a radioactive atom is equal to the reciprocal of λ. The amount of time for the number of parent atoms to decrease to half the original number is defined as half-life, $t_{1/2}$, and is a factor of 1/ln2 longer than τ (e.g. Faure, 1986; Dickin, 1997).

A mass spectrometer is an instrument designed to separate charged atoms and molecules based on the motions of their masses in electric fields or magnetic fields. The present Nier-type mass spectrometers consists a source of positively charged ion

beam, a magnetic analyser and an ion collector. The ion beam is generated, such as, by heat (thermal ionisation) or inductive coupling of high-frequency energy plasma (ICP) to ionise of the element in question. When the ion beam enters the magnetic field, it deflects the ions into circular paths whose radii are proportional to the mass/charge (m/z) of the isotopes. The deflected ions finally enter the detectors, which will pick up the electron collisions and translate them into currents as the output signals (e.g. Faure, 1986, Fig. 1.1a).

Element such as hafnium (Hf) has high first ionisation potential (7.0 eV). This normally requires large amount of samples for processing and high purity from chemical separation when employing solid-source mass spectrometry, i.e. thermal ionisation mass spectrometer (TIMS) (e.g. Patchett and Tatsumoto, 1980). The inductively coupled plasma (ICP) ionisation approach can provide higher ionisation potentials and overcome the difficulties in measuring high ionisation potential elements. As the ion beam produced by the plasma is more unstable than the ion beam of TIMS, multiple collectors are necessary to simultaneously measure isotopes of interest and cancel out the effects of plasma instability. Because samples are introduced at atmospheric pressure in a plasma source mass spectrometer, it facilitates external mass bias normalisation by mixing elements that cover similar mass range, such as Tl for Pb (Longerich *et al.*, 1987) and Cu-Zn (Maréchal *et al.*, 1999), or the coupling with a laser ablation (LA) system for *in situ* measurement with high sampling resolution and fast data acquisition (e.g.Christensen *et al.*, 1997). Therefore, the MC-ICP-MS (Multicollector Inductively Coupled Plasma Mass Spectrometry, e.g. IsoProbe, Micromass UK Ltd, Fig. 1.1b) combining the ionisation efficiency of the ICP ion source and improved precision from multiple Faraday cups had encouraged wide applications in various Earth sciences fields.

(a) Nier-type Magnetic Sector Mass Spectrometer

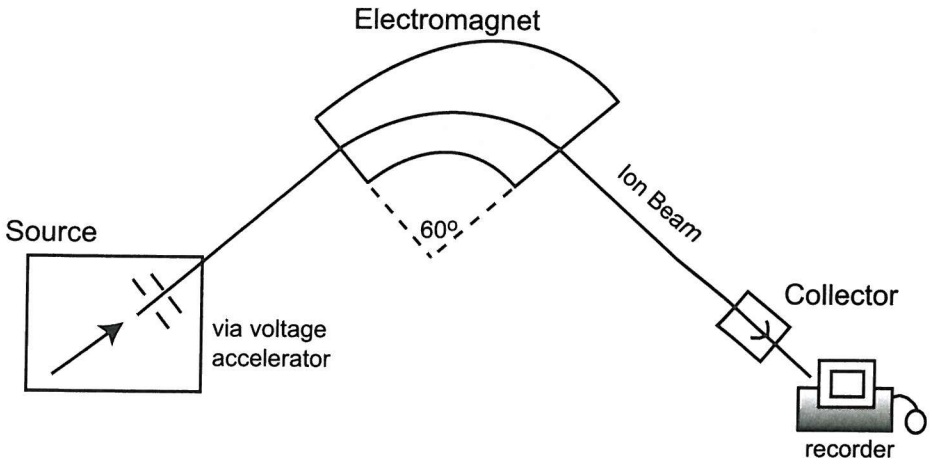

(b) Micromass IsoProbe

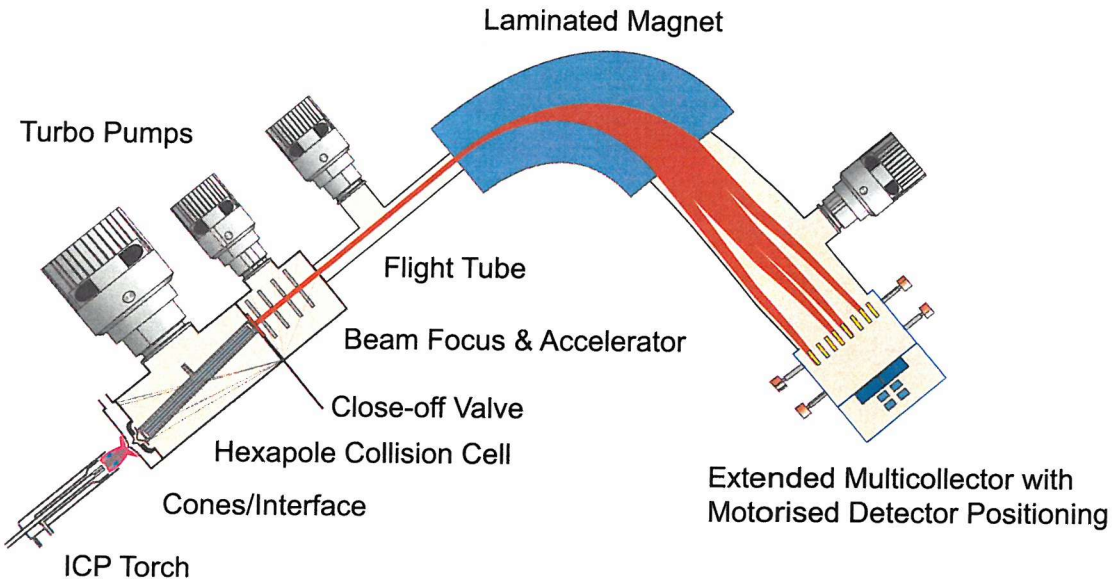

Fig. 1.1 Schematic outlines of (a) Nier-type single collector mass spectrometer (b) Micromass Multicollector ICP Mass Spectrometer (IsoProbe).

1-3 Isotopes in Marine Geochemistry

1-3-1 Radiogenic isotopes (Sr, Nd, U-Th-Pb, Os, Hf)

The radiogenic isotopes commonly analysed in marine authigenic precipitates (described later) exhibit no systematic variations induced by either biological fractionation (cf $\delta^{13}C$) or physico-chemical processes such as evaporation (cf $\delta^{18}O$). Instead, the variations observed in the radiogenic isotope composition of a water mass, or any proxy thereof, is believed to be dominated by the addition of this material to the oceans from reservoirs with differing isotopic compositions. Radiogenic isotopes, therefore, can provide valuable information on both past ocean circulation patterns and the relative strengths, through time, of source inputs and sinks important to maintain marine geochemical budgets.

Assuming the composition of the oceans to be maintained at steady state, the average time that any element spends in the ocean before being removed into some (e.g. sedimentary, hydrothermal) sink can be described in terms of its 'residence time' (Broecker and Peng, 1982). This term in chemical oceanography is defined by dividing the total content of any given element 'A' dissolved in the sea by the rates of supply (or removal) each year.

$$\tau = A/(dA/dt)$$

To be useful as a tracer of present and, hence, past water mass circulation, the residence time of any given element/isotope system should be on the order of, or shorter than, the average circulation time of the global ocean, approximately 1500 years (e.g. Broecker and Peng, 1982), estimated by ^{14}C measurements. The residence times of Os and Sr, by contrast, are on the order of tens of thousands years to millions years (Hodell *et al.*, 1990; Palmer and Edmond, 1992; Richter and Turekian, 1993; Oxburgh, 2001 and reference therein) and so are not suitable as water mass tracers because individual water mass signatures should be expected to become well-mixed and homogenised over some (great) number of cycles through the deep oceans before these metals are removed into the sedimentary record. That does not mean that such tracers are without benefit in marine geochemistry, of course. The long residence-time of Sr, for example, has been put to particularly good use in resolving the relative inputs from major sources (riverine vs hydrothermal) to the oceans (e.g. Palmer and Edmond, 1989).

The half-lives of the daughter products in any isotopic system to be studied should also be long enough to allow that isotopic composition to be preserved faithfully over paleoceanographic reconstruction timescales. Tracers such as Nd, Pb and Hf therefore fit all the above requirements because they exhibit short residence times in the deep-ocean but exhibit sufficiently long half-lives of both the parent and daughter isotopes of interest (Table 2.2).

Table 1.2 Radiogenic isotopic systems applied as oceanic tracers and their mean residence time in the ocean

Element	Isotopic ratios of interests	Parent-Daughter Decay	Half-life	Residence Time (yrs)	Ref for Residence Time
Nd	$^{143}Nd/^{144}Nd$	^{147}Sm-^{143}Nd	106 Gyr	600-2000	Jeandel *et al*. (1993, 1995); Tachikawa *et al*. (1999)
Pb	$^{206}Pb/^{204}Pb$	^{238}U-^{206}Pb	4.47 Gyr	>100	Schaule and Patterson (1981)
	$^{207}Pb/^{204}Pb$	^{235}U-^{207}Pb	704 Myr		Henderson and Maier-Reimer (2002)
	$^{208}Pb/^{204}Pb$	^{232}Th-^{208}Pb	14 Gyr		
Hf	$^{176}Hf/^{177}Hf$	^{176}Lu-^{176}Hf	37.5 Gyr	~2000	Godfrey *et al*. (1996, 1997); McKelvey and Orians (1998); Lee *et al*. (1999)

It is well recognised that hydrogenetic Fe-Mn crusts (Section 1.4) *do* record reliably the isotopic composition of the ambient deep ocean. This was first demonstrated from the study of REE, Sr and Nd isotopes (O'Nions *et al.*, 1978; Piepgras *et al.*, 1979; Elderfield *et al.*, 1981; Goldstein and O'Nions, 1981). Most recent marine isotope studies have continued to use Fe-Mn crusts to investigate oceanic trace metal isotopic distributions and paleo-ocean circulation (e.g. Frank, 2002; van de Flierdt *et al.*, 2003). In addition, however, recent improvements in chemical preparation treatments have also permitted investigations of other Fe-Mn materials such as authigenic Mn oxide coatings on forams (Burton and Vance, 2000) and the authigenic Fe-Mn fractions leached from bulk marine sediments (e.g. Rutberg *et al.*, 2000; Bayon *et al.*, 2002) or fish teeth (Martin and Haley, 2000). Although their slow growth rates generate relatively low resolution records, the long-term continuous record accumulation of Fe-Mn crusts, together with their insignificant perturbations when compared to sediment cores deposited over the same time-frame, mean that these crusts still provide a preferred first order tool, both for whole-ocean

paleoceanographic observations and for testing new isotopic systems. Therefore, this same material will also be the focus of the discussion here and this study.

Nd isotopes. The isotopic distributions of Nd (Fig. 1.2) show a general correlation between ocean basins and, hence, water masses. This provinciality is caused by differences in the weathering inputs from the surrounding continents since large cratons of old continental rocks (strongly negative ε_{Nd}) surround the relatively small Atlantic Ocean whereas provinces rich in young volcanics (more positive ε_{Nd}) ring the margins of the much larger deep Pacific Ocean. Time-series studies of Nd isotopes in the Atlantic Ocean correlated well with major tectonic events such as the closure of the Panama Gateway (Frank *et al.*, 1999b; Reynolds *et al.*, 1999), and with variations in water mass transport, e.g. the relative importances of NADW and AABW (Bayon *et al.*, 2003) and the trajectory of NADW export into the Indian and Southern Oceans (Frank *et al.*, 2002b).

Pb isotopes: Pb has a shorter oceanic residence time than Nd and, therefore, the variations of Pb isotopic compositions between adjacent ocean-basins are generally larger than they are for Nd (Henderson and Maier-Reimer, 2002). Pb isotopes are strongly influenced by local inputs from riverine (weathering of local source rocks) and aeolian inputs, exhibiting much less efficient mixing in the ocean than is the case for Nd (Abouchami *et al.*, 1997; Frank and O'Nions, 1998). Another advantage of investigating Pb isotopes is that one can potentially trace back the exact weathering source for any given sample using combinations of its three decay systems (^{238}U-^{206}Pb, ^{235}U-^{207}Pb and ^{232}Th-^{208}Pb). For example, the corresponding Pb isotopic compositions of Himalayan granites and Fe-Mn crusts in the Indian Ocean suggest that weathering sources were a direct result of Himalayan uplift (Frank and O'Nions, 1998).

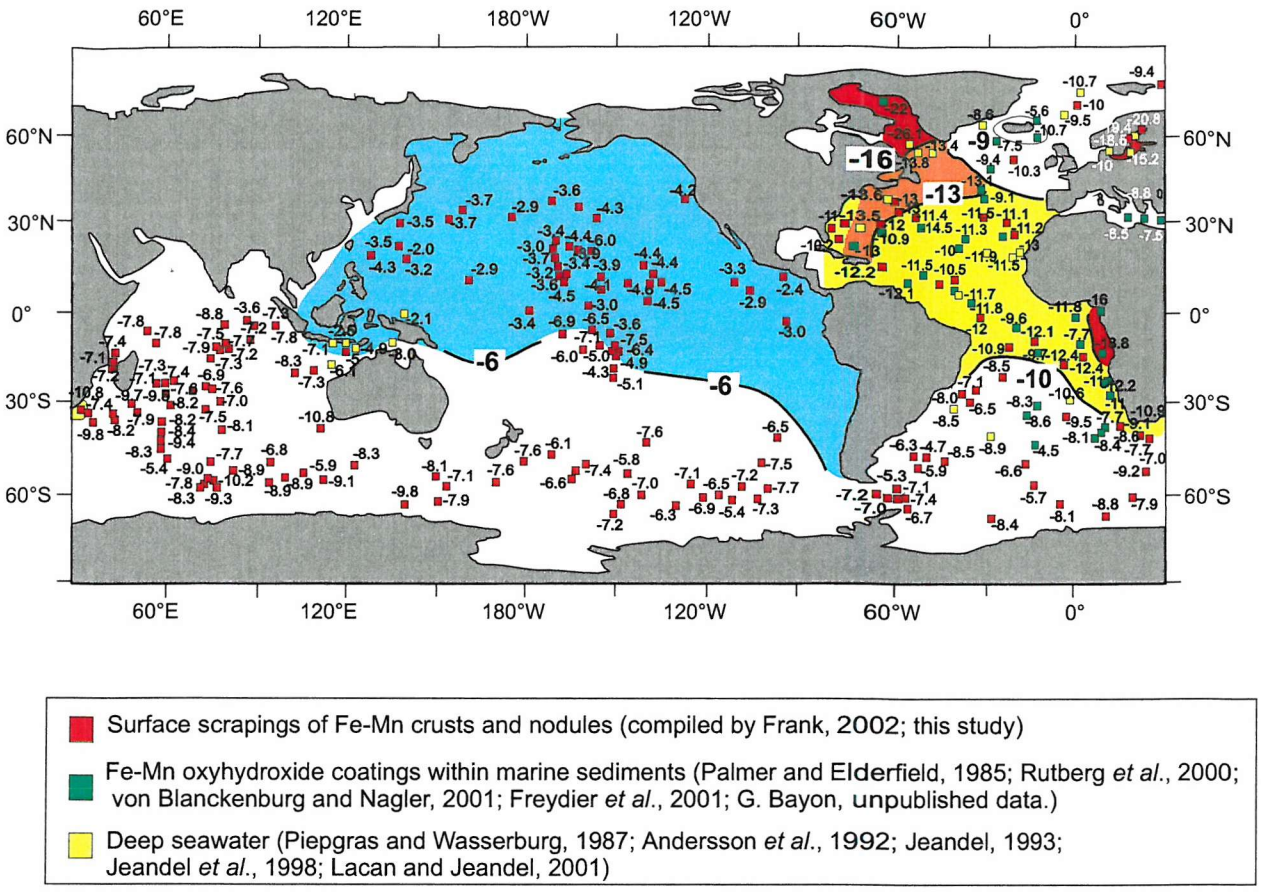

Fig. 1.2 Global distribution of Nd isotope ratios in the deep ocean (below 1000m).

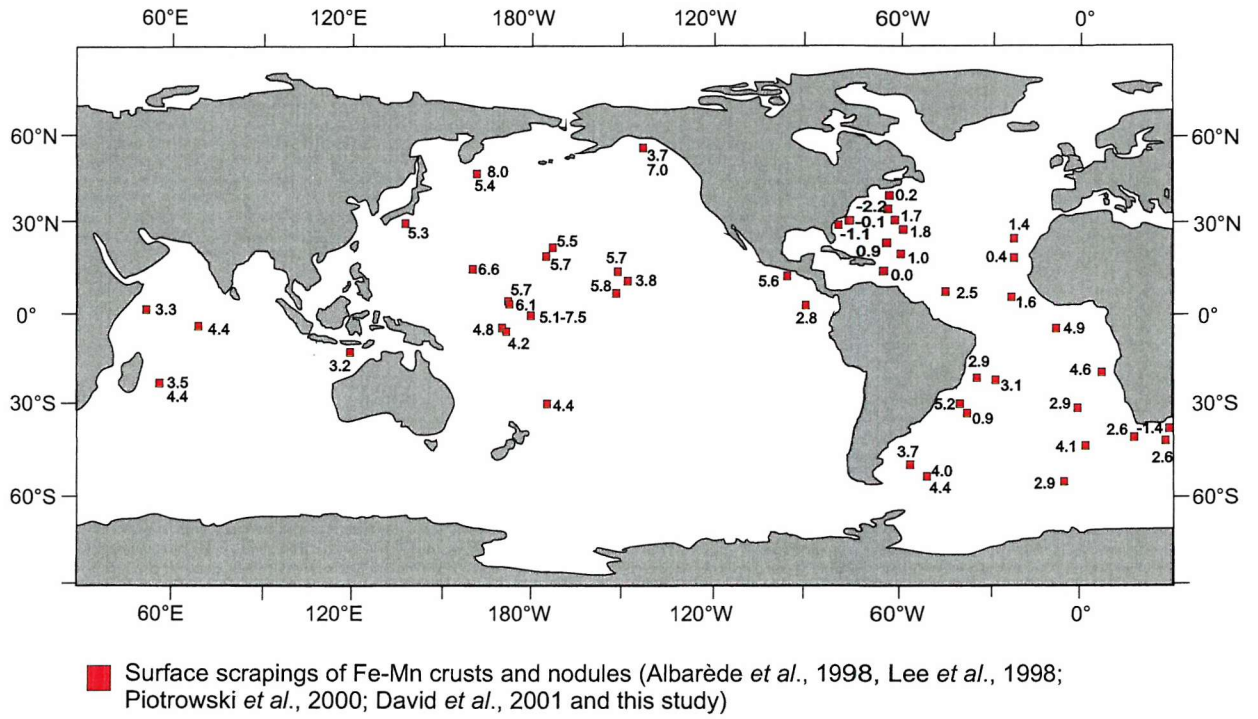

Fig. 1.3 Global distribution of Hf isotope ratios in the deep ocean (below 1000m).

Hf isotopes: Because the study of Lu-Hf isotope system is relatively new to marine geochemistry I present a more detailed discussion of the Lu-Hf system, here. The Lu-Hf system has a half-life of ~37 billion years with the decay constant of $1.865\pm 0.015\times10^{-11}$ yr^{-1} (Scherer *et al.*, 2001). The Lu-Hf system is in many respects similar to the Sm-Nd system in that both the parent and daughter elements of these two systems are refractory and lithophile (i.e. elements that are incompatible and are preferentially concentrated in the liquid phase during melting and crystallization) and moderately to strongly incompatible. Because of their coherent behaviours within the Earth's interior, the Nd-Hf isotopic composition of all mantle sources form a positive correlation when plotted against one another (Fig. 1.4a).

While Sm and Nd, both REEs, exhibit close similarities that result in no significant geochemical fractionation from one another, the same is not the case for Lu (another REE) and Hf, one of the HFSE (high field strength elements). Consequently, important fractionations in the Lu-Hf system can be imparted from mineralogy - notably by zircon which is particularly enriched in Hf, but not Lu (Patchett *et al.*, 1984). This provides a potential tool for deciphering various weathering-dissolution processes that cannot be resolved from the Sm-Nd system because both the Lu/Hf and the $^{176}Hf/^{177}Hf$ ratio of the coarse (zircon-rich) sand fraction of continental and near shore sediments/turbidites are lower than in more fine-grained, clay-rich pelagic sediments. Indeed, it is believed that the, Hf isotopic composition of seawater must be controlled by incongruent weathering, in which weathering processes systematically have less impact on resistant minerals (e.g. zircons) such that their relatively unradiogenic Hf-isotope signal is preferentially retained in the detrital phase rather than being released into seawater. This is clearly demonstrated by the seawater array in a plot of ε_{Hf} vs ε_{Nd} (Fig. 1.4b). The difference in slope between the terrestrial and seawater data-arrays has been interpreted as a direct result of this "zircon-effect" which prevents unradiogenic Hf (compared to Nd) entering the ocean. In addition, of course, contributions from both hydrothermal systems (White *et al.*, 1986; Godfrey *et al.*, 1997) and from rivers (for which no direct measurements yet exist) may also contribute to the oceanic Hf budget. The behaviour of Hf isotopes and their distributions, however, remain only poorly studied to date, if at all. Further, dissolved Hf concentrations in seawater are very low (0.1-1.1 pmol/kg) (Boswell and Elderfield, 1988; Godfrey *et al.*, 1996; McKelvey and Orians,

1998) making direct isotopic measurements difficult. For this reason, the use of Fe-Mn crusts/nodules has been made, both in the literature and the work presented here, because they pre-concentrate Hf from seawater during precipitation allowing the Hf isotopic composition of present and past oceanic water masses to be inferred.

Like Nd, the isotopic composition of Hf also shows inter-basin variations (Fig. 1.3). It has been suggested, therefore, that continental weathering must also control the Hf isotope composition of seawater (Albarède *et al.*, 1998). A decrease of ε_{Hf} observed over the past 3 Ma in two crusts from the NW Atlantic Ocean has been attributed to an enhanced contribution of unradiogenic Hf which is released from zircons (known to be enriched in Hf, compared to bulk continental crust compositions) during mechanical weathering (Piotrowski *et al.*, 2000; van de Flierdt *et al.*, 2002). The well-mixed Pacific Ocean, by contrast, is believed to be responsible for buffering and preserving the consistent long-term ε_{Hf} trend which has been observed in Central Pacific records (Lee *et al.*, 1999; David *et al.*, 2001). However, the detailed behaviour of Hf isotopes in the deep ocean remains unclear. Obtaining additional records from new locations, to complement the scarce records available to-date, has been one of the prime foci of this investigation.

(a)

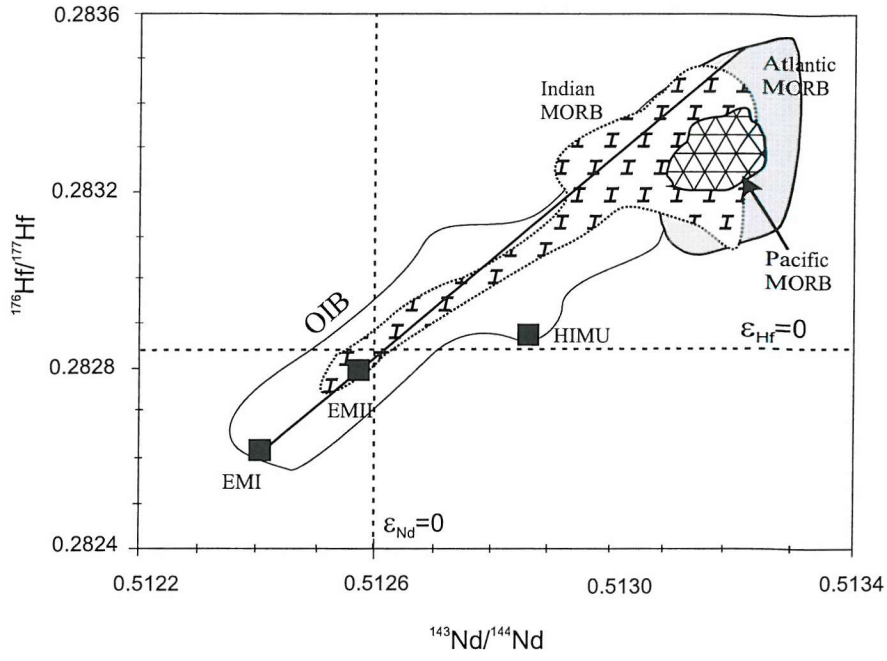

(b)

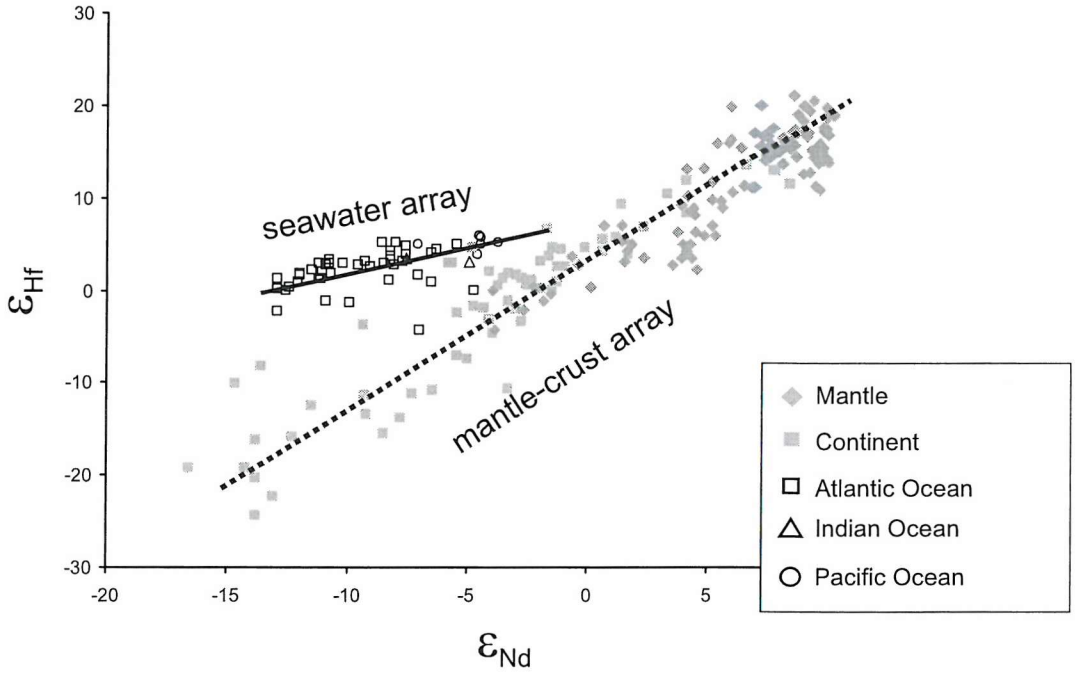

Fig. 1.4 (a) Nd and Hf isotopic compositions of mantle end-members. (modified from Salters *et al.*, 1996 and Chauvel and Blichert-Toft, 2001) (b) ε_{Hf} vs ε_{Nd} of seawater and mantle-crust array. The seawater array was determined by Fe-Mn crusts/ nodules (Albarede *et al.*, 1998; David *et al.*, 2001). Mantle data from Salters and Hart, 1991; Salters and White, 1998; Nowell *et al.*, 1991; Chauvel and Blichert-Toft, 2001. Continent data from Vervoort *et al.*, 1996 and 1999.

1-3-2 Transition metal isotopes - Iron isotopes

Stable isotope geochemistry is concerned with the fractionation of different isotopes of a common element from one another as a result of biological and/or physicochemical processes (e.g. Hoefs, 1997). The study of transition metal isotopes, which can be considered as 'heavier' stable isotopes, has advanced very rapidly in recent years following the improvement of analytical techniques – notably the introduction of multi-collector ICP-MS. Natural variations in the isotopic compositions of all of Fe, Cu, Zn, Mo and Tl have been reported recently in Fe-Mn crusts and/or nodules (e.g. Maréchal *et al.*, 1999; Zhu *et al.*, 2000b; Barling *et al.*, 2001; Rehkämper *et al.*, 2002; Siebert *et al.*, 2003) offering the promise of potential new proxies in marine isotope geochemistry studies and improved understanding of the balance for these elemental budgets in the oceans.

The exceedingly low concentration of dissolved Fe in the modern ocean (<1 nM in the open ocean (e.g. Johnson *et al.*, 1997) makes direct isotopic measurement of this element, in particular, extremely challenging. Zhu *et al.* (2000) reported the first time series of Fe isotope variations in a Fe-Mn crust from the North Atlantic Ocean in which an increasing Fe isotope variation covariate with increasing $^{206}Pb/^{204}Pb$ ratios after 1.7 Ma was observed. It has been shown a remarkable constancy in the present-day Fe isotope compositions in all of the following: igneous rocks and their weathering products; loess; aerosols; continental sediments; suspended river loads and marine turbidites (Fig. 1.5). Therefore this current, much larger database (Beard *et al.*, 2003a; Beard *et al.*, 2003b) suggests that, instead of reflecting changes in the Fe and Pb isotopic composition of lithologic material that reach the ocean, it was an increase in the detrital flux to the open oceans caused by ice rafting or increased riverine and/or atmospheric fluxes associated with the initiation of Northern Hemisphere glaciation at 2.6 Ma that raised the average seawater Fe-isotope signature from its previously lower values (possibly dominated by the hydrothermal flux) (Beard *et al.*, 2003b).

(a)

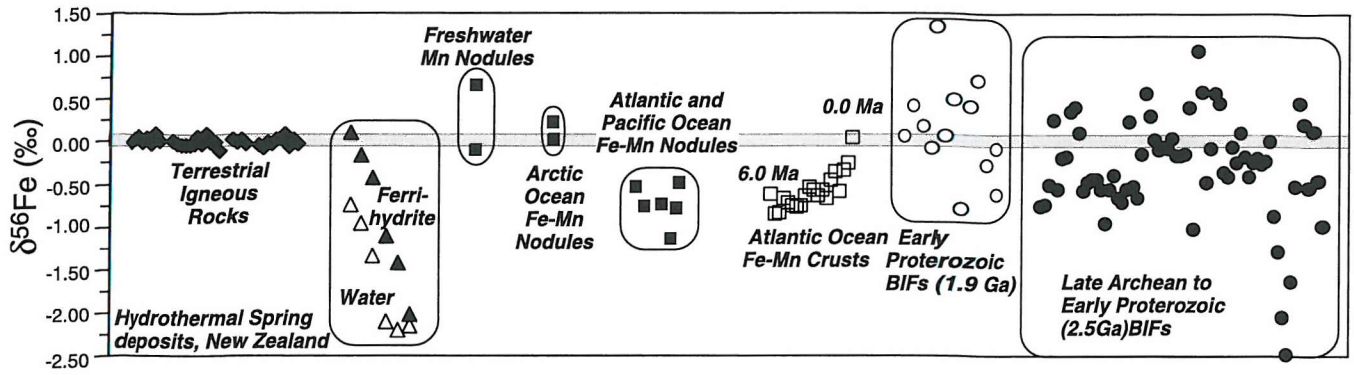

(b)

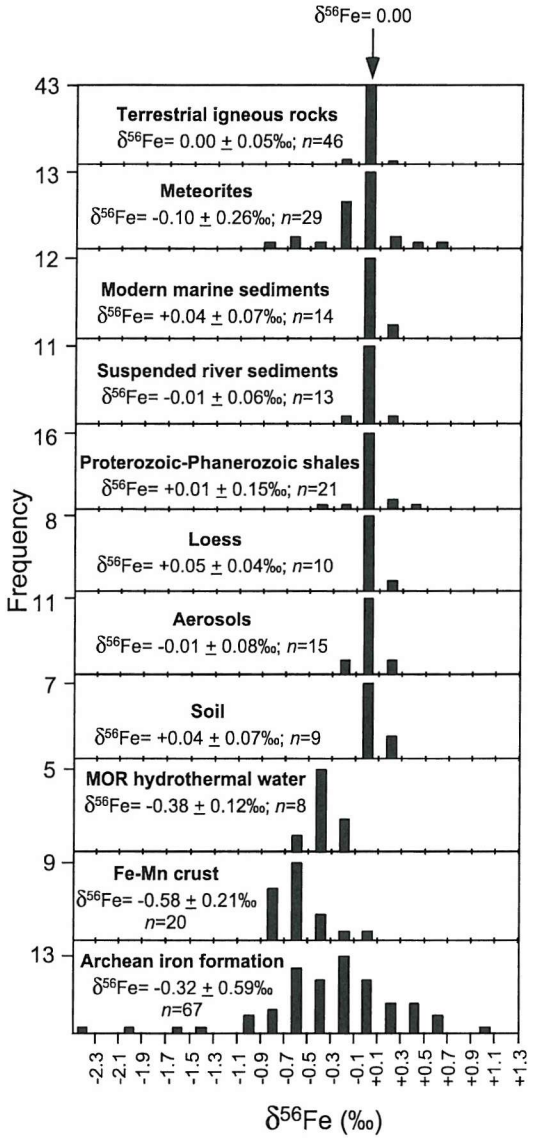

Figure taken from Beard *et al.* (2003 a, b)

Fig. 1.5 Fe isotope variations in natural samples. (a) Values are relative to igneous Fe (gray band ± 0.05 ‰); values have corrected for interlaboratory differences between UW-Madison and Oxford from standard IRMM-014 with a value of 0.09‰. Data are from Beard and Johnson (1999), Beard *et al.* (1999), Bullen *et al.* (2001), Zhu *et al.* (2000), Johnson *et al.* (2003), Beard *et al.* (2003) and Johnson *et al.*, unpublished data. (b) Frequency plot of Fe isotopic variations. Meteorite data from Zhu *et al.* (2001).

The residence time of Fe (<100 yr, Johnson *et al.*, 1997) is at the same order or shorter than Pb (~100 yr, Henderson and Maier-Reimer, 2002) and is expected to have regional variability. The discovery of low Fe isotopic values in hydrothermal sources (Sharma *et al.*, 2001; Beard *et al.*, 2003b) suggests that these, too, must act as an important source of dissolved Fe to balance the isotopic budget of Fe in the ocean. The paucity of data available from hydrothermal systems to date, however, makes this issue difficult to resolve at present.

1-4 Fe-Mn crusts

As described earlier, a key aspect of the work described here is the reliance upon Fe-Mn crusts as natural pre-concentrators of dissolved metals from the oceans for detailed isotopic analysis. Before proceeding to a discussion of the particular samples chosen and any presentation of the analytical data obtained from those samples, however, it is first important to consider how such samples are first formed.

1-4-1 The growth of Fe-Mn precipitates

Fe-Mn crusts occur in three principal types of formation which have been classified as "hydrogenetic", "diagenetic" and "hydrothermal" deposits (Arrhenius *et al.*, 1964; Lynn and Bonatti, 1965; Cronan, 1967; Bonatti *et al.*, 1972). The classification of "hydrothermal" was actually predates first discovery of submarine hydrothermal venting at the Galapagos Spreading Centre in 1977 (Corliss *et al.*, 1979). Hydrogenetic deposits, characterized by slow growth rate, form directly from seawater in an oxidizing environment where Mn^{2+} is transformed to insoluble Mn^{4+} in hydrated MnO_2 particles. Diagenetic deposits develop within/or at the interface of sediment columns through precipitation of dissolved Mn (± Fe) from reduced pore waters. These deposits are characterized by faster growth rates (10-100 mm/Ma) and are found on siliceous oozes. Hydrothermal deposits precipitate directly from hydrothermal solutions in areas with high heat flow, for example along mid-ocean ridges. They are characterized by high to extremely high growth rates (>1000 mm/Ma) and low to very low trace element contents. They tend to be associated with hydrothermal sulfide deposits and iron oxi-hydroxide crusts.

Fe-Mn crusts and nodules consist of manganese oxides (δ-MnO_2, vernadite and todorokite) and amorphous iron oxyhydroxides $FeOOH^{*}xH_2O$. Three principal manganese oxides minerals are (1) birnessite (also called 7 Å manganite) which is

associated with hydrothermal processes (Roy, 1981 and references therein); (2) δ-MnO_2 (Fe-vernadite or disordered birnessite) with X-ray lines at 2.40 Å and 1.40 Å (Burns and Burns, 1977) - a typical hydrogenetic feature and (3) 10 Å manganate (todorokite, burserite) - a typical indicator of diagenetic processes.

A growth model for ferromanganese precipitates by a colloidal-chemical mechanism is demonstrated in Fig. 1.6 (Koschinsky and Halbach, 1995). With the supply of oxygen, oxidation of Mn and Fe will form oxides and hydroxide colloids. These colloidal phases will then scavenge dissolved trace metals from the surrounding seawater, where hydrated cations of (e.g.) Co, Ni, Zn, Pb, Cd, Tl) are attracted to the negatively charged surface of Mn oxyhydroxides. By contrast, anions and elements that form large oxyanions and other complexes with low charge-density (e.g. V, As, P, Zr, Hf) will be attracted to the slightly positive charge of Fe oxy-hydroxide surfaces. Mixed Fe and Mn colloids, together with these other, adsorbed metals, then precipitate onto hard-rock surfaces as poorly crystalline or amorphous oxyhydroxides. Continuing crust accretion, after precipitation of that first molecular layer, is autocatalytic but is probably also enhanced to some degree by bacterial processes (see, e.g., Hein *et al.*, 2000 and references therein).

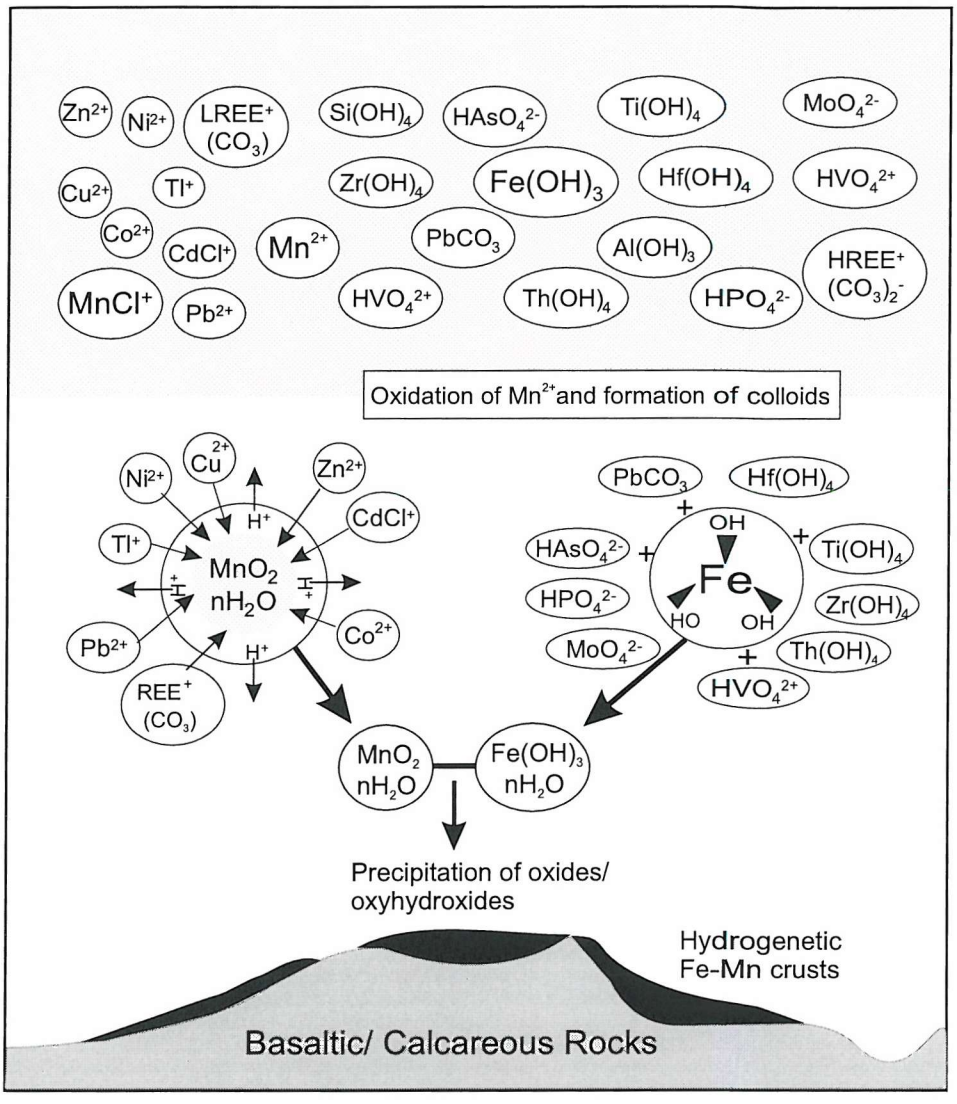

(After Koschinsky and Halbach, 1995 and Hein *et al.*, 2000)

Fig. 1.6 Colloidal-chemical model for hydrogenetic crusts formation. It shows the formation of complexes and colloidal phases, adsorption of metals and precipitation of oxides on seamount rock substrates.

1-4-2 Different types of Fe-Mn deposit and how to tell them apart

Morphologically, there are two main types of Fe-Mn deposit: Fe-Mn nodules and Fe-Mn crusts. Nodules usually grow concentrically around a discrete nucleus and occur mainly in deep-ocean basins (>4000 m) characterized by low sedimentation rates (i.e. <5 mm $10^3 yr^{-1}$) where inputs of calcareous ooze, turbidity flows and volcanic ash are low. They therefore occur in highest abundances on red clays and siliceous oozes, far from land and its detrital inputs. As AABW flows north and east across the bottom of the Pacific Ocean, for example, as the sedimentation rate decreases, so the nodule abundance increases, along this flow path. The composition of deep-sea manganese nodules is often chemically hetereogeneous, both within individual nodules and over small distances on the sea floor, as well as on a worldwide scale. This is because of the rotation of the nodules at the sediment-water interface interrupting a continuous growth records and possible diagenetic interactions between the host sediments' pore-fluids and the Fe-Mn nodules themselves (see Glasby, 2000 and references therein).

Fe-Mn crusts accumulate on submarine seamounts and plateaus at depths >1000m where bottom currents prevent sediment accumulation. This type of ferromanganese precipitate anchors itself onto a rock or calcareous basement and therefore, does not become involve any processes of rotation or diagenesis during growth. This characteristic thus allows one to determine the growth direction and identify definite layers representing consecutive episode of growth back times. As a primary chemical precipitates formed directly from, and directly in contact with local ocean water, Fe-Mn crust can provide confident seawater isotopic compositions records the of elements in questions.

1-5 Thesis Outline

The focus of this project has been to improve our understanding of the geochemistry of Hf and Fe isotopes in the marine environment. This has been achieved by setting the Hf and Fe data presented in the context of complementary, better-understood analyses of Pb, Nd and REE systematics. All measurements have been made upon a suite of Pacific Fe-Mn crusts; the Fe-Mn crusts selected were taken from the Central and Western Pacific Ocean (Izu-Bonin Back Arc Basin) and encompass two quite different geographic and geological settings. The present day oceanographic settings of these locations are reviewed in Chapter 2.

In Chapter 3, I describe the first establishment of Hf isotope analytical methods at SOC. This includes the newly-proposed ytterbium (Yb) isotopic ratios, which are crucial when Yb interference is present or applying a laser ablation technique to Hf isotopic analysis. This part of the thesis has already been published in the international peer-reviewed literature (Chu *et al.*, 2002). The chronology determinations for the Fe-Mn crusts used in this study, obtained from beryllium (^{10}Be) dating conducted during a visit to ETH (Zurich) in 2002, are described in the final section of Chapter 3.

Chapter 4 presents the compiled radiogenic isotope and elemental results from the analyses of the *surface*-layers of the entire suite of Fe-Mn crusts analysed. These surface-layer data represent an average of ocean composition over just the most recent few thousand years. As such, these seawater signatures can be compared with present ocean physical properties (e.g. WOCE data) to establish the best constraints on the marine geochemitsry of Hf-isotopes that can be achieved in the continuing absence of direct seawater Hf-isotope analyses. Properties and source inputs for Hf to the Central Pacific Ocean are suggested based upon correlations between the reported Hf isotope results and associated physical tracers and complementary geochemical results (e.g. REE and Nd isotopes). In this chapter, I also demonstrate the importance, for Hf isotopes, of avoiding all detrital phases incorporated into Fe-Mn crusts during their growth.

In Chapter 5 I present time-series records of Nd, Pb and Hf isotopes in three Fe-Mn crusts, one from the already relatively well-characterised Central Pacific Ocean and two from a completely novel setting: the Izu-Bonin back-arc basin area. The

various sources, signatures and oceanic residence times of these three isotopic systems provide deeper insights into our understanding of Hf-isotope paleoceanography. For example, a pronounced decoupling between Hf and Nd isotopes is observed in the Izu-Bonin Fe-Mn crusts and possible causes and consequences are discussed.

In Chapter 6, I present data showing secular variation in the Fe isotopic composition of the same set of samples presented in Chapter 5. These are the first time-series Fe isotope measurements to be obtained from anywhere in the Pacific Ocean. The aim of this chapter is to provide improved understanding of the Fe budget, controlled by direct input and/or biogeochemical processing within the ocean interior, in the modern and the paleo-ocean. This final analytical part of my thesis study was carried out in the Department of Geology and Geophysics, Univ. of Wisconsin-Madison, funded by a Worldwide University Network studentship exchange scheme.

Finally, the conclusions which can be drawn from this study are summarised in Chapter 7. That chapter also includes a discussion on the relative potencies among the present suite of isotopic tracers available as (pale)oceanographic 'proxies' and closes with some suggestions on important future directions for marine isotope geochemistry.

Chapter 2. Materials

2-1 Abstract

Fe-Mn crust samples analysed in this study have been collected from the Central Pacific Ocean and the Izu-Bonin Back Arc Basin of the Western Pacific. Based on their physical descriptions, mineralogical and chemical characteristics, it was possible to select samples from both the surfaces and growth layers which were free of diagenesis alterations. The samples used are therefore hydrogenetic in origin and ideally suitable for palaeoceanographic studies. Detailed present day hydrological settings were described in this chapter. Physical and nutrient tracer information of the seawater at the sample locations was derived from the WOCE database for the present day comparison interpretation (see Chapter 4).

2-2 Samples and methods

Sixteen Fe-Mn crusts analysed in this work were collected from Central Pacific Ocean and Izu-Bonin Back-Arc Seamounts (Table. 2.1; Fig. 2.1; Plate 2.1-2.3). The Central Pacific samples were collected by dredging from two cruises- SO46 (1986) and SO66 (1990) under the MIDPAC project 3 and 4 (PI: Prof. Dr.-Ing.P. Halbach): there are 5 samples from the North Central Pacific (NC1~5, open circle) and 9 samples from the South Central Pacific (SC1~9). Samples from South Central Pacific (SCP) were divided into three subgroups according to their locations: from North to South are SC-a (SC1~5, half-filled squares), SC-b (SC6&7, open squares), and SC-c (SC8&9, solid squares). Two Izu-Bonin Back Arc crusts (IB1&2; open and solid triangle) were collected by dredging during R/V *Moana Wave* cruise MW9507 (1996) as part of the UCSC-UH-GSJ-ORI joint project 'Cross-Chain and Remnant Volcanism in the Izu Region' (Shallenberger *et al.*, 1995; Usui *et al.*, 1996).

Table 2.1 Locations of Fe-Mn crusts in this study

Sample/ Symbol	Lierature Name	Depth (m)	Lat./Long.	Sample description	Thickness (mm)
North Central Pacific ○					
NC1	107DSK1	1275	15°42'N / 169°29'W	non-phosphatized (d) SR: basalt breccia	49.0
NC2	120DSK1	1565	15°37'N / 169°16'W	non-phosphatised (d) SR: volcanoclastite	50.0
NC3	79DSK4	1585	15°39'N / 170°24'W	young generation with old phosphatized part characterised as white veins closed to the substrate (d) SR: basalt breccia	40.0
NC4	69DSK1	1930	15°39'N / 170°21'W	non-phosphatized (d) SR: basalt breccia	38.0
NC5	92DSK1	2255	15°44'N / 171°08'W	a layer of detritals incorporated in the growth layer (d) SR: basalt	90.0
South Central Pacific					
SC-a ◪					
SC1	13DSR3	1664	4°08'S / 174°52'W	non-phosphatized (b) SR: phosphatized limestone	39.0
SC2	10DSR14	1984	4°10'S / 174°51'W	non-phosphatized (b) SR: phosphatized limestone	40.0-60.0
SC3	43DSO5	2260	4°08'S / 174°53'W	non-phosphatized (b) SR: phosphatized limestone	46.0
SC4	5DSR8	2500	4°09'S / 174°54'W	Mainly young generation with old phoshpatized growth layers (a) SR: volcanoclasite in phosph. matrix	80.0
SC5	28DSR3/9	3033	4°10'S / 174°54'W	non-phosphatized (b) SR: phosphatized limestone	34.0
SC-b □					
SC6	80DSK2	1787	2°01'S / 176°10'E	non-phosphatized (b) SR: carbonate clastite partly phosphat.	47.0
SC7	69DSO3	2000	2°03'S / 176°14'E	non-phosphatized (b) SR: volcanoclastite	49.0
SC-c ■					
SC8	59DSR1	2545	8°23'S / 177°19'E	Mainly young generation with old phoshpatized growth layers (a) Thin todorokite-rich layers occur at the contact to carbonate phases. (c) Isolated Fe-Ti-rich layers with characteristic light colour. (c) SR: volcanoclastite	50.0
SC9	85DSK2	2600	9°57'S / 179°56'E	Young generation covered on old phosphatized old generation, zeolites at the contact to the substrate (a) SR: carbonate clastite	40.0
NW Pacific- Izu-Bonin Back Arc					
IB1 △	D105-5AB	1860	31°22'N / 138°41'E	non-phosphat. (d) SR: basalt	24.0
IB2 ▲	D97-1	2600	30°53'N / 138°22'E	non-phosphat., white banding patterns within the crust (d) SR: basalt	46.0

SR= Substrate Rock

Ref: a: Kochinsky and Halbach (1995); b: Bau *et al*. (1996); c: Kochinsky *et al*. (1997); d: this study.

(a)

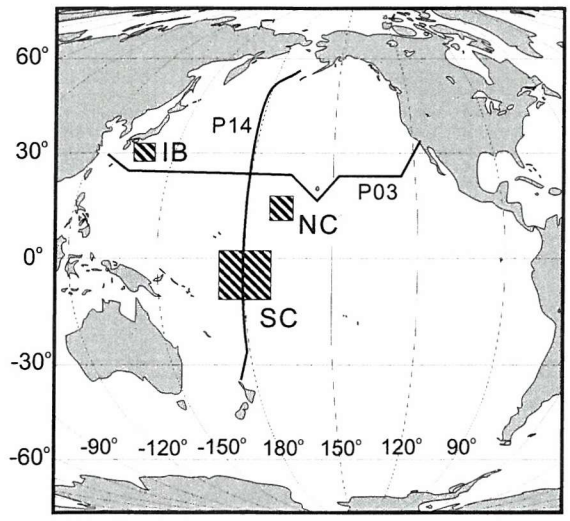

(b)

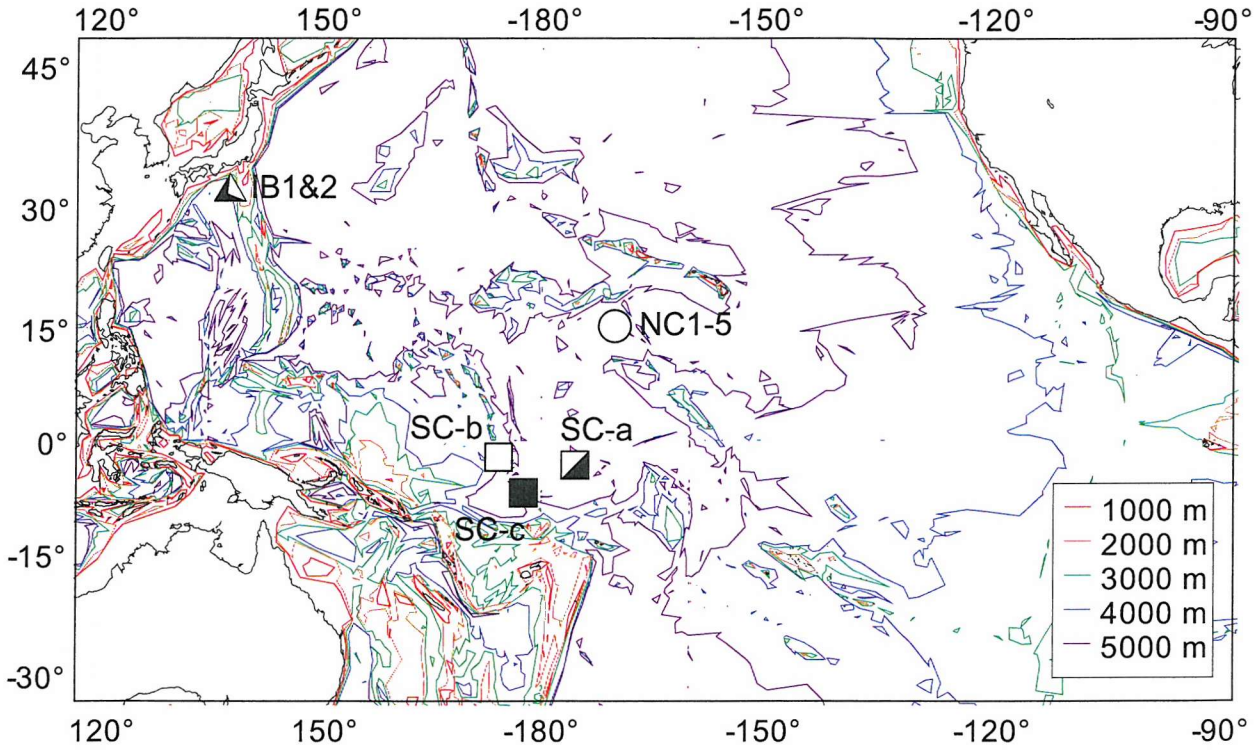

Fig. 2.1 (a) Sample locations (shaded area). P03 and P14 are the WOCE sections. (b) Sample location with bathymetric map (Source: GEBCO). SC-a includes SC1-5; SC-b includes SC6&7 and SC-c includes SC8&9.

NC1 (107DSK1)

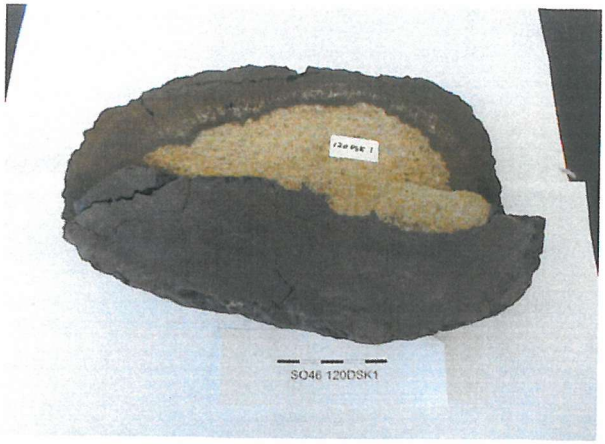

NC2 (120DSK1)

NC3 (79DSK4)

NC4 (69DSK1)

NC5 (92DSK1)

SC1 (13DSR3)

Plate 2.1 Fe-Mn crusts of this study (descriptions see table 2.1)

SC2 (10DSR14)

SC3 (43DSO5)

SC4 (5DSR8)

SC5 (28DSR9)

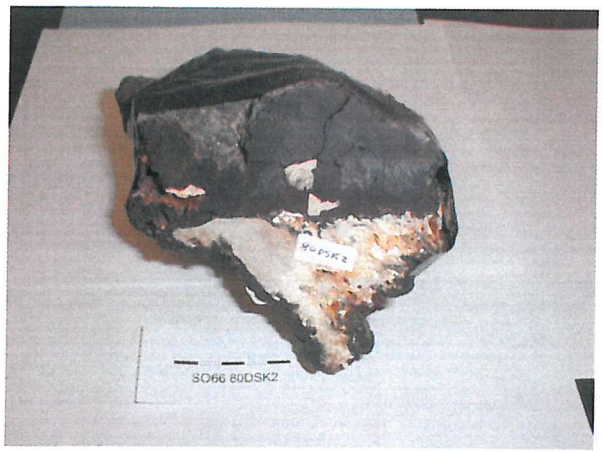

SC6 (80DSK2)

SC7 (69DSO3)

Plate 2.2 SC2-SC7 (description see table 2.1)

SC8 (59DSR1)

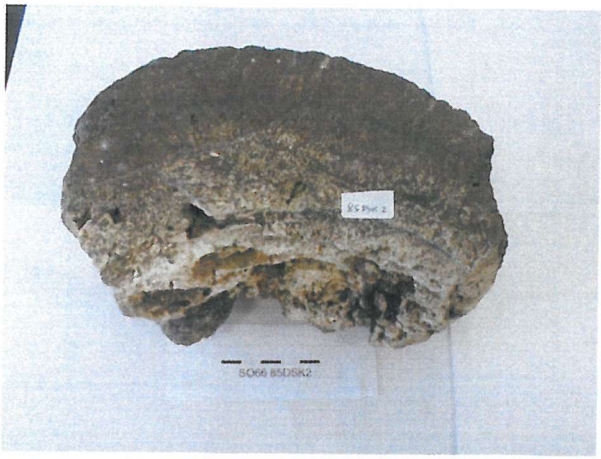

SC9 (85DSK2)

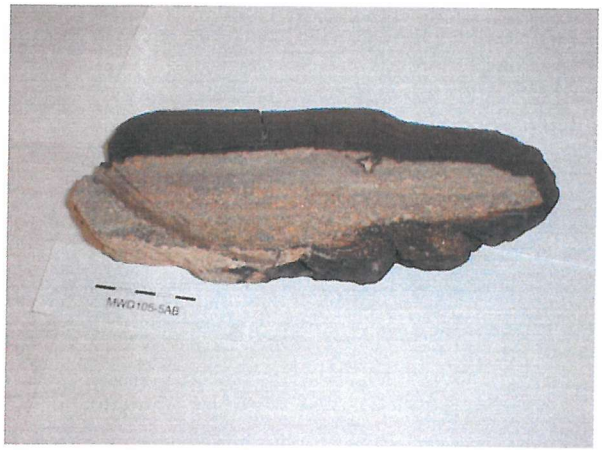

IB1 (D105-5AB)

IB2 (D97-1)

Plate 2.3 SC8-9 and IB1-2. (Description see table 2.1)

Mineralogical and elemental studies had previously been carried out and published for most of these samples (see, e.g. Koschinsky and Halbach, 1995; Bau *et al.*, 1996; Koschinsky *et al.*, 1997; Joshima and Usui, 1998 and appendix I); and sample IB1 has already been dated using the $^{10}Be/^{9}Be$ method (Usui *et al.*, unpublished data). The thicknesses of the crusts range between 2.4 and 9.0 cm and the values listed in Table 2.1 represent the thickest parts of the samples provided. The substrate rocks consisted variously of basalt, basalt breccia, hyaloclastite, limestone, phosphorite, and reef limestone breccia (Koschinsky *et al.*, 1997; Ishizuka *et al.*, 1998).

Most of the crusts were non-phosphatized pure hydrogenetic deposits (Bau *et al.*, 1996) although some represented young non-phosphatized material covering older phosphatized part (Koschinsky *et al.*, 1997), the later being characterised by the impregnation of carbonate fluorapatite (CFA), which could be recognized as white vents that grew at the bottom part of the crusts (detailed in section 2-3-1) and are indicative of diagenetic remobilization effects. When selecting crusts for this study, phosphatized sections were therefore avoided.

Surface samples were scraped with steel scalpel blades and the blades were either discarded or cleaned with distilled water and acetone between sampling. The sub-sampling for $^{10}Be/^{9}Be$ dating was carried out by fixing the sample on a drill stand (Plate 2.4) with a 1 mm diameter steel drill bit. New drill bits were used each time during one layer drilling. Depth profile sampling was carried out on resin-impregnated (Epoxy resin AY105) section by a computer-controlled micro-milling machine (at ETH, Zurich) (Plate 2.5) to obtain continuous profiles with 0.5-1mm intervals parallel to the $^{10}Be/^{9}Be$ dating profiles. Drill bit was cleaned each time with acetone after one layer sampling.

The sample powders (either from scraping, drilling or milling) were firstly leached/ digested in hot 6N HCl for 4 hours and the undissolved detritus fractions then removed by centrifuging. The major/ minor elements were analysed by an Elmer-Perkin Optima 2000DV ICP-AES; and trace element results were obtained using an ICP-MS (PlasmaQuad 2+, VG Elemental). All analyses carried out were from the same dissolution.

Plate. 2.4 Sampling for Be profiles.

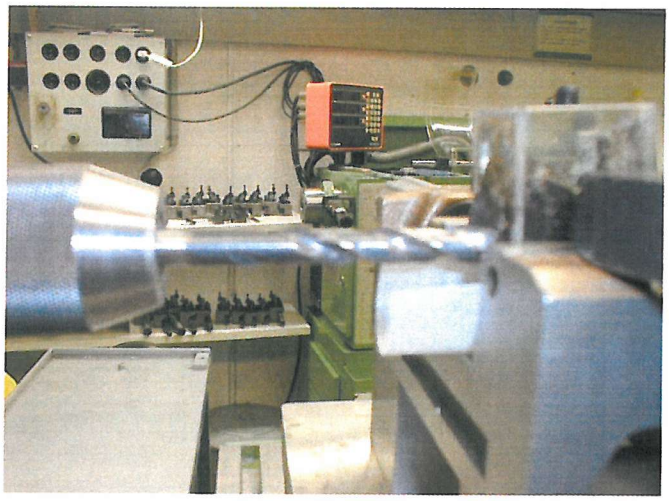

Plate. 2.5 Depth profile sampling. Sampling was carried out at Department of Earth Sciences, ETH Zurich.

2-3 Origin of the samples- element variations and diagenesis effects

2-3-1 Major element and the phosphorus problem

Dissolved Mn^{2+} (and Fe) exhibits a maximum concentration in the oxygen minimum zone (OMZ) from the degradation of organic material and the *in situ* reduction of Mn-bearing solid phases in this zone. In the Central Pacific the OMZ is found between 800 to 1,200 m (Klinkhammer and Bender, 1980). Below the OMZ, the presence of oxygen forces the oxidation of Mn^{2+} to particulate MnO_2 and it adsorbs cations such as Ni^{2+}, Cu^{2+}, and Zn^{2+}, from natural waters. Higher δ–MnO_2 content, lower colloidal Fe-hydroxide (smaller dilution effect) or slower growth rate will increase the amount of these minor metals. Hydrogenetic Fe-Mn crusts are therefore characterised by high (up to 1%) Co contents (Manheim and Lane-Bostwick, 1988).

When interpreting present or past seawater variation, diagenesis can be a major pitfall as this results in the alteration of both the major/trace element and isotopic characteristics. Commonly, the end result of this process is an enrichment of Mn due to its high mobility in pore water (Hein *et al.*, 1994 and reference therein). Based on these chemical features it has been proposed (e.g. Bonatti *et al.*, 1972; Usui and Someya, 1997) that it is possible, to use Fe/Mn ratios and Cu-Ni concentrations, to distinguish the various types of Fe-Mn crusts in the ocean. The ternary diagram ((Cu+Ni)×10)-Fe-Mn can be used to differentiate the growth origin of the Fe-Mn crusts (e.g. Halbach *et al.*, 1981; Miller and Cronan, 1994; Ohta *et al.*, 1999; Takahashi *et al.*, 2000). The major element compositions of both the surface and growth layers of the Fe-Mn crusts used in this study are listed in Table 2.2 and Table 2.3 and are plotted in Fig. 2.2. The figures show rather convincingly that the samples fall within the hydrogenetic area defined by the others (Halbach *et al.*, 1981; Miller and Cronan, 1994; Ohta *et al.*, 1999; Takahashi *et al.*, 2000).

Table 2.2 Major element compositions of the surface Fe-Mn crusts

Sample	Mn (%)	Fe (%)	Cu (%)	Ni (%)	Zn (%)	Co (%)	P (%)
NC1	23.71	13.60	0.017	0.490	0.058	1.181	0.590
NC2	23.08	12.95	0.041	0.529	0.073	1.180	0.550
NC3	27.49	10.60	0.075	0.918	0.109	1.038	0.378
NC4	18.67	14.03	0.059	0.379	0.060	0.773	0.404
NC5	18.61	17.65	0.044	0.304	0.063	0.603	0.496
SC1	21.33	14.00	0.019	0.456	0.071	1.016	0.418
SC2	20.08	15.27	0.028	0.422	0.069	0.869	0.407
SC3	21.31	13.85	0.033	0.487	0.064	0.994	0.334
SC4	22.86	13.57	0.123	0.656	0.089	0.675	0.309
SC5	19.69	15.89	0.038	0.423	0.069	0.561	0.416
	20.11	15.30	0.040	0.444	0.061	0.599	0.426
SC6	20.71	16.53	0.024	0.403	0.076	0.731	0.517
SC7	21.03	18.45	0.093	0.453	0.075	0.465	0.439
SC8	17.57	16.90	0.035	0.336	0.060	0.437	0.451
SC9	16.10	20.17	0.056	0.268	0.062	0.315	0.469
IB1	15.34	20.67	0.022	0.188	0.061	0.191	0.582
IB2	17.50	12.97	0.158	0.630	0.106	0.141	0.226

Phosphorus (P) is also one indicator for diagenesis and appears in the samples as carbonate fluorapaptite (CFA). The impreganation of CFA in the inner part of Fe-Mn crusts is caused by phosphatization events from the later Eocene through the Miocene (Hein *et al.*, 1993). A typical phosphatised crust is characterised by its P concentration up to 5.5 wt% (Koschinsky *et al.*, 1997 and references therein).

The P is thought to result from intense chemical weathering. After biological uptake in the surface ocean, maximum levels of dissolved P are regenerated at intermediate depths in the awater column, within the oxygen-minimum zone (OMZ). When this OMZ layer becomes more intense and expands (e.g. due to increased surface-ocean productivity), suboxic (phosphate-rich) waters can extend down to the seafloor where they interact with existing Fe-Mn deposits, inhibiting further crust precipitation and impregnating the older crust generation with CFA (Halbach *et al.*, 1989). The overall effect of phosphatization within Fe-Mn crusts is to mobilize certain elements and generate a second precipitation of nutrient-type elements (Koschinsky *et al.*, 1997) making them much less suitable for paleoceanography studies.

Since samples from the surface of the Fe-Mn crusts are younger than the phosphatization event they should not be affected by P introduction and this is demonstrated by the phosophorus data in Table 2.2 where all of the P values are low

(0.2 to 0.6% P). Parts of the crusts, by contrast, are older than the phosphatization event and some discrimination factor must be used to aid sample selection. Bau *et al.* (1996) have suggested that samples having P concentrations lower than 0.7% are suitable for palaeoceanographic studies and this value has been adopted in the present study. On this basis, the growth layers of three Fe-Mn crusts (SC5, IB1&2, Table 2.3) did not show significant phosphatization signatures throughout, except high carbon and phosphorus contents were observed in the oldest layer (10.41Ma) in sample SC5 and consequently this particular layer was omitted in the later depth profile results (Chapter 5 and 6).

2-3-2 Rare earth element patterns

Hydrogenetic Fe-Mn crusts from the major oceans show remarkably similar rare earth element (REE) patterns (Hein *et al.*, 2000). Hydrogenetic Fe-Mn crusts are characterized by high REE contents and a positive Ce anomaly (Aplin, 1984). This latter feature is due to the preferential oxidation of Ce from Ce(III) to insoluble Ce(IV) under typical oxidizing conditions (e.g. Goldberg *et al.*, 1963; Elderfield, 1988; Koeppenkastrop and De Carlo, 1992; Ohta and Kawabe, 2001).

The REE contents of the surface and growth layers Fe-Mn crusts are listed in Table 2.3 and plotted in Fig. 2.3. The similar REE patterns of all surfaces and growth layers (SC5, IB1&2) demonstrate that the consistency origin among/ within these crusts.

Table 2.3 Major element composition of depth profile of crust IB1, IB2 and SC5

Depth (mm)	Age (Ma)*	Mn	Fe	Cu	Ni	Zn	Co	P	Ca
IB1 (D105-5AB)									
surface	0.02	15.34	20.67	0.02	0.19	0.061	0.19	0.58	2.17
1-1.5	0.23	11.97	18.09	0.02	0.12	0.049	0.13	0.45	1.66
3-3.5	0.60	11.86	18.49	0.02	0.13	0.049	0.12	0.42	1.56
5.5-6.0	1.06	10.11	17.53	0.02	0.11	0.044	0.10	0.36	1.34
10.0-10.5	1.90	11.55	18.95	0.03	0.12	0.051	0.12	0.40	1.49
13.0-13.5	2.45	12.50	19.61	0.03	0.14	0.053	0.12	0.41	1.56
15.0-16.0	2.88	12.29	18.45	0.03	0.14	0.050	0.11	0.39	1.53
17.0-18.0	3.24	14.27	19.34	0.03	0.15	0.055	0.14	0.43	1.70
21.0-22.0	3.98	14.76	19.55	0.02	0.17	0.058	0.14	0.44	1.77
24.0-25.0	4.52	11.63	16.48	0.02	0.14	0.053	0.11	0.36	1.49
IB2 (D97-1)									
surface	0.01	17.50	12.97	0.16	0.63	0.106	0.14	0.23	1.52
1.5-2.0	0.26	N/A	N/A	N/A	N/A	N/A	N/A	N/A	N/A
3.0-3.5	0.49	10.78	12.36	0.13	0.37	0.062	0.10	0.19	1.29
4.0-4.5	0.63	N/A	N/A	N/A	N/A	N/A	N/A	N/A	N/A
5.5-6.0	0.86	13.51	11.27	0.21	0.73	0.101	0.04	0.12	1.34
6.5-7.0	1.01	12.84	11.91	0.19	0.67	0.095	0.05	0.14	1.26
8.0-8.5	1.23	13.51	12.25	0.19	0.68	0.097	0.05	0.15	1.32
9.5-10.0	1.46	12.54	12.45	0.18	0.63	0.090	0.05	0.15	1.25
11.0-12.0	1.72	12.36	14.56	0.17	0.64	0.092	0.05	0.16	1.21
13.0-14.0	2.01	11.82	14.91	0.17	0.65	0.091	0.05	0.15	1.10
17.0-18.0	2.61	11.86	16.19	0.16	0.57	0.090	0.06	0.15	1.16
21.0-22.0	3.21	11.61	13.42	0.15	0.52	0.080	0.07	0.16	1.34
23.0-24.0	3.51	10.67	12.19	0.14	0.48	0.077	0.07	0.14	1.23
26.0-27.0	3.96	8.99	11.98	0.12	0.39	0.067	0.06	0.12	1.22
28.0-29.0	4.25	7.10	9.25	0.10	0.31	0.054	0.04	0.10	1.03
30.0-31.0	4.57	5.81	8.31	0.08	0.24	0.045	0.03	0.09	1.03
SC5 (28DSR9)									
surface	0.03	19.69	15.89	0.04	0.42	0.069	0.56	0.42	2.56
1.0-1.5	0.34	16.77	13.71	0.04	0.34	0.049	0.42	0.35	2.04
2.6-3.0	0.75	17.54	15.19	0.05	0.33	0.050	0.44	0.33	1.93
5.5-6.0	1.56	18.80	17.14	0.06	0.34	0.056	0.48	0.35	2.05
8.0-8.5	2.23	18.77	16.30	0.07	0.38	0.057	0.56	0.32	1.95
11.0-12.0	3.11	19.75	15.47	0.09	0.41	0.058	0.54	0.29	2.00
13.0-14.0	3.65	18.09	13.79	0.09	0.42	0.053	0.47	0.24	1.80
16.0-17.0	4.46	19.28	13.78	0.10	0.44	0.055	0.50	0.25	1.90
19.0-20.0	5.27	20.80	13.71	0.12	0.51	0.062	0.50	0.25	2.00
23.0-24.0	6.35	18.64	14.24	0.11	0.36	0.057	0.46	0.26	1.91
27.0-28.0	7.43	19.79	15.30	0.14	0.36	0.070	0.66	0.30	2.11
30.0-31.0	8.24	20.75	14.24	0.15	0.37	0.070	0.81	0.26	2.12
33.0-34.0	9.05	20.97	15.74	0.15	0.39	0.076	0.62	0.31	2.30
38.0-39.0	10.41	6.63	7.70	0.10	0.24	0.046	0.10	6.77	17.52

N/A: Not analysed.

* Age determination by ^{10}Be method, described in Chapter 3.

(a) Surface Fe-Mn crusts

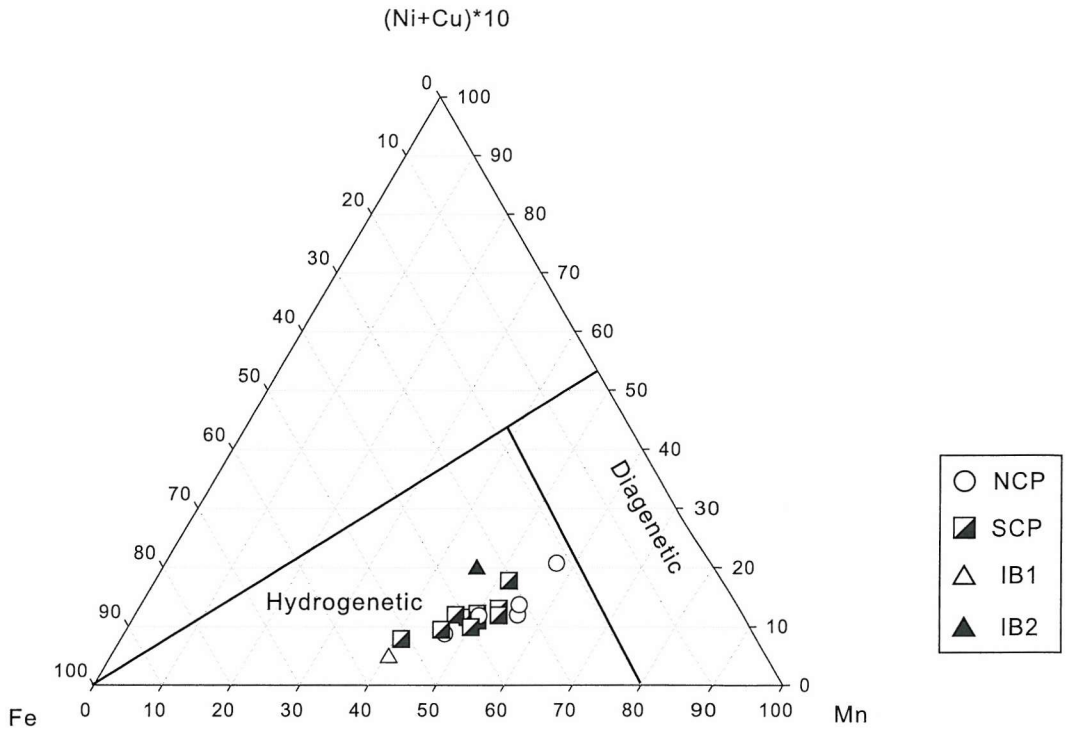

(b) Depth Profile

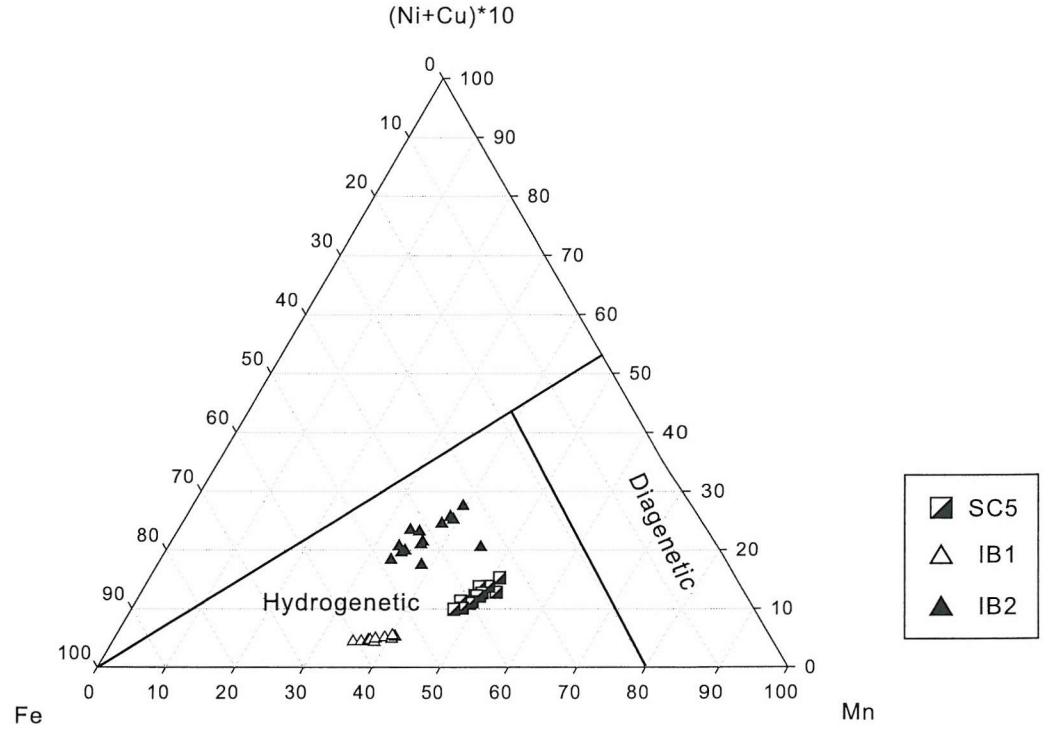

Fig. 2.2 Ternary diagram, Fe-Mn-(Cu+Ni)*10, of Fe-Mn crusts from (a) surface and (b) growth layers. Genesis area are defined after Halbach *et al.* (1981), Usui (1983/1984) Usui and Someya (1997) and Ohta *et al.* (1999).

Table 2.4 REE contents in surface and growth layers of Fe-Mn crusts (ppm)

Sample	Water Depth(m)/ Age (Ma)	La	Ce	Pr	Nd	Sm	Eu	Gd	Tb	Dy	Ho	Er	Tm	Yb	Lu
NCP															
NC1	1275	217	784	43.5	172	33.6	8.0	39.1	6.35	33.9	7.3	19.7	2.5	18.1	2.8
NC2	1565	201	790	40.4	159	31.6	7.1	34.7	5.61	30.9	6.2	17.2	2.1	15.9	2.4
NC3	1585	130	716	24.6	97	19.3	4.5	22.2	3.68	19.7	4.3	12.0	1.5	11.0	1.7
NC4	1930	202	819	41.4	164	32.3	7.6	36.9	5.91	31.0	6.3	17.2	2.2	15.8	2.3
NC5	2255	271	975	64.1	245	50.4	11.4	54.1	8.66	43.3	8.4	22.2	2.8	20.2	2.9
SCP-1															
SC1	1664	195	464	36.2	151	29.5	7.1	32.7	5.50	31.2	6.5	17.8	2.4	16.3	2.6
SC2	1984	196	531	35.5	148	28.5	6.9	32.8	5.43	30.3	6.4	17.7	2.5	17.1	2.7
SC3	2260	222	681	40.6	169	32.9	7.8	35.5	6.21	35.1	7.6	19.8	2.7	19.0	2.9
SC4	2500	142	354	22.3	95	17.5	4.2	21.6	3.74	21.7	4.9	14.3	2.1	14.7	2.3
SC5	3033	200	458	40.3	169	33.3	8.2	36.0	6.10	32.4	6.7	17.4	2.4	16.8	2.5
SC5 (bis)		205	468	41.4	173	34.9	7.9	36.3	6.25	33.6	6.9	18.3	2.4	16.5	2.5
SCP-2															
SC6	1787	203	536	34.8	146	28.6	7.1	35.1	5.71	32.7	7.4	19.5	2.5	18.5	2.9
SC7	2000	179	524	29.2	123	23.3	5.8	28.8	4.92	27.9	6.2	17.4	2.2	16.6	2.6
SCP-3															
SC8	2545	241	480	49.5	204	40.7	9.4	43.1	7.23	38.6	7.8	19.5	2.5	18.0	2.7
SC9	2600	234	483	47.0	190	37.8	9.0	42.8	7.07	37.7	7.9	20.1	2.6	18.5	2.9
IB															
IB1	1860	95	454	22.7	90	19.8	4.5	21.2	3.27	17.2	3.2	8.8	1.1	8.0	1.2
IB2	2600	246	903	57.9	231	47.5	11.0	50.4	8.04	41.9	7.7	20.6	2.6	17.8	2.5
IB1															
surface	0.02	246	903	57.9	231	47.5	11.0	50.4	8.04	41.9	7.7	20.6	2.6	17.8	2.5
0.5-1.0	0.14	291	1098	69.0	286	65.6	13.9	63.4	8.28	53.6	10.1	27.7	3.7	23.3	3.3
1.5-2.0	0.32	255	983	58.0	240	53.6	11.5	53.4	7.43	47.1	9.0	24.9	3.3	21.4	2.9
2.5-3.0	0.51	249	937	55.2	230	49.8	10.9	52.7	7.13	45.2	8.6	24.3	3.3	22.5	2.8
3.5-4.0	0.70	260	1028	57.9	240	51.2	11.3	54.1	7.38	45.7	9.0	24.9	3.4	21.8	2.9
4.5-5.0	0.88	288	1197	64.8	274	58.2	12.9	61.6	8.12	50.7	9.8	27.0	3.8	24.4	3.3
8.0-8.5	1.53	299	1093	63.5	268	57.9	12.7	60.7	8.26	51.6	9.9	27.2	3.8	25.0	3.4
12.0-12.5	2.27	290	1055	60.4	258	55.0	12.3	58.3	8.12	50.6	9.6	27.5	3.7	25.6	3.5
16.0-17.0	3.06	327	1102	65.1	275	57.4	13.2	64.6	8.59	54.3	10.7	29.9	4.1	27.2	3.6
20.0-21.0	3.80	297	979	57.2	244	51.4	11.6	56.6	7.78	49.5	9.6	29.1	3.7	26.0	3.4
23.1-24.0	4.37	246	838	47.3	201	41.5	9.31	46.0	6.40	41.2	8.1	24.4	3.32	22.4	3.1
IB2															
surface	0.01	95	454	22.7	90	19.8	4.5	21.2	3.27	17.2	3.2	8.8	1.1	8.0	1.2
1.0-2.0	0.22	138	773	31.4	128	27.9	6.0	26.8	3.81	24.0	4.3	12.5	1.6	11.0	1.6
9.0-10.0	1.42	40	142	9.4	41	9.3	2.2	10.0	1.40	9.1	1.6	4.9	0.6	4.3	0.6
14.0-15.0	2.16	56	278	12.4	53	11.8	2.6	12.7	1.84	11.7	2.4	7.0	0.9	6.3	0.9
25.0-26.0	3.81	92	491	19.7	85	18.1	4.0	19.5	2.72	18.0	3.5	9.9	1.4	9.4	1.3
31.0-32.0	4.70	77	488	17.2	73	15.6	3.6	15.9	2.41	15.0	2.9	8.0	1.1	7.6	1.1
SC5															
surface	0.03	200	458	40.3	169	33.3	8.2	36.0	6.10	32.4	6.7	17.4	2.4	16.8	2.5
1.0-2.0	0.41	226	513	39.9	170	33.9	7.9	39.0	5.53	38.4	7.8	23.8	3.3	21.9	3.2
6.0-7.0	1.76	187	482	28.9	127	24.0	5.7	31.0	4.18	31.3	6.9	21.4	3.1	21.4	3.1
9.0-10.0	2.57	154	445	21.3	93	17.4	4.2	23.3	3.23	25.8	6.0	19.7	2.8	19.4	2.9
13.0-14.0	3.65	129	502	18.7	81	15.2	3.6	19.8	2.84	20.9	5.0	16.4	2.3	16.1	2.5
29.0-30.0	7.97	163	843	27.6	114	21.8	5.0	24.3	3.59	25.1	5.2	16.6	2.4	16.4	2.5

(a)

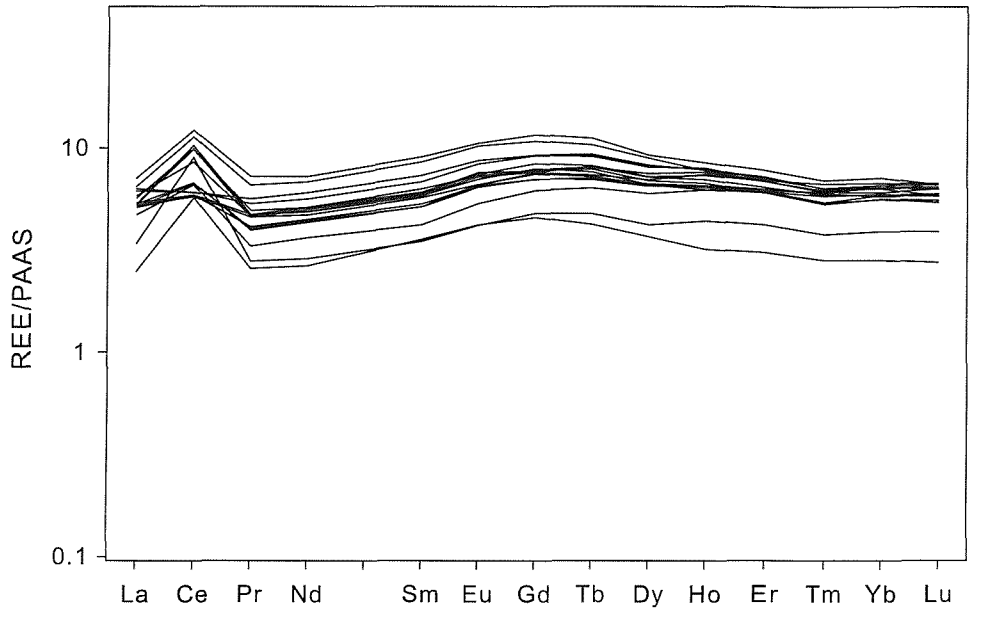

(b)

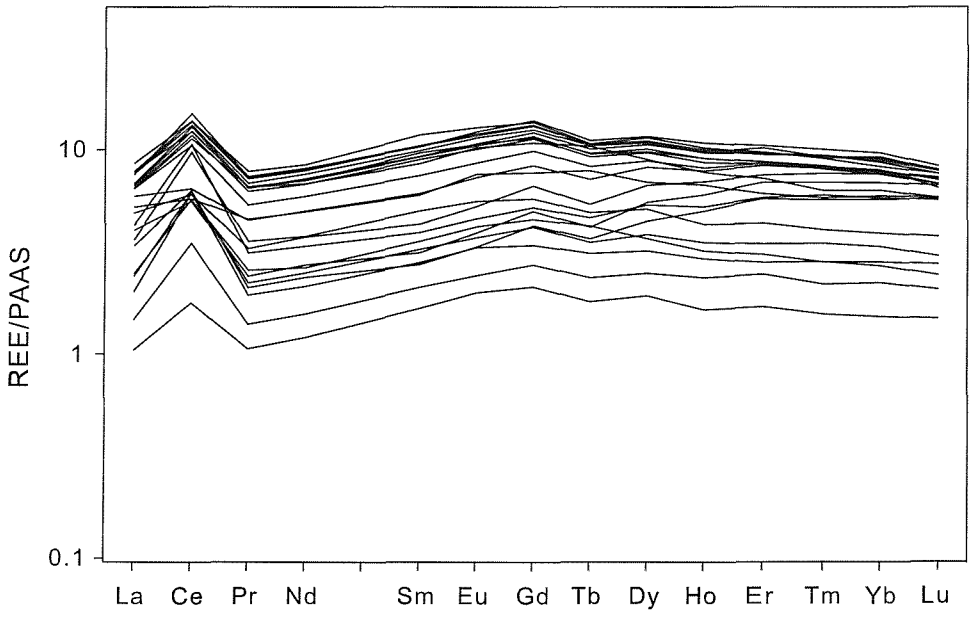

Fig. 2.3 REE patterns of (a) Surface and (b) growth layers of Fe-Mn crusts in this study.

2-4 Modern hydrological settings at sample sites

One of the objectives of this study is to investigate the chemical properties of modern day Pacific water-masses using the geochemical characteristics of Fe-Mn crusts as a proxy. To some extent, a significant amount of such information is available through the World Ocean Circulation Experiments (WOCE). In this section the WOCE and other published data are extrapolated into the geographic and depth regions of the Fe-Mn crust samples and from this, estimates are made of the water-masses surrounding the sample localities

2-4-1 Modern Pacific Ocean

The deep Pacific Ocean below 1000 m comprises four principal water-masses: North Pacific Intermediate Water (NPIW), Antarctic Intermediate Water (AAIW), Pacific Deep Water (PDW) and Antarctic Bottom Water (AABW) (e.g. Dietrich *et al.*, 1980) (Table 2.4). Situated toward the end of the global conveyer belt (Broecker, 1991), Pacific deepwater-masses are characterised by sluggish movement and uniform properties. AABW, originated from the Circumpolar Deep Water that flows around Antarctica, enters the Pacific Ocean via Macquarie Ridge south of New Zealand and then flows northward through the Samoa Passage (10°S, 169°W), following the 4000 m contour lines (Reid and Lonsdale, 1973; Warren, 1973). This bottom water then divides into two toward the northwest and northeast branches after crossing the Equator. Unlike the Atlantic Ocean, the salinity in the north Pacific is too low to allow the formation of deep water from winter cooling. Instead, the bottom water ends in the North Pacific and upwells to a less dense layer of deepwater- mass as PDW before returning south and completing the conveyor loop (Roemmich and McCallister, 1989). PDW acquires its hydrological properties from the mixtures of overlying intermediate waters and underlying bottom waters (Reid and Lynn, 1971).

Two trans-oceanic sections, P14 (179°E, 1996) and P03 (24°N, 1985) (Fig. 2.1), from the WOCE (World Ocean Circulation Experiments) database were chosen as representing the modern day hydrology in the Central Pacific. Plate 2.6 – 2.11 present the potential temperature, salinity, silicate, oxygen, phosphate and nitrate properties of these two sections. These modern day properties from the two sections will be applied in Chapter 4 as a parameter and comparing with the geochemical data acquired from surface Fe-Mn crusts samples.

Table 2.5 Physical properties and depth range of water masses in the Pacific Ocean

Abbrev.	Watermass	Approx. Range (m)	Typical physical properties (θ, σ_θ, S)
NPIW	North Pacific Intermediate Water	500-2000m	θ=6-8°C, σ_θ=26.4-27.2, S~ 34.2°/$_{oo}$
AAIW	Antarctic Intermediate Water	1000-2000m	θ=6-8°C, σ_θ=27.2-27.6, S~34.4 °/$_{oo}$
PDW	Pacific Deep Water	2000-4000 m	θ=1.1-2.2°C, σ_θ=27.8, S= 34.65-34.75°/$_{oo}$
AABW	Antarctic Bottom Water	> 4000 m	θ=0°C, σ_θ=45.8, S= 34.69°/$_{oo}$

note: θ = potential temperature, σ= potential density(kg/m^3) and S= salinity
θ and σ are approximate values from water masses at Central Pacific.
Ref. Broecker and Takahashi, 1980; Pickard and Emery, 1990; Wong *et al*., 1999; and WOCE P14.

2-4-2 Water masses properties from WOCE sections

The two intermediate waters (AAIW from south and NIPW from north) can be identified in the salinity and temperature properties in P14 section (Plate 2.6 and 2.7) at around 500-2000 m. The lower temperature and salinity values are caused by fresh water released from the polar areas.

PDW is marked by high content of silicate contents (Plate 2.8) because the sluggish flow and lack of deepwater formation tends to build up nutrients in the deepwater. It is apparent that there is more silicate content in the north and east of the Pacific Ocean than the south and the west. Similar patterns can be observed in nitrate and phosphate section plots (Plate 2.10 and 2.11), except their maximum layers are ~1000 m shallower than slilicate. As at the end of the conveyor belt, PDW has low oxygen content (Plate 2.9).

AABW is characterised by low temperature, high salinity and high oxygen and can be identified at below ~4000 m (Plate 2.6, 7 & 9). The oxygen level decreases as this water mass gradually moving north.

2-4-3 North Central Pacific

The North Pacific samples (NC1-NC5) are collected at water depth of 1275-2255 m (Fig. 2.4). This is located at the transition from the bottom of NIPW to the top of the PDW. The local water column property plot selected from a station of section P03 (dash line in Fig. 2.5) marks the low salinity intermediate water (NIPW) in a temperature-salinity plot and high silicate PDW in temperature-silicate plot. If the sample depths are applied to these trends, the hydrological properties of each sample

location can be estimated (as shown in the inset of Fig. 2.5b). These values are given in Table 2.6.

2-4-4 South Central Pacific

The close grouping of the NCP samples means, without other samples, we can only study variations in the Pacific water-mass at one site. Therefore, a group of samples lying approximately due south of the NC samples was also selected for study. These are located on WOCE line P14 in the Southern Central Pacific and are labelled SC samples. Based on their geographical location, (Fig. 2.4) the SC groups are divided into three subgroups (a to c in Table 2.1) with a depth range from 1664 m to 3033 m. The addition of these sites to the sample coverage means that the deeper parts of the PDW can be examined.

Using the WOCE data and the same approach as applied to the NC samples, the water-mass characteristics surrounding the SC samples have been estimated. These are given in Table 2.6 and are plotted as square symbols in Fig. 2.5b.

Table 2.6 Estimated temperature, silicate and salinity from the sample sites [(a)]

Sample ID	Depth (m)	Tpot θ (°C)	Silicate (umol/kg)	Salinity (°/oo)
NC1	1275	3.07	125.77	34.537
NC2	1565	2.59	135.69	34.572
NC3	1585	2.56	136.33	34.574
NC4	1930	2.06	146.68	34.611
NC5	2255	1.66	155.07	34.640
SC1	1664	2.63	118.83	34.607
SC2	1984	2.19	128.93	34.631
SC3	2260	1.84	136.89	34.649
SC4	2500	1.57	142.24	34.664
SC5	3033	1.04	139.50	34.692
SC6	1787	2.46	126.74	34.619
SC7	2000	2.17	132.88	34.633
SC8	2545	1.52	138.50	34.666
SC9	2600	1.46	140.50	34.669

(a) Estimate is based on WOCE experiment database of profile P3 and P14.

Plate 2.6 (a) Salinity for P14 179E (1000:1)

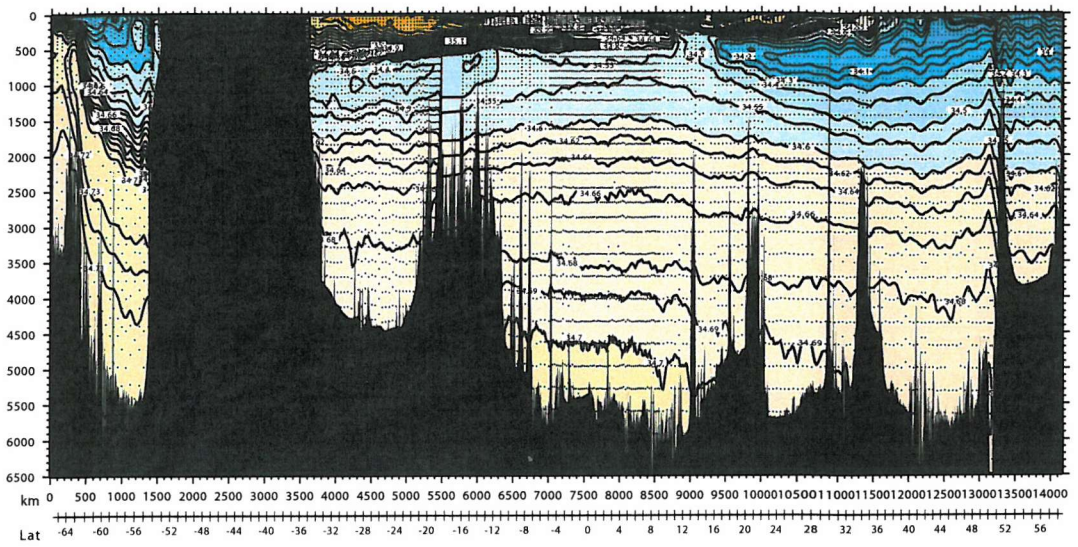

Plate 2.6 (b) Salinity for P03 24N (1000:1)

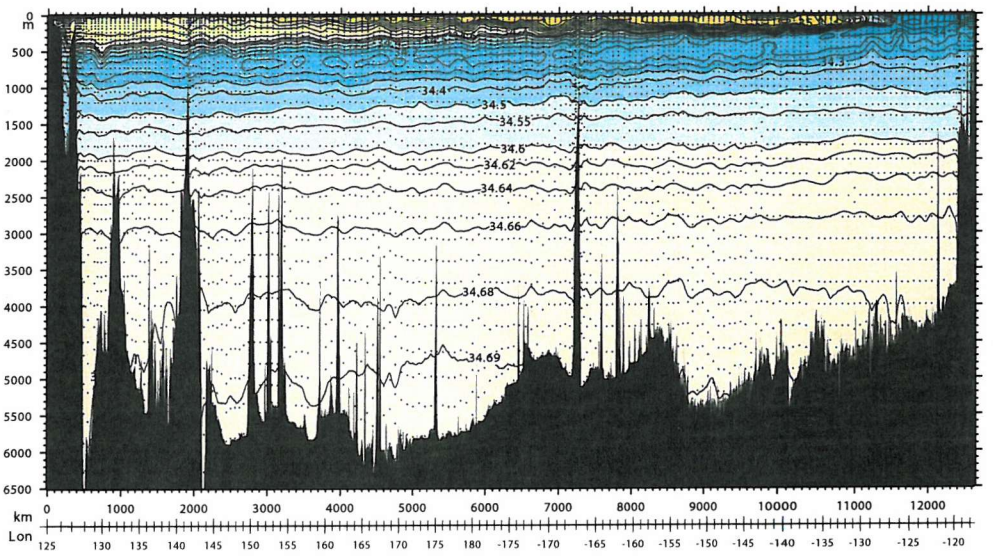

Plate 2.7 (a) Potential Temperature (C) for P14 179E (1000:1)

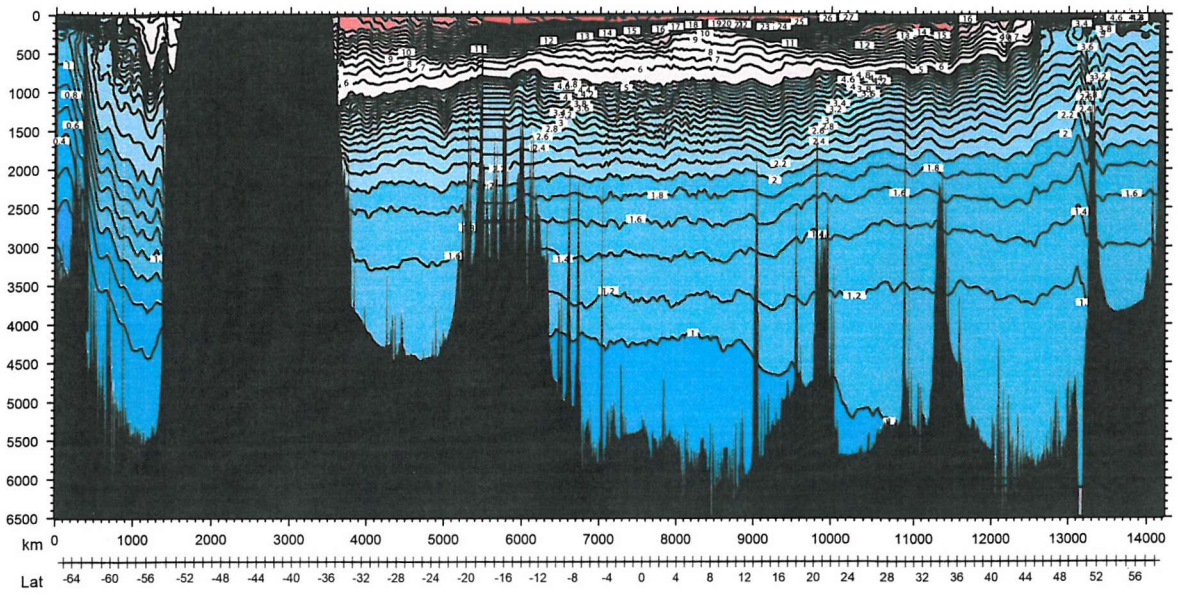

Plate 2.7 (b) Potential Temperature (C) for P03 24N (1000:1)

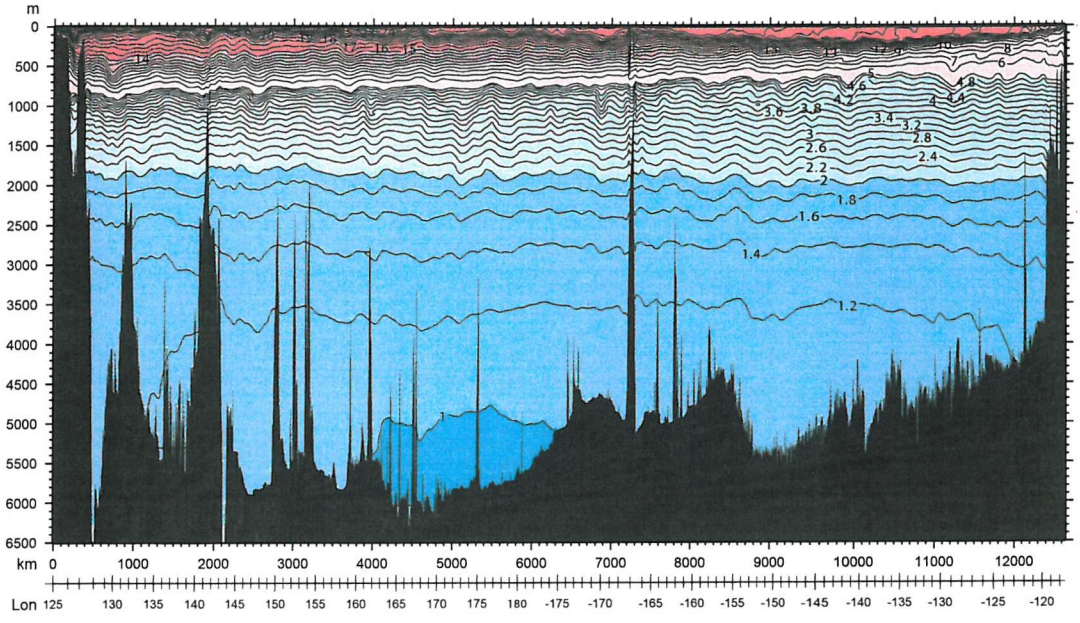

Plate 2.8 (a) Silicate (μM/kg) for P14 179E (1000:1)

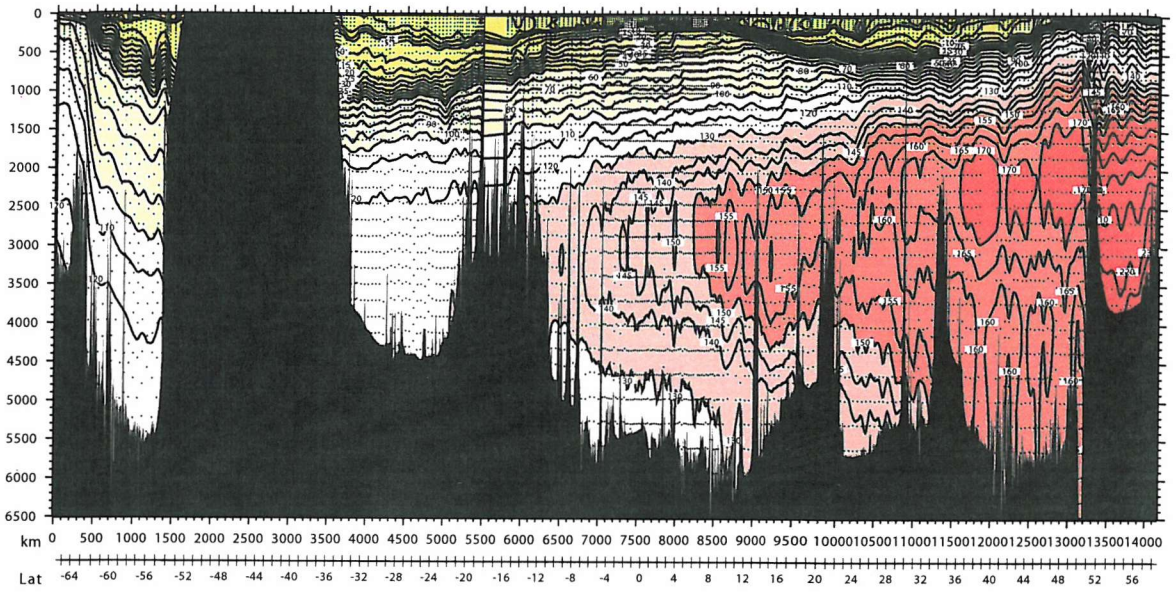

Plate 2.8 (b) Silicate (μM/kg) for P03 24N (1000:1)

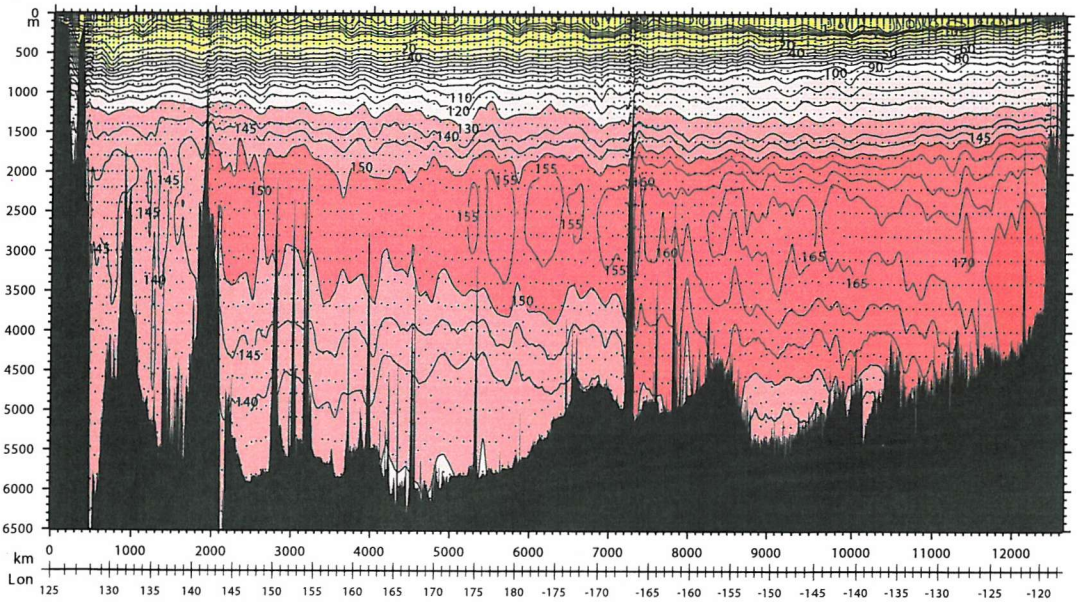

Plate 2.9 (a) Oxygen (μM/kg) for P14 179E (1000:1)

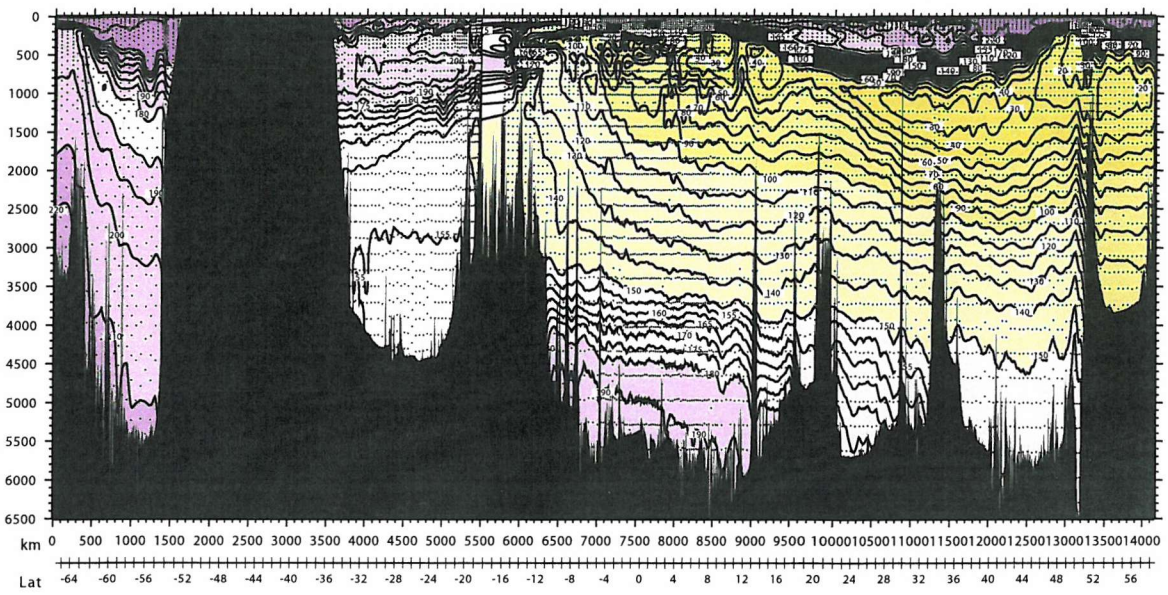

Plate 2.9 (b) Oxygen (μM/kg) for P03 24N (1000:1)

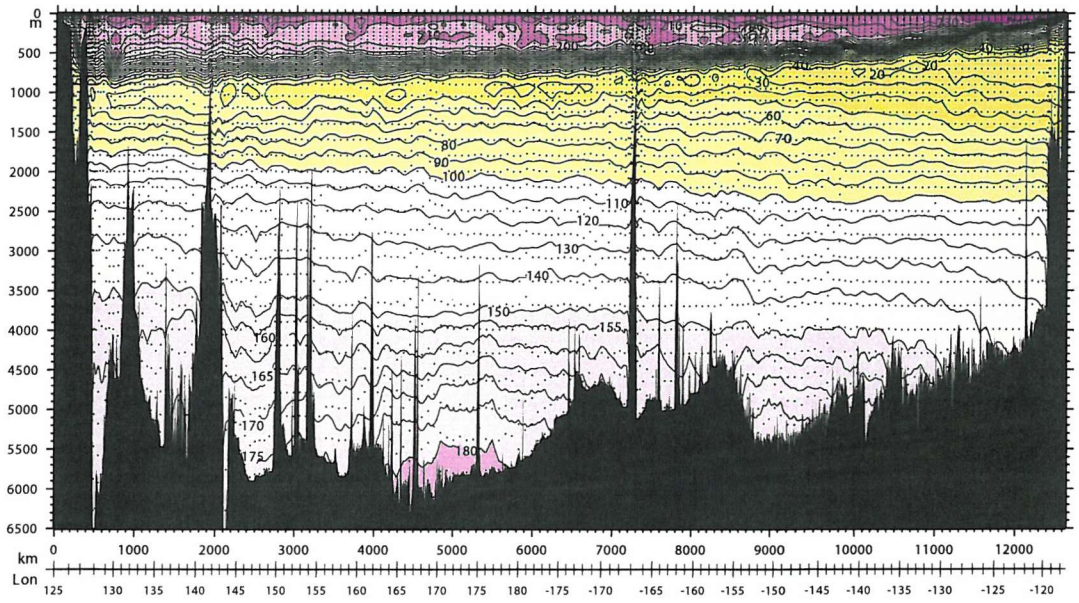

Plate 2.10 (a) Nitrate (μM/kg) for P14 179E (1000:1)

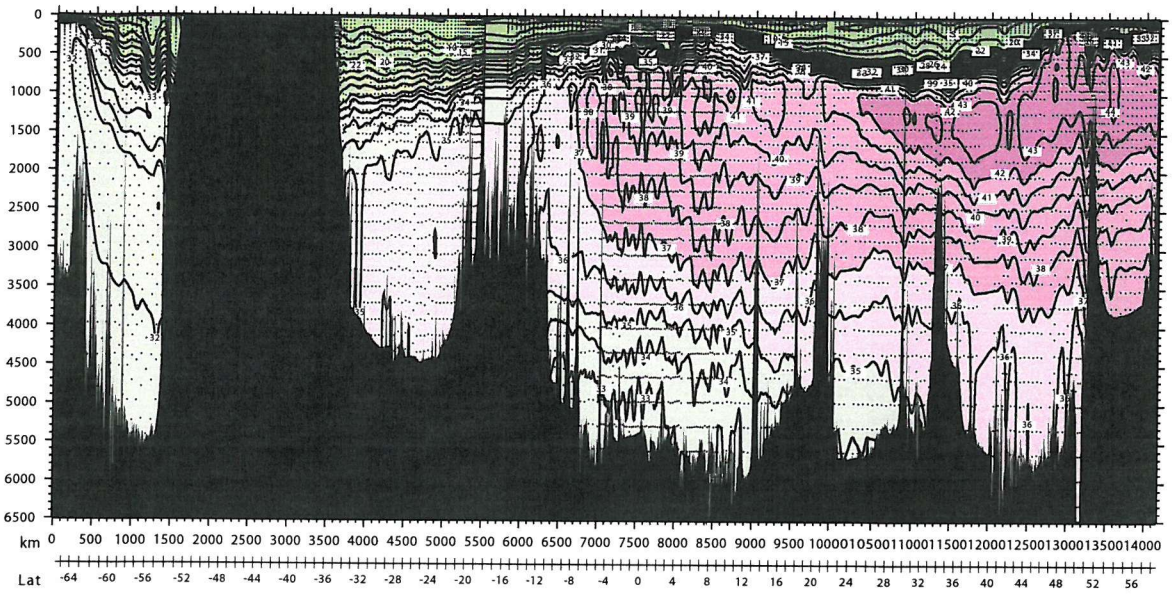

Plate 2.10 (b) Nitrate (μM/kg) for P03 24N (1000:1)

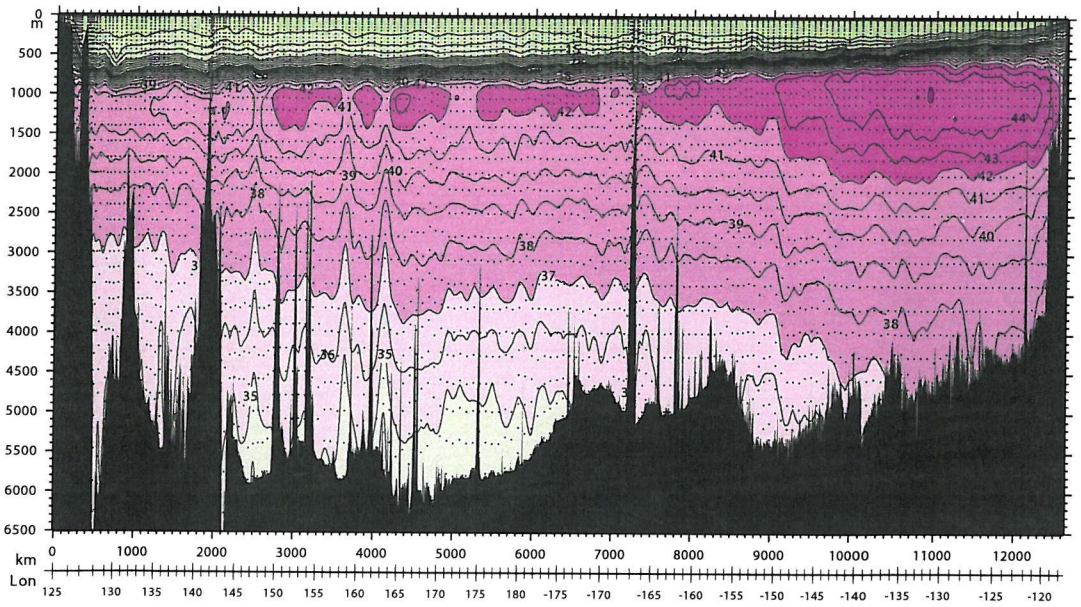

Plate 2.11 (a) Phosphate (μM/kg) for P14 179E (1000:1)

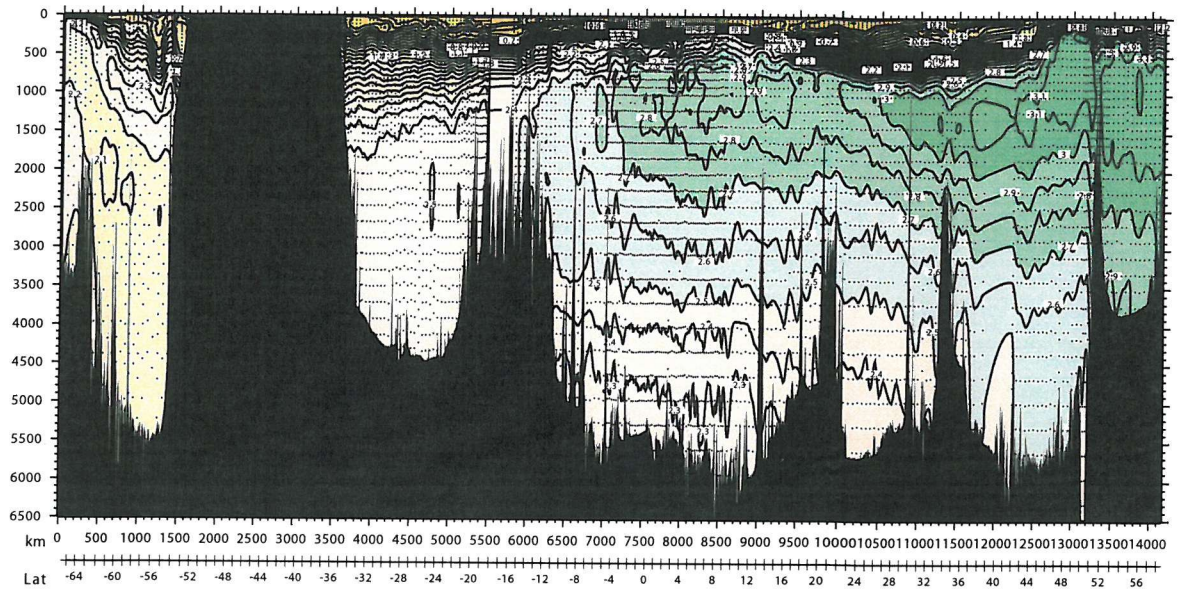

Plate 2.11 (b) Phosphate (μM/kg) for P03 24N (1000:1)

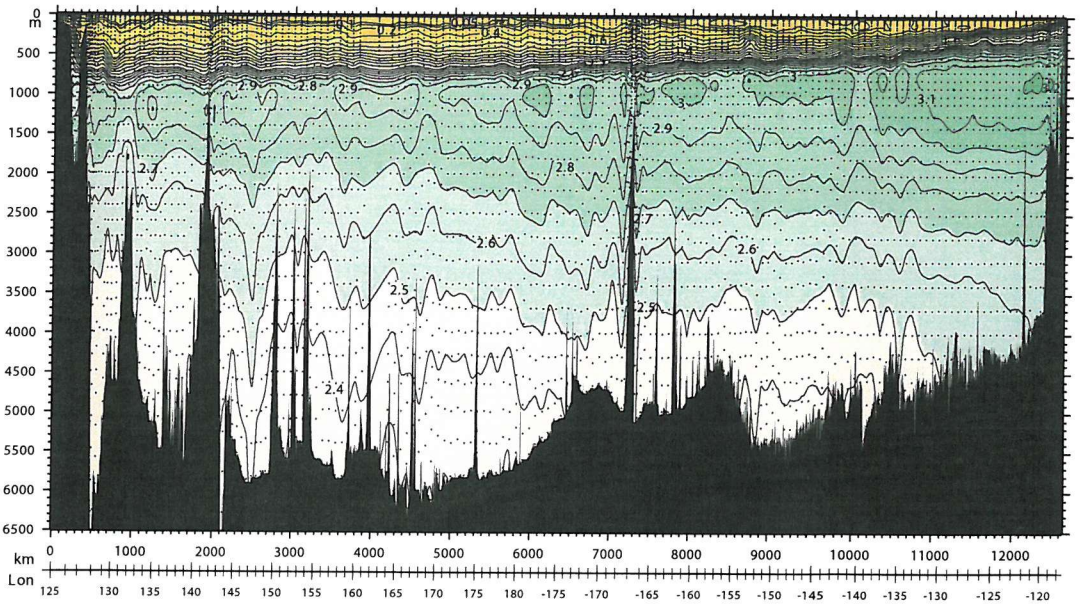

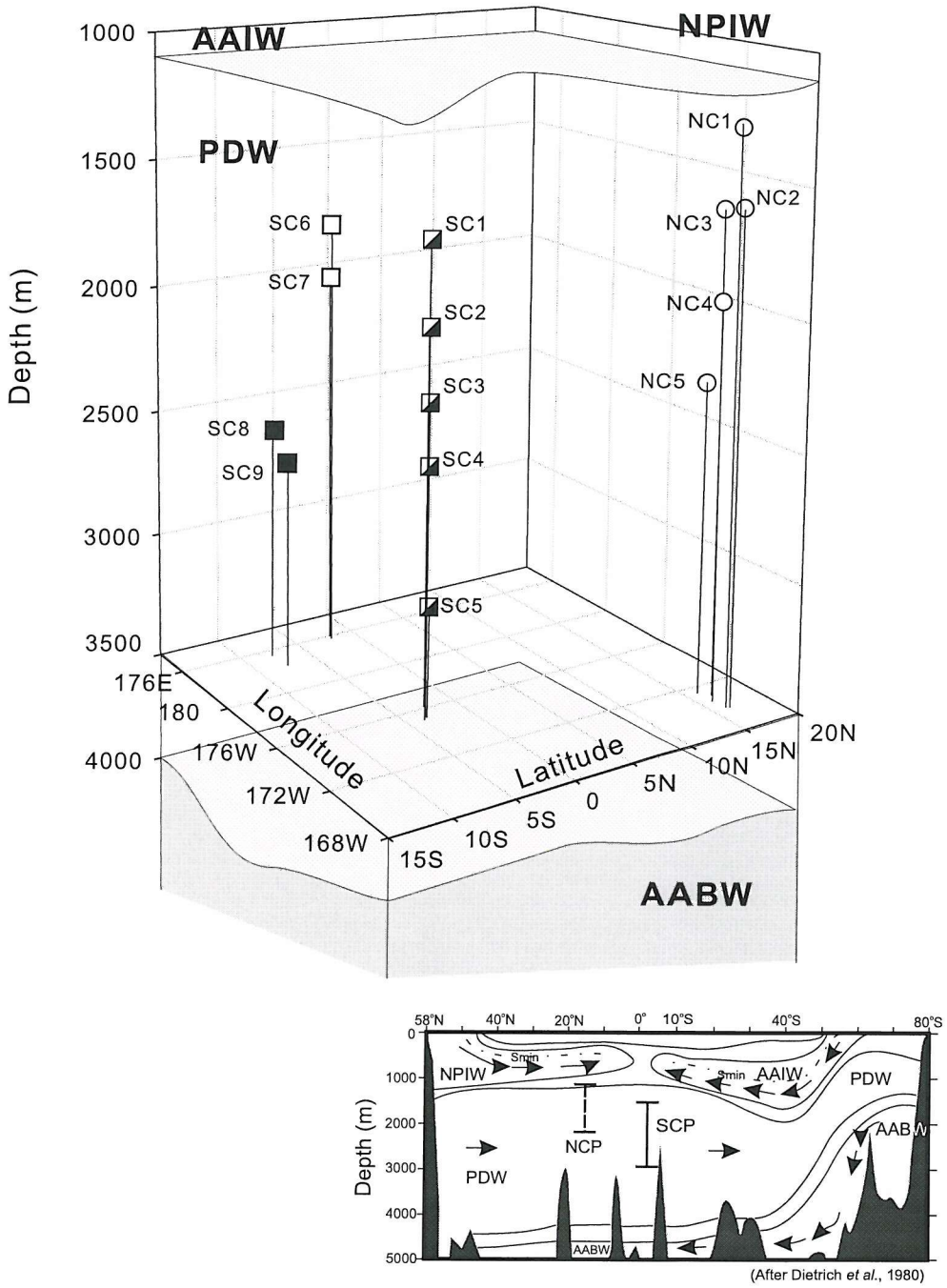

Fig. 2.4 Fe-Mn crusts locations and depths in this study. Inset shows the major circulation direction of the present-day water masses. The water mass boundaries are drawn schematically along 160°W of the Pacific Ocean.

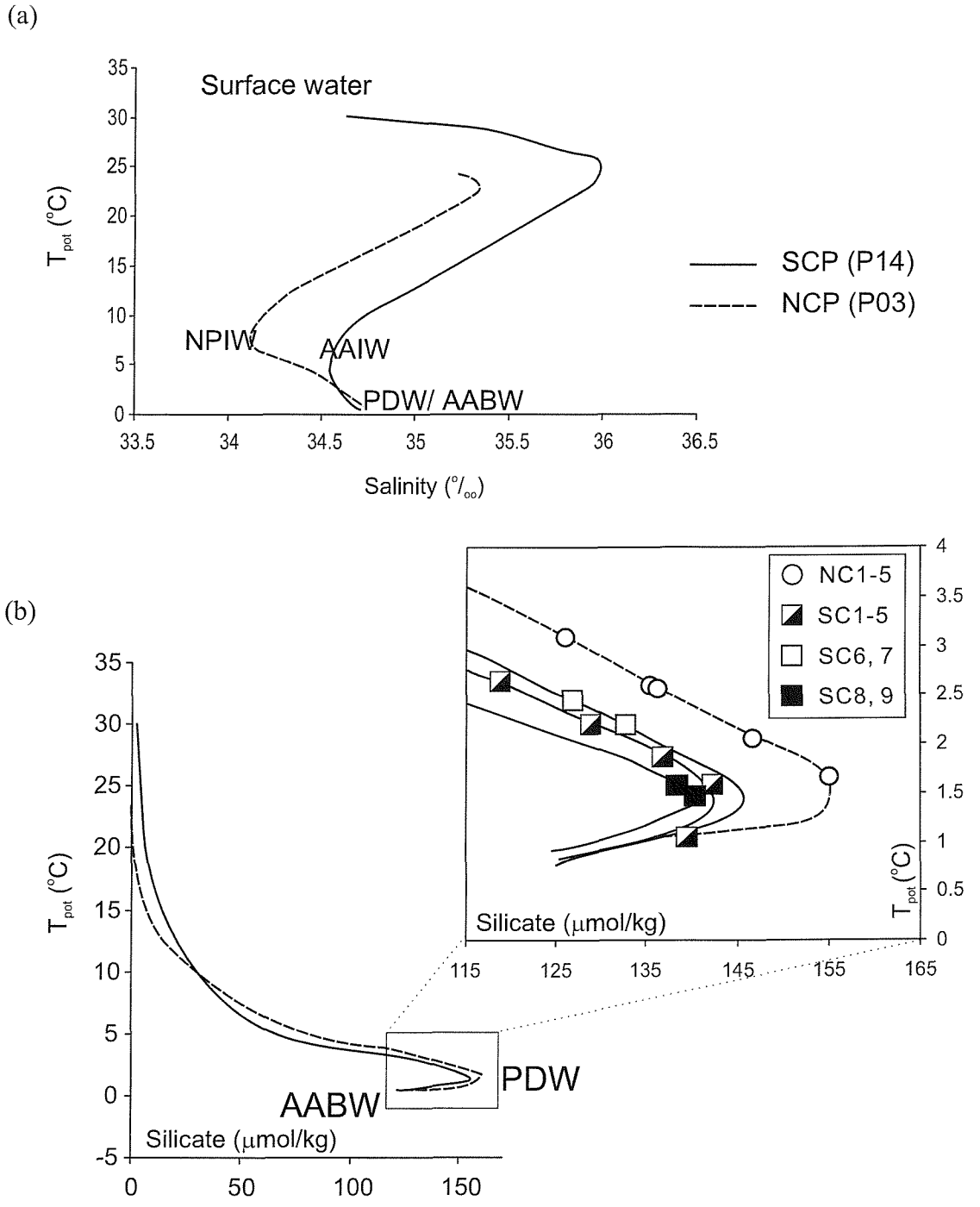

Fig. 2.5 (a) Temperature versus salinity of two selected WOCE profiles: P14 (179E, solid lines) and P3 (24N, dash line) to represent SC and NC group samples respectively. (b) Temperature versus silicate. Inset shows the values of seawater for the locations where samples were collected.

2-5 Conclusions

Several locations of Fe-Mn crusts were chosen for this study. In addition to the North Central Pacific where three previous Fe-Mn crusts studies are available (Christensen *et al.*, 1997; Ling *et al.*, 1997; Lee *et al.*, 1998; David *et al.*, 2001), a group of South Central Pacific Fe-Mn crusts were also selected in order to extend the study area and depths. Two Fe-Mn crusts from Izu-Bonin Back Arc Basin were chosen for their marginal sea location and different geological setting.

Mineralogical and geochemical data on these Fe-Mn crusts demonstrate that, other than patchy phosphatisation (which can be avoided during sampling) the samples have a hydrogenetic origin and represent suitable material for oceanographic studies.

Modern day hydrological sections (WOCE data) are presented as a background for oceanographic information. Fe-Mn crusts of this study were located in the Pacific Deep Water. Based on their collection depth the physical and nutrient tracer data of the Central Pacific samples (NC and SC) have been estimated from the WOCE database. In Chapter 4, these seawater properties estimates are compared with the isotopic tracers.

Chapter 3. Methods

I. Hf isotope ratio analysis using multi-collector inductively coupled plasma mass spectrometry: an evaluation of isobaric interference corrections[*]

3-1 Abstract

From measurements of Hf-Yb mixtures, we have found that the correction of isobaric interferences involving accepted Yb isotope ratios and reasonable estimates of mass bias result in a significantly under-corrected ^{176}Hf, which is proportional to the amount of Yb added. This can be explained by 1) a significant difference in the instrumental mass bias between Hf and Yb, and 2) that the accepted values for isotopic ratios within the Yb and/or Hf systems are incorrect.

We have evaluated these possibilities by measuring mixed solutions of Yb and Hf on two MC-ICP-MS instruments and undertaking a series of REE fractionation experiments using a thermal ionisation mass spectrometer (TIMS). Our results indicate that the presently accepted abundances of the Yb isotopes are not appropriate. We present new values for Yb isotopic abundances based on the TIMS and MC-ICP-MS results.

Using the newly defined Yb values, we demonstrate that Yb and Hf have similar levels of mass bias in plasma ionisation instruments, and that Hf isotope ratios can be used to correct Yb mass bias before subsequent correction of isobaric interference. A laser ablation comparison of Yb and Hf indicates that similar relationships exist, and can be applied to micro analytical techniques where chemical separation is not possible.

[*] Published in Chu *et al.* (2002), *J. Anal. At. Spectrom.*, 17, 1567-1574.

3-2 Introduction

Hafnium isotope studies have increased in number since the advent of plasma source mass spectrometry, which, unlike traditional thermal ionisation mass spectrometry (TIMS), overcomes the difficulties of analysing elements with high first ionisation potential. Most analytical protocols and correction procedures for MC-ICP-MS are directly transferred from TIMS. However, as the mass bias of a multi-collector ICP-MS is about 10 times that of a TIMS, it has been suggested (Vance and Thirlwall, 2002) that the mass bias behaviour should be better characterised, especially where isobaric interferences need to be corrected. This is particularly true where hafnium purification is not possible prior to sample introduction to MC-ICP-MS. For example, the laser ablation of solid samples frequently involves coincident ionisation of the REE. Yb so introduced results in the isobaric ^{176}Yb interference onto the radiogenic ^{176}Hf, which is the isotope of interest in the hafnium system. As such, the correction of isobaric interferences needs to be rigorously constrained to achieve a satisfactory accuracy of Hf isotope ratios.

It has been suggested that the extent of mass bias in plasma source instruments varies with mass in a coherent fashion (Longerich *et al.*, 1987; Maréchal *et al.*, 1999). Therefore, it should be plausible to use the mass bias determined for isotopes of one element to correct externally the isotopic mass bias of an element with similar mass (e.g. Tl-Pb (Longerich *et al.*, 1987) and Zn-Cu (Maréchal *et al.*, 1999)). It is also recognised that even neighbouring elements are not biased to exactly the same extent but that the relative mass bias remains constant over one measurement session (Maréchal *et al.*, 1999; White *et al.*, 2000). To achieve high precision and better accuracy these authors have applied a modified correction based on the correlation between the mass bias of element pairs. For isotopic systems with well-determined and invariant isotope pairs, the magnitude of mass bias during a run can be assessed (e.g. ^{146}Nd/^{144}Nd and ^{179}Hf/^{177}Hf) and the calculated instrumental bias applied to radiogenic isotopes of interest and to relevant isobaric interferences (Blichert-Toft *et al.*, 1997; Luais *et al.*, 1997). If differences exist between the level of ionisation of element pairs in a plasma, as proposed by Maréchal *et al.* (1999) and White *et al.* (2000), better constraints on inter-element mass bias are needed to correct isobaric interferences, especially where (interfering element: object element) ratios are high.

^{176}Yb is a major isobaric interference that has to be corrected by monitoring another Yb isotope (e.g. ^{171}Yb or ^{173}Yb) during a Hf measurement. Some previous laser ablation studies (Thirlwall and Walder, 1995; Griffin *et al.*, 2000) have argued that the accepted isotopic abundances of Yb (McCulloch *et al.*, 1977; Griffin *et al.*, 2000) do not result in a consistently corrected ^{176}Hf/^{177}Hf. Such studies have modified the values by empirically deriving a correction by generating a suitable Yb isotope ratio, which results in a consistent ^{176}Hf/^{177}Hf. This method is limited by the assumption that the Yb mass bias is consistent between the empirically derived solution and the sample measurements. In reality the degree of bias is likely to vary with the nature of the sample matrix and through time.

In this study, we have evaluated the possible pitfalls in Hf isotope measurements on different instruments in order to achieve accurate results even with high levels of interference.

3-3 Experimental

3-3-1 Chemistry separation

The Hf separation method used at the Southampton Oceanography Centre (SOC) and The Open University is derived from two previously published methods (Blichert-Toft *et al.*, 1997; Lee *et al.*, 1999). Its purpose is to separate Hf rapidly and efficiently from isobaric and non-isobaric interfering elements, e.g. Yb and Ti. Two columns are employed for this separation scheme, anion exchange resin AG1-X8 (Bio-Rad) and EICHROM© Ln-resin (Table 3.1).

Table 3.1 Hf Ion-exchange column specification and elution profile

Resin type	Column dimension	Eluent	Elements
Bio-Rad AG1-X8	4 cm height	sample in 2 ml 4 M HF	Bulk
(200-400 mesh)	0.8 cm ø	elute 8 ml 4 M HF	Matrix
		collect 8 ml 6 M HCl : 1 M HF	Ti, Zr, Hf ± HREE
Eichrom Ln	8.3 cm height	sample in 100µl 2.2M HCl : 1% H_2O_2	Ti, Zr, Hf
(100-150 mm)	0.4 cm ø	elute 200 µl 2.2M HCl : 1% H_2O_2	Ti
		elute 3.7 ml 2.2 M HCl : 1% H_2O_2	Ti
		elute 12 ml 6M HCl	HREE
		collect 6 ml 1 M HF	Hf and Zr

Ti in the analyte suppresses the ionisation of Hf, and thus Ti needs to be removed from the sample such that the Ti concentration is less than 1 μg g^{-1} in the measurement solution (Münker *et al.*, 2001). The use of hydrogen peroxide enabling the complexation of the yellow-tinted peroxytitanyl compound $Ti(O\text{-}O)^{2+}$, results in a satisfactory separation of Hf and Ti. 1% of H_2O_2 is added to the HCl elute in the second column stage (Table 3.1). The collected fraction from the second column is converted to a 2% HNO_3 matrix for analysis. The recovery of this chemical separation is generally about 90%. Detailed Hf chemistry set up is described in Appendix II at the end of this thesis.

3-3-2 Instrumentation and measurement systematics

Two different types of MC-ICPMS have been used to measure Hf isotopes in this study. An IsoProbe (Micromass Ltd., UK) at Southampton Oceanography Centre and a Nu Plasma (Nu Instruments, Wrexham, UK) at The Open University. Details of these two instruments have been described elsewhere (Belshaw *et al.*, 1998; Taylor *et al.*, 2001). All standards and samples were prepared with 2% HNO_3 and introduced via two types of desolvating nebulizers, the MCN 6000 and the Aridus (both from CETAC, Omaha, USA) for the IsoProbe and the Nu Plasma respectively. The normal operating conditions of the two instruments are summarised in Table 3.2.

Hf isotopes on the IsoProbe and Nu Plasma are measured statically in the Faraday collector arrays shown in Table 3.3. Various collector configurations were examined with the JMC 475 Hf standard on the IsoProbe; the results were indistinguishable within the error of the measurements (Table 3.4). This suggests that there are negligible differences between the collector efficiencies of each Faraday collector and justifies the use of static analysis. In both instruments, collectors were set to measure both ^{171}Yb and ^{173}Yb to calculate the ^{176}Yb interference on ^{176}Hf and to determine the mass bias of Yb isotopes (detailed below). On the IsoProbe, the collector positions were checked before each analytical session using a mixed solution of Hf, Lu and Yb (Hf at ~12 ng ml^{-1}, Lu at ~1 ng ml^{-1} and Yb at ~0.1 ng ml^{-1}). On the Nu Plasma, the zoom lens system was set at the values determined to accommodate the dispersion of the Hf isotopes amongst the fixed collectors. The beam intensities of both instruments were then optimised by adjusting the torch position, gas flows, ion focusing and magnet field settings. The overall input/output efficiency, i.e. the

final ion current measured relative to the amount of Hf introduced, was 0.5% for the IsoProbe and 0.2% for the Nu Plasma.

The collector baselines were measured on-peak on the IsoProbe using the same 2% HNO_3 used for the sample matrix. These baselines were then subtracted from the appropriate peaks of subsequent standard or sample measurements. On the Nu Plasma, the baseline was measured at half masses and corrected on-line during each measurement. For both instruments, the sample analysis baselines were remeasured after cleaning the sample introduction system with 10% HNO_3, 1% HF, MQ (high purity deionised water) and isopropyl alcohol (IPA) for 15 minutes, followed by 5 minutes of equilibration in 2% HNO_3. Following the cleaning procedure no differences were detected between the on-peak 2% HNO_3 baselines and the instrument baselines.

Table 3.2 Operating conditions of the Micromass IsoProbe and Nu Plasma for Hf measurement

	IsoProbe	Nu Plasma
Argon gas flow rates-		
Cool Gas	14.0 l min^{-1}	13.0 l min^{-1}
Auxiliary gas	1.0 l min^{-1}	1.0 l min^{-1}
Nebuliser gas	1.05 l min^{-1}	0 l min^{-1}
Collision gas flow rate (Ar)	1.2 ml min^{-1}	N/A
Nebuliser type	Cetac MCN 6000	Cetac Aridus
Spray chamber temperature	75°C	70°C
Desolvator temperature	160°C	160°C
N2 gas flow	0.10 $lmin^{-1}$	0.07-0.11 $lmin^{-1}$
Sweep gas flow (Ar)	2.25-2.60 l min^{-1}	3.00-3.75 l min^{-1}
Solution uptake rate	60 $\mu l.min^{-1}$	50 $\mu l.min^{-1}$
Forward (rf) power	1350 W	1300 W
Interface cones	Nickel	Nickel
Analyser Vacuum	3×10^{-8} Pa	5×10^{-9} Pa
Acceleration voltage	5.5 kV	4.0 kV
Ion lens setting (IsoProbe)/ Focusing Optics (Nu)	Optimised for maximum intensity with Extract (Ex) focusing at 35%	Optimised for maximum intensity
Detector used	9 Faraday collectors	10 Faraday collectors
Typical Hf sensitivity	300V/ppm	130 V/ppm
Sampling time	4 blocks of 25 ratios (~12 mins)	4 blocks of 25 ratios (~10 mins)
Typical Hf introduced (ng)/ analysis	28 ng	30 ng

Table 3.3 Faraday collector array scheme of the IsoProbe and Nu Plasma, typical baseline signals and elemental abundances

Iso-Probe	Faraday Collector	L3	L2	Axial	H1	H2	H3	H4	H5	H6		
Nu Plasma	Faraday Collector	F10	F9	N/A	F8	F7	F6	F5	F4	F3	F2	F1
m/z measure		**171**	**173**	**174**	**175**	**176**	**177**	**178**	**179**	**180**	**181**	**183**
Abundance[a]	Yb	14.28%	16.13%	31.83%		12.76%						
	Lu				97.41%	2.59%						
	Hf			0.16%		5.26%	18.60%	27.28%	13.62%	35.08%		
	Ta									0.01%	99.98%	
	W									0.12%		14.31%

[a] IUPAC Commission on Atomic Weights and Isotopic Abundances report in *Isotopic Compositions of the Elements 1997*, Pure and Appl. Chem., 1998, 70, No. 1, 217.

Table 3.4 Various static mode collector configurations and corresponding JMC475 ratios

IsoProbe										
Faraday	**L3**	**L2**	**Axial**	**H1**	**H2**	**H3**	**H4**	**H5**	**H6**	^{176}**Hf/**^{177}**Hf ±2sd (no of analysis)**
	171	173	175	176	177	178	179	180	181	0.282162 ± 24 (55)
m/z measure	171	173	174	175	176	177	178	179	180	0.282168 ± 33 (21)
		171	173	174	175	176	177	178	179	0.282165 ± 5 (4)

Laser ablation analyses on the IsoProbe at the SOC were achieved using an ArF excimer laser system operating at a wavelength of 193 nm (4D Engineering, Hanover, Germany). The laser produces a beam size of 40 μm, has a pulse duration of 10 ns and an optimised repetition rate of 4 Hz. Ablated sample material is carried to the IsoProbe using a mixed He+Ar carrier gas. Analysis time was in the range 60-200 seconds. For the duration of the ablation the laser position and focus was fixed; no rastering was used. This typically gave total Hf signals of 7×10^{-15} A μg g^{-1} sec^{-1}.

To investigate fractionation relationships and determine the isotopic abundance of Yb, we have used a VG Sector 54 thermal ionisation mass spectrometer (TIMS). REE solutions used in the experiments were measured in either static or dynamic collector arrays using ion beams generated from triple filament assemblies with Ta side and Re centre filaments.

3-3-3 Tail correction

It is recognised that the scatter of ions from a high abundance signal produces a 'tail' of extraneous ions across adjacent masses. This effect is proportional to the analyser vacuum condition (Thirlwall, 2000; Münker *et al.*, 2001; Thirlwall, 2001) and will induce a background over-correction if baselines are measured at inter-peak (half mass) positions. The tail effect is the contribution of the signal from a given peak at 1 Dalton on the low mass side, e.g. the proportion of a ^{209}Bi ion beam measured at m/z 208. This abundance sensitivity is expressed in ppm and is generally proportional to the analyser vacuum (Fig. 3.1). If the analyser vacuum remains constant (e.g. at ~3×10^{-8} mBar), the tail effect is a constant factor.

Abundance sensitivity measurements on the IsoProbe are approximately a factor of 3 higher than on the Nu Plasma (Thirlwall, 2001), and as such the tail effect is significant and requires correction. We have determined the low and high mass tail effects on the IsoProbe across the Hf mass range by using ^{181}Ta and ^{169}Tm respectively (Fig. 3.2). Signals measured at 0.5, 1.5, 2.5 and 3.5 Dalton away from 181 and 169 are used to interpolate the abundance sensitivity at 1 to 4 Dalton. The tail factors in the Hf isotope range on the low mass side are 8, 3, and 1 ppm at 1, 2, and 3 Dalton, and on the high side are 6 and 1 ppm at 1 and 2 Dalton, respectively. During Hf measurement each mass is corrected for the tails of all other peaks, for example in the case of ^{176}Hf:

$$^{176}Hf_{tailcorr} = 176_{meas} - (^{177}Hf \times T_{L1} + ^{178}Hf \times T_{L2} + ^{179}Hf \times T_{L3}) - (^{175}Lu \times T_{H1} + ^{174}Hf \times T_{H2}) \quad \text{eq. 3.1}$$

Where T_{L1} is the tail proportion expected at 1 Dalton light and T_{H1} is the tail at 1 Dalton heavy, and so on. The effects of tail are most significant where a low abundance isotope is close in mass to a high abundance isotope. In the Hf system this is particularly true for ^{175}Lu, which is adjacent to $^{176\text{-}178}Hf$.

Tail corrections on the Nu Plasma resulted in a 0.000003 shift in the $^{176}Hf/^{177}Hf$ result. This indicates that any errors resulting from the use of half-mass baselines are negligible as they are considerably smaller than the in-run errors on the measurements.

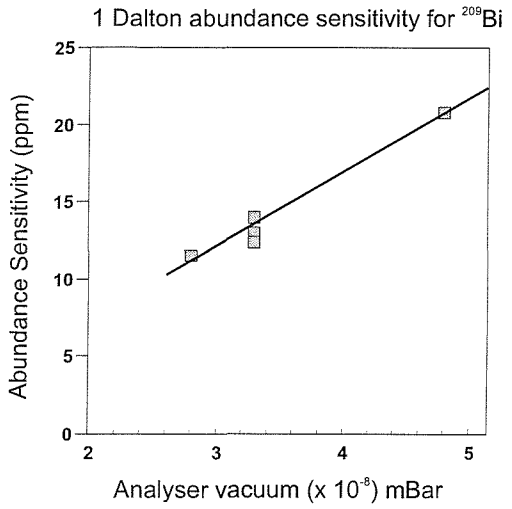

Fig. 3.1 Abundance sensitivity at m/z 208 relative to a ^{209}Bi signal under different analyser vacuum conditions.

(a)

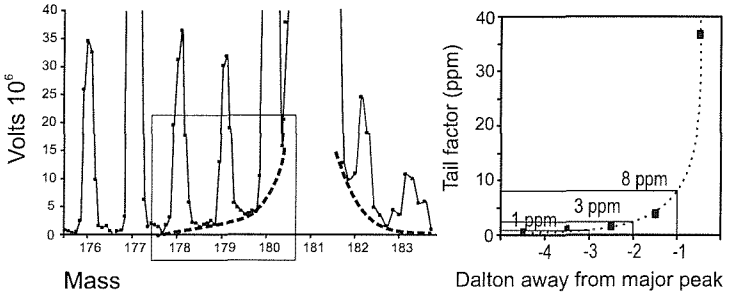

(b)

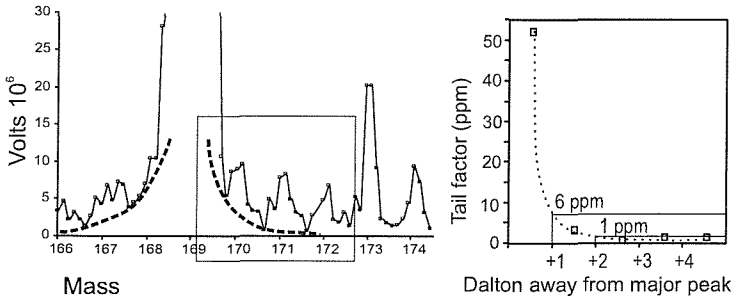

Fig. 3.2 Tail effects within the Hf mass range on the IsoProbe. Slow scan and half-mass measurements demonstrate the tail factor on (a) mass scan m/z 176-183 with a solution of 66 μg l^{-1} ^{181}Ta, and (b) mass scan m/z 166-174 with a solution of 10 μg l^{-1} ^{169}Tm. Inset graphs show the calculated abundance sensitivity (tail correction factors) interpolated from the scans.

3-3-4 JMC 475 standard and rock standards

A solution of the JMC 475 Hf standard with concentrations of 40 ng ml^{-1} (IsoProbe) or 50 ng ml^{-1} (Nu Plasma) was used for instrumental set up and routine standard measurements. The $^{176}Hf/^{177}Hf$ ratio gives an average of 0.282163 ± 26 (n=79) (± $2\sigma_D$) on the IsoProbe with good consistency over a 1-year measuring period, and 0.282159 ± 38 (n= 20) (± $2\sigma_D$; Fig. 3.3) on the Nu Plasma during 5 analytical sessions. The results of $^{176}Hf/^{177}Hf$ of the IsoProbe for a selection of international rock standards (BRR, BCR-1, BCR-2 and BE-N (Table 3.5)) fall within the range of published data (Kempton *et al.*, 2000; Blichert-Toft, 2001; David *et al.*, 2001; Le Fèvre and Pin, 2001; Münker *et al.*, 2001).

Table 3.5 The $^{176}Hf/^{177}Hf$ values of international rock reference samples measured in this study in comparison with previously published values[a]

Rock standard comparison		
	$^{176}Hf/^{177}Hf$ (2se)	**Reference**
BRR[b]	0.283368 ± 10	this study[c]
	0.283366 ± 8	this study
	0.283368 ± 16	Kempton et al. (2000)
	0.283351 ± 16	Kempton et al. (2000)
	0.283363 ± 16	average ± 2sd
BCR-1	0.282845 ± 10	this study
	0.282866 ± 9	this study
	0.282860 ± 11	David et al. (2001)
	0.282817 ± 8	Le Fèvre and Pin (2001)
	0.282879 ± 8	Blichert-Toft (2001)
	0.282892 ± 6	Münker et al. (2001)
	0.282860 ± 53	average ± 2sd
BCR-2	0.282859 ± 9	this study
	0.282884 ± 7	Le Fèvre and Pin (2001)
	0.282872 ± 35	average ± 2sd
BE-N	0.282929 ± 12	this study
	0.282939 ± 4	Münker et al. (2001)
	0.282923 ± 9	Münker et al. (2001)
	0.282921 ± 6	Münker et al. (2001)
	0.282921 ± 7	Blichert-Toft (2001)
	0.282927± 15	average ± 2sd

[a]All $^{176}Hf/^{177}Hf$ data are reported relative to 0.282160 for JMC-475.

[b]BRR is identical to sample CD80-WP02-D6 in ref. 18; SOC standard-Basalt Reykjanes Ridge, 1.5 μg g^{-1} Hf.

[c]All rock standard data acquired for this study were made using the IsoProbe.

(a)

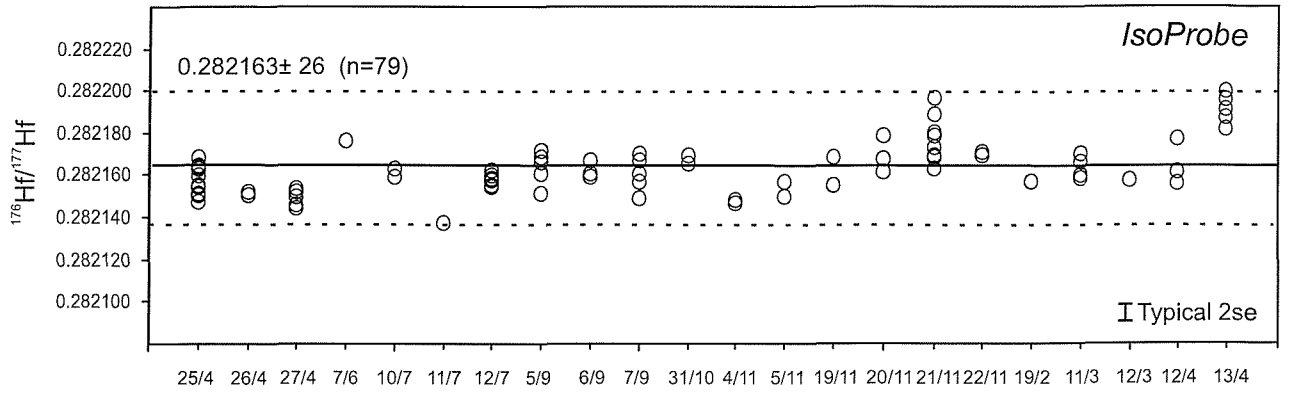

(b)

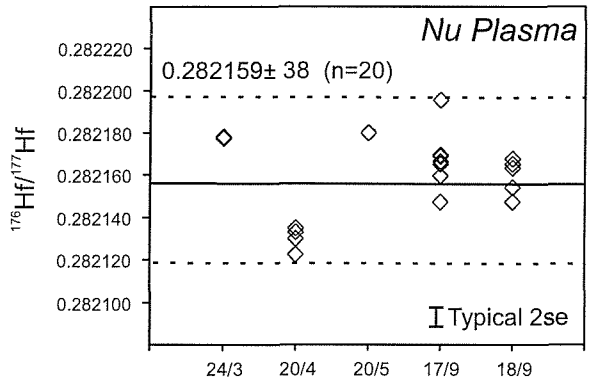

Fig. 3.3 (a) JMC 475 Hf standard measurement from April 2001 to April 2002 for the IsoProbe. The average from this study gives $^{176}Hf/^{177}Hf = 0.282163+/-26$ ($+/-2\sigma_D$, n=79) (b) Equivalent measurements made on the Nu Plasma during the period March 2002 to September 2002. Average $^{176}Hf/^{177}Hf = 0.282159+/-38$ ($+/-2\sigma_D$; n= 20). For both instruments, each group of symbols represents one measuring day. Errors of individual analysis are typically 0.000007 (+/-2se).

3-3-5 Mass fractionation

In this study, we have assessed the instrumental mass bias using an exponential law (Russell *et al.*, 1978):

$$R_t = R_m (M_B/M_A)^{\beta} \quad \text{eq. 3.2}$$

where R_m is the measured ratio of an isotope of exact mass M_B to an isotope with exact mass M_A, and R_t is the accepted ratio of the two isotopes and hence β is the mass bias coefficient

$$\beta = \ln(R_m/R_t)/\ln(M_A/M_B) \quad \text{eq. 3.3}$$

β is calculated using an invariant isotope ratio with accepted values. In the case of the Hf system, $R_t = {}^{179}Hf/{}^{177}Hf = 0.7325$ (Patchett and Tatsumoto, 1980). Other measured Hf isotope ratios can be corrected for mass bias using the β determined for ${}^{179}Hf/{}^{177}Hf$ (Table 3.6). This assumes that the bias across the Hf mass range can be described by the exponential law. In the case of Nd isotopes, the experimental relationship results in a slightly decreasing β value for ratios involving progressively heavier isotopes (Vance and Thirlwall, 2002), suggesting that the mass bias deviates marginally from the exponential law. Table 3.6 compares the proposed values with the values determined on the IsoProbe and Nu Plasma in this study. All ratios are similar, except for ${}^{178}Hf/{}^{177}Hf$, for which results from both instruments in this study are slightly higher (~0.000200) than published values.

3-3-6 Interference correction of Hf isotopes

To obtain accurate ${}^{176}Hf/{}^{177}Hf$, isobaric interferences from ${}^{176}Lu$ and ${}^{176}Yb$ must be accounted for. Using interference–free masses, i.e. ${}^{175}Lu$ and ${}^{173}Yb$ or ${}^{171}Yb$, interferences can be subtracted according to their accepted isotopic abundances of 0.02656 for ${}^{176}Lu/{}^{175}Lu$ and 0.7876 for ${}^{176}Yb/{}^{173}Yb$ or 0.8859 for ${}^{176}Yb/{}^{171}Yb$ (Table 3.7). The mass 176 isobaric interference correction functions can be expressed as

$${}^{176}Hf = 176_m - [{}^{175}Lu \times ({}^{176}Lu/{}^{175}Lu)_t (M_{176}/M_{175})^{\beta Lu} + {}^{173}Yb \times ({}^{176}Yb/{}^{173}Yb)_t (M_{176}/M_{173})^{\beta Yb}] \quad \text{eq. 3.4}$$

In this study, we have used a series of Yb-doped JMC 475 Hf solutions, so that the total Yb/Hf ranged between 0.0002 to 0.05, to evaluate the capability of the interference corrections on both the IsoProbe and the Nu Plasma. The results of these experiments are described below.

Table 3.6 Hf isotopic composition values for JMC 475 from the literature and this study

	Patchett (83) (ID-TIMS)[a]			Blicher-Toft *et al.* (97)[b]	Kleinhanns *et al.*[c]		This study (±2sd)			This study (±2sd)		
	IUPAC (98)		n	TIMS/P54	(Nu Plasma)		(IsoProbe)		n	(Nu Plasma)		n
$^{174}Hf/^{177}Hf$	0.008710	± 50	25	N/A			0.008674	± 32	41	N/A		
$^{176}Hf/^{177}Hf$	0.282195	± 15	25	0.28216	0.282169	± 16	0.282163	± 26	79	0.282159	± 38	20
$^{178}Hf/^{177}Hf$	1.467100	± 100	25	1.467168	1.467290	± 80	1.467417	± 232	79	1.467304	± 147	20
$^{179}Hf/^{177}Hf$	**0.732500**			**0.732500**			**0.732500**			**0.732500**		
$^{180}Hf/^{177}Hf$	1.886510	± 120	25	1.886666	1.88680	± 30	1.886765	± 290	75	1.886683	± 625	20

[a] The author has suggested a baseline interference by Re and some values may not be final.

[b] No error value was reported.

[c] Kleinhanns, I.C., Kreissig, K., Kamber, B.S., Meisel, T., Nägler, T.F. and Kramers, J.D. *Anal. Chem.*, 2002, **74(1)**, 67.

Table 3.7 Yb isotopic composition values

	TIMS/P54[a]	IUPAC (98)[b]	This study ± 2sd (TIMS)		n	This study (IsoProbe)		n
$^{168}Yb/^{171}Yb$	0.00951	0.00889	0.008865	± 22	2	0.008845	± 63	19
$^{170}Yb/^{171}Yb$	0.21370	0.21289	0.212645	± 6	2	0.212531	± 49	19
$^{172}Yb/^{171}Yb$	1.52640	1.52871	1.532075	± 272	6	1.532227	± 75	19
$^{173}Yb/^{171}Yb$	1.12480	1.12955	**1.132685**			**1.132685**		
$^{174}Yb/^{171}Yb$	2.21630	2.22899	2.242466	± 160	6	2.242716	± 266	19
$^{176}Yb/^{171}Yb$	0.88590	0.89356	0.901821	± 189	4	0.901864	± 508	19
$^{176}Lu/^{175}Lu$	0.02656	0.026512	**0.026549**			#N/A		

[a] McCulloch *et al.*, (1977) and Blichert-Toft *et al.* (1997)

[b] Holliger and Devillers (1981)

3-4 The mass bias relationship between Yb and Hf

If plasma ion sources provide similar levels of ionisation of elements with similar masses then it is plausible to use the measured Hf mass bias to correct bias within the interfering elements, Yb and Lu (i.e. assuming $\beta_{Hf}=\beta_{Lu}=\beta_{Yb}$ in eq.3). Fig. 3.4a shows the $^{176}Hf/^{177}Hf$ measurements of the Yb-Hf mixtures corrected using the Yb isotope abundances of McCulloch *et al.* (1977) and Blichert-Toft *et al.* (1997) using various mass bias schemes for Yb. The crossed symbols are Hf measurements corrected for Yb interference assuming no mass bias of Yb (i.e. $\beta_{Yb}=0$ in eq. 4). Solid symbols denote $^{176}Hf/^{177}Hf$ corrected for Yb interference using β_{Hf} from $^{179}Hf/^{177}Hf$ (i.e. $\beta_{Yb}=\beta_{Hf}$). In the case where no mass bias correction is used, both instruments show a marked positive correlation between $^{176}Hf/^{177}Hf$ and Yb/Hf. Positive trends are also produced on the instruments where β_{Hf} is applied to Yb (i.e. $\beta_{Yb}=\beta_{Hf}$). This suggests

two possibilities: firstly, that $\beta_{Yb} \neq \beta_{Hf}$ due to a difference in the way these elements ionise; secondly that the isotope abundances used in calculating the β values for one of the two elements are inappropriate.

To investigate this further we have obtained an empirical Yb and Hf mass bias relationship by measuring mixtures of Hf-free Yb solution (SPEX 'Assurance', ICP standard solution) and the JMC475 Hf standard with Yb/Hf=1 and Yb/Hf=0.3. β values measured for Hf and Yb in these mixtures are shown as the open symbols (squares for IsoProbe; circles for Nu Plasma) in Fig. 3.5. Nu Plasma β values are lower than those obtained on the IsoProbe, but data from both instruments lie approximately on a line passing through the origin, which is shown as a dashed line in Fig. 3.5. The correlation has the form:

$$\beta(^{173}Yb/^{171}Yb)=1.272 \times \beta(^{179}Hf/^{177}Hf) \qquad \text{eq. 3.5}$$

From this equation it is clear that β_{Yb} is apparently greater than β_{Hf}, which would lead to the under correction of the ^{176}Yb and produce an overly radiogenic Hf isotope ratio in analyses where Yb is present. It should also be noted that the trends produced by each instrument from variations in mass bias cut across the overall correlation line (Fig. 3.5). The relationship of β_{Hf} to β_{Yb} given by this line could potentially be used to correct the Yb mass bias in the determination of $^{176}Hf/^{177}Hf$. Results of this correction procedure on the range of mixed Hf-Yb solutions are shown as the open symbols in Figure 3.4a. Over the range of mixtures used, the $^{176}Hf/^{177}Hf$ is invariant within error, indicating a satisfactory correction.

Despite the success of the empirical correction, it does not solve the question of whether the results from Hf-Yb mixtures are a product of different ionisation of the two elements or are related to inappropriate isotopic abundances. To test this further we have investigated Yb isotope abundances using TIMS.

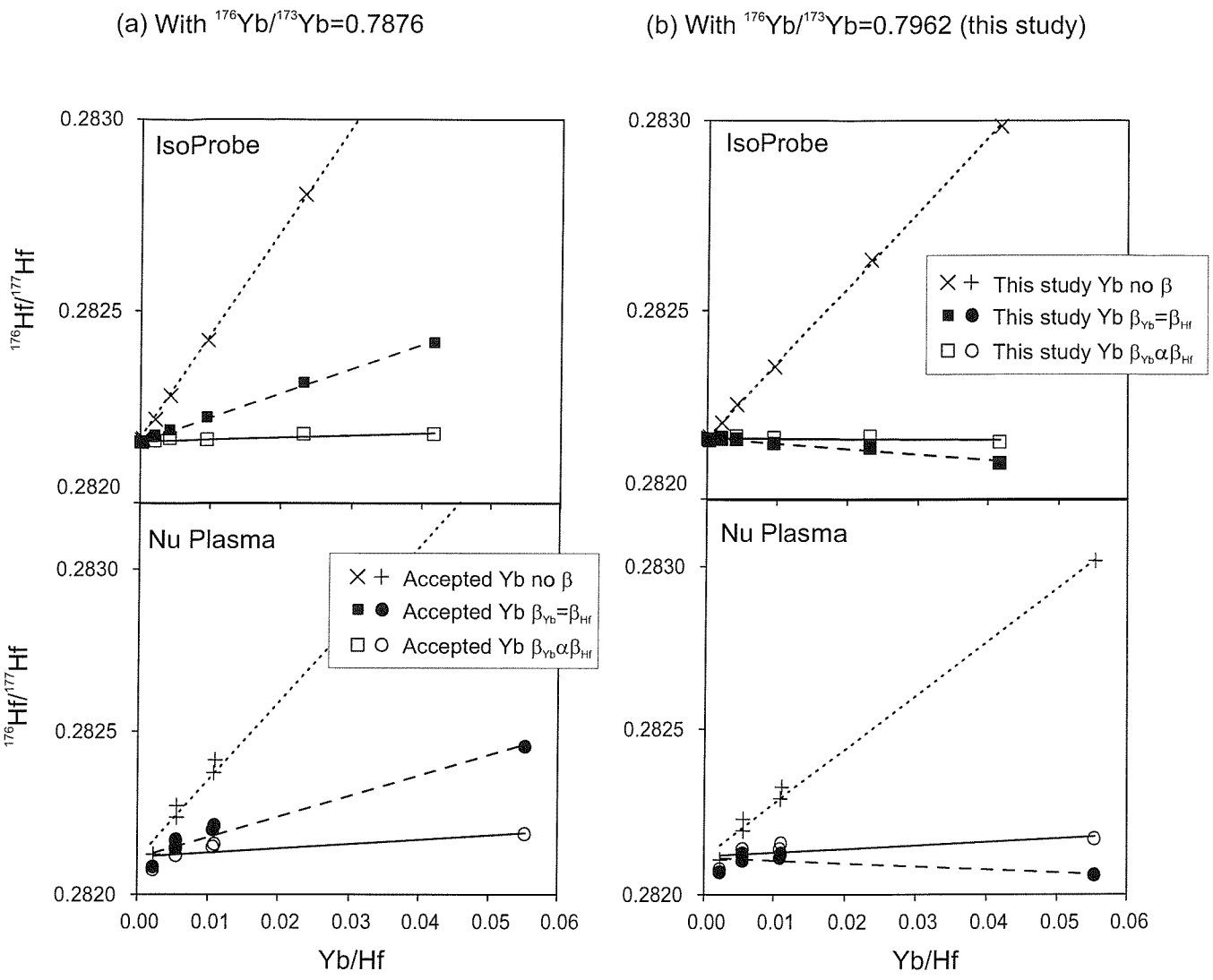

Fig. 3.4 $^{176}Hf/^{177}Hf$ plotted against Yb/Hf for mixtures of JMC475 and Yb. Upper plot for the IsoProbe; lower plot for the Nu Plasma. Symbols '+' and '×'represent ^{176}Yb corrected using natural $^{173}Yb/^{176}Hf$; solid symbols (squares or circles) are ^{176}Yb corrected using $\beta_{Yb}=\beta_{Hf}$, and open squares or circles are ^{176}Yb corrected using $\beta_{Yb}=1.272\times\beta_{Hf}$ (eq. 5, Fig 3.5 dashed line). Left panels: all correction made using the accepted $^{176}Yb/^{173}Yb$ natural abundance ratio of 0.7876. Right panel: the same corrections but made using the new proposed Yb isotope values (Table 3.7).

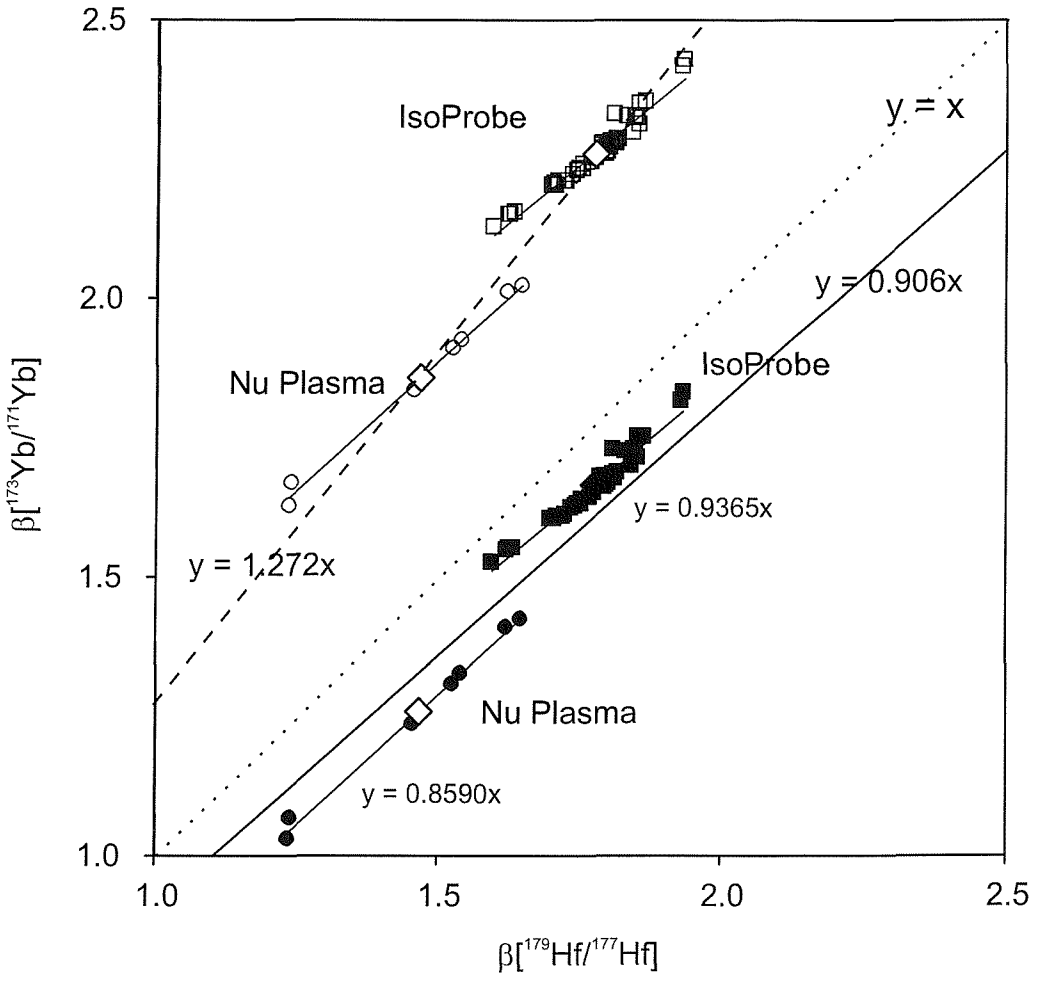

Fig. 3.5 $\beta(^{179}Hf/^{177}Hf)$ plotted against $\beta(^{173}Yb/^{171}Yb)$. Open squares/circles are individual Hf-Yb measurements with the present Yb isotope values (Table 3.7, TIMS/P54) on the IsoProbe and Nu Plasma, respectively. The correlation derived from present Yb values is presented in dashed line as y=1.272x. Solid square/circles are the same measurements using the new Yb values from this study; they are parallel to the correlation line.

3-5 Yb isotope abundances measured on TIMS

Yb isotope abundances have been measured previously by McCulloch *et al.* (1977) using ID-TIMS, by Holliger and Devillers (1981) using TIMS and Blichert-Toft *et al.* (1997) using MC-ICP-MS. The IUPAC values currently accepted are those of Holliger and Devillers (1981). It has been suggested by laser ablation studies (Thirlwall and Walder, 1995; Griffin *et al.*, 2000) that the $^{176}Yb/^{171}Yb$ and $^{176}Yb/^{173}Yb$ accepted ratios may be too low. We have carried out a series of TIMS measurements to attempt to evaluate the validity of the currently accepted Yb isotopic ratios. To do this we have utilised other rare earth elements, Nd and Ce, which have well constrained isotopic abundances (Wasserburg *et al.*, 1981; Makishima *et al.*, 1987) based on analysis of gravimetric compounds or rigorous examination for geochronological measurements. These elements are used here as analogues of the fractionation behaviour of Yb during thermal ionisation.

It is recognised that in TIMS analysis pure fractions of elements consistently produce light isotope enriched ratios during the initial stages of ionisation at a given temperature and sample quantity on the filament. This is one of the fundamental principals of external fractionation correction of Pb isotopes used through the last 40 years. The use of double spike Pb techniques on TIMS has superseded the external fractionation correction as the method of choice (Galer and Abouchami, 1998; Thirlwall, 2000) but within the errors of the external correction technique, good estimates of the level of fractionation can be achieved. In the case of Nd, large sample loads (~1 μg) of purified Nd result in $^{146}Nd/^{144}Nd$ ratios that focus around a particular value, particularly during the initial stages of the ionisation.

We have examined 37 measurements of Nd isotopic standards (JMC321, La Jolla and JNdi) with Nd loads in excess of 500ng. During the first 15 minutes of measurement (30 ratios) the average $^{146}Nd/^{144}Nd = 0.719433 \pm 0.00139$ (2se), which is lighter than the accepted value of $^{146}Nd/^{144}Nd$ (0.7219), and equates to a β value of -0.248 (Table 3.8). These measurements, performed over a period of 6 years, conform to the typical light to heavy thermal fractionation progression. A similar comparison for Ce isotopes using the $^{138}Ce/^{142}Ce$ produces a β value of -0.219, indicating that the level of initial fractionation is similar between these elements, despite variations in their first ionisation potentials. If we assume that the behaviour of Yb using identical

analytical protocols is comparable to that of Nd and Ce, we can apply the β value generated from the other rare earths to correct the measured Yb isotope ratios. Taking $^{173}Yb/^{171}Yb$ as a reference, we have taken the average initial value measured on the TIMS (1.129416) and fractionation corrected it using β= -0.248 to give $^{173}Yb/^{171}Yb$ = 1.132685. Using this as a normalising ratio (i.e. as R_t in eq. 2) the other Yb ratios can be internally corrected for fractionation. The resulting ratios are presented in Table 3.8. Using the same $^{173}Yb/^{171}Yb$ value, Yb ratios measured on the MC-ICP-MS instruments are normalised in the same way and shown for comparison in Table 3.7.

Table 3.8 Exponential deviation of accepted values and initial thermal ionisation results

HREE isotope pair	accepted values [ref]	ini. ionisation average [c]	± 2se	n	β
$^{146}Nd/^{144}Nd$	0.7219[a]	0.719433	± 139	37	-0.248
$^{136}Ce/^{142}Ce$	0.01688[b]	0.017080	± 61	2	-0.272

[a] Wasserburg *et al.* (1981)

[b] Makishima *et al.* (1987)

[c] The ratios were taken from the first 15 mins of the ionisations during TIMS analysis

The Yb isotope ratios calculated in this thermal ionisation experiment can now be applied to the Hf-Yb measurements. These are plotted as solid symbols in Figure 3.5, and lie much closer to the $\beta_{Hf}=\beta_{Yb}$ line than data calculated using the currently accepted Yb ratios. Furthermore, the data from each instrument lie parallel to, rather than across, lines intersecting the origin. In a similar fashion, the new Yb ratios can be applied to the series of Hf-Yb mixtures, the recalculations of which are shown in Fig. 3.4b. In this plot the crossed symbols, where $\beta_{Yb}=0$, define a positive trend. The solid squares, where $\beta_{Yb}=\beta_{Hf}$, lie close to a constant $^{176}Hf/^{177}Hf$, but with a slight tendency to decreasing $^{176}Hf/^{177}Hf$ with increasing Yb content in the mixture. This could suggest that the revised values for Yb defined in this study are slightly offset, or that a difference does exist between the mass bias of Hf and Yb. The subtly different behaviour of Yb and Hf is the most likely explanation as data from each of the instruments used in this study lie on a different trend in Figure 3.5, with different Hf coefficients (0.9365 for the IsoProbe and 0.8590 for the Nu Plasma). A comparison between the Yb and Hf mass bias across the two isotope systems is displayed in Figure 3.6. This figure shows mass bias for a range of Yb and Hf isotope pairs, and

plots the β values against the average mass of the pair. It shows that the β_{Yb} generated using the Yb abundances determined in this study produce 1) similar β values for Hf and Yb, 2) roughly consistent β values across the Yb mass range and 3) a slight increase in the mass bias (higher β_{Yb}) with decreasing mass. This contrasts with the β_{Yb} generated using the existing values, which are shown as open squares in Figure 3.6. These show a scatter of β across the Yb mass range, and significantly higher mass bias of Yb relative to Hf. Differences in mass bias between elements across a large range in masses is clearly recognised in MC-ICP-MS instruments (Hirata, 1996; Rehkämper *et al.*, 2001). Mass discrimination ($\alpha=\beta/M$) on the IsoProbe for a range of masses are U ~1.2, Pb ~1.3, Hf ~1.9, Nd ~2.3, and Sr ~2.5. However, slight increases in bias towards lower mass ratios have also been observed in the isotopic spectrum of individual elements (Vance and Thirlwall, 2002), which may be the case in the Yb data presented in this study.

The discrepancy between the Hf-Yb mixtures corrected using $\beta_{Hf}=\beta_{Yb}$ and a constant $^{176}Hf/^{177}Hf$ (Figure 3.4b, solid symbols) can be adjusted using a correction developed in a similar way to 3.5, except that the level of adjustment is smaller. The result of this additional correction is shown in Figure 3.4b as the open symbols.

Lu can be investigated in a similar fashion to Yb. Values suggested for $^{176}Lu/^{175}Lu$ vary considerably (McCulloch *et al.*, 1976; Holliger and Devillers, 1981; Patchett, 1983), including the commonly used value of 0.02656 (Blichert-Toft *et al.*, 1997) This variation is related to the difficulty in determining the Lu isotopic ratio since only two isotopes exist in nature and the proportion of ^{176}Lu is very small (2.59%). Fractionation analyses performed on TIMS and adjusted in the same way as Yb produce a ratio of 0.02655 (Table 3.7), which is close to the present recommended value (Blichert-Toft *et al.*, 1997). Figure 3.7 shows the β_{Lu}-β_{Hf} correlation based on the measurement of a 1:1 Hf:Lu solution and the $^{176}Lu/^{175}Lu = 0.02655$. The results, shown as diamonds in figure 3.7, form an array displaced from the $\beta_{Lu}=\beta_{Hf}$ correlation (Fig. 3.7, diamond symbols), with $\beta_{Lu} = 0.7966\times\beta_{Hf}$. This is surprising given the equivalence of β_{Yb} and β_{Hf} generated by our experiments in this study. It is unlikely that the R_t of $^{176}Lu/^{175}Lu$ is in error as a value of ~0.02647 would be required to generate $\beta_{Lu}=\beta_{Hf}$, which is lighter than any initial stage TIMS values. It is therefore likely that the measurement of Lu in the presence of equivalent amounts of Hf on the

plasma source instruments is the source of the problem, as large corrections have to be made for the isobaric ^{176}Hf on the ^{176}Lu. In most natural samples the Lu content is about an order of magnitude lower than the Yb and Hf and thus the correction is relatively small.

3-6 Yb correction of laser ablation analysis by MC-ICP-MS

For comparison, the Yb and Hf mass bias relationship described above was tested using laser ablation as an alternate sample introduction method. The NIST SRM 610 glass standard, containing Hf 417.7 $\mu g\ g^{-1}$, Yb 416.5 $\mu g\ g^{-1}$ (Pearce *et al.*, 1997), was ablated and analysed using the IsoProbe MC-ICP-MS. The results are shown in Fig. 3.7 as solid triangles. The β_{Hf}-β_{Yb} covariation from the laser analysis is close to the range of values generated by solution nebulisation on the same instrument (open squares), but lie slightly closer to the $\beta_{Hf}=\beta_{Yb}$ line. The differences between the solution and laser mass bias are likely to be small as both introduction methods present the plasma with sample in the form of a dry aerosol. Although the signal levels generated by laser are lower, these results indicate that a similar correction procedure to the solution analysis can be applied.

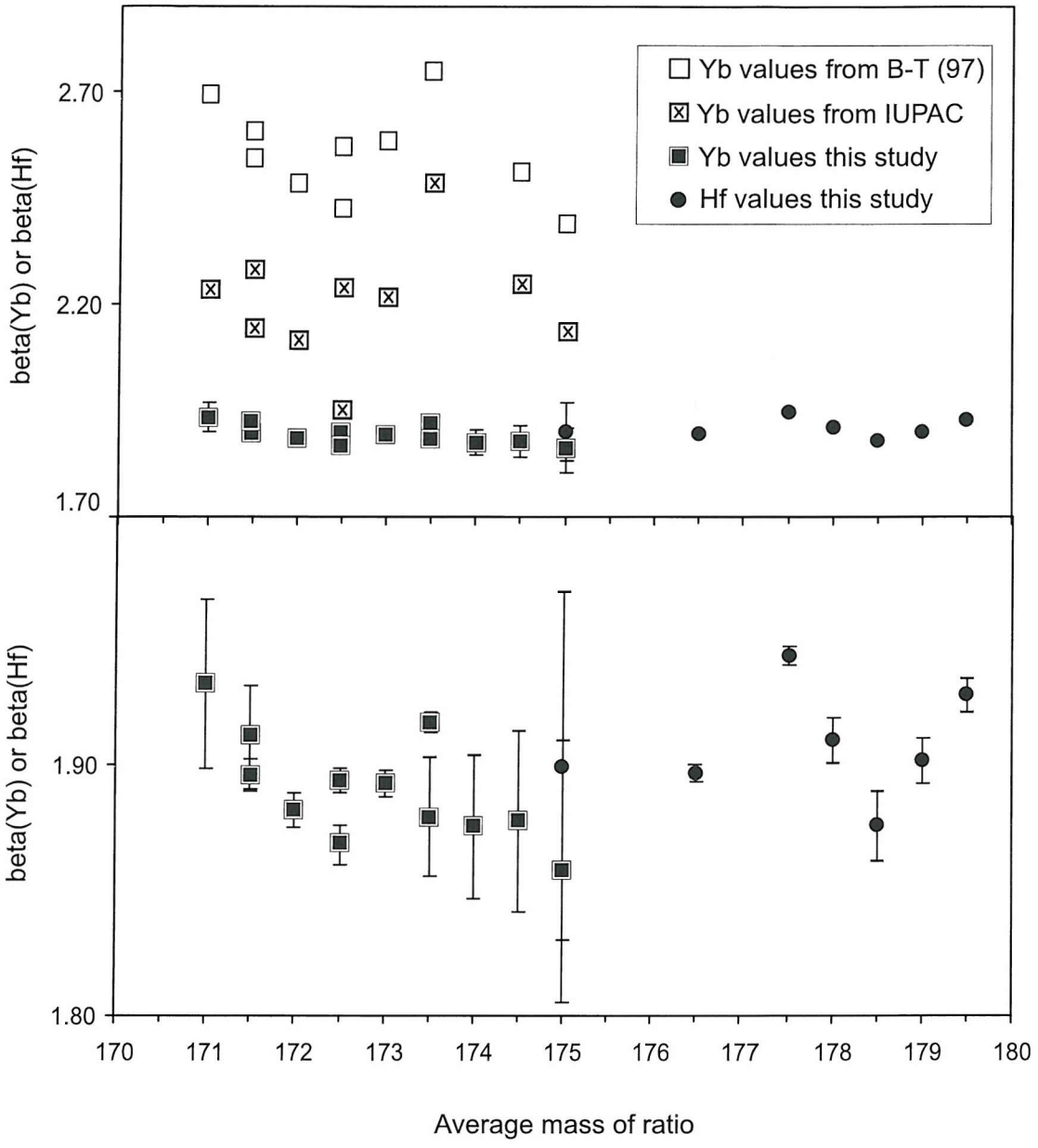

Fig. 3.6 Variations of the exponential mass bias function β relative to the average mass of M_A-M_B for the Yb and Hf isotope systems (the lower plot has an expanded scale). Analyses were done separately during the same analysis session with single element solutions. The three sets of square symbols are β values for Yb derived from various Yb values (open squares from McCulloch *et al.* (1976) and Blichert-Toft *et al* (1997); crossed squares from Holliger and Devillers (1981), and solid squares from this study, Table 3.7) and solid circles are those for Hf. Some mass averages are derived from 2 sets of isotope ratios, i.e. $^{174}Yb/^{173}Yb$ and $^{176}Yb/^{171}Yb$ both result in an average of 173.5.

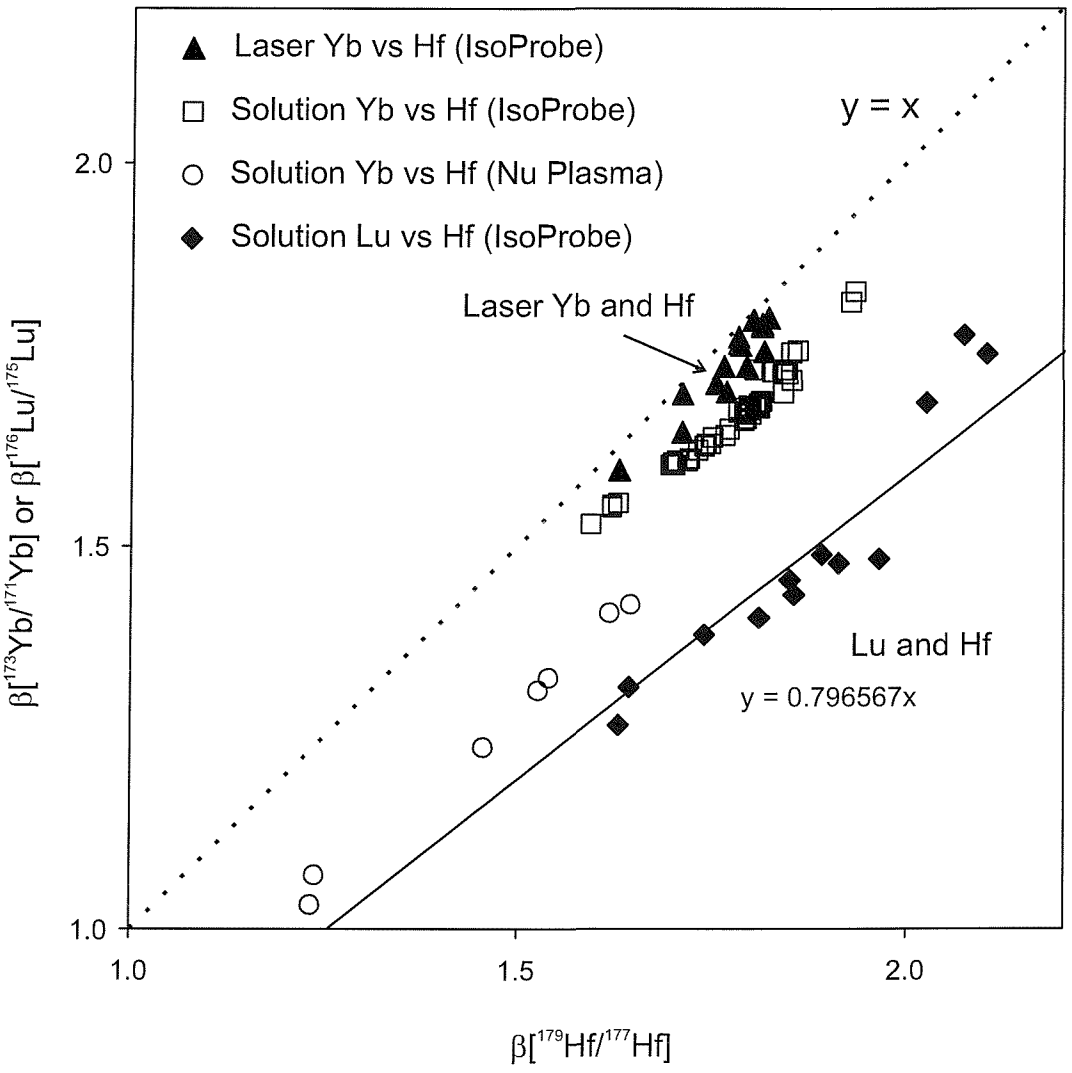

Fig. 3.7 $\beta(^{176}Lu/^{175}Lu)$ and $\beta(^{173}Yb/^{171}Yb)$ versus $\beta(^{179}Hf/^{177}Hf)$ for solution and laser ablation analysis. Laser determinations are from NIST SRM 610 glass standard (416.5 μg g^{-1} Yb, 417.7 μg g^{-1} Hf); solution measurements are those from Fig. 3.5 corrected using the Yb values proposed in this study, and JMC 475 Hf doped with pure Lu, where Lu/Hf= 0.5. Solid triangles are the laser ablation results of Yb and Hf correlations, which fall within same range as samples introduced by solution. The Lu and Hf correlation is slightly below that of Yb and Hf.

3-7 Conclusions

In this study we have examined the relationship between Yb and Hf mass bias with a view to improving isobaric interference corrections. Two different MC-ICP-MS instruments (IsoProbe and Nu Plasma) demonstrate that if currently accepted values for Yb isotope ratios are employed in the corrections, large deviations in $^{176}Hf/^{177}Hf$ are found in solutions with increasing Yb/Hf ratios. Using thermal ionisation mass spectrometry we have defined an internally consistent set of Yb isotope ratios that were tested as an independent calibration of the plasma source results. Using the new values, it can be concluded that Yb and Hf have similar levels of mass bias and that consistent $^{176}Hf/^{177}Hf$ can be achieved following the application of a simple empirical correction. Laser ablation sample introduction demonstrates that the same Yb correction is potentially applicable to the analysis of solid samples where chemical separations are not possible.

II. Be-10 Chronology for Fe-Mn crusts time series

3-8 Dating techniques for Fe-Mn crusts

Various methods have been applied to date Fe-Mn crusts. For example, a maximum age is given by dating the substrate with an assumption that the crust began growing soon after formation of the rock (e.g. Koski *et al.*, 1985; VonderHaar *et al.*, 1988); however this does not detail the growth rate. Paleontological methods using nannofossil biostratigraphy (e.g. from coccolith imprints, Cowen *et al.*, 1993), although reliable, are time consuming and have not been widely applied.

Most modern methods of dating Mn nodules and crusts, instead, rely on radiometric determination base on U and Th methods (Banakar and Borole, 1991; Eisenhauer *et al.*, 1992; Chabaux *et al.*, 1995; Chabaux *et al.*, 1997), Sr isotopes (Futa *et al.*, 1988; Ingram *et al.*, 1990) or ^{10}Be (Segl *et al.*, 1984; Segl *et al.*, 1989). These methods rely on the assumption that slow-growing Fe-Mn crusts incorporate these elements and nuclides from seawater as they grow but that post-depositional diffusion has had negligible subsequent effect. The most precise ^{230}Th method, however, is restricted to an upper age limit of about 400 kyrs, equivalent to the outer few mm of any deep-sea crust (Segl *et al.*, 1984; Banakar and Borole, 1991). The Sr isotope method is based on comparing Sr values in any crust with the ^{87}Sr/^{86}Sr seawater curve to determine the age and the growth rate of that crust. Although this method can be used to identify hiatuses in the growth of the crusts to ages in excess of 20 Ma, the presence of Sr-rich detrital or secondary phases, diagenesis or diffusional exchange with seawater make the Sr isotope method less reliable (Ingram *et al.*, 1990; VonderHaar *et al.*, 1995; Ling *et al.*, 1997). Some alternative methods, such as magnetostratigraphy (Joshima and Usui, 1998), also provide some age information; however, that approach still has to be supported with other conventional dating methods.

Cosmogenic ^{10}Be is produced in the atmosphere by spallation of O and N (Arnold, 1957) and enters the ocean predominantly by precipitation at an essentially constant rate (Ku *et al.*, 1990). The ^{10}Be production rate is $1.12 \pm 0.26 \times 10^6$ atms cm^{-2} yr^{-1} of the global average (Monaghan *et al.*, 1985/1986; Mchargue and Damon, 1991; Morris, 1991)). Because the half life for ^{10}Be (1.51 ± 0.06 Ma, (Hofmann *et al.*, 1987) is of the same order as the time needed for a few millimetres of crust material

to grow, the ^{10}Be method is a very suitable dating tool for Fe-Mn crusts. After normalising to the stable isotope ^{9}Be, as a product of erosion, the method can readily be applied back to ~10 Ma. Extrapolation of this age model is used when the age is beyond 10 Ma, but possible errors will occur if the growth rate of the crusts has changed beyond 10 Ma. It is thought that the flux incorporation of cobalt (Co) into any Fe-Mn crust is constant (Halbach *et al.*, 1983) and therefore, the Co-chronometer can compensate for ^{10}Be deficiency by applying empirical equations to yield a maximum age of ~24 Ma for studied Fe-Mn crusts (Manheim, 1986; Puteanus and Halbach, 1988; Frank *et al.*, 1999a).

3-9 Samples and methods

Four crusts of this study, NC4, SC1, SC5, and IB2, were selected for ^{10}Be dating. All chemical separations and measurements were carried out at ETH, Zurich. The sub-sampling for ^{10}Be/^{9}Be dating was carried out by fixing the sample on a drill stand (Plate 2.4) with a 1 mm diameter steel drill bit. Drill bits were discarded after sampling of each individual growth layer. Samples were weighed at around 10 mg and dissolved in 6N HCl. Digestion of material collected from each growth layer followed the descriptions provided earlier (section 2.2). 1 ml of ^{9}Be (with a concentration of 1000 mg/l) was spiked into dissolved samples as the Be-carrier.

Beryllium separation was done based on co-precipitation at different levels of pH. For this purpose, trace of EDTA (ethylene diamine tetra acetic acid, 1.5 ml) was added for complexation below pH of 2.5. Beryllium and Fe were later co-precipitated overnight when the pH level was raised back to 7-8. The residues were redissolved in conc. NaOH (1 ml) to separate Fe (precipitate) and Be (dissolved phase). Beryllium was finally precipitated after decanting when the pH is up to 8-9.

Several washings with MQ in the final precipitations are necessary to reduce the remaining amount of B, as ^{10}B would interfere with the ^{10}Be measurements. After washing, samples were collected on a cellulose acetate filter (pore size: 0.45 μm) and $Be(OH)_3$ was ashed to BeO at 1000°C and prepared for accelerator mass spectrometry (AMS) measurements at the AMS facility of ETH Zurich and the Paul Scherrer Insititute following standard procedures (Ender *et al.*, 1997). The concentrations were normalised to internal standard S555 with a nominal ^{10}Be/^{9}Be ratio of 95.5×10^{-12} (Frank *et al.*, 2002a).

^{10}Be counts, presented as atoms/g, have been corrected by subtraction of procedure blanks. The values are divided by stable ^{9}Be, measured separately by ICP-MS, for correcting the dilution effect from the stable Be erosion input. The growth rates were derived from the half-life of ^{10}Be of 1.5 Myr (decay constant $\lambda = 4.56*10^{-7}$ y^{-1}). In the case of ^{10}Be measured as a function of depth in a manganese crust this writes as

$$^{10}Be_{measured} = {}^{10}Be_{initial} * e^{-\lambda t} \qquad \text{eq. 3.6}$$

Assuming the ^{10}Be flux into the Fe-Mn crust was constant, $^{10}Be_{initial}$ was constant. Thus the growth rate s over time can be calculated with $s = \frac{x}{t}$

with x = depth below the top of the crust

Thus the above can be written as

$$^{10}Be_{measured} = {}^{10}Be_{initial} \cdot e^{-\frac{\lambda \cdot x}{s}} \qquad \text{eq. 3.7}$$

or

$$\ln {}^{10}Be_{measured} = \ln {}^{10}Be_{initial} - \frac{\lambda \cdot x}{s} \qquad \text{eq. 3.8}$$

This results in a straight line in coordinate of $ln\ ^{10}Be_{measured}$ and x, with the slope m = $-\lambda/s$ and the intercept with the ordinate is $ln\ ^{10}Be_{initial}$.

Thus: $\dfrac{x\ -\lambda}{\ln\left(\dfrac{^{10}Be_{measured}}{^{10}Be_{initial}}\right)} = s$, and this is the growth rate we require.

3-10 Results

The age models derived from ^{10}Be/^{9}Be and ^{9}Be concentrations for this study are listed in Table 3.9 and plotted in Fig 3.8. The results for these crusts are all younger than 10 Ma and the Co-chronometer is therefore not necessary. The growth rate for NC4 is 2.5 mm/Ma for all ages before 5 Ma and 0.63 mm/Ma from 5 Ma till present; for SC1, the growth rate is 2.5 mm/Ma; for SC5 it is 3.7 mm/Ma and IB2 it is 6.7 mm/Ma.

In general, the Central Pacific crusts (NC4, SC1 and SC5) have slower growth rates compared to the 'ocean-margin' crust (IB2). The fast growth rate of IB2 is also consistent with another previously dated crust (IB1; Usui *et al.*, unpublished data), which has a growth rate of 5.4 mm/Ma.

Table 3.9 Be concentration, $^{10}Be/^{9}Be$ ratios and age models of Fe-Mn crusts

Depth (mm)	$^{10}Be*10^{-8} \pm 1\sigma$ (atoms/g) [a]	^{9}Be (ppm) [b]	$^{10}Be/^{9}Be *10^{-8} \pm 1\sigma$	Age (Ma) $\pm 1\sigma$ [c]
NC4				
surface	237.33 ± 6.46	2.99	11.87 ± 0.40	0.25 ± 0.01
1.0-2.0	53.20 ± 2.38	3.31	2.40 ± 0.12	3.75 ± 0.18
3.0-4.0	30.72 ± 1.75	3.73	1.23 ± 0.07	5.22 ± 0.31
6.0-7.0	16.40 ± 1.41	2.90	0.85 ± 0.07	6.04 ± 0.53
9.0-10.0	5.79 ± 0.89	3.51	0.25 ± 0.04	8.75 ± 1.35
13.0-14.0	3.01 ± 0.55	3.24	0.14 ± 0.03	10.01 ± 1.84
16.0-17.0	1.97 ± 0.72	3.16	0.09 ± 0.03	10.87 ± 3.97
21.0-22.0	1.47 ± 0.78	4.27	0.05 ± 0.03	12.18 ± 6.49
SC1				
surface	280.20 ± 7.05	2.09	20.08 ± 0.65	0.06 ± 0.00
2.0-3.0	187.63 ± 4.37	2.78	10.09 ± 0.31	1.57 ± 0.05
4.0-5.0	130.69 ± 3.72	2.90	6.75 ± 0.23	2.45 ± 0.09
8.0-9.0	62.65 ± 4.06	2.19	4.28 ± 0.29	3.45 ± 0.23
10.0-11.0	39.80 ± 1.66	1.92	3.10 ± 0.14	4.16 ± 0.19
13.0-14.0	20.25 ± 1.18	1.33	2.29 ± 0.14	4.83 ± 0.30
16.0-17.0	9.61 ± 0.93	1.84	0.78 ± 0.08	7.18 ± 0.71
21.0-22.0	4.57 ± 0.57	2.01	0.34 ± 0.04	9.00 ± 1.13
SC5				
surface	265.75 ± 9.89	2.31	17.22 ± 0.73	0.08 ± 0.00
1.0-2.0	219.83 ± 5.99	3.11	10.59 ± 0.36	1.14 ± 0.04
6.0-7.0	162.37 ± 9.50	3.52	6.91 ± 0.43	2.08 ± 0.13
9.0-10.0	92.48 ± 3.78	3.39	4.09 ± 0.19	3.23 ± 0.15
13.0-14.0	84.93 ± 3.22	3.21	3.96 ± 0.17	3.30 ± 0.14
16.0-17.0	49.04 ± 3.65	3.31	2.22 ± 0.17	4.57 ± 0.35
20.0-21.0	26.68 ± 1.87	4.07	0.98 ± 0.07	6.36 ± 0.46
IB2				
surface	146.07 ± 4.89	1.70	12.83 ± 0.50	0.02 ± 0.00
1.0-2.0	163.51 ± 3.98	2.19	11.16 ± 0.35	0.33 ± 0.01
5.0-6.0	51.52 ± 1.95	1.21	6.37 ± 0.27	1.56 ± 0.07
9.0-10.0	34.88 ± 1.65	0.99	5.25 ± 0.27	1.98 ± 0.10
14.0-15.0	44.77 ± 2.03	1.47	4.56 ± 0.23	2.29 ± 0.11
19.0-20.0	35.80 ± 1.98	1.99	2.69 ± 0.16	3.45 ± 0.20
25.0-26.0	28.94 ± 1.43	2.33	1.86 ± 0.10	4.26 ± 0.23
31.0-32.0	20.95 ± 1.37	2.08	1.51 ± 0.10	4.72 ± 0.32
40.0-41.0	21.91 ± 1.84	2.70	1.21 ± 0.10	5.20 ± 0.45

(a) Data obtained by a AMS at ETH, Zurich.

(b) The external reproducibility for ^{9}Be is 2%.

(c) Calculated from ^{10}Be half-life=1.5 Myr.

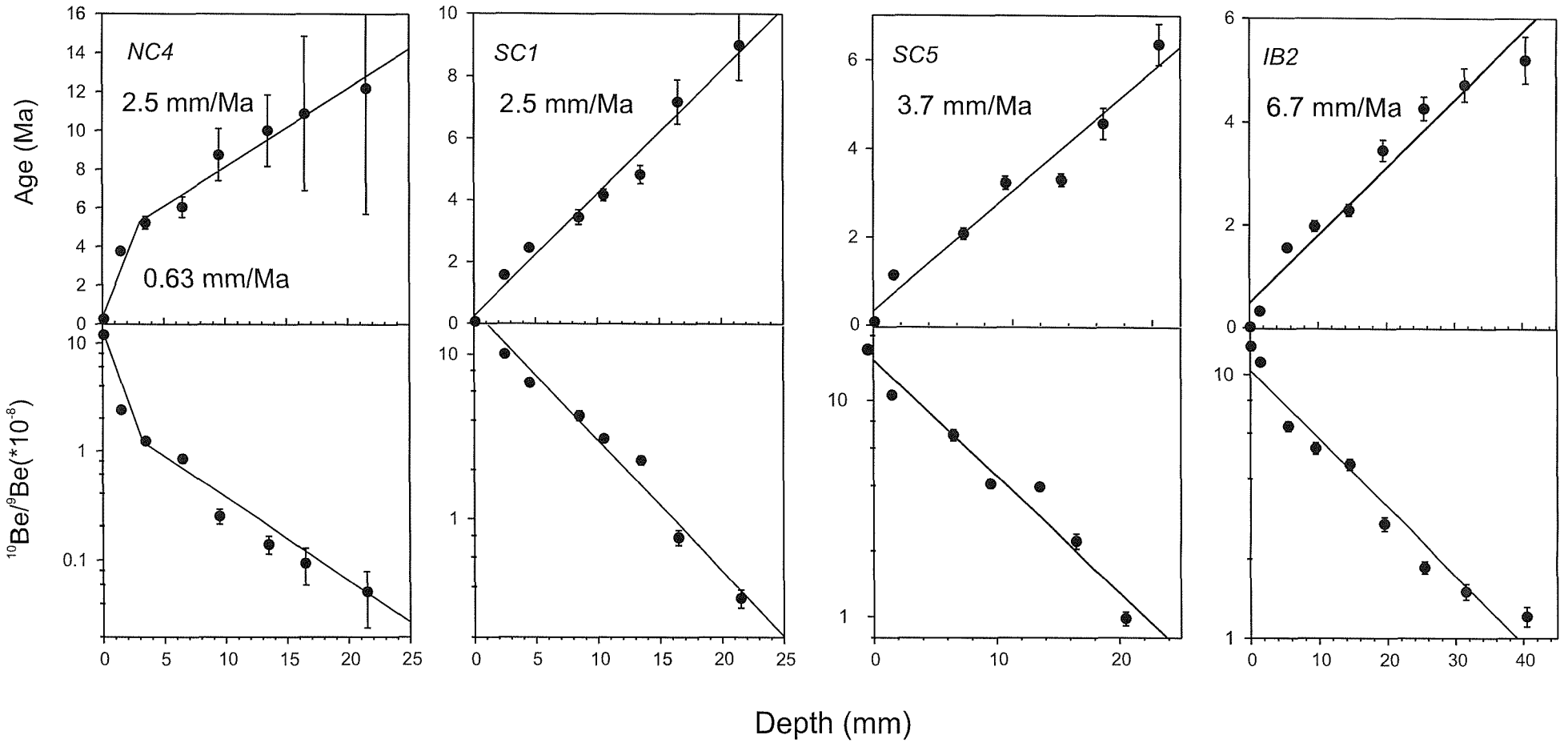

Fig. 3.8 Age model for Fe-Mn crusts with $^{10}Be/^{9}Be$ chronology. $^{10}Be/^{9}Be$ ratios and corresponding ages (Ma) versus depth (mm) for crusts NC4, NC1, SC5, IB2. The growth rate calculated for these crusts are marked on the plots.

Chapter 4. Present day Fe-Mn crusts study and interpretation for seawater Hf isotopic compositions

4-1 Abstract

Because *in situ* Hf isotope seawater measurements are still unavailable, the aim of this chapter is to reconstruct modern day Hf isotopic compositions in the water column using surface scrapings of Fe-Mn crusts. The basis of this study is that the growth of a Fe-Mn crust records ambient seawater properties and if this is the case the surface composition of crusts collected from different depths can provide information on modern day Hf isotopic variations in the water column.

The interpretation of the observed Hf isotopic variability involves using a combination of standard geochemistry of Nd isotopes plus REE and the hydrology/ nutrient tracers (WOCE database). The REE patterns and radiogenic Nd isotopic signatures of the Fe-Mn crusts suggest an input from volcanic materials of the Papua New Guinea area. The consistency of (1) the Nd mixing model derived from seawater and surface Fe-Mn crusts results and (2) the strong correlation with present day hydrological tracers supports the validity in using Fe-Mn crusts surfaces to infer present day seawater Hf signatures. The results of Hf isotope show less significant correlation with the hydrology properties than Nd, suggesting Hf has a longer ocean residence time. Hf isotopic signatures of two water masses in the Pacific Ocean are proposed from the Hf mixing model, in which the Pacific Deep Water has a ε_{Hf} value of 6-7 and the Intermediate Water at around 3-4.

In addition, leaching experiments carried out on the Fe-Mn crusts demonstrate the importance of removing detrital fractions when interpreting data as past seawater signatures. This is especially true when measuring Hf isotopes since zircon, which is enriched in Hf, is an important component in many detrital fractions.

4-2 Introduction

Godfrey *et al.* (1996) and McKelvey and Orians (1998) have reported extremely low Hf values in seawater (0.1 to 1.1 pmol/kg) and this makes direct isotopic measurements extremely difficult. Consequently, reliable Hf isotopic data have not yet been reported and the potential of using Hf isotopic composition in the ocean is still to be realised. Numerous studies (e.g. O'Nions *et al.*, 1978; Piepgras *et al.*, 1979; Elderfield *et al.*, 1981; Goldstein and O'Nions, 1981; Aplin *et al.*, 1986/1987; Futa *et al.*, 1988; Amakawa *et al.*, 1991; Albarède and Goldstein, 1992; Abouchami and Goldstein, 1995; von Blanckenburg *et al.*, 1996a; von Blanckenburg *et al.*, 1996b; Albarède, 1997; David *et al.*, 2001; Vlastélic *et al.*, 2001) have demonstrated that hydrogenetic Fe-Mn crusts and nodules record the trace metal isotope composition of the ambient deepwater. In addition, because Fe-Mn oxides pre-concentrate elements (including Hf) during their precipitation, the use of Fe-Mn crusts/nodules makes it possible to infer seawater Hf isotopic compositions. In this study, Hf isotope compositions from the surface of Fe-Mn crusts collected at various depths are measured in attempts to reconstruct the Hf isotopic composition of the Central Pacific water column.

Rare earth elements (REE) and Nd isotopes in seawater have been extensively studied; either through direct measurements (Piepgras *et al.*, 1979 and references herein) or inferred from Fe-Mn crusts or nodules (e.g. Goldstein and O'Nions, 1981; Albarède and Goldstein, 1992). The dissolved REE distribution is determined by the competition between soluble carbonate-REE(III)$^{+}$ complexes and the removal of REE(III)$^{+}$ by particle scavenging (Elderfield, 1988). This competition results in fractionation between light and heavy REE, plus the preferential oxidation of Ce, hence caused the Ce anomaly, and form the REE patterns. The pattern is a useful tool to identify which marine process could have modified the distribution of the REE in seawater (adsorption, desorption, redox process and so on) (Elderfield, 1988; Zhang and Nozaki, 1996; Sholkovitz *et al.*, 1999). Nd isotopes have been applied as an important water masses tracer (Piepgras and Wasserburg, 1982; Piepgras and Wasserburg, 1987; Piepgras and Jacobsen, 1988; Jeandel, 1993; Jeandel *et al.*, 1998). Because they are not affected by evaporation or any removal processes, Nd isotopic compositions reflect source input with continental sources result in low isotopic Nd

values or radiogenic Nd values coming from the weathering of LREE-depleted volcanic rocks. REE and Nd isotopes were therefore measured on the surface Fe-Mn crusts and applied as proxies to constrain the source input of the water masses from which the crusts were precipitated (see also De Carlo, 1991; Piepgras and Jacobsen, 1992; Sholkovitz *et al.*, 1999; Amakawa *et al.*, 2000; Nozaki and Alibo, 2003).

Previous studies (e.g. Piepgras and Jacobsen, 1988; Piepgras and Jacobsen, 1992; German *et al.*, 1993; Jeandel, 1993; Jeandel *et al.*, 1998; Lacan and Jeandel, 2001; Nozaki and Alibo, 2003) have demonstrated the relationships between seawater REE, Nd isotopes and water masses by comparing with their physical/ nutrient properties (e.g. salinity, temperature or Si content). Modern day physical/ nutrient tracers obtained near the sample locations (described in Chapter 2) were compared with the surface Fe-Mn crusts geochemical data. Because even a few mm of the Fe-Mn crust might represent a significant time interval and average out the seawater signatures due to the very slow growth rates. Besides the careful sampling with only superficial surface scrapes, their Nd isotope results can be compared with these hydrological properties to provide assurance for further investigations. Hence, the Hf isotope systematics in modern day seawater can be inferred.

Terrigenous components, though rare, could be incorporated as detrital phases during the growth of the Fe-Mn crusts (e.g. De Carlo *et al.*, 2000). The fractions represent local sedimentation inputs and have geochemical properties which are quite distinct from the seawater signatures. Since large fractions of weathering-resistant zircons, hence Hf, exist in this phase, there is a real potential that a distortion of the seawater signature will occur if the detrital fraction is not removed. In a separate investigation a series of leaching experiments were carried out to determine the influence of the detrital fraction. The results clearly demonstrate that in order to obtain meaningful proxy data for seawater, it is essential to avoid the detrital fractions.

4-3 Materials and analytical method

Fe-Mn crusts in this study were collected during various cruises in the North-Central (NC) and South-Central (SC) Pacific Ocean. Sample locations are shown in Fig. 2.1, 4.1, and Table 2.1. Sampling and digestion of the ferromanganese oxide phase follow the method described in Chapter 2.

The silicate detritus included in the growth of Fe-Mn crusts was separated and analysed. Since the amount of silicate detrital fractions in Fe-Mn crusts is low (< 5%) it was necessary to process reasonably large quantities (~100 mg) of material from the surface of the Fe-Mn crusts. The detrital fractions were left as the residual fraction following thorough digestion of the ferromanganese oxide phase. The residues were separated by centrifugation, dried and weighed before being digested by mixed HF and HNO_3 at 150°C. Final solutions for the detrital fractions were made in 6N HCl with a trace of HF.

Trace elements were determined by an ICP-MS (PlasmaQuad 2+, VG Elemental). Nd and Hf isotope compositions were measured on a TIMS (VG-Micromass Sector 54) and a MC-ICP-MS (Micromass, IsoProbe) respectively after column purification (see Appendix II, III and Chapter 3). Analyses were processed from the same aliquots.

4-4 Results

4-4-1 Rare earth elements

The REE patterns of surface materials taken from the Fe-Mn crusts used in this study are shown in Fig. 4.2, where they are normalised to the Post-Archaean Australian Shale (PAAS) (Taylor and McLennan, 1985). The samples all have a characteristic convex upward shape (due to MREE enrichment) and, except SC-c samples, all others display a positive Ce anomaly (expressed as $Ce/Ce^*=3Ce_{sh}/(2La_{sh}+Nd_{sh})$ (where Ce_{sh} means shale normalised, after (de Baar *et al.*, 1985). Using this expression, most of the samples have Ce anomalies between 1.1 to 2.8 with the strongest anomaly being found in the NCP group, which are the shallowest samples (Fig 4.3a). Nd, Gd and Lu are chosen here in representing LREE, MREE and HREE respectively. Fig 4.3 (b-d) show the normalised Gd/Lu, Lu/Nd and Gd/Nd ratios of

each sample along their water depth. Among them, the highest (Gd_n/Nd_n) values demonstrate the shape of the MREE quantitatively.

Table 4.1 Zr, Hf and REE in surface Fe-Mn crusts (ppm)

Sample	Depth(m)	La	Ce	Pr	Nd	Sm	Eu	Gd	Tb	Dy	Ho	Er	Tm	Yb	Lu	Zr	Hf
NCP																	
NC1	1275	217	784	43.5	172	33.6	8.0	39.1	6.35	33.9	7.3	19.7	2.5	18.1	2.8	236	2.4
NC2	1565	201	790	40.4	159	31.6	7.1	34.7	5.61	30.9	6.2	17.2	2.1	15.9	2.4	284	3.1
NC3	1585	130	716	24.6	97	19.3	4.5	22.2	3.68	19.7	4.3	12.0	1.5	11.0	1.7	268	2.8
NC4	1930	202	819	41.4	164	32.3	7.6	36.9	5.91	31.0	6.3	17.2	2.2	15.8	2.3	362	4.0
NC5	2255	271	975	64.1	245	50.4	11.4	54.1	8.66	43.3	8.4	22.2	2.8	20.2	2.9	327	3.7
SCP-a																	
SC1	1664	195	464	36.2	151	29.5	7.1	32.7	5.50	31.2	6.5	17.8	2.4	16.3	2.6	268	3.1
SC2	1984	196	531	35.5	148	28.5	6.9	32.8	5.43	30.3	6.4	17.7	2.5	17.1	2.7	345	4.2
SC3	2260	222	681	40.6	169	32.9	7.8	35.5	6.21	35.1	7.6	19.8	2.7	19.0	2.9	335	4.0
SC4	2500	142	354	22.3	95	17.5	4.2	21.6	3.74	21.7	4.9	14.3	2.1	14.7	2.3	390	3.4
SC5	3033	200	458	40.3	169	33.3	8.2	36.0	6.10	32.4	6.7	17.4	2.4	16.8	2.5	223	2.3
SC5 (bis)		205	468	41.4	173	34.9	7.9	36.3	6.25	33.6	6.9	18.3	2.4	16.5	2.5	181	1.8
SCP-b																	
SC6	1787	203	536	34.8	146	28.6	7.1	35.1	5.71	32.7	7.4	19.5	2.5	18.5	2.9	285	3.1
SC7	2000	179	524	29.2	123	23.3	5.8	28.8	4.92	27.9	6.2	17.4	2.2	16.6	2.6	405	4.4
SCP-c																	
SC8	2545	241	480	49.5	204	40.7	9.4	43.1	7.23	38.6	7.8	19.5	2.5	18.0	2.7	285	3.3
SC9	2600	234	483	47.0	190	37.8	9.0	42.8	7.07	37.7	7.9	20.1	2.6	18.5	2.9	422	5.2

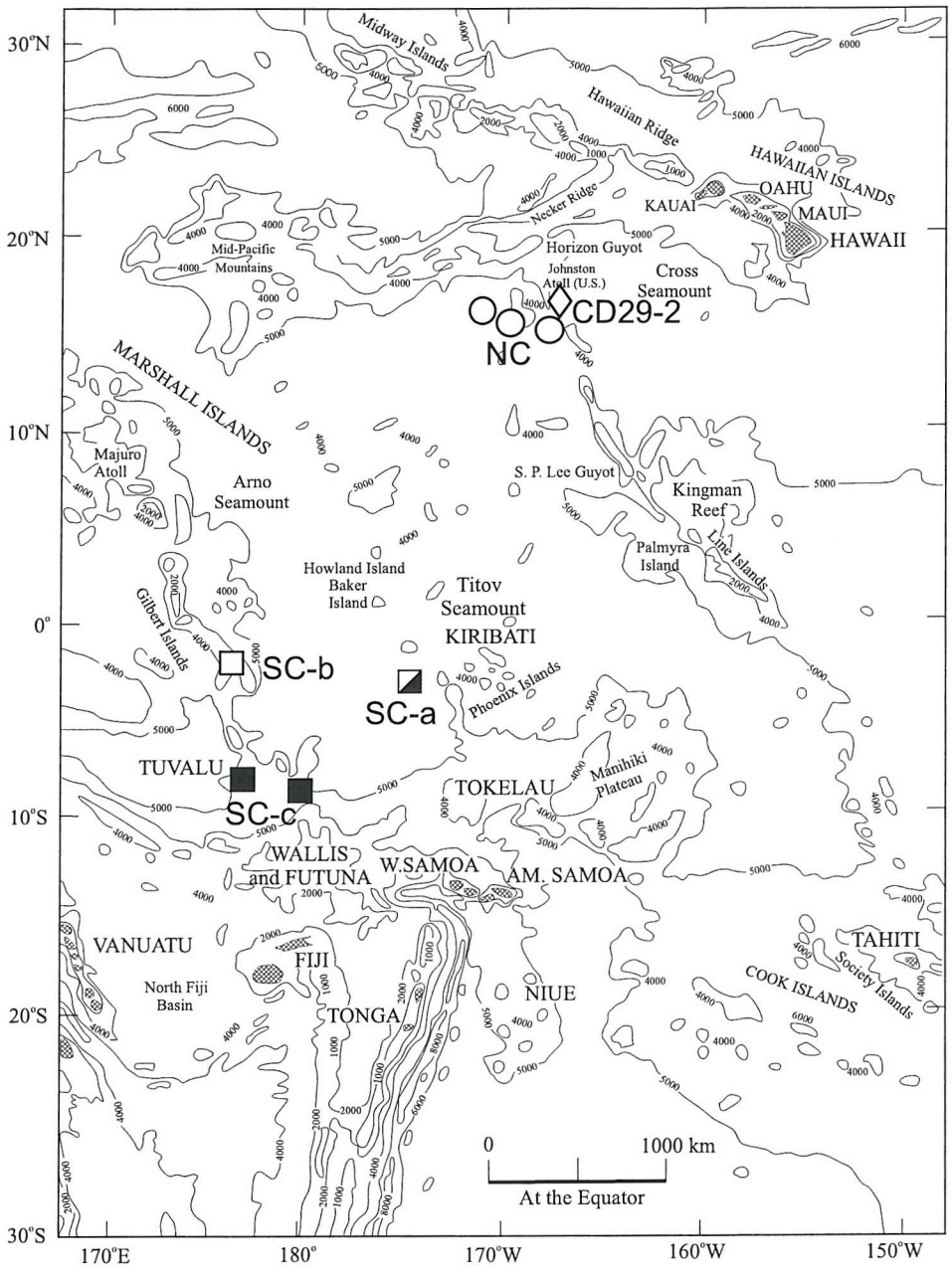

Fig. 4.1 Locations of Central Pacific Fe-Mn crusts with one previously reported sample CD29-2. (For locations of another literature sample D11-1 see Fig. 5.1.)

(a)

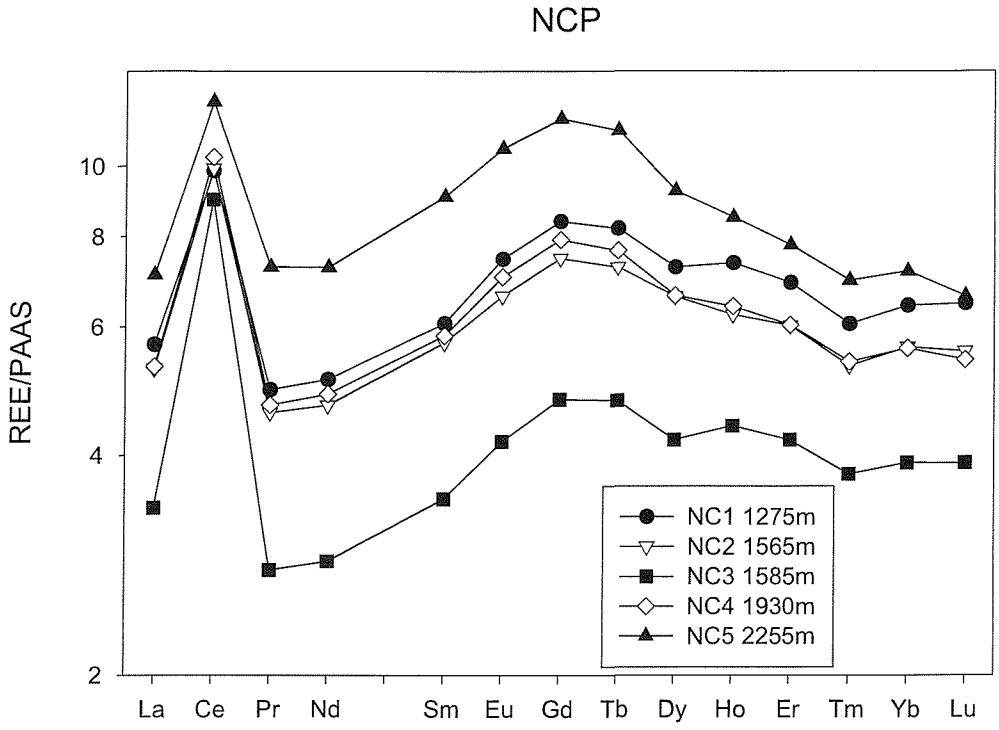

(b)

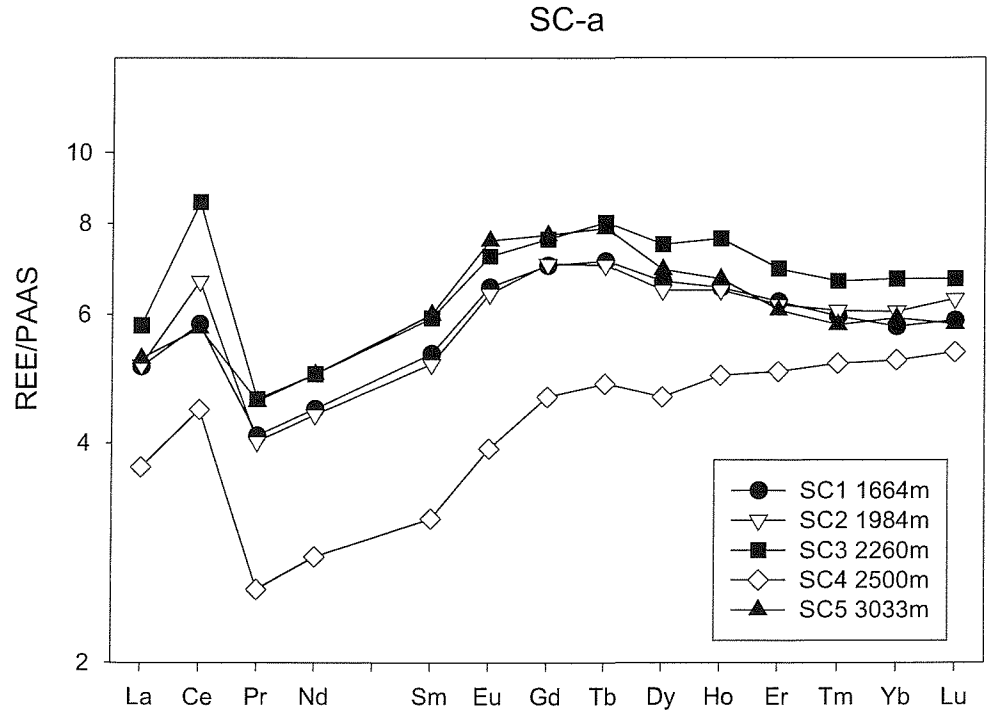

Fig. 4.2 Shale normalised REE pattern of NC and SC samples.

(c)

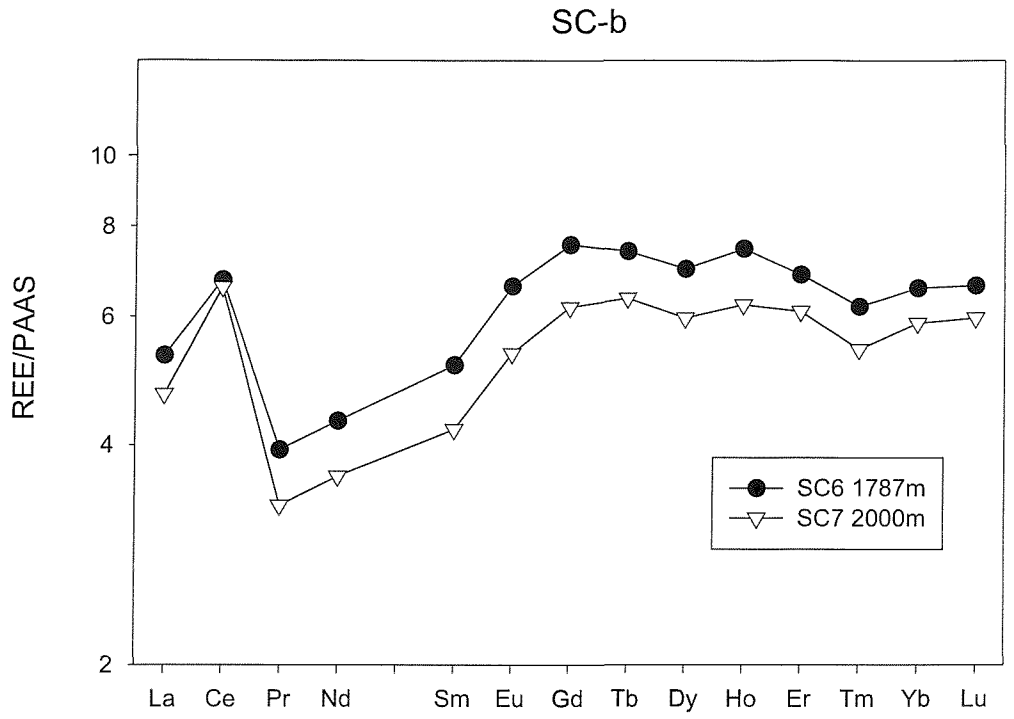

(d)

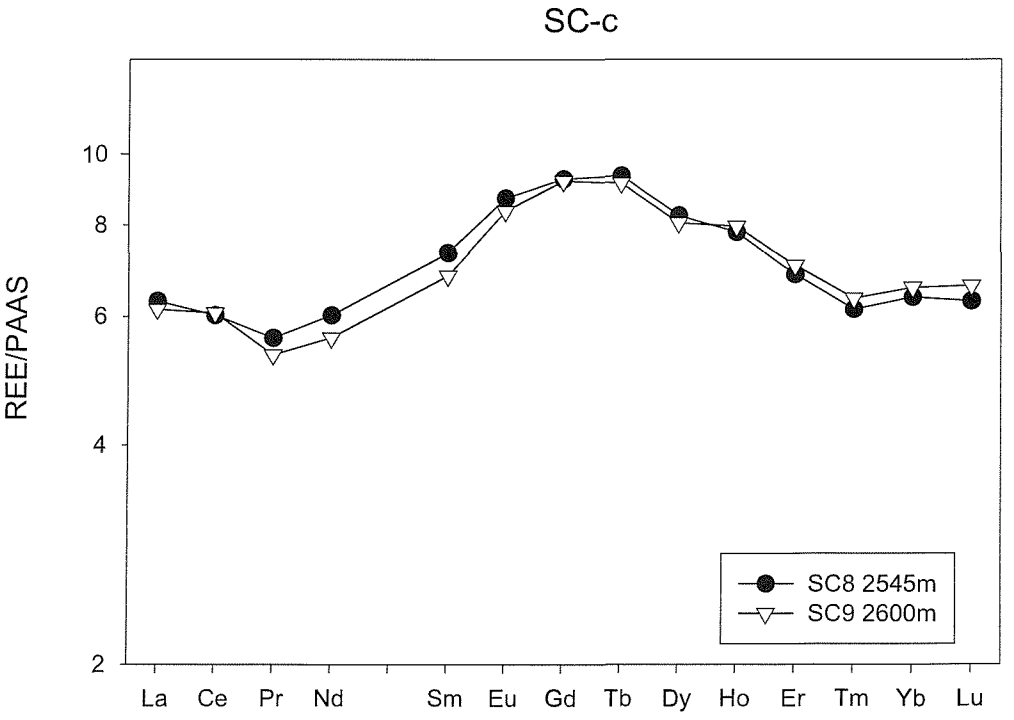

Fig. 4.2 (cont.)

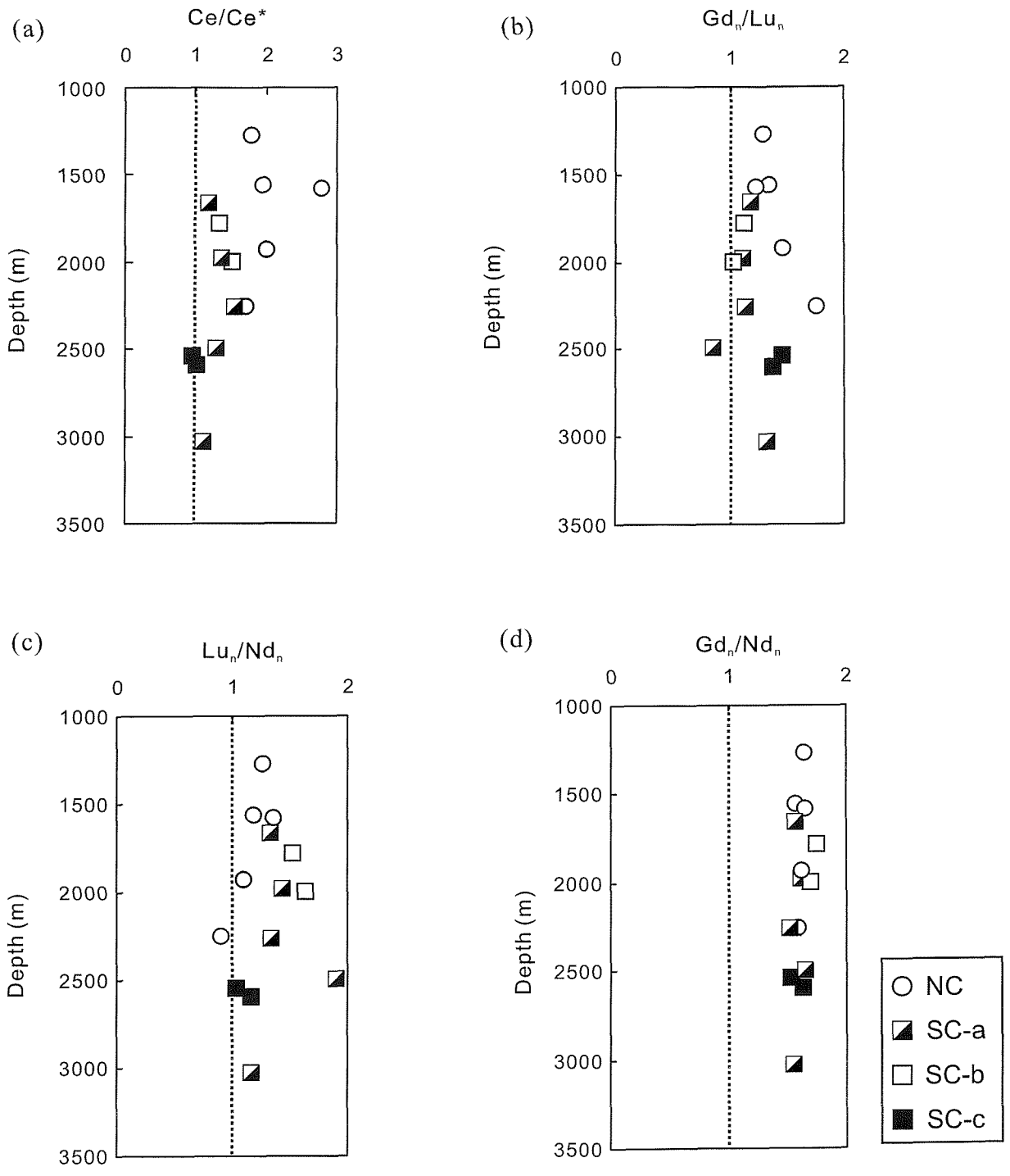

Fig. 4.3 (a) Ce/Ce* and normalised ratios of (b) Gd/Lu (MREE/HREE) (c) Lu/Nd (HREE/LREE) and (d) Gd/Nd (MREE/LREE) of surface Fe-Mn crusts.

4-4-2 Nd and Hf isotopic compositions

Nd and Hf isotopic compositions of the surface Fe-Mn crusts are listed in Table 4.2 and plotted against depths in Fig. 4.4. Nd isotope ratios, expressed as ε_{Nd} as relative deviation of the $^{143}Nd/^{144}Nd$ ratio from the chondritic ratio in parts in 10^4. Similar notation is also applied to $^{176}Hf/^{177}Hf$ as ε_{Hf}. The ε_{Nd} values range between –2.2 and –3.7, whereas the ε_{Hf} values vary from 4.2 to 7.5. Two Fe-Mn crusts published previously (designated as diamond symbols in Fig. 4.4. D11-1: 1800m; 11°39N, 161°41E and CD29-2: 2300m; 16°42N, 168°14W. Locations see Fig. 4.1 and 5.1) are compared here as they were collected near to the NC group of this study.

NC, SC-a and SC-b&c formed three decreasing trends with increasing water depths in a tight range (Fig. 4.4). The ε_{Nd} values of two literature samples (Ling *et al.*, 1997) are consistent with the NC trend (open circle). The ε_{Nd} signature profiles from the Fe-Mn crust-tops follow the same trend of that from NW Pacific seawater (dash line in Fig. 4.4, after Piepgras and Jacobsen, 1988; Shimizu *et al.*, 1994) but exhibit more radiogenic signatures.

ε_{Hf} values from the surfaces of the crusts generate two groups with rather similar patterns. Both show a pronounced radiogenic trend at about 2000m with the SC-a group having higher ε_{Hf} values. Two literatures samples, D11-1 and CD29-2 (David *et al.*, 2001), also follow the ε_{Hf} trend.

Table 4.2 Fe-Mn crusts locations and their Nd and Hf isotopic sompositions

Sample	Depth (m)	$^{143}Nd/^{144}Nd \pm 2se$ [(a)]	$\varepsilon_{Nd}(0)$ [(b)]	$^{176}Hf/^{177}Hf \pm 2se$ [(c)]	$\varepsilon_{Hf}(0)$ [(d)]
NCP					
NC1	1275	0.512523 ± 5	-2.24 ± 0.14	0.282915 ± 21	5.05 ± 0.74
NC2	1565	0.512511 ± 5	-2.47 ± 0.14	0.282927 ± 08	5.48 ± 0.28
NC3	1585	0.512518 ± 5	-2.33 ± 0.14	0.282933 ± 06	5.70 ± 0.20
NC4	1930	0.512485 ± 6	-2.98 ± 0.16	0.282947 ± 06	6.18 ± 0.20
NC5	2255	0.512476 ± 5	-3.15 ± 0.14	0.282932 ± 18	5.65 ± 0.62
SCP-1					
SC1	1664	0.512496 ± 6	-2.76 ± 0.16	0.282953 ± 21	6.40 ± 0.74
SC2	1984	0.512504 ± 6	-2.61 ± 0.16	0.282980 ± 19	7.36 ± 0.66
SC3	2260	0.512484 ± 5	-3.00 ± 0.14	0.282984 ± 05	7.49 ± 0.16
SC4	2500	0.512507 ± 5	-2.55 ± 0.14	0.282945 ± 24	6.10 ± 0.84
SC5	3033	0.512454 ± 5	-3.58 ± 0.14	0.282936 ± 11	5.80 ± 0.38
SC5 (bis)				0.282938 ± 19	5.88 ± 0.66
SCP-2					
SC6	1787	0.512507 ± 5	-2.55 ± 0.14	0.282933 ± 06	5.71 ± 0.20
SC7	2000	0.512508 ± 9	-2.53 ± 0.14	0.282944 ± 06	6.07 ± 0.20
SCP-3					
SC8	2545	0.512451 ± 5	-3.64 ± 0.14	0.282909 ± 06	4.84 ± 0.21
SC9	2600	0.512447 ± 5	-3.72 ± 0.14	0.282892 ± 06	4.24 ± 0.20

(a) The average of Nd standard, JNdi = 0.512104 ± 8 (2sd, n=21) and normalised $^{143}Nd/^{144}Nd$ are reported to recommended values of 0.512115.

(b) $\varepsilon_{Nd(0)}=[(^{143}Nd/^{144}Nd)_{sample}/(^{143}Nd/^{144}Nd)_{CHUR}-1]\times10^4$, where $(^{143}Nd/^{144}Nd)_{CHUR}=0.512638$. Reported error are in-run 2se.

(c) Average Hf JMC 475 standard yields an average of $^{176}Hf/^{177}Hf=0.282163 \pm 26$ (2sd, n=79). $^{176}Hf/^{177}Hf$ values are reported relative to 0.282160 for JMC475.

(d) $\varepsilon_{Hf(0)}=[(^{176}Hf/^{177}Hf)_{sample}/(^{176}Hf/^{177}Hf)_{CHUR}-1]\times10^4$, where $(^{176}Hf/^{177}Hf)_{CHUR}=0.282772$.

(e) Hf value was collected from crust depth of 0.5 -1 mm, equivalent of age= 0.14 Ma.

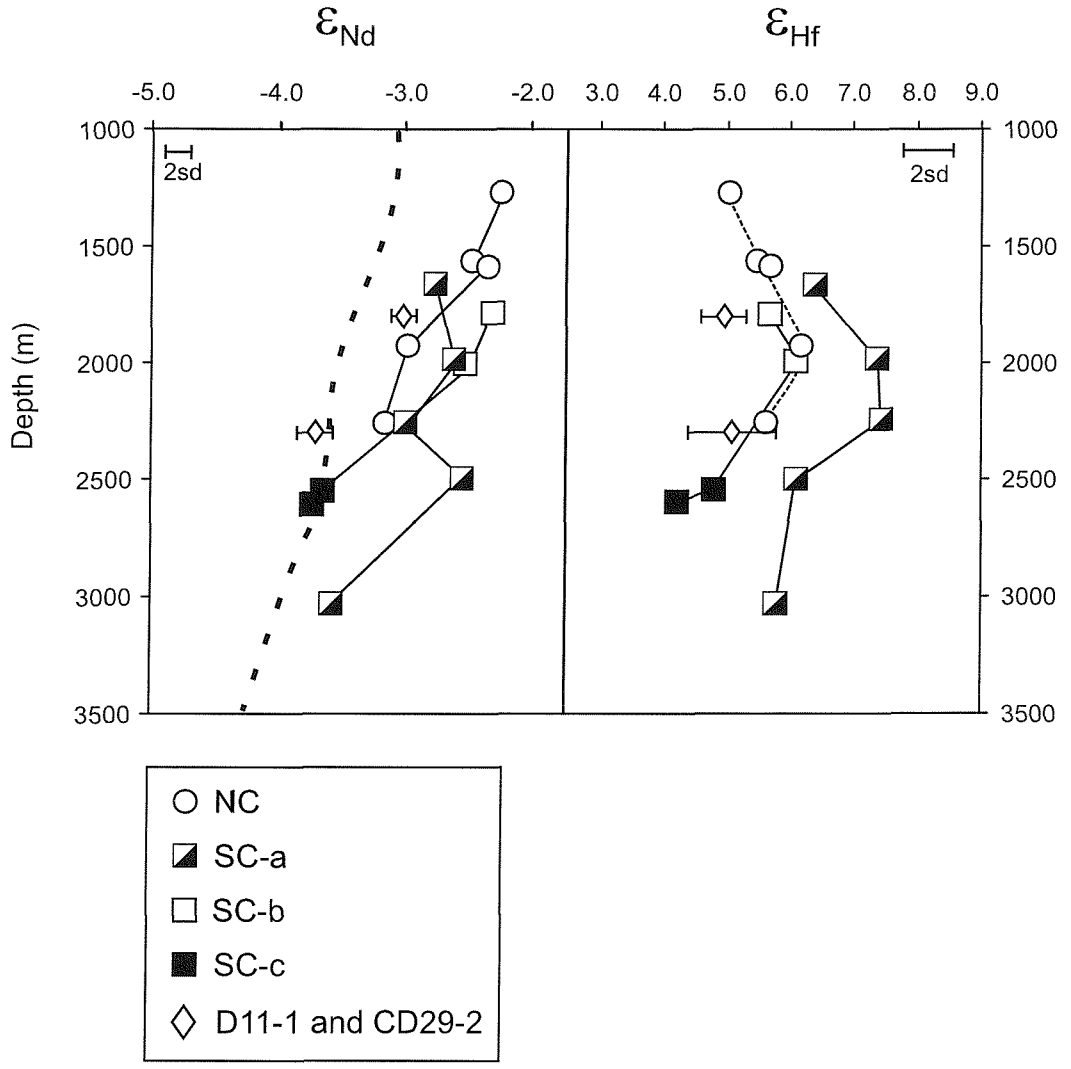

Fig. 4.4 Surface Fe-Mn crusts Nd and Hf isotopic compositions. Dash line in the ε_{Nd} plot is the seawater ε_{Nd} composition of NW Pacific (Piepgras and Jacobson, 1988 and Shimizu *et al.*, 1994). Diamond symbols are two literature crusts (Ling *et al.*, 1997; David *et al.*, 2001)

4-4-3 Detrital fraction REEs and Hf isotopes

The REE compositions of the detrital fractions leached from surface Fe-Mn crusts are listed in Table 4.3. The shale normalised REE patterns of the detritus (Fig. 4.5) are entirely different to that of the host ferromanganese oxyhydroxide phase (Fig. 4.2) and show HREE enrichment and Eu anomaly similar to adjacent pelagic sediment (Toyoda *et al.*, 1990). However, although the patterns of detrital fraction and sediment are similar, the pelagic sediment clearly has higher concentration of the REE.

In terms of Hf concentrations the detrital fractions vary over a wide range, from 3-60 ppm (Table 4.3) whilst their variation in Hf isotopic compositions (between 5 and 6) is smaller (Fig. 4.6). Fig 4.6 shows a plot of ε_{Hf} for the leachates (=Fe-Mn crust) and the detrital fractions, where the 1:1 solid line defines whether the detrital ε_{Hf} is larger (left) or smaller (right) than the leachate ε_{Hf}. Whilst sub-samples from individual sites (NC, SC-a, b& c) plot close together on this figure, there does not appear to be any systematic trend as a result of detrital fraction removal. It is apparent, however, that the Hf isotopic compositions of Fe-Mn oxides (seawater signatures) are nearly 4 times more variable than the included detritus.

Table 4.3 REE concentrations in the detrital fraction of surface Fe-Mn crusts (ppm)

Sample	La	Ce	Pr	Nd	Sm	Eu	Gd	Tb	Dy	Ho	Er	Tm	Yb	Lu
NCP														
D-NC1	0.338	0.690	0.064	0.212	0.034	0.017	0.034	0.007	0.056	0.014	0.046	0.007	0.050	0.008
D-NC2	2.387	4.608	0.439	1.454	0.233	0.091	0.225	0.049	0.384	0.096	0.307	0.046	0.353	0.057
D-NC3	1.256	2.755	0.307	1.147	0.195	0.069	0.166	0.028	0.189	0.042	0.125	0.018	0.126	0.021
D-NC4	2.257	4.348	0.407	1.424	0.239	0.111	0.225	0.045	0.350	0.083	0.274	0.040	0.305	0.050
D-NC5	2.925	5.405	0.518	1.685	0.269	0.140	0.244	0.056	0.425	0.105	0.342	0.051	0.395	0.064
SCP-a														
D-SC1	0.258	0.620	0.050	0.192	0.038	0.014	0.081	0.016	0.050	0.011	0.039	0.005	0.027	0.007
D-SC2	0.107	0.209	0.020	0.075	0.014	0.006	0.015	0.003	0.023	0.005	0.020	0.003	0.018	0.003
D-SC3	0.045	0.101	0.009	0.031	0.005	0.002	0.006	0.001	0.009	0.002	0.007	0.001	0.009	0.001
D-SC4	0.113	0.187	0.018	0.063	0.011	0.011	0.012	0.002	0.016	0.003	0.013	0.002	0.013	0.002
D-SC5	0.077	0.164	0.014	0.053	0.010	0.005	0.011	0.002	0.012	0.003	0.010	0.001	0.008	0.002
SCP-b														
D-SC6	0.246	0.565	0.047	0.171	0.031	0.011	0.031	0.005	0.040	0.009	0.029	0.004	0.026	0.005
D-SC7	0.164	0.317	0.035	0.140	0.031	0.015	0.027	0.004	0.029	0.006	0.018	0.003	0.019	0.003
SCP-c														
D-SC8	0.071	0.140	0.014	0.056	0.012	0.008	0.012	0.002	0.014	0.004	0.011	0.002	0.011	0.002
D-SC9	0.167	0.272	0.029	0.112	0.023	0.024	0.023	0.004	0.027	0.006	0.019	0.003	0.018	0.003

Table 4.4 Hf isotopic somposition of detrital fractions

Sample	Depth (m)	Hf (ppm)	$^{176}Hf/^{177}Hf \pm 2se$ [(a)]	$\varepsilon_{Hf}(0)$ [(b)]
NCP				
D-NC1	1275	11.8	0.282941 ± 4	5.97 ± 0.14
D-NC2	1565	65.6	0.282944 ± 5	6.08 ± 0.16
D-NC3	1585	19.6	0.282916 ± 9	5.07 ± 0.32
D-NC4	1930	49.3	0.282950 ± 5	6.28 ± 0.18
D-NC5	2255	56.5	0.282940 ± 6	5.92 ± 0.22
SCP-1				
D-SC1	1664	56.3	0.282935 ± 5	5.75 ± 0.18
D-SC2	1984	14.9	0.282925 ± 5	5.42 ± 0.18
D-SC3	2260	2.8	0.282911 ± 8	4.90 ± 0.28
D-SC4	2500	8.6	0.282922 ± 7	5.31 ± 0.26
D-SC5	3033	8.4	0.282914 ± 3	5.03 ± 0.12
D-SC5 (bis)*			0.282915 ± 5	5.04 ± 0.16
SCP-2				
D-SC6	1787	26.6	0.282936 ± 8	5.81 ± 0.30
D-SC7	2000	9.4	0.282933 ± 4	5.68 ± 0.14
SCP-3				
D-SC8	2545	5.9	0.282912 ± 3	4.96 ± 0.12
D-SC9	2600	12.1	0.282915 ± 5	5.04 ± 0.16
IB				
D-IB1	1860	5.9	0.282930 ± 4	5.59 ± 0.15
D-IB2	2600	5.4	0.282916 ± 5	5.09 ± 0.16

(a) $^{176}Hf/^{177}Hf$ values are reported relative to 0.282160 for JMC475.

(b) $\varepsilon_{Hf(0)}=[(^{176}Hf/^{177}Hf)_{sample}/(^{176}Hf/^{177}Hf)_{CHUR}-1]\times10^4$, where $(^{176}Hf/^{177}Hf)_{CHUR}=0.282772$.

*Duplicates of D-SC5

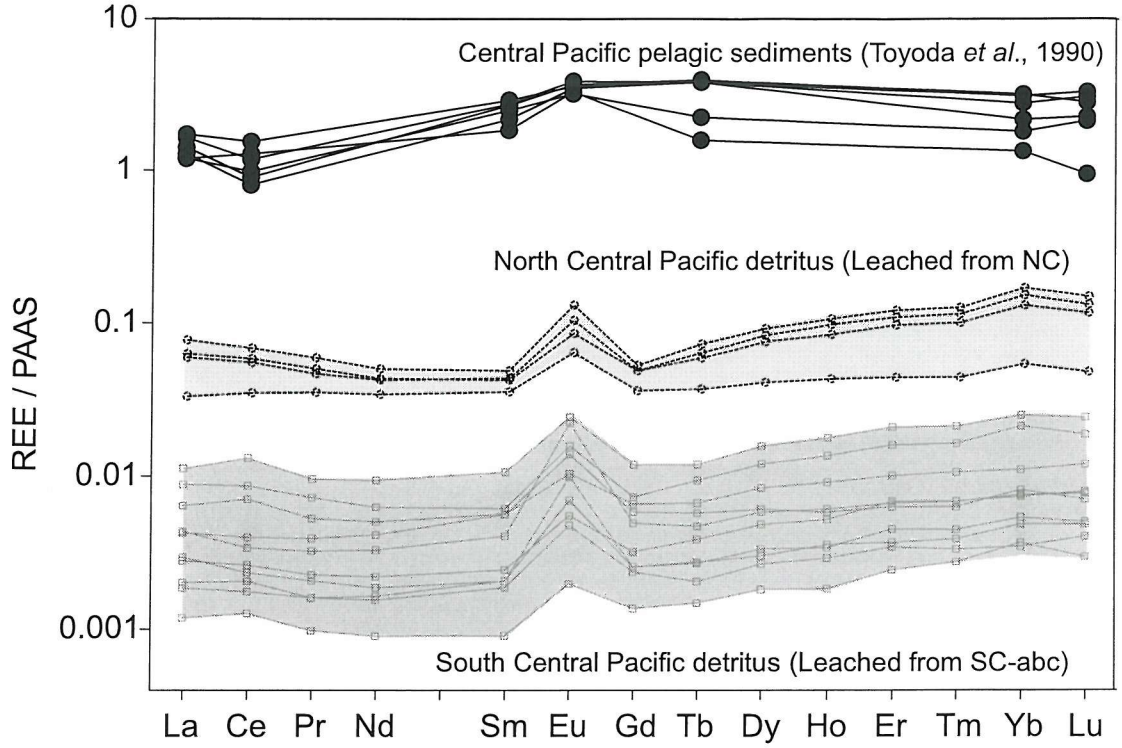

Fig. 4.5 Shale normalised REE patterns of detritus fraction separated from surface Fe-Mn crusts. Patterned squares are the pelagic sediment from Toyoda *et al.* (1990).

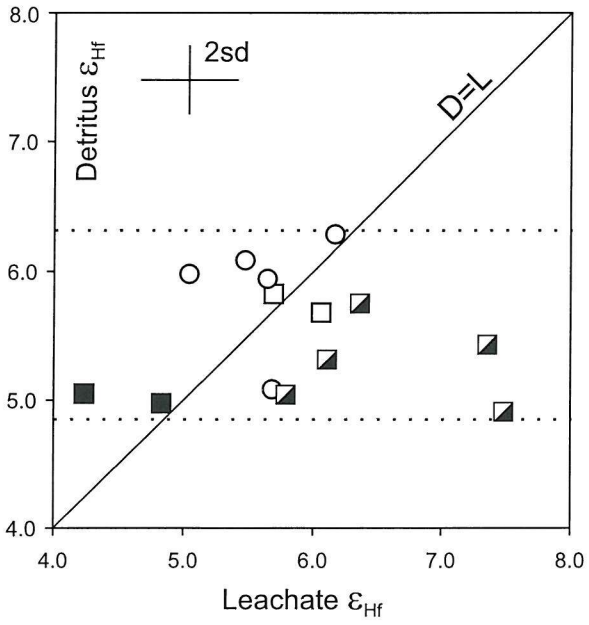

Fig. 4.6 ε_{Hf} vs ε_{Nd} of Fe-Mn oxyhydroxide and detrital fraction from surface Fe-Mn crusts.

4-5 Discussion

4-5-1 Detritus contamination in Fe-Mn crusts

Typically the Hf concentration of a Fe-Mn crust is less than 10 ppm whilst the value for the detrital fraction is highly dependent on the amount present as well as the nature of the silicate fraction in the detritus. What is clear from Fig. 4.6 is the variation in ε_{Hf} between coexisting Fe-Mn crust and detrital fraction. From this it is evident that failure to remove the detrital fraction (which has no relation to seawater composition) from the Fe-Mn crust would lead to a series of systematic results. Because of the possibility of high concentrations of zircon (and therefore Hf) the disparity between the leached and combined leach plus detrital fraction can be expected to be greater when dealing with Hf isotopes. When dealing with Nd isotopes, the effect will be rather small because of the very high REE concentrations in the Fe-Mn crusts (with $Nd_{detritus}/Nd_{Fe\text{-}Mn\ oxides}>0.01$).

4-5-2 Elemental supply from REE and Nd isotope evidence

The oceanic budget of REE and Nd isotopes is controlled by riverine input and particle-water exchange (Goldstein and Jacobsen, 1987; Elderfield *et al.*, 1990; Bertram and Elderfield, 1993; Amakawa *et al.*, 2000; Lacan and Jeandel, 2001). It has been proposed that the major REE supply to the Central Pacific are either from dissolved riverine input of Papua New Guinea (PNG) (Sholkovitz *et al.*, 1999) or erosion and dissolution of the PNG volcanic materials on the continental slopes (Lacan and Jeandel, 2001). These authors propose that the equatorial current system is able to transport these signals into the Central Pacific water mass.

In order to directly compare two types of material: solid phase as in this study and dissolved phase as in the literature, one has to apply the seawater Fe-Mn oxide partitioning coefficients of Bau *et al.* (1996) and convert the unit from pmol/kg to ppm for seawater data. The shale-normalised dissolved riverine REE from PNG (Sholkovitz *et al.*, 1999) and adjacent seawater (Zhang and Nozaki, 1996) exhibit MREE enrichments and are consistent with REE patterns observed in the surface Fe-Mn crusts of this study (Fig. 4.7). The similarity of MREE enrichment, especially in terms of MREE/LREE fractionation, implies that the seawater below the equatorial current system may be affected by nearby island weathering input as the particles sink through the water column.

ε_{Nd} of surface samples decreases with increasing seawater depth (Fig. 4.4) consistent with unradiogenic input of AABW underneath (see Chapter 2). Seawater Nd isotopic profiles from NW Pacific (TPS39-1, 47°N, 161°08.2'E and TPS271-1, 24°17.2'N, 150°28.2'N, Piepgras and Jacobsen, 1988), consistent with IB surface samples, were chosen here for comparison. The higher ε_{Nd} values of the Central Pacific Fe-Mn crust surface samples (Fig. 4.4), plus the REE evidence, suggest a young volcanic weathering input with radiogenic Nd signatures, possibly from the Papua New Guinea area, has contributed to the seawater in this region.

Theoretical Nd concentrations in Fe-Mn oxides precipitated from seawater (Piepgras and Jacobsen, 1988) were obtained by applying the partitioning coefficient values for seawater and Fe-Mn crusts (Bau *et al.*, 1996) to derive a 'NW Pacific seawater ε_{Nd} mixing line' (grey area in Fig. 4.8). The Nd isotopic compositions from the surficial Fe-Mn crusts in this study exhibit a pattern (with water depths marked next to the symbol, Fig. 4.8) that is offset from this 'seawater mixing line', with lower Nd concentrations and more radiogenic isotopic signatures. This offset is likely due to differences in seawater properties between these two locations (e.g. the previously discussed island arc weathering input in the Western Pacific Ocean).

From this trend, two end-members can be derived: the Intermediate Water (IW) and Pacific Deep Water (PDW). Note that the IW does not specifically indicate for NPIW or AAIW as described in Chapter 2 as the sample distribution covers both North and South of the Equators. A recent study proposed seawater ε_{Nd} values (Central Antarctic Intermediate Water, CAAIW) adjacent to this area (Lacan and Jeandel, 2001) of –2.1 and –3.4. Combining with the *Kd* modified Nd contents from E. PNG (Zhang and Nozaki, 1996), this represents *in situ* local Intermediate Water mass signature (marked as a 'plus' in Fig. 4.8). The data interestingly agrees with the derived IW end-member from the Fe-Mn crusts trend, suggesting some first level credibility in using this model. The same approach will be applied for Hf isotopic systems and is discussed in later section.

(a)

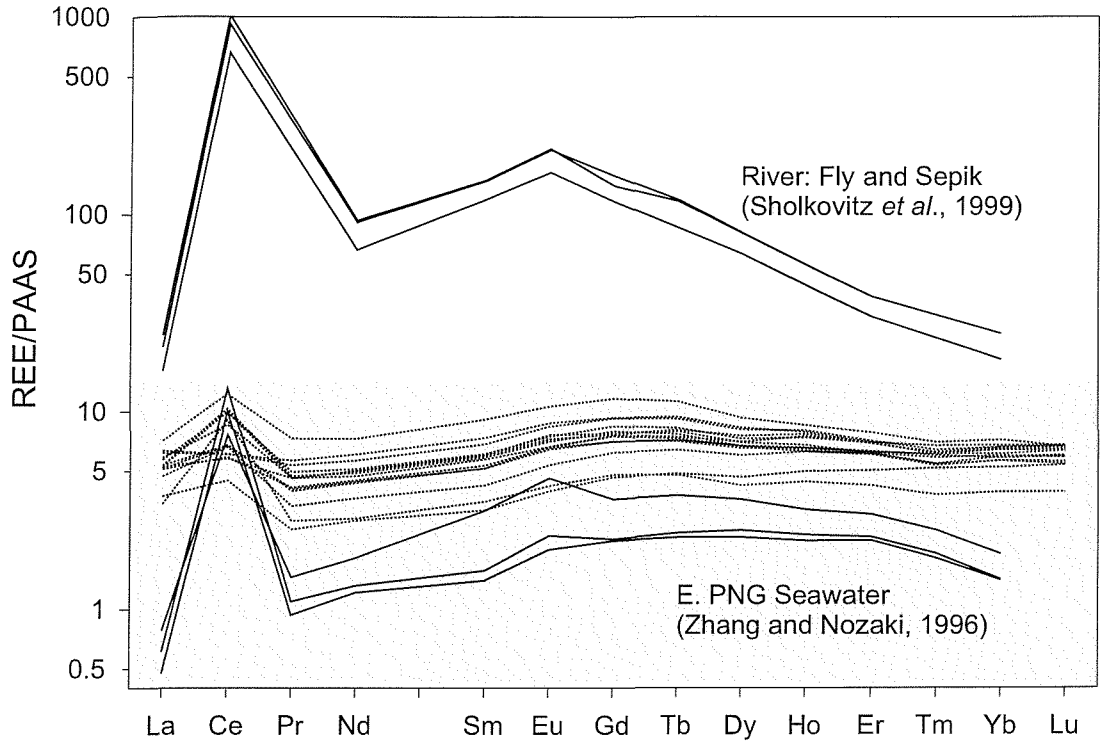

(b)

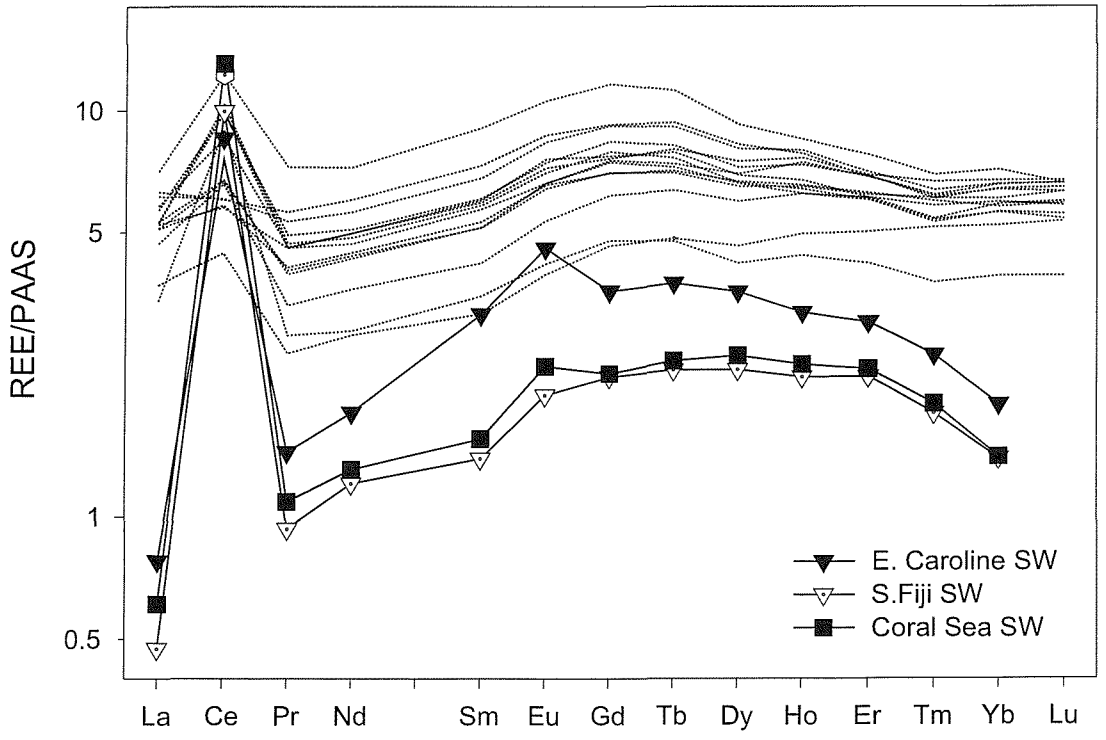

Fig. 4.7 (a) REE patterns of surface Fe-Mn crust (dotted lines, this study) and *Kd* modified (Bau *et al.*, 1996) PNG river (Sholkovitz *et al.*, 1999) and E. PNG seawater (Zhang and Nozaki, 1996). Grey area is magnified as the (b) seawater and surface Fe-Mn crusts REE patterns.

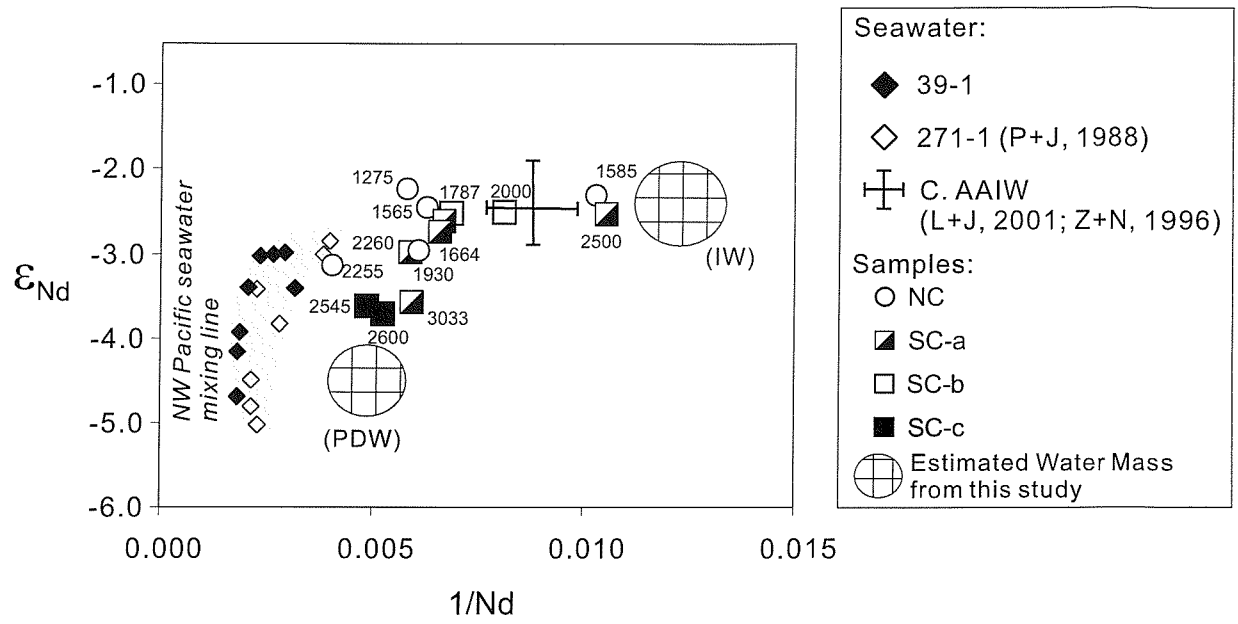

Fig. 4.8 Seawater mixing model by ε_{Nd} vs 1/Nd. The surface Fe-Mn crusts, representing present seawater compositions of the Central Pacific Ocean, compose a mixing trend similar to real seawater measurements (NW Pacific, Piepgras and Jacobsen, 1988). Further, the seawater ε_{Nd} and Nd concentration from the adjacent area (Lacan and Jeandel, 2001 and Zhang and Nozaki, 1996), proposed as Central Antarctic Intermediate Water (AAIW) by the authors, is close to the estimated Intermediate Water (IW) from this study Seawater data were modified by the *Kd* of Bau *et al.* (1996).

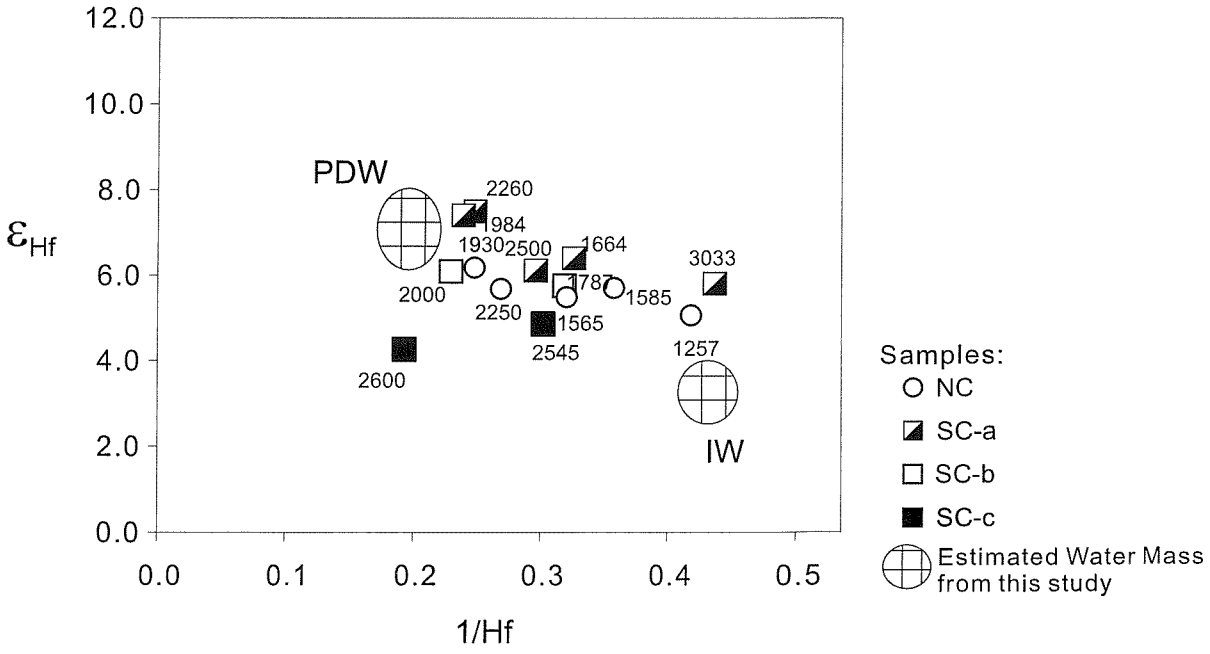

Fig. 4.9 ε_{Hf} vs 1/Hf plot of surface Fe-Mn crusts as the Central Pacific seawater Hf-model. Sample depths marked next to the symbols. Two water mass are estimated here following the Nd mixing model approach.

4-5-3 Hf isotope composition in the Pacific seawater derived from Fe-Mn crusts

As no direct seawater Hf isotopic measurements are available, an indirect method must be applied for inferring water mass Hf isotopic compositions. As demonstrated in the previous section for Nd isotopes, the proposed model can provide information on present seawater compositions. Similarily, Hf isotopic compositions from surface Fe-Mn crusts form a mixing line (Fig. 4.9). One end of this mixing trend extends toward the depth at ~ 2000 m, which correspond to the PDW in modern physical oceanography definition. The other end possibly indicates the Intermediate Water as the Hf concentrations of NC samples decreases with the depths towards this end-member. The deepest sample of this study, SC5 at 3033m, also exhibit a value close the IW end member and could possibly imply bottom water influences. Nevertheless, no samples from deeper locations allow us for further inversitigation.

4-5-4 Hydrological properties with Nd and Hf isotopic composition

In this study, the Fe-Mn crust surface isotopic results and the 'on-site' hydrology properties (Table 2.6) are directly compared in an attempt to evaluate the isotope behaviour of seawater. Comparison between ε_{Nd} of seawater and the hydrological properties have been applied in several studies (e.g. Piepgras and Wasserburg, 1987; Jeandel, 1993; Jeandel *et al.*, 1998). They show a good correlation of temperature, salinity and silicate content with ε_{Nd}, and suggest that Nd isotopes behave conservatively. In this study, the ε_{Nd} of surface Fe-Mn crusts are well correlated with the sample site hydrological properties (Fig. 4.10) which further reassures the sampling has not averaged out the 'present seawater' signatures and Fe-Mn crust growth is closely related to the ambient seawater properties.

In comparison to ε_{Nd}, ε_{Hf} has a much less pronounced correlation with hydrological properties. As Fig 4.10 shows, there is very little variation of ε_{Hf} irrespective of the physical or nutrient properties of seawater. This behaviour, which contrasts to that of Nd, suggests that the residence time of Hf is apparently longer than Nd.

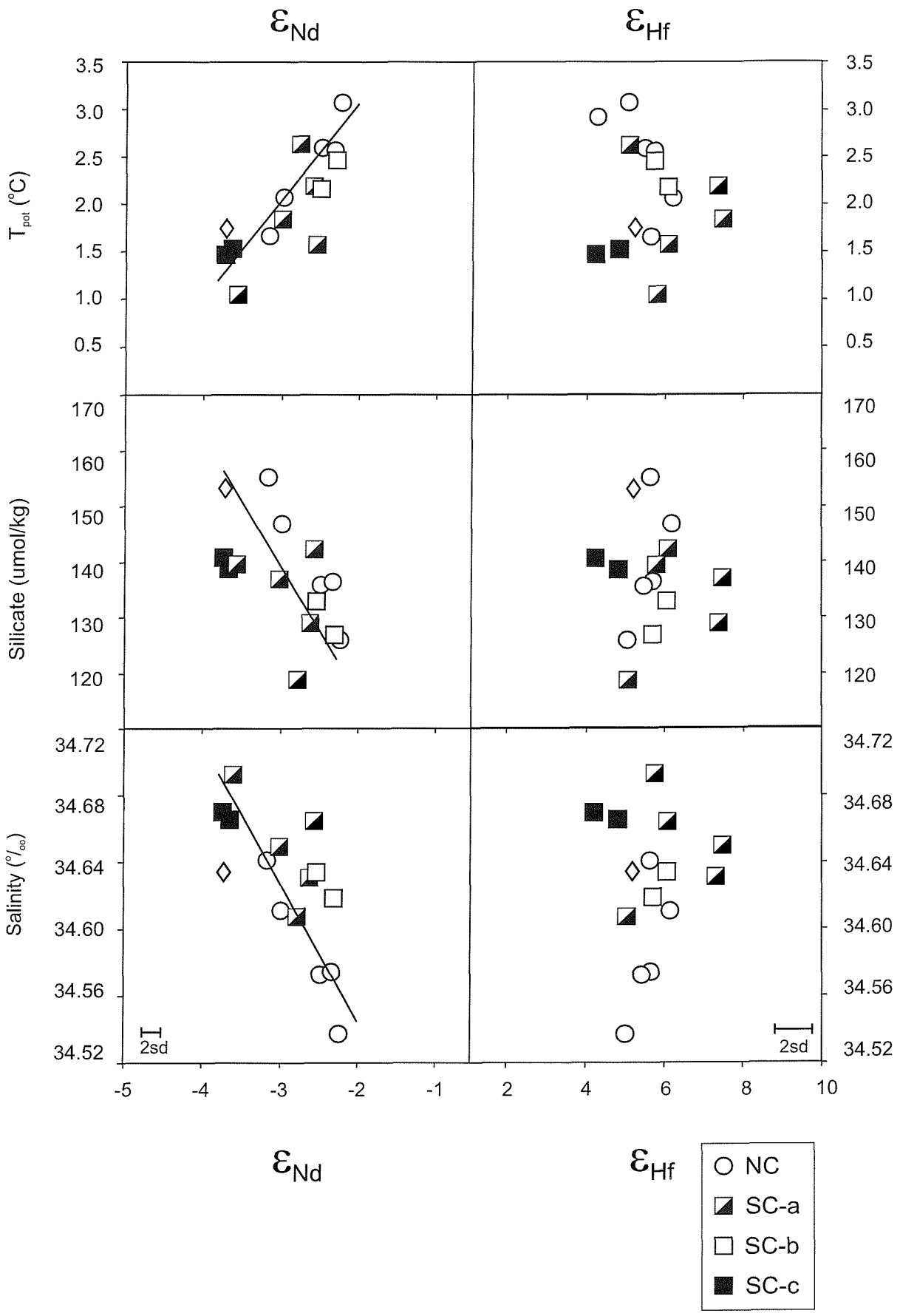

Fig. 4.10 Surface Fe-Mn crusts Nd and Hf isotopic compositions with physical and nutrient tracers on sites where samples were collected (see Table 2.6).

4-6 Conclusions

The distinct characters of REE and Hf isotopic values in the detritus fraction, separated from hydrogenetic components, suggest that careful chemical digestion treatment is important to remove this detrital contamination when inferring seawater signatures. Surface Fe-Mn crusts were carefully sampled to reconstruct the present day seawater column composition. When comparing Nd isotopic compositions with derived 'on-site' hydrology properties, it is clear that the Nd isotopic compositions of surface Fe-Mn crusts are controlled by the nature of the water masses. The REE patterns and Nd isotope results suggest that there is a contribution from the weathering products of nearby volcanic islands, possibly from the Papua New Guinea.

Hf isotopic compositions show insignificant correlations with hydrological property comparisons, confirming a longer residence time of Hf than Nd in seawater. Hf isotopic compositions in two water masses of the Central Pacific are proposed from the depth profiles and mixing model inferred from the surface Fe-Mn crusts: the IW has the ε_{Hf} value between 3-4 and the PDW between 6-7.

Chapter 5. Secular variation of Hf, Nd and Pb isotopes in the Central and Western Pacific Ocean, as recorded in Fe-Mn crusts

5-1 Abstract

Radiogenic isotope distributions have been investigated in three Fe-Mn crusts for time series studies of South-Central Equatorial Pacific (SCP) and Izu-Bonin Back Arc Basin (IB) seawater compositions. The geochemical results for the South-Central Pacific crust agree with previously published North-Central Pacific Fe-Mn crust studies over the past 5 Ma. A shift to more unradiogenic values is observed at 5.5Ma in this South-Central Pacific crust, however, consistent with an increased input from the Southern Ocean to this site, at that time. The Pb isotope distributions in the two Izu-Bonin Fe-Mn crusts are quite different from those observed in the Central Pacific. Those data are indicative of (a) two-component mixing between W. Pacific volcanic and aeolian dust sources and (b) efficient transport of Pb by the Kuroshio Current, which delivers a characteristic Ryukyu/Okinawa Trough signature to the IB crusts. Constrained by the evidence provided from Pb isotope systematics, two causes could be responsible for a decoupling which is observed between the Nd and Hf isotopic profiles of both IB crusts at around 4 Ma: (1) hydrothermal inputs and (2) weathering effects. Mechanisms by which this could be achieved include: (a) Hf, unlike Nd, may be relatively un-reactive in hydrothermal plumes, leading to a more significant dissolved hydrothermal Hf flux to the local deep waters, unaccompanied by Nd; (b) because the Nd/Hf value in seawater is almost an order of magnitude greater than that in volcanic rocks, local dissolution of a minor component of fresh young volcanic rocks could potentially perturb the local Hf isotopic composition of IB seawater without having any equivalent impact upon the local Nd isotopic budget. While the above interpretations are all consistent with the data presented, those same data are insufficient to constrain one single unequivocal interpretation.

5-2 Introduction

Several sources account for the radiogenic isotopic tracer distributions of the modern open ocean: continental weathering and riverine, aeolian and hydrothermal inputs. In cases where the oceanic residence time of an element is short relative to ocean mixing, the isotopic composition of that element can be used to record inter-basin variations and, hence, to investigate circulation and/or source/input variations.

Nd isotopes: Previous studies have shown that different water masses exhibit distinct Nd isotope signatures (e.g. Piepgras *et al.*, 1979, Chapter 4 and references therein), which are related to the weathering of Nd from different types and ages of continental crust. For example, the Pacific Ocean, surrounded by island-arcs, exhibits more radiogenic seawater ε_{Nd} values than the "continent-bounded" Atlantic Ocean. It is evident that these systematic variations in Nd isotope distributions in the ocean should not be contributed to significantly by submarine hydrothermal fluxes because, although hydrothermal vent-fluids are very enriched in REE (e.g. Klinkhammer *et al.*, 1994) it is known that the REE released are scavenged very efficiently back from seawater, very close to their sources (German *et al.*, 1990; Sherrell *et al.*, 1999; Edmonds and German, 2003). While weathering fluxes should dominate the Nd isotopic composition of the oceans, however, the relative contributions from aeolian and riverine inputs to provide this flux remain unclear. For example, Jones *et al.* (1994; 2000) suggested that the influence of aeolian sources upon dissolved Nd budgets should be minor compared to riverine runoff. By contrast, Pettke et al. (2002) have argued that the long-term trend of decreasing ε_{Nd} that has been observed in both sediments and Fe-Mn crusts over the past 3 Ma is entirely consistent with a ten-fold increase of aeolian input over the same time-frame, suggesting that dust-bound Nd can contribute an important fraction of the total dissolved Nd budget in the Pacific Ocean. (NB The latter argument holds only if one discounts the potential influence of intensifying NADW input over the same period (Frank *et al.*, 2002b).

Pb isotopes: The residence time of Pb (<100 yrs, Schaule and Patterson, 1981; Henderson and Maier-Reimer, 2002) is an order of magnitude shorter than Nd (600-2000 yr, Jeandel, 1993; Jeandel *et al.*, 1995; Tachikawa *et al.*, 1999); therefore, the Pb isotopic signatures recorded in the oceans, e.g. in Fe-Mn crusts, are much more indicative of variations in local influences than is the case for Nd. Aeolian sources

have previously been suggested to provide an important component of the Pb input to the ocean, particularly in areas characterised by low hemipelagic fluxes and/or slow deep-water advection rates (Jones *et al.*, 2000; Godfrey, 2002). However, Pettke *et al.* (2002) have argued that the exchangeable Pb adhering to dust in the leach experiments conducted by Jones *et al.* (2000) may have derived from volcanic aerosol. This, in turn, is more consistent with the fact that the preanthropogenic Pb isotopic signature of the Pacific Ocean is very similar to that of the island arcs surrounding this ocean basin (von Blanckenburg *et al.*, 1996b). In their model, von Blanckenburg and Igel (1999) indicate that efficient thermocline mixing should render island arc sources responsible for controlling the dissolved Pb isotope budget of the Pacific Ocean.

Fractionation of Pb isotopes can occur during weathering of ancient (e.g. cratonic) continental rocks in which case they are known to release an incongruently radiogenic fraction (Erel *et al.*, 1994; Harlavan *et al.*, 1998; Jones *et al.*, 2000), such that the dissolved Pb isotopic composition of the ocean may not directly reflect the isotopic composition of the source rocks from the surrounding continents (von Blanckenburg and Nägler, 2001) or may not reflect the aeolian sources by its bulk compositions (Jones *et al.*, 2000; Godfrey, 2002).

Another possible source of dissolved Pb to the deep-oceans is from sediment-water interactions (Vlastélic *et al.*, 2001; van de Flierdt *et al.*, 2003), similar to the mechanism invoked for remobilisation of Nd from continental slope sediments (Lacan and Jeandel, 2001). Like Nd, Pb is enriched in seafloor hydrothermal vent fluids (German and Von Damm, 2003). However, Pb precipitates rapidly in near-field hydrothermal systems (e.g. Mottl and McConachy, 1990; German *et al.*, 2002). Near-field sediments show that this precipitation removes most of the hydrothermal Pb at this stage (Godfrey *et al.*, 1994; German *et al.*, 1999) while ridge-flank metalliferous sediments show a mixing between seawater and basaltic/hydrothermal components (e.g. Barrett *et al.*, 1987; German *et al.*, 1997) indicating further scavenging of dissolved Pb from seawater (see also Godfrey *et al.*, 1994). This absence of any significant large-scale hydrothermal source is further supported by two observations: (*i*) the isotopic homogeneity of Pacific Pb is inconsistent with geographically variable (hydrothermal) sources of MORB-like Pb (von Blanckenburg *et al.*, 1996b) (*ii*) only a

few nodules, located very close to mid-ocean ridges show, significant "MORB" Pb signatures (Abouchami and Goldstein, 1995).

Hf isotopes: The importance of various sources in controlling the dissolved Hf isotope composition of the ocean remains unclear at the present, mainly because direct measurements of seawater Hf isotopes have not yet been achieved. What has been demonstrated, however, from Fe-Mn crust and nodule data, is that marked, incongruent weathering exerts a significant influence upon the dissolved Hf isotopic composition of seawater. Weathering-resistant zircons, which are concentrated into the coarse, sand fraction of continental and near-shore marine sediments or turbidites, exhibit low Lu/Hf ratios, leading to low $^{176}Hf/^{177}Hf$ ratios, causing a fractionation between the marine Nd and Hf isotopic systems (Albarède *et al.*, 1998, Fig. 1.2b). In addition to this zircon effect, it has been suggested that hydrothermal contributions may also play an important role in the dissolved Hf budget of the ocean (White *et al.*, 1986; Godfrey *et al.*, 1997). However, direct vent fluid or near-field sediment Hf measurements are still absent from the literature and first riverine source data also remain unavailable to-date.

Previous time series studies of Nd, Pb and Hf isotope records in three North-Central Pacific Fe-Mn crusts, CD29-2, D11-1 and VA13-2 (Christensen *et al.*, 1997; Ling *et al.*, 1997; Lee *et al.*, 1998; David *et al.*, 2001), show a well-characterised pattern of Pacific deep-water mixing over the past 10 Ma. In detail, a constant offset in Nd isotopic compositions by about 1 ε_{Nd} unit is observed between the signature of Anatarctic bottom water (AABW) as recorded by crust VA13/2 (collected at 4800 m depth in the Eastern Pacific at 9°25'N, 146°03'W) and shallower Pacific Deep Water as recorded by crusts CD29-2 and D11-1 (2300 m, 16°42'N, 168°14'N and 1800 m 11°39'N, 161°41'N). It is interpreted that this offset is probably caused by a long-standing advection to this VA13/2 site from some Circum-Antarctic water mass (CDW) which exhibits a consistently lower (more terrigeneous) Nd isotope ratio than the overlying central Pacific Deep Water (Ling *et al.*, 1997). Unlike Nd, the Pb isotope records of all three crusts are very similar throughout the past 10 Ma, indicating an extremely homogenous isotopic composition for all inputs to the central Pacific Ocean and/or an efficient mixing and homogenisation of Pb derived from varying input sources to the Pacific, despite its relatively short oceanic residence time (von Blanckenburg *et al.*, 1996b; Abouchami *et al.*, 1997; Christensen *et al.*, 1997;

Ling *et al.*, 1997). A similar interpretation was derived for Hf isotopes - that the Central Pacific seawater has been very well mixed more than 10 Ma (Lee *et al.*, 1998; David *et al.*, 2001). Island arc weathering, especially prior to 5 Ma, is thought to have controlled these isotopic compositions in the Equatorial Pacific (von Blanckenburg *et al.*, 1996b; David *et al.*, 2001; Frank, 2002) contributing radiogenic Nd and Hf and unradiogenic Pb. Since 5 Ma, the most likely cause of the observed changes (slightly decreasing Nd and increasing Pb isotope ratios) would appear to be an increase in aeolian (loess) inputs (Pettke *et al.*, 2002a), consistent with the order-of-magnitude increase in Asian dust input reported to have occurred at around 3 Ma (Duce *et al.*, 1991; Rea, 1994).

In this study, one crust from the deep (~3000m) South Central Pacific (SC5; Fig. 5.1) just 2500 km south of CD29-2, has been analysed, together with two samples (IB1 and IB2) from ~1800m and ~2600m water depth in the Izu-Bonin Back-Arc Basin, a location previously univestigated in terms of Fe-Mn crust, time-series radiogenic isotopic compositions. The objectives of this chapter are: (1) to compare variations in South-Central Equatorial Pacific (SC5) seawater's radiogenic isotopic composition variation through time with data from the previously reported North-Central Pacific; (2) to observe and understand the radiogenic isotope budgets of a semi-enclosed back-arc basin, a region quite different from that of the open ocean, and one where past hydrothermal events have also been reported.

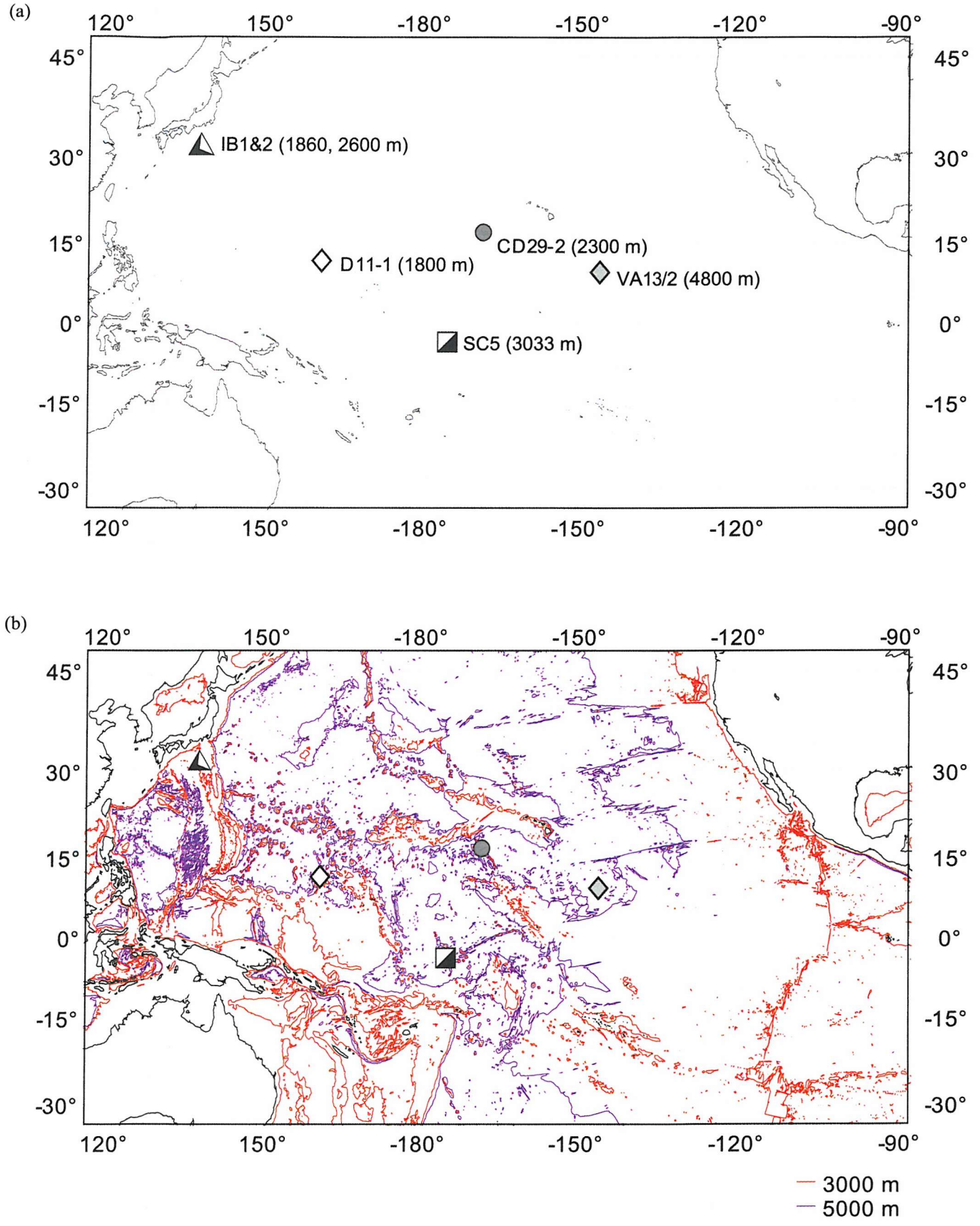

Fig. 5.1 (a) Locations of samples and three previously reported Fe-Mn crusts with their recovering depth in brackets.(b) Contour map with 3000 (red) and 5000 (blue) water depth. Coutour data from General Bathymetric Chart of the Oceans (GEBCO).

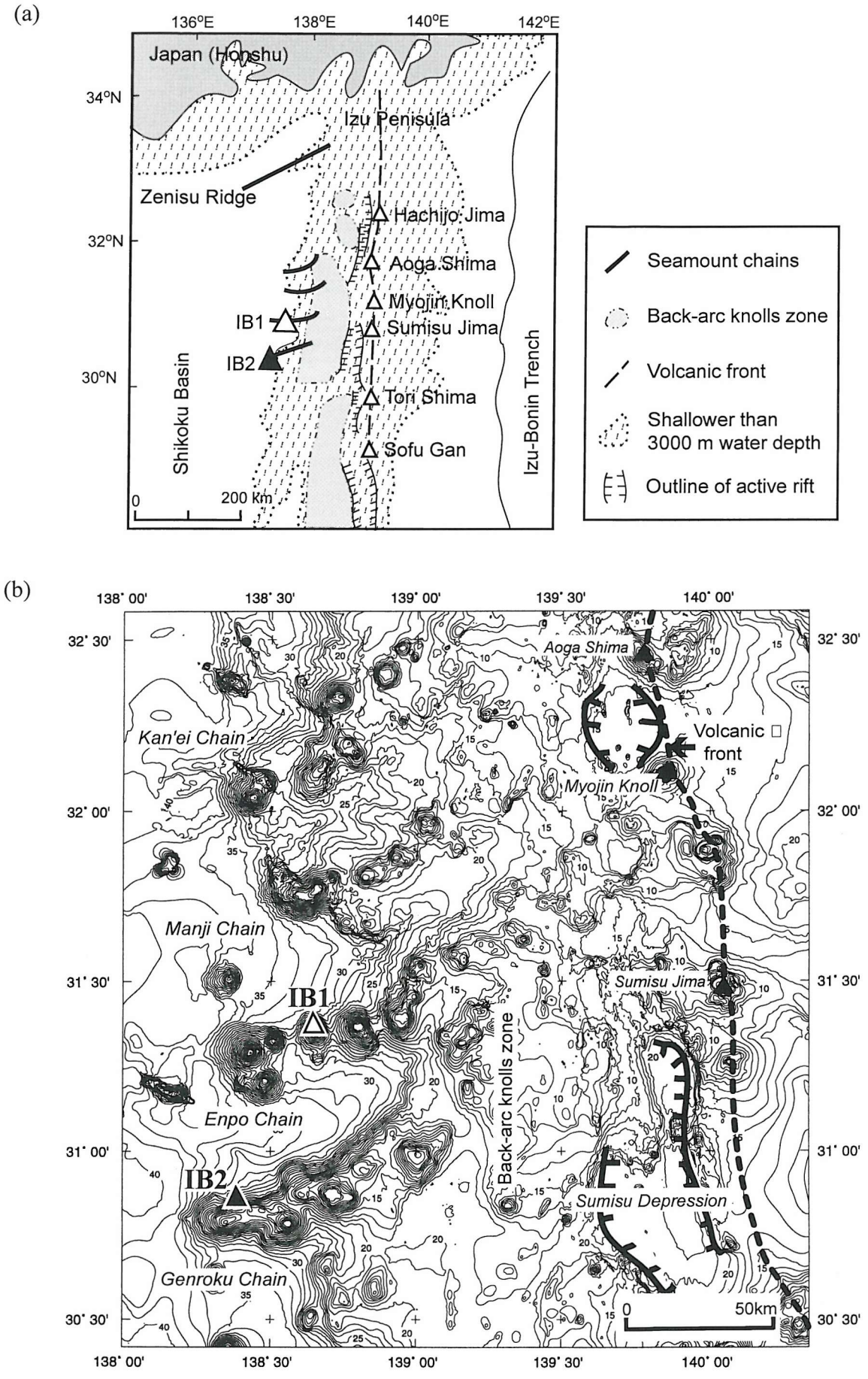

Fig. 5.2 (a) Schematic map of the Izu-Bonin Arc area and (b) Bathymetric map of the middle part of the Izu-Bonin Arc. Sample locations are shown as open and solid triangles.

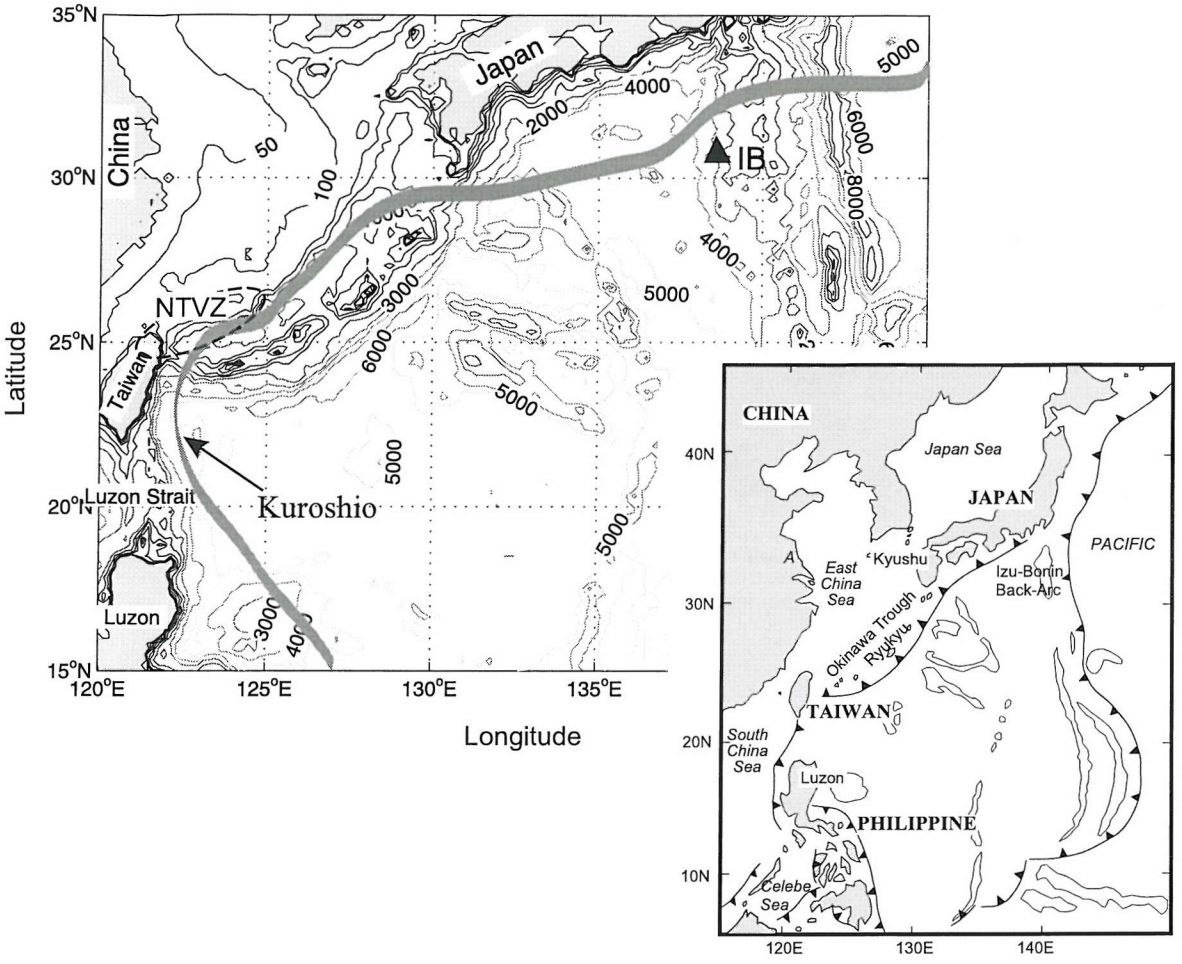

Fig. 5.3 Tectonic and bathymetric map of the Luzon/Ryukyu/Izu-Bonin area. Grey line indicates the flow direction of the Kuroshio Current. NTVZ stands for North Taiwan Volcanic Zone.

5-3 Geological background of the Izu-Bonin area and the nature of the Kuroshio Current

5-3-1 Izu-Bonin System

The Izu-Bonin (Ogasawara) arc is located in the northeastern margin of the Philippine Sea Plate. The arc extends N-S and is bounded by the Izu-Bonin Trench to the east and by the Shikoku Basin to the west (Fig. 5.2). Four key topographic features dominate within this broad (~400 km wide) volcanic zone: a) the active volcanic front, b) the back-arc rift basin, c) the "back-arc knolls" zone, and d) a series of back-arc seamount chains (Fig. 5.2). The volcanic front includes both subaerial stratovolcanoes (e.g. Hachijyo Jima and Aoga Shima islands) and large submarine calderas (e.g. Myojin knoll) and is characterized by production of both basaltic and rhyolitic tephras (Fujioka *et al.*, 1992; Rodolfo *et al.*, 1992). The active back-arc rifts (Sumisu and Aoga Shima Rifts) are delineated by north-south trending, inward-facing faults (Klaus *et al.*, 1992; Taylor, 1992). Holocene basalts (<0.1Ma) and hydrothermal activity occur along the central axis of the Sumisu Rift, whereas older lavas (~1.4 Ma) crop out along the rift-walls (Hochstaeder *et al.*, 1990; Urabe and Kusakabe, 1990). The back-arc knolls zone lies west of the active rifts, consisting of numerous small submarine volcanoes. The back-arc seamount chains extend into the Shikoku Basin, striking ENE-WSW, oblique to the trend of both the volcanic front and back-arc rifting. The IB1 and IB2 Fe-Mn crusts were recovered from two of these seamount chains, Enpo and Genroku, at depths of ~1800m and ~2600m respectively. Hydrothermal activity has previously been reported in association with the back-arc seamount chains, e.g. Manji Chain, and was associated with voluminous back-arc volcanism in an oceanic setting (Ishizuka *et al.*, 2002b).

From the K-Ar ages of the volcanic seamounts (Ishizuka *et al.*, 1998; Ishizuka *et al.*, 2002a), volcanism in the back-arc seamount chains was active between 12.5 and 2.9 Ma, i.e. after the cessation of spreading of the Shikoku Basin, to the west. Volcanism at the frontal arc is thought to have resumed at about 3.8 Ma and continued until at least 2.35 Ma based upon an apparent lull in arc activity inferred from pumice production and magma compositions (Nishimura *et al.*, 1991; Gill *et al.*, 1992; Hiscott and Gill, 1992). Volcanism in the back-arc knoll zone was active from ~2.8 Ma until 1 Ma. After 1 Ma, active volcanism ceased in the area west of the currently

active rift zone since when volcanism and rifting have been confined to the currently active rift zone.

5-3-2 Kuroshio Current

The Kuroshio current forms part of the larger North Pacific gyre system of the Western Boundary Current (Fig. 5.3). This water has its origins in the North Equatorial Current and flows northward along the east coast of Taiwan before turning northeast along the East China Sea continental slope and flowing over the Okinawa trough before exiting the area as the Kuroshio Extension once it separates from the SE Japan coast (see, e.g., Roemmich and McCallister, 1989). The reported transport-rate for the Kuroshio Current in the Okinawa section of its flow-cycle is about 30 Sv ($1Sv=10^6\ m^3s^{-1}$) (Roemmich and McCallister, 1989; Bingham and Talley, 1991). It exhibits a mean current speed of 3-30 cm s^{-1} but this can range up to greater than 150 cm s^{-1}, the exact value varying with both region and depth (Chung and Hung, 2000; Tang *et al.*, 2000; Zhang *et al.*, 2001; Hwang and Kao, 2002; Kashima *et al.*, 2003; Zhu *et al.*, 2003 and references therein). In general, the Kuroshio is a warm current which flows at high speed; it extends across a great width (150-200 km) and also extends to a significant depth below the surface (~1 km).

5-4 Samples and Analytical Methods

Three Fe-Mn crusts were selected for this secular variation study: SC5 (4°10S, 174°54W; 3033 m) from the South Central Pacific and IB1 (1860 m) and IB2 (2600 m) from the Izu-Bonin Back Arc Basin (Table 2.1; Fig. 5.1; 5.2). The sampling method, dating techniques, and chemical preparations employed were all described previously, in Chapters 2 and 3. Average growth rates, determined from Be-10 chronology, were 5.4, 6.7 and 3.7 mm/Ma for IB1, IB2 and SC5, respectively.

The Nd and Hf isotope chemistry and their analytical protocols have been described in Appendix II, III and Chapter 3. Pb isotope compositions were determined on just 2-4 mg of solid samples because of the generally high Pb concentrations in these Fe-Mn crusts. Chemical procedures were detailed in appendix IV after Ishizuka *et al.* (2003). Compared to the amount of total Pb loaded in the column (~1 μg), the total procedural blank was negligible. Pb isotopic compositions were obtained using a Tl-doping technique (Longerich *et al.*, 1987; Walder and Furuta, 1993; Rehkämper and Halliday, 1998) on a MC-ICP-MS (Micromass,

IsoProbe). All Pb isotopic compositions reported here have been normalised to reported NBS981 standard values (Galer and Abouchami, 1998; Thirlwall, 2000) for interlaboratorial comparison ($^{206}Pb/^{204}Pb$=16.9407, $^{207}Pb/^{204}Pb$=15.4960 and $^{208}Pb/^{204}Pb$=36.7224).

5-5 Results

Nd, Hf and Pb isotope results for the three Fe-Mn crusts studied are listed in Table 5.1 and 5.2. The reported age models were obtained by ^{10}Be dating, as described in Chapter 3.

Table 5.1 Nd and Hf isotopic compositions

Depth (mm)	Age (Ma)	$^{143}Nd/^{144}Nd$ [(a)] ± 2se	ε_{Nd} (T) [(c)] ± 0.16 (2sd)	$^{176}Hf/^{177}Hf$ [(c)] ± 2se	ε_{Hf} (T) [(d)] ± 0.70 (2sd)
D105-5AB (IB1)					
surface	0.02	0.512459 ± 5	-3.49	n/a	n/a
0.5-1.0	0.14	n/a	n/a	0.282920 ± 10	5.22
4.5-5.0	0.88	0.512437 ± 4	-3.93	0.282928 ± 13	5.48
8.0-8.5	1.53	n/a	n/a	0.282918 ± 13	5.15
12.0-12.5	2.27	n/a	n/a	0.282945 ± 11	6.06
16.0-17.0	3.06	0.512436 ± 5	-3.99	0.282948 ± 09	6.15
20.0-21.0	3.80	n/a	n/a	0.283033 ± 07	9.16
23.1-24.0	4.37	0.512470 ± 4	-3.34	0.282953 ± 18	6.29
D97-1 (IB2)					
surface	0.01	0.512435 ± 8	-3.95	0.282923 ± 18	5.34
1.0-2.0	0.22	n/a	n/a	0.282925 ± 13	5.41
9.0-10.0	1.42	0.512463 ± 5	-3.43	0.282941 ± 19	5.93
14.0-15.0	2.16	0.512445 ± 6	-3.80	0.282938 ± 13	5.83
25.0-26.0	3.81	0.512423 ± 5	-4.25	0.283029 ± 12	9.01
31.0-32.0	4.70	0.512420 ± 5	-4.32	0.282989 ± 09	7.57
28DSR9 (SC5)					
surface	0.03	0.512454 ± 5	-3.58	0.282936 ± 11	5.80
0-1.0	0.14	n/a	n/a	0.282914 ± 14	5.03
1.0-2.0	0.41	n/a	n/a	0.282935 ± 11	5.75
6.0-7.0	1.76	0.512487 ± 5	-2.97	0.282971 ± 11	7.01
9.0-10.0	2.57	0.512483 ± 6	-3.06	0.282958 ± 09	6.53
13.0-14.0	3.65	n/a	n/a	0.282951 ± 13	6.25
16.0-17.0	4.46	n/a	n/a	0.282956 ± 09	6.41
20.0-21.0	5.54	0.512432 ± 5	-4.10	0.282921 ± 11	5.14
20.5-21.0	5.61	n/a	n/a	0.282929 ± 09	5.43
29.0-30.0	7.97	n/a	n/a	0.282953 ± 09	6.21

(a) The average of Nd standard, JNdi = 0.512104 ± 8 (2sd, n=21) and normalised $^{143}Nd/^{144}Nd$ are reported to recommended values of 0.512115 (ref).

(b) $\varepsilon_{Nd\,(0)}=[(^{143}Nd/^{144}Nd)_{sample}/(^{143}Nd/^{144}Nd)_{CHUR}-1]\times10^4$, where $(^{143}Nd/^{144}Nd)_{CHUR}$=0.512638.

(c) Average Hf JMC 475 standard yields an average of $^{176}Hf/^{177}Hf$=0.282163 ± 26 (2sd, n=79). $^{176}Hf/^{177}Hf$ values are reported relative to 0.282160 for JMC475.

(d) $\varepsilon_{Hf\,(0)}=[(^{176}Hf/^{177}Hf)_{sample}/(^{176}Hf/^{177}Hf)_{CHUR}-1]\times10^4$, where $(^{176}Hf/^{177}Hf)_{CHUR}$=0.282772.

Table 5.2 Pb isotopic compositions

Depth (mm)	Age (Ma)	$^{206}Pb/^{204}Pb$ ± 0.0043	$^{207}Pb/^{204}Pb$ ± 0.0039	$^{208}Pb/^{204}Pb$ ± 0.0092	$^{208}Pb/^{206}Pb$	$^{207}Pb/^{206}Pb$
D105-5AB (IB1)						
surface	0.02	18.5775	15.6475	38.8171	2.0895	0.8423
0.5-1.0	0.14	18.5798	15.6448	38.8108	2.0889	0.8420
1.5-2.0	0.32	18.5708	15.6422	38.8027	2.0894	0.8423
2.5-3.0	0.51	18.5715	15.6456	38.8125	2.0899	0.8425
4.5-5.0	0.88	18.5812	15.6462	38.8153	2.0890	0.8420
6.5-7.0	1.25	18.5888	15.6572	38.8549	2.0902	0.8423
8.0-8.5	1.53	18.5755	15.6440	38.8093	2.0893	0.8422
10.0-10.5	1.90	18.5934	15.6525	38.8380	2.0888	0.8418
12.0-12.5	2.27	18.5916	15.6471	38.8217	2.0881	0.8416
13.0-13.5	2.45	18.5846	15.6487	38.8259	2.0891	0.8420
14.0-14.5	2.64	18.5836	15.6516	38.8314	2.0896	0.8422
16.0-17.0	3.06	18.5681	15.6494	38.8246	2.0909	0.8428
20.0-21.0	3.80	18.5655	15.6489	38.8197	2.0910	0.8429
23.1-24.0	4.37	18.5557	15.6448	38.8022	2.0911	0.8431
D97-1 (IB2)						
surface	0.01	18.5791	15.6485	38.8221	2.0896	0.8423
1.0-1.5	0.19	18.5762	15.6452	38.8121	2.0894	0.8422
5.0-6.0	0.82	18.5667	15.6460	38.8055	2.0901	0.8427
14.0-15.0	2.16	18.5487	15.6463	38.8040	2.0920	0.8435
19.0-20.0	2.91	18.5510	15.6531	38.8197	2.0926	0.8438
25.0-26.0	3.81	18.5485	15.6493	38.8063	2.0922	0.8437
31.0-32.0	4.70	18.5425	15.6448	38.7893	2.0919	0.8437
28DSR9 (SC5)						
surface	0.03	18.7093	15.6268	38.7123	2.0692	0.8352
0-1.0	0.14	18.7160	15.6332	38.7252	2.0691	0.8353
1.0-2.0	0.41	18.7294	15.6289	38.7159	2.0671	0.8345
6.0-7.0	1.76	18.7347	15.6317	38.7197	2.0667	0.8344
13.0-14.0	3.65	18.7255	15.6358	38.7366	2.0687	0.8350
20.0-21.0	5.54	18.7261	15.6442	38.7743	2.0706	0.8354

5-5-1 Central Pacific Ocean

The Nd, Hf and Pb isotopic compositions of the South Central Pacific Fe-Mn crust (SC5) fall within the range defined by three previously reported Central Pacific Fe-Mn crusts: D11-1 (1800m; 11°39N, 161°41E), CD29-2 (2300m; 16°42N, 168°14W) and VA13-2 (4800m; 09°25N, 146°03W) (Fig. 5.1, Fig.5.4, 5.5). The Nd isotopic compositions all vary within 1ε unit (-3.1~ -4.1; Table 5.1), increasing from –4.1 at 5.5 Ma to –3.1 at 1.8 Ma before decreasing to –3.6, the present day value, comparable to the *in situ* Pacific seawater ε_{Nd} at equivalent depth (Piepgras and Jacobsen, 1988). ε_{Hf} ranges between 5.0 and 7.0 throughout the record and at 5.5 Ma ε_{Hf} exhibits a minimum radiogenic value of 5.1, coincident with the pronounced drop in the Nd isotope record at the same interval. Since 5.5Mn, the ε_{Hf} has increased and remained constant at 6.5 before starting to decrease at 1.8 Ma toward ε_{Hf} = 5-6. Throughout the 0-5 Ma period, both the Nd and Hf isotopic compositions of SC5 correlate well with the North Central Pacific Deep Water records reported previously (CD29-2 and D11-1, Ling *et al.*, 1997; Lee *et al.*, 1999; David *et al.*, 2001). At 5.5 Ma, by contrast, the Nd and Hf isotopes of SC5 are more similar to the bottom water signatures represented by deeper (4800 m) crust VA13/2.

SC5 only exhibits a very limited range in Pb isotope compositions: $^{206}Pb/^{204}Pb$, $^{207}Pb/^{204}Pb$ and $^{208}Pb/^{204}Pb$ vary in the range 18.71 - 18.73, 15.63 - 15.64 and 38.71 - 38.77 respectively (Table 5.2). $^{206}Pb/^{204}Pb$ values are constant from 5.5 to 0.4 Ma before decreasing slightly to 18.71. $^{207}Pb/^{204}Pb$ and $^{208}Pb/^{204}Pb$ show a slightly decreasing trend from (15.64, 38.77) at 5.5 Ma to (15.63, 38.72) at 0.4 Ma. Most of the results fall in the range defined previously by the North-Central Pacific Fe-Mn crusts; the exception to this rule occurs at 5.5 Ma where higher $^{207}Pb/^{204}Pb$ and $^{208}Pb/^{204}Pb$ ratios are observed (Fig. 5.5).

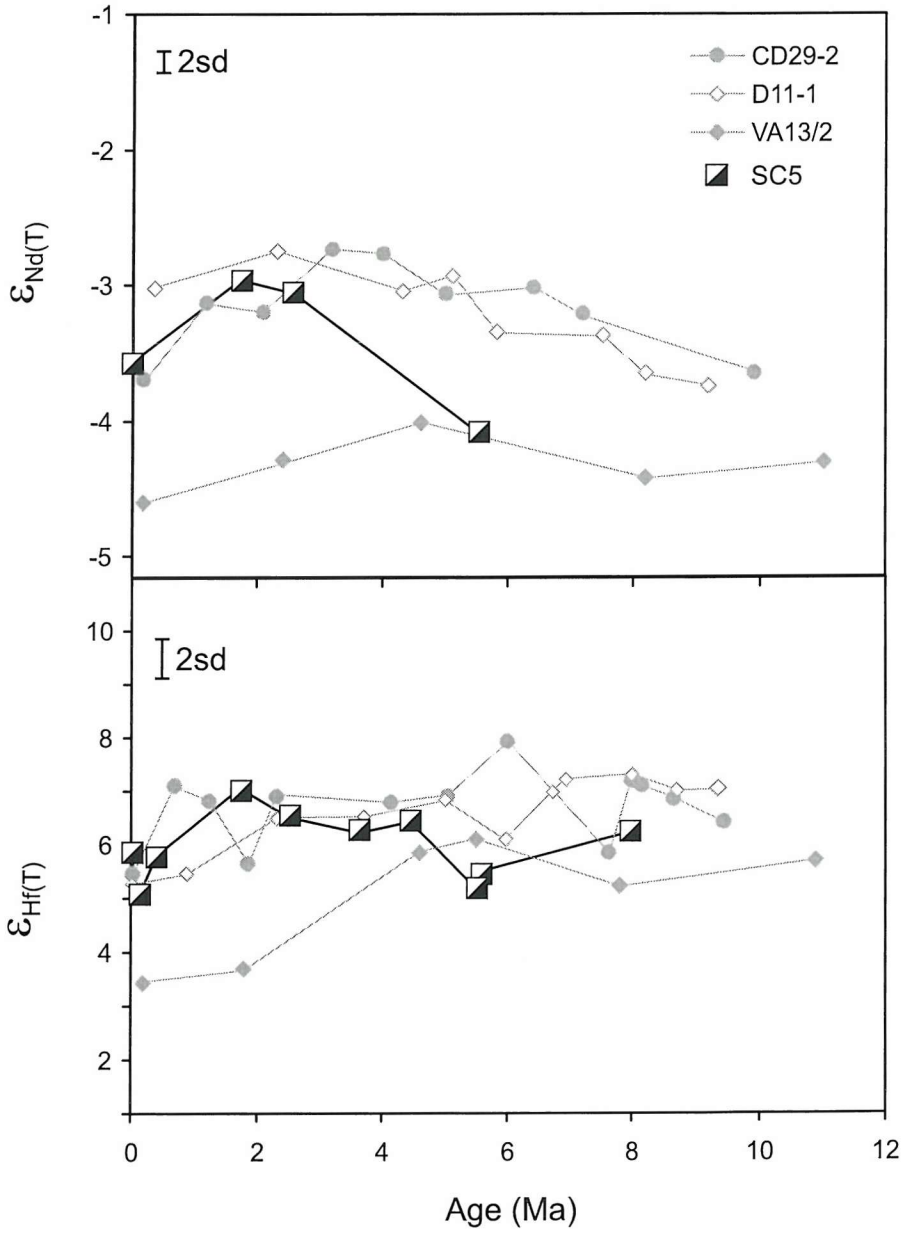

Fig. 5.4 Nd and Hf isotope variations of SC5 and three other previously reported Fe-Mn crusts (Ling *et al.*, 1997; Lee *et al.*, 1999; David *et al.*, 2001).

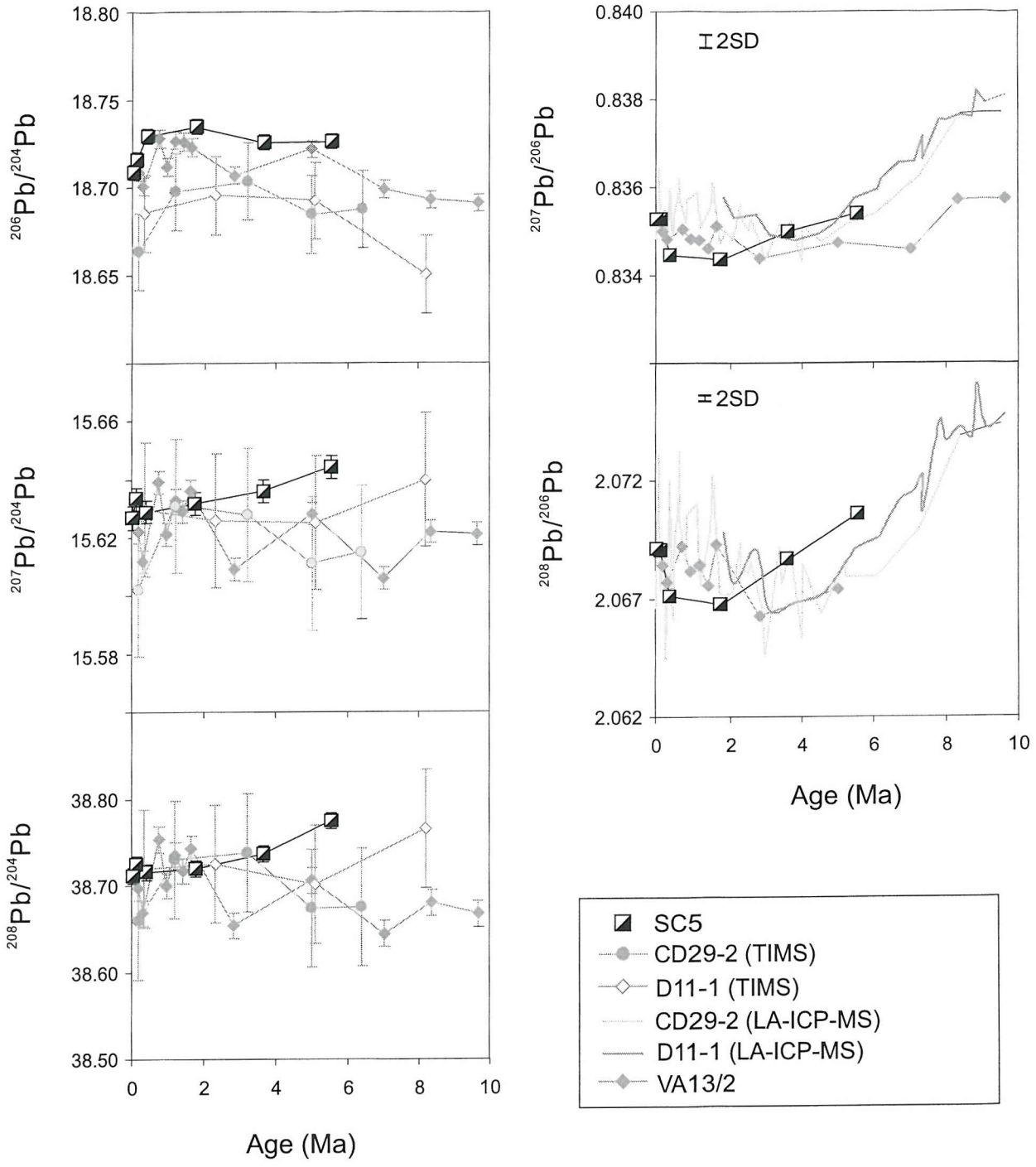

Fig. 5.5 Pb isotope variations of SC5 compared with other Central Pacific Fe-Mn crusts (CD29-2, D11-1and VA13/2, Ling *et al.* (1997) and Abouchami *et al.* (1997)). Laser results of $^{208}Pb/^{206}Pb$ and $^{207}Pb/^{206}Pb$ from Christensen *et al.* (1997).

5-5-2 Izu-Bonin Fe-Mn crusts

Nd isotope compositions in both the IB1 and the IB2 crust exhibit secular variations smaller than 1ε unit (Fig. 5.6). IB1 shows an ε_{Nd} value of –3.3 at 4.4 Ma before decreasing to –4.0 and then increasing to –3.5 at present. IB2 shows an increase from –4.32 at 4.7 Ma to –3.43 at 1.4 Ma then decreases again to –4.0 at present. At the oldest part of the record (~4.5 Ma), IB1 shows a more radiogenic signature than IB2. In general, however, the two records can be considered as consistent over the past 5 Ma. Further, they exhibit both less radiogenic profiles than Central Pacific Deep Water (e.g. SC5; ~3000 m) and more radiogenic profiles than Central Pacific Bottom water (below 4000 m) (Ling *et al.*, 1997) (Fig. 5.6).

Radiogenic peaks of ε_{Hf} at ~9 are observed in both IB crusts at 3.8 Ma. From 3.8Ma to the present ε_{Hf} values remain constant at 5.6. The Hf isotopic compositions of both IB crusts from 0-4 Ma also exhibit signatures similar to those of North-Central Pacific Deep Water (Fig. 5.6, Lee *et al.*, 1999).

Pb isotopic compositions in IB and IB2 (Fig. 5.7) exhibit relatively tight variations over the past 5 Ma, with $^{206}Pb/^{204}Pb$=18.59-18.54, $^{207}Pb/^{204}Pb$=15.65-15.64 and $^{208}Pb/^{204}Pb$=38.84-38.79. Both crusts exhibit relatively unradiogenic signatures in $^{206}Pb/^{204}Pb$ when compared to the open-ocean values of both Central Pacific Deep and Bottom Waters (Abouchami *et al.*, 1997; Christensen *et al.*, 1997; Ling *et al.*, 1997). In $^{207}Pb/^{204}Pb$ and $^{208}Pb/^{204}Pb$ systematics, any differences between the IB crusts and all other Central Pacific Mn crusts (including the SC5 data reported here) are less obvious than they are from the $^{206}Pb/^{204}Pb$ data. Both crusts also show an age correlation when plotted in mixed Pb-Pb space (Fig. 5.8). For both crusts, what is observed is that the Pb becomes more radiogenic with decreasing age (a significant increase in $^{206}Pb/^{204}Pb$ is observed at around 3 Ma) suggesting a possible change in the provenance of Pb supplied to these IB crusts at that time.

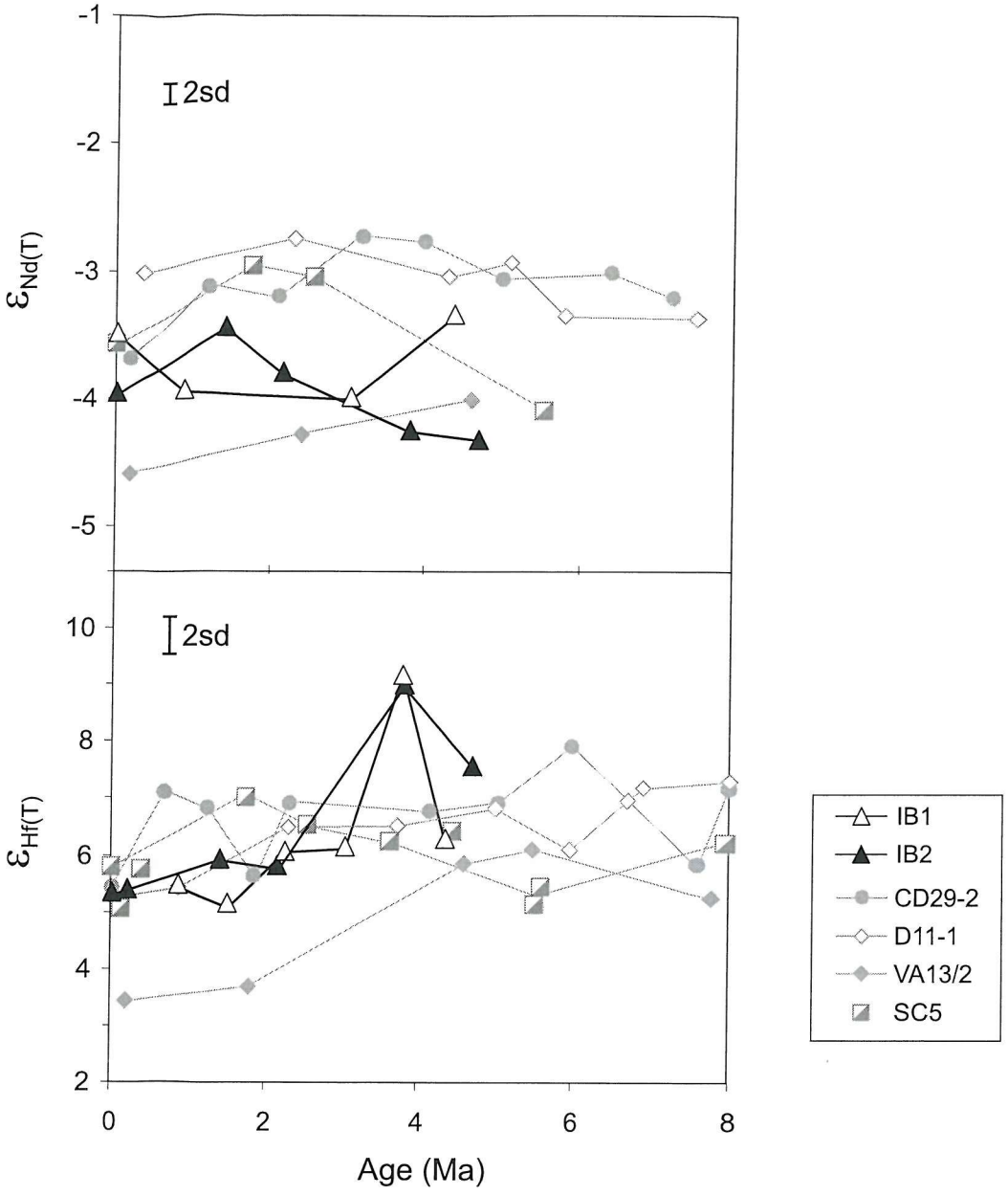

Fig. 5.6 Nd and Hf isotope variations of IB1 & IB2 in comparison with Central Pacific Fe-Mn crusts.

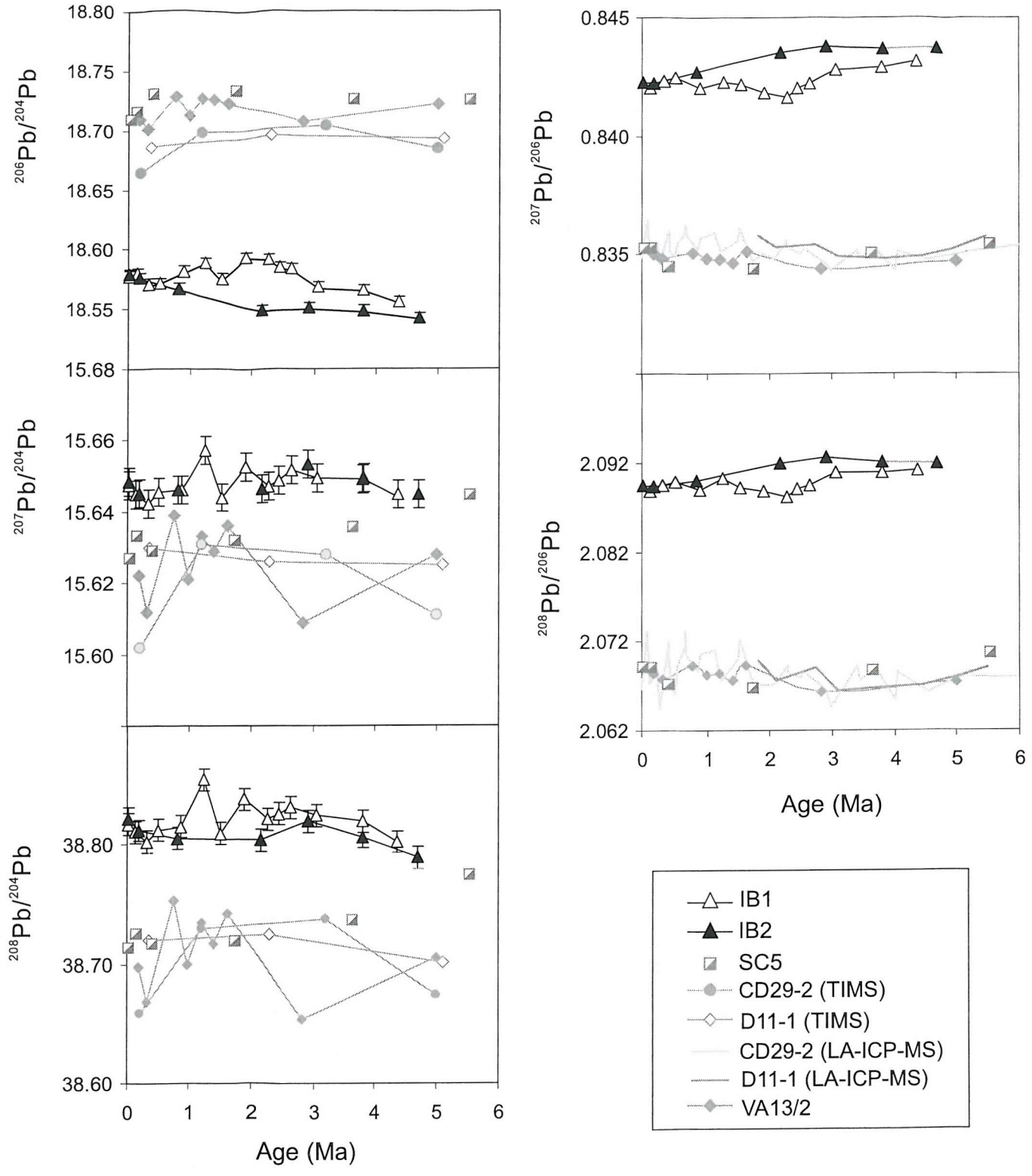

Fig. 5.7 Pb isotope variations of IB1 and IB2

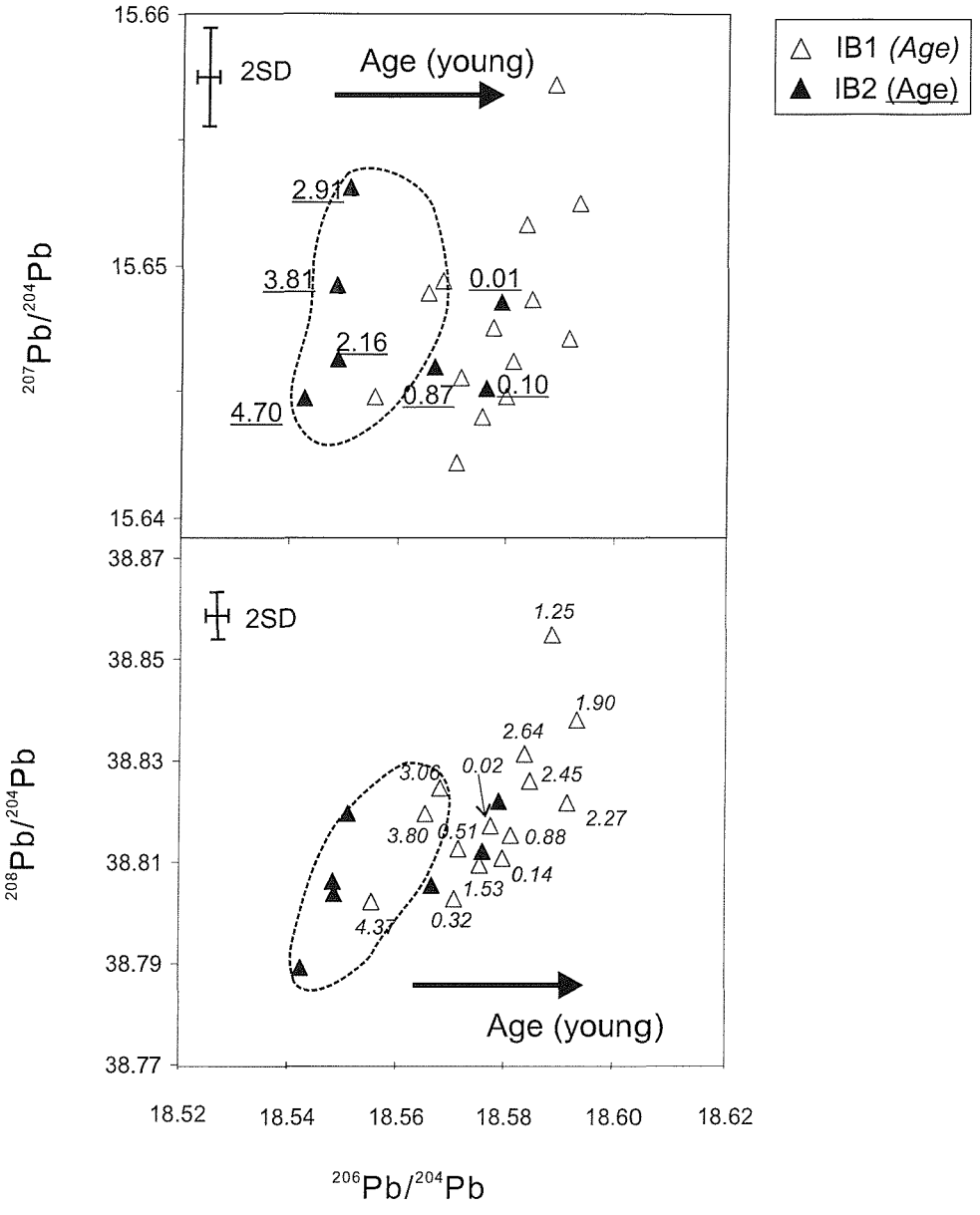

Fig. 5.8 Pb isotope of IB1 and IB2 in $^{208}Pb/^{204}Pb$ versus $^{206}Pb/^{204}Pb$ and $^{207}Pb/^{204}Pb$ versus $^{206}Pb/^{204}Pb$ space. Individual ages (Ma) are marked next to the symbol: IB1 in $^{208}Pb/^{204}Pb$ versus $^{206}Pb/^{204}Pb$ and IB2 in $^{207}Pb/^{204}Pb$ versus $^{206}Pb/^{204}Pb$ plots. Arrows indicates the decreasing age, and the circled area is the oldest parts of two IB crusts.

5-6 Discussion

5-6-1 Radiogenic isotope variations in the South-Central Equatorial Pacific over the past 6 Ma

(a) Ocean circulation

The least radiogenic Nd and Hf and the more radiogenic $^{207}Pb/^{204}Pb$ and $^{208}Pb/^{204}Pb$ (Fig. 5.5, 5.9) signatures in Fe-Mn crust SC5 were observed at 5.5 Ma. When compared to the existing North-Central Pacific Fe-Mn crust data, this sample exhibits signatures closer to the ~4800m deep bottom water signatures recorded by VA13/2 (filled diamonds, Fig. 5.4, 5.5) than to the overlying Pacific Deep Water records present in crusts D11-1 and CD29-2. As previously discussed, Nd and Hf input to the Central Pacific, prior to 5 Ma was dominated by island arc weathering and the release of these typically more radiogenic young island materials explains the continuous build up of the radiogenic signatures in seawater. Therefore, the 'unradiogenic excursion' observed at 5.5Ma in the South-Central Equatorial Pacific could be attributed to either (1) a sudden interruption to island-arc weathering or (2) an anomalous unradiogenic input caused by some perturbation of prevailing ocean circulation patterns. It has been suggested that the rate of production of Pacific island-arcs increased strongly after 8Ma (Kaiho and Saito, 1994) but there have been no reports on any slow-down or cessation of island-arc production at 5-6 Ma. It seems unlikely, therefore, that island-arc weathering ceased at this particular time.

SC5 is located at the exit of the Samoa Passage (see Chapter 2 for detailed descriptions), where Antarctic Bottom Water from the Southern Ocean enters the deep Equatorial Pacific bearing unradiogenic Hf, Nd and radiogenic Pb signatures (see, e.g., Southern Ocean Pb data reported by Frank *et al.*, 2002). The location of crust SC5 and the observation that this crust is sited significantly deeper than crusts D11-1 and CD29-2 raise the possibility that what is recorded at 5.5Ma represents an episode in the strengthening of local Bottom Water input, either as a result of diversion of the flow path of waters bathing site VA 13/2 past site SC5 or simple shallowing of an already extant current which is normally restricted to greater water depths in this region of the Equatorial Pacific but which was present sufficiently shallow in the water column at 5.5Ma to influence this 3033m-deep crust at that particular time. This event is also supported by an adjacent Fe-Mn crust (Nova, 01°08'S, 168°04'W,

7000 km) which shows unradiogenic Nd and Hf signatures at exactly the same time interval (van de Flierdt *et al.*, submitted). If a general change on Pacific Ocean water masses is the cause of the negative anomalies seen in SC5 this might also help explain the more subtle decreases in Nd and Hf isotope values reported for crust D11-1 before 5 Ma (open diamonds, Fig. 5.4) which lies at both shallower water depth and also further NW along the modern-day flow-path of Antarctic Bottom Water progressing across the floor of the deep Pacific Ocean (Chapter 2).

(b) Input sources

The slight decrease in ε_{Nd}, less obvious in ε_{Hf}, observed from 2 to 0 Ma in SC5 (Fig. 5.4) along with other decreasing trends in the three N. Central Pacific Crusts agrees with the large increase in aeolian input argued for by Pettke *et al.* (2002) over this time-frame. This would appear to imply that influence of aeolian input upon the Nd and Hf isotopic composition in seawater must extend at least as far as the South Equatorial Pacific Ocean. However, this aeolian input cannot be discerned from a consideration of Pb-Pb plots (Fig. 5.9). This requires that, unlike the case for Hf and Nd, dust-bound Pb must not be an important input function to Pacific deep water, whereas island arc volcanics provide a much more significant Pb contribution, even far away from these landmasses, *via* efficient lateral mixing (von Blanckenburg and Igel, 1999; Pettke *et al.*, 2002a).

Another intriguing feature among the three N. Pacific crusts is the difference in Nd and Hf isotopic compositions between *N Pacific Deep Water* and *Bottom Water*: prior to 5 Ma, the ε_{Hf} value for *bottom water* (VA13/2) exhibited consistent values which were indistinguishable from the two *deep water* crusts (CD29-2, D11-1). During the last 5 Ma, however, a pronounced difference between these isotope values is observed; for ε_{Nd} by contrast, a neat constant (1ε unit) difference has been sustained throughout this time. The shift in ε_{Hf} values in VA13/2 at ca. 6 Ma was about -3ε unit, from +6 to +3. This might suggest that a potential decoupling mechanism may exist between the Hf and Nd isotope systems when island arc weathering is a dominant source. This topic will be discussed further in a later section of this chapter describing the Izu-Bonin Fe- Mn crust data sets.

In summary, SC5 shows radiogenic isotopic compositions which are consistent with other North Central Pacific Crusts, demonstrating that the Central Pacific has

been relatively well mixed, at least throughout the past 5 Ma. At 5-6 Ma, however, more unradiogenic signatures have been recorded in SC5, perhaps indicative of an increased influence at this site and this water depth from some form of Southern Ocean input.

5-6-2 Izu-Bonin Arc Crusts: Sources and mechanisms- evidence from Pb isotopes.

Fig. 5.10 presents combined $^{206}Pb/^{204}Pb$ and $^{207}Pb/^{204}Pb$, $^{208}Pb/^{204}Pb$ plots which can be applied to help constrain the input sources of Pb to the Izu-Bonin Back Arc Basin (IB) crusts. Intriguingly, the Pb isotopic compositions of the IB crusts over the past 5Ma do not coincide with the Pb isotopic compositions of any IB volcanic rocks, the local rift zone or even the back-arc seamounts, upon which the IB 1&2 crusts grew (Hochstaeder *et al.*, 1990; Gill *et al.*, 1994; Taylor and Nesbitt, 1998; Ishizuka *et al.*, 2003a). Nor do they coincide with any of the Northern or Central Ryukyu or Southern Kyushu volcanics (Shinjo *et al.*, 2000). One set of samples which do plot toward one end of the array defined by the IB crust samples (Fig. 5.11) are loess leachates from Lanzhou and from Luochuan in China (Jones *et al.*, 2000) although those samples actually exhibit even more radiogenic $^{206}Pb/^{204}Pb$ values than the IB 1&2 sample trends. Turbidites from South China Sea and Celebe Sea (marked as Luzon turbidites in Figs. 5.10, 5.11, Hemming and McLennan, 2001), coincide with the IB samples in a plot of $^{208}Pb/^{204}Pb$ vs $^{206}Pb/^{204}Pb$, but exhibit more radiogenic $^{207}Pb/^{204}Pb$ values make these unlikely to be a dominant source to the IB crusts. By contrast, the S. Ryukyu/Okinawa volcanic systems - labelled in Figs. 5.10 and 5.11 as NTVZ (north Taiwan volcanic zones) (Sun, 1980; Shinjo *et al.*, 2000, Wang et al., in press) also appear to offer potential as an appropriate source of Pb to the IB Fe-Mn crusts assuming two-component mixing with some more radiogenic second end-member (e.g. Loess, Fig. 5.11). In this interpretation, all IB 1&2 crust samples younger than 3Ma in age, as shown in Fig. 5.8, would exhibit Pb isotopic compositions consistent with a move toward some increased radiogenic aeolian input component.

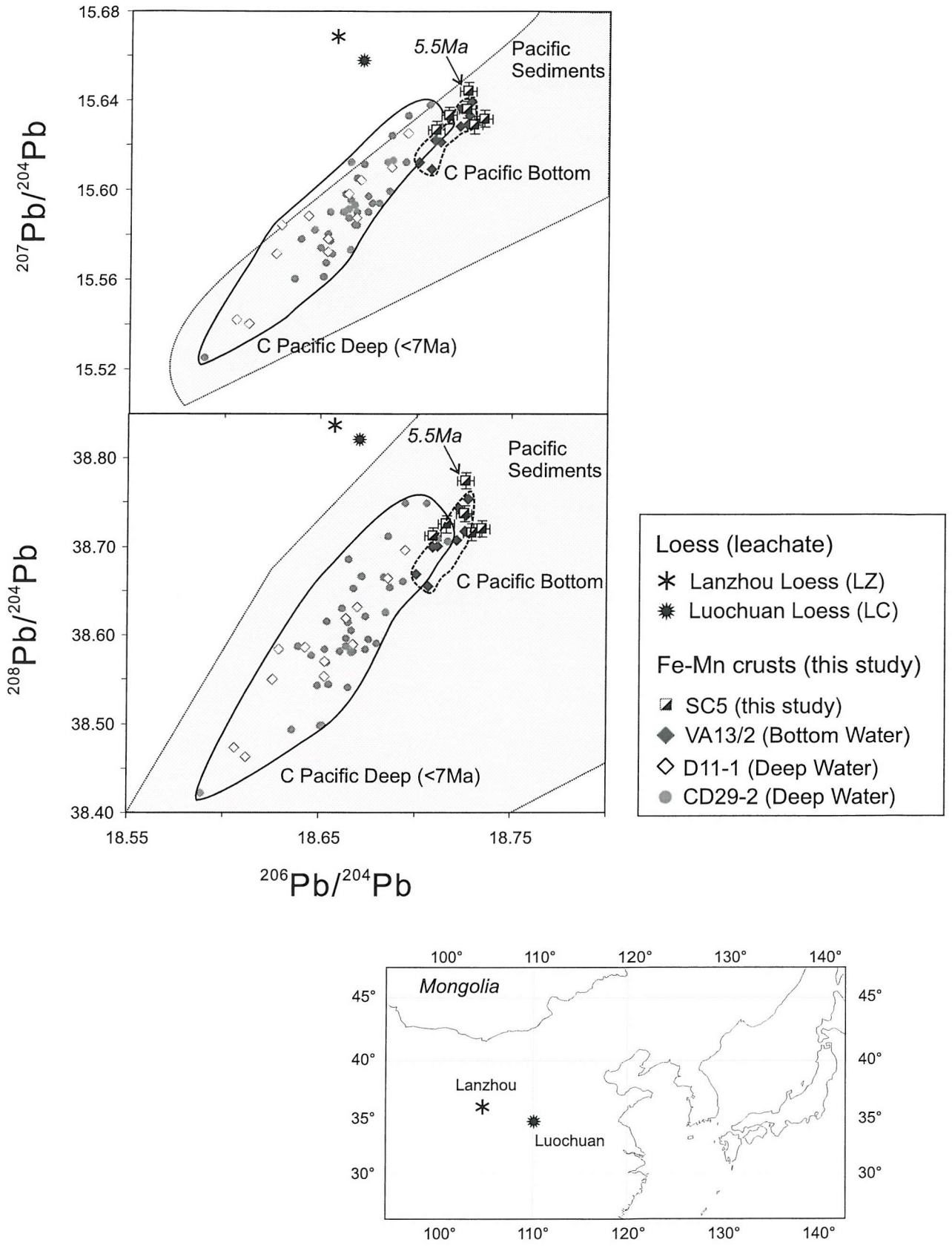

Fig. 5.9 Pb isotope of SC5 in $^{208}Pb/^{204}Pb$ and $^{207}Pb/^{204}Pb$ versus $^{206}Pb/^{204}Pb$ plots. Central Pacific Bottom water is defined by VA13/2 (Abouchami *et al.*, 1997) and Central Pacific Deep water is defined by CD29-2 and D11-1of the past 7 Ma (Christensen *et al.*, 1997). Gray area corresponds to the C. Pacific Fe-Mn crusts area in Fig. 5.10. Star symbols representing leached loess (Jones *et al.*, 2000) with their locations marked as inset map. The most radiogenic $^{208}Pb/^{204}Pb$ and $^{207}Pb/^{204}Pb$ signature of SC5 is marked with its age of 5.5 Ma.

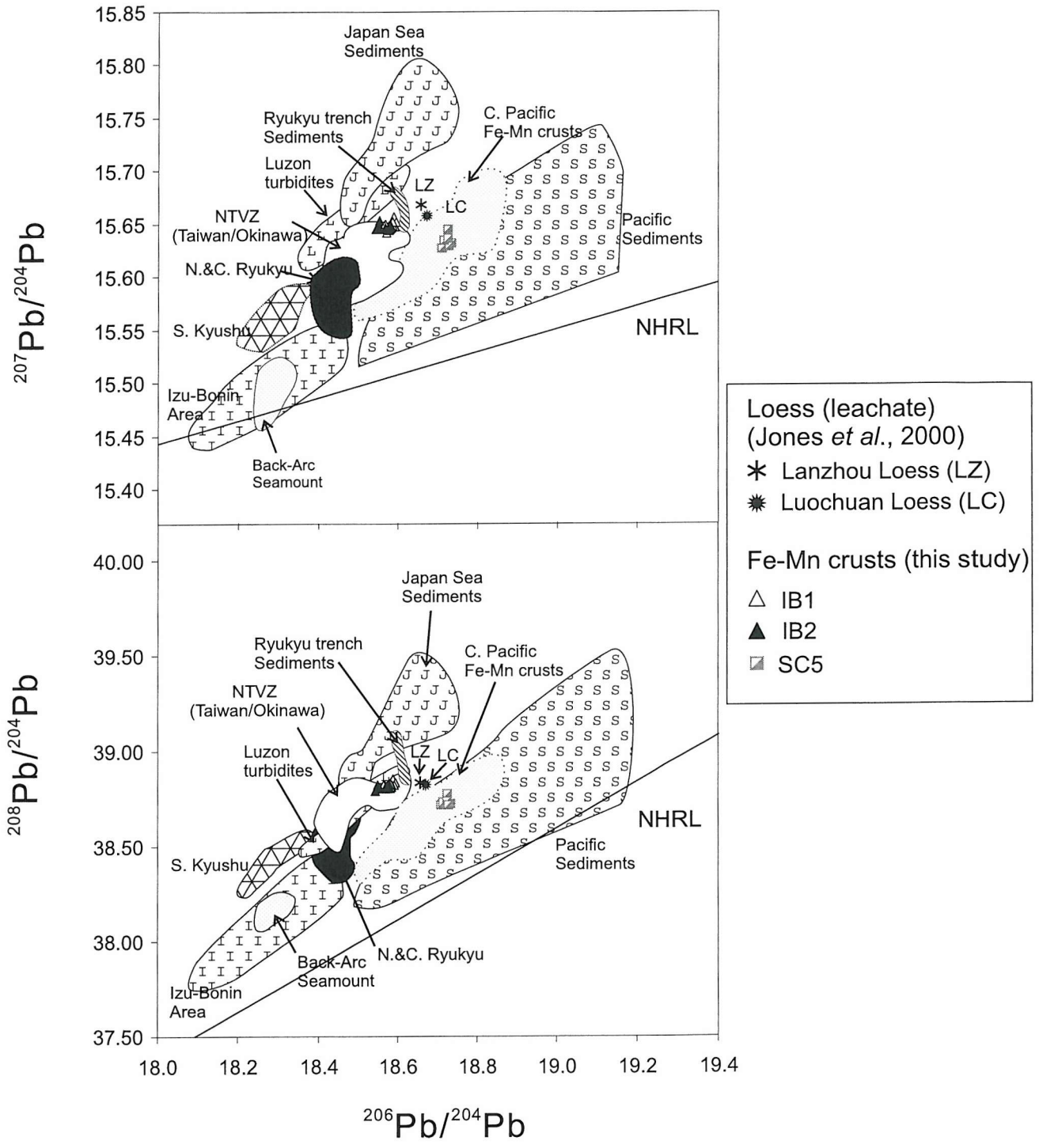

Fig. 5.10 $^{208}Pb/^{204}Pb$ and $^{207}Pb/^{204}Pb$ versus $^{206}Pb/^{204}Pb$ space plots, with potential sources of Pb to the Izu-Bonin back arc basin seawater: Japan Sea sediments, Luzon turbidites (Hemming and McLennan, 2001); Pacific Sediments (Jones *et al.*, 2000 and Pettke *et al.*, 2000), loess (Jones *et al.*, 2000), Central Pacific Fe-Mn crusts (as in text), Izu-Bonin area, including Arc volcanics (Taylor *et al.*, 1998), Sumisu Rift (Hochstadeter *et al*, 1990; Gill *et al.*, 1994) turbidites (Gill *et al.*, 1994) and Back-Arc Seamounts (Ishizuka *et al.*, 2003), Kyushu and Ryukyu volcanics (Shijo *et al.*,2000), NTVZ (Sun, 1980 and Wang *et al.*, 2004) and Ryukyu sediments (Sun, 1980). The Northern Hemisphere Reference Line defined by MORB and OIB data (Hart, 1984).

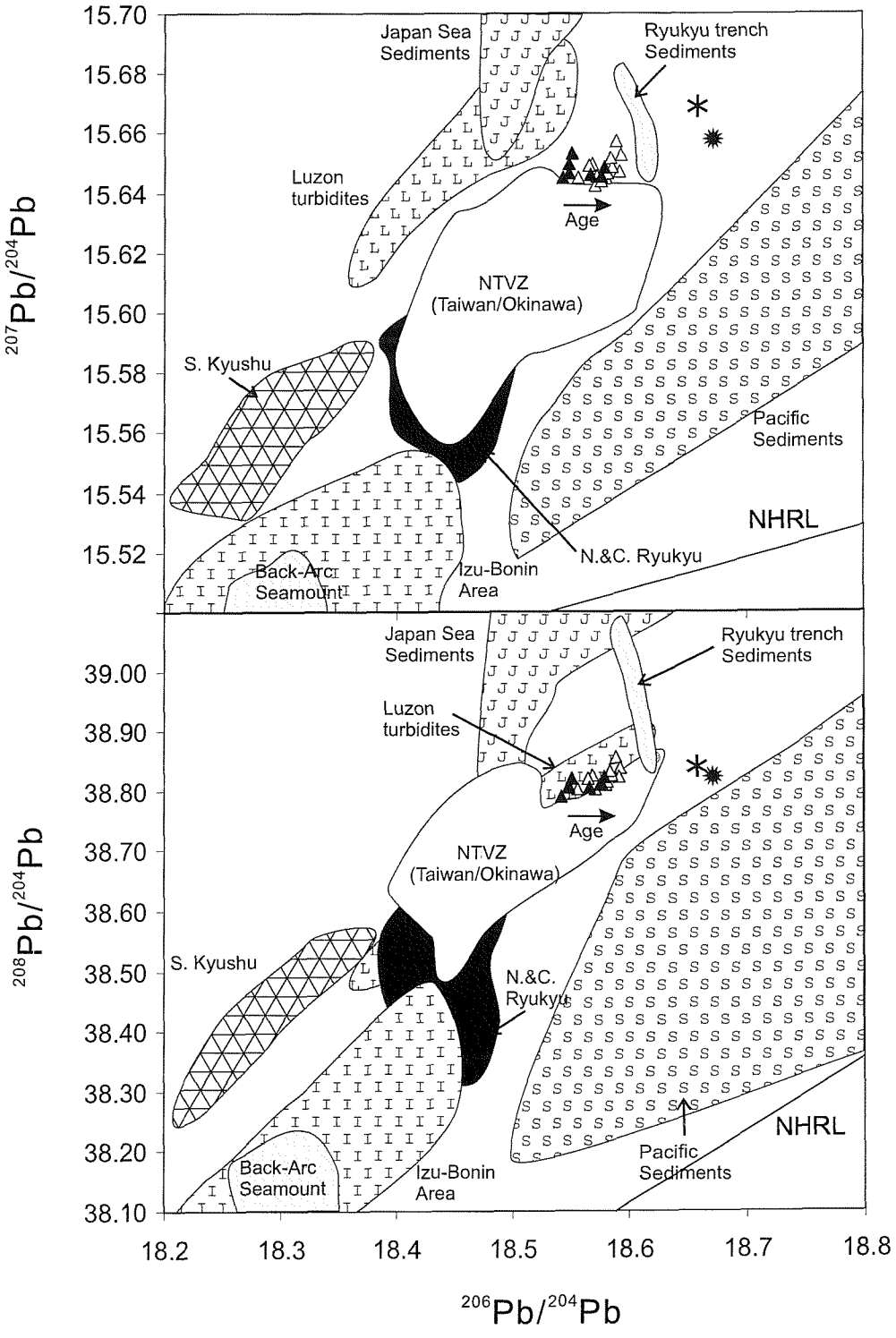

Fig. 5.11 Close up of Fig. 5.10.

(a) Aeolian input

The available aeolian data included here are from leached Asian dust (Jones *et al.*, 2000). It is this fraction which can most easily release its isotopic composition into seawater. In the West Pacific it has been predicted that it is the area of surface ocean closest to the Asian landmass which receives the highest loess input (e.g. Duce *et al.*, 1991). Thus, the IB area chosen for this study should provide an appropriate location to investigate such inputs.

Although these aeolian components may lie off the mixing trend for IB crust records of past and present seawater (too unradiogenic in $^{207}Pb/^{204}Pb$ and $^{208}Pb/^{204}Pb$; Fig. 5.8, 5.10, 5.11), the ten-fold increase in aeolian input to the surface of the Pacific Ocean since 3 Ma (Duce *et al.*, 1991) would certainly be consistent with having influenced the IB1&2 mixing trends toward more radiogenic $^{206}Pb/^{204}Pb$ values at that time. It has been demonstrated previously (von Blanckenburg *et al.*, 1996b; Henderson and Maier-Reimer, 2002; Pettke *et al.*, 2002a) that arc-weathering input should dominate in the dissolved Pb input to the oceans, especially close to any volcanic landmass. Nevertheless, the shift in Pb isotopic composition observed after 3 Ma in this study remains strongly indicative of a long-term change caused by increased aeolian input.

(b) Trench sediments

Ryukyu trench sediments (Fig. 5.11) exhibit more radiogenic Pb isotopic signatures than IB seawater and, hence, offer a potential alternate to aeolian loess as one end-member in a two-component mixing system that would explain these data. However, it is difficult to envisage how a surface current (Kuroshio) which extends to no more than ca. 1000 m water depth (see earlier) could interact with bottom sediments from the Ryuku Trench in such a way as to transport dissolved Pb with that Pb isotopic character to the sites of IB 1 & 2 crust-formation.

(c) The Northern Taiwan Volcanic Zone and lateral transportation.

The Okinawa Trough is a curved back-arc basin located behind the Ryukyu arc-trench system (Fig. 5.3). Its southern extent is termed the NTVZ (northern Taiwan volcanic zone), which has been active from ~2.8 Ma until the present (Wang *et al.*, 2002 and references therein). Although distant from the sites of formation Izu-Bonin back-arc basin crusts, the NTVZ area appears to represent one plausible source for the

IB seawater compositions, especially based on Pb-isotopes. Possible mechanisms need to be established, however, to explain how such distal material could act as an end-member source of material preserved in the IB 1&2 compositional records. Certainly, weathering is thought to be an important mechanism in this W. Pacific island-arc area and local rivers from such islands are believed to have the potential to provide significant dissolved tracer contributions to *global* ocean budgets (e.g. (Sholkovitz *et al.*, 1999). Continuous volcanic eruptions, for example, coupled with heavy subtropical-tropical precipitation and mountain-river runoff render these locations as very rich potential sources in balancing the isotopic signatures of seawater.

Further, if one considers the distance between the NTVZ and the site of the Izu-Bonin crusts (ca. 2000 km) and compares that with an average flow rate for the Kuroshio current of 30 cm/s (Tang *et al.*, 2000), then one can calculate that the approximate time taken for material entering the surface ocean at the NTVZ to arrive in the IB area is less than 80 days, which is much shorter than both the mean Pb residence time in the ocean (80 years) or 3-10 years of the modelled Pb residence time in this area (Henderson and Maier-Reimer, 2002) This helps support any argument that the Kuroshio Current is and/or has been an efficient mechanism for transporting dissolved radiogenic isotopic material from the Ryukyu/Okinawa volcanic region to provide a significant input to the IB 1 & 2 crusts.

(d) Local volcanics

Although they plot farther away from the Pb isotopic compositions measured in the IB 1&2 Fe-Mn crusts, the Izu-Bonin arc volcanic system also exhibits Pb isotopic values that could lie on a potential 2-component mixing line that would extend through the IB 1&2 data-set toward some more radiogenic second end-member (e.g. Ryukyu Trench Sediments; Fig. 5.11). In that case, however, the relative contribution to the Pb isotopic composition of the IB 1&2 crusts from local volcanics would have to be much less pronounced that would be the case for input from the NTVZ, and other factors, such as radiogenic sediments and/or some aeolian source, would have to provide a somewhat greater contribution to the overall seawater compositions.

In ancient continental rocks, where high U and Th concentrations have led to the production of significant decay product Pb isotopes, incongruous weathering of

releasing radiogenic Pb can arise by the decay weakness (Erel *et al.*, 1994). By contrast, because of the young ages of the island-arc volcanic rocks surrounding the western Pacific, little or no such isotopic contrasts are expected during the dissolution of different mineral phases and any Pb leached from local sediments should closely match that of any bulk silicate-sediment Pb isotopically (Jones *et al.*, 2000). Certainly, the Pb isotopic compositions of the leachates from the IB seamounts also do not show significantly more radiogenic signatures than the local volcanic rocks themselves upon which they have grown (R. Taylor, pers. com.). This precludes, therefore, the possibility of there being any incongruent weathering in the Izu-Bonin area (cf. von Blanckenburg and Nägler, 2001).

In summary, over the past 5 Ma, seawater in the Izu-Bonin area has been dominated by inputs from island arc weathering and, especially after 3 Ma, from aeolian (loess) input from Asia. The island arc input cannot be resolved but either represents (1) strong input from Okinawa/ South Ryukyu (NTVZ) volcanics brought in by the fast-flowing Kuroshio current, (2) less pronounced input from local volcanics with a more unradiogenic isotopic composition or some intermediate contributions from both sources.

5-6-3 Decoupling of Nd from Hf isotopes

Decoupling is observed between Nd and Hf isotopes in both Izu-Bonin Fe-Mn crusts (Fig. 5.6) in the form of a very radiogenic Hf input to the local seawater at ca. 3.8 Ma with no accompanying radiogenic Nd signature. Coincidentally, volcanic activity also resumed within the Izu-Bonin back arc system at 3.8 Ma (Nishimura *et al.*, 1991; Hiscott and Gill, 1992). The Izu-Bonin arc has undergone several such episodes of significant volcanic activity and related hydrothermal events have also been reported, e.g. at the fontal arc (Iizasa *et al.*, 1999; Tsunogai *et al.*, 2000), in the rift zone (Urabe and Kusakabe, 1990), and associated with the back-arc seamount chains (Ishizuka *et al.*, 2002b). Here, several possible cases are examined that may explain the observed Nd and Hf isotopic records.

(a) Incorporation of Volcanic Ash

Because they are situated in an intensely volcanically active area, one possibility exists that the IB Fe-Mn crusts may have incorporated material directly from volcanic ash fall out during growth. Typical Izu-Bonin volcanic rocks have ε_{Nd} values of 7-9

(Hochstaeder *et al.*, 2001) and ε_{Hf} values of ~13 or higher (Pearce *et al.*, 1999). If 'ash materials' had accidentally been incorporated into the Fe-Mn crust leaching analysis, therefore, it would be quite unexpected to observe an apparent decoupling of ε_{Nd} and ε_{Hf} in any single sample dissolution. Further, because pronounced decoupling is also observed in the Pb isotopic system between I-B arc volcanics and the IB Fe-Mn crusts (Fig 5.10) it seems quite clear that the anomalously positive Hf isotope values observed in IB 1&2 at 3.8Ma cannot result from direct incorporation of IB volcanic ash material within the 3.8Ma crust layers. This argument is further supported by the examination of REE patterns of the IB crusts which throughout all growth layers, including the 3.8Ma layer, exhibit characteristic seawater distribution patterns (e.g. Elderfield, 1988) which are quite distinct from the signature for local island arc volcanics (e.g. Pearce *et al.*, 1999). In summary, the data at 3.8Ma cannot be explained as resulting from incorporation of volcanic ash fall-out into this layer of the IB 1&2 Fe-Mn crusts.

(b) Hydrothermal/ aeolian input

Hydrothermal inputs have long been proposed as a possible source of dissolved Hf to the oceans (White *et al.*, 1986; Godfrey *et al.*, 1997). Further, it is quite plausible that hydrothermal discharge might have been particularly enhanced following the resumption of volcanic activity in the IB arc at 3.8 Ma (Nishimura *et al.*, 1991; Hiscott and Gill, 1992). For such hydrothermal activity to be responsible for the observed decoupling of Hf and Nd, would require that dissolved Hf, unlike Nd, could remain in solution and be advected some distance away from its source vent-site unlike Nd which, like all hydrothermally-sourced REEs, is known to be quantitatively co-precipiated with and/or scavenged onto Fe oxyhydroxide particulates within the buoyant portion of hydrothermal plumes, immediately following eruption (German *et al.*, 1990; Mitra *et al.*, 1994). Because the Izu-Bonin back arc basin is a geographically restrained semi-enclosed marine basin, this 'hydrothermal Hf' hypothesis has particular validity in that "hydrothermally perturbed" local bottom waters could readily be retained so as to result in an anomalous signature in the Fe-Mn crust layers recorded immediately following volcanic activity's resumption.

An important caveat, however, is that no further, comparable radiogenic Hf peaks have been observed throughout the following 3.8Ma that might correlate with any later episodes of continuing volcanic and/or hydrothermal events in the intervening period. As observed in the Pb isotopic systems, of course, aeolian input appears to have increased significantly in the Izu-Bonin region since 3 Ma (Duce *et al.*, 1991). One possibility, therefore, is that further hydrothermal "event" episodes have continued within the Izu-Bonin region but that, since 3Ma, and such events' isotopic records have been masked by the overwhelming influence of aeolian material which overprints and averages out any volcanically-stimulated hydrothermal "eruptions" with its a much more unradiogenic Hf component (ε_{Hf} = -4.7~2.5) (Pettke *et al.*, 2002b) resulting from the efficient dissolution of settling aeolian materials.

A further complication to any hydrothermal explanation of the data is that no hydrothermal Pb-isotope signatures (which should be unradiogenic like MORB) have been observed in the IB 1&2 crusts throughout the past 5 Ma. Conversely, however, one still cannot fully eliminate a "hydrothermal" explanation for the decoupling in Nd and Hf because the lack of MORB like Pb isotope signatures could also arise (1) because island arc weathering has overwhelmed the hydrothermal input signature or (2) because, like Nd, most of the hydrothermal Pb was scavenged from solution very close to any vent sources and the amount of dissolved Pb remaining in solution and available to be incorporated into the 3.8Ma layer of the IB 1&2 Fe-Mn crusts was negligible when compared to the equivalent dissolved Hf input to this layer.

(c) Island Arc Weathering

From Pb isotope systematics, island arc weathering is thought to have exerted an important influence upon the composition of the Izu-Bonin crusts, either through local inputs or via transported by the Kuroshio surface current from more distal (NTVZ) volcanic arcs (see previous section). Local seawater concentrations for Nd and Hf have been reported to be ~25 pmol/kg (Alibo and Nozaki, 1999) and >0.6 pmol/kg (McKelvey and Orians, 1998). This yields a Nd/Hf values for seawater which is approximately 8 times greater than in typical arc volcanics ([Nd] and [Hf]=10ppm and 2 ppm, respectively) (Pearce *et al.*, 1999; Ishizuka *et al.*, 2003a). If it is assumed that the dissolution behaviours of Nd and Hf are similar, it can be argued, then, that (a) any sudden increase localised dissolution of island arc material released into the Kuoshio current "upstream" of the IB 1&2 crusts (e.g. in response to suddenly re-

activiated volcanic activity) would preferentially perturb the Hf isotopic signatuire of that water mass when compared to its Nd isotopic composition and (b) any such "perturbed" isotopic signature should be retained within that water mass over timescales which are long relative to the transport of the Kuroshio current past the IB 1&2 crust sites (but short when compared to homogenisation of the larger, central Pacific deepwaters). Of course, all the above is highly speculative and it is unfortunate that no local riverine Hf data, potentially representative of weathering signatures, is available in order to help constrain such arguments. Nevertheless, one can take some encouragement from the previously discussed long-term records from Central Pacific Fe-Mn crusts. There, it has been shown that the dissolved Nd and Hf budgets of Central Pacific seawater have been dominated by island arc weathering up until ca.5 Ma (von Blanckenburg *et al.*, 1996b; David *et al.*, 2001; Frank, 2002). A decoupling between bottom (4800m) and deep (1800-2600m) water masses has also been observed, however, in which ε_{Nd} and ε_{Hf} vary respectively less and more coherently, within these two distinct water masses, before and after 5 Ma (Fig. 5.4). Those observations are at least partly consistent with the arguments presented here for IB 1&2, therefore, because they at least demonstrate a separate occasion in which the Hf isotopic composition of an Fe-Mn crust can show significant excursions from past values with no accompanying variations in the reported Nd isotopic composition.

Although the "event" like data in the IB 1&2 crusts suggest some direct correlation with the resumption of volcanic activity at this time (Nishimura *et al.*, 1991; Hiscott and Gill, 1992) any "Island Arc Weathering" hypothesis, like the preceding "hydrothermal" hypothesis would still require explanation of why such anomalous signals are preserved as a "one-off" event and not preserved as a continuous signal contiguous with the continuing volcanic activity that has continued to the present day.

In summary, it is difficult to elucidate whether the decoupling of Nd and Hf observed in the two Izu-Bonin Fe-Mn crusts investigated here may have been caused by some form of hydrothermal activity, by island-arc weathering or by some further, as-yet-unidentified process. Evidence provided by Pb isotopic systems may suggest that the "hydrothermal" hypothesis is less favoured, but the interpretations that can be gleaned from those data are far from unequivocal. One way to solve this problem might be if one could identify some additional geochemical tracer, not influenced by

varying terrigenous inputs, but which is known to exhibit a quite distinct, characteristic signature in deep-sea hydrothermal systems. Fe isotopes match this description very closely (Beard *et al.*, 2003b) and it is the Fe isotopic composition of crusts IB 1&2 crusts, compared with that of South-Central Pacific crust SC5 that is studied and presented in the following chapter of this thesis.

5-7 Conclusions

Three Fe-Mn crusts from two locations in the Pacific Ocean have been investigated in an attempt to decipher secular variations in the radiogenic isotope budgets of the Pacific Ocean. The results from one South-Central Equatorial Pacific Fe-Mn crust agree well with previously published records from North Central Pacific crusts over the period from 5 Ma to the present. An shift toward unradiogenic Nd, Hf values and radiogenic ^{207}Pb and ^{208}Pb at 5.5 Ma was also observed, however, which would be consistent with an increased strength of input from the Southern Ocean to this (~3000 m deep) site at that time.

Two Fe-Mn crusts from the Izu-Bonin Back-Arc Basin appear to demonstrate, based upon Pb isotopic signatures, two-component mixing between aeolian loess input and weathering from volcanic island arcs. A decoupling of Nd from Hf isotope records is observed in both these two crusts at ~4Ma. It is argued that this decoupling could be a direct consequence of localised hydrothermal activity or arc weathering that preferentially impacts the Hf isotopic record over that of Nd. In the continuing absence of either end-member riverine and hydrothermal Hf isotopic data or identification of some other geochemical tracer better suited to track the varying inputs of dissolved material to the Izu-Bonin back-arc basin these issues remain extremely difficult to resolve.

Chapter 6. Secular variation of Fe isotope in Fe-Mn crusts*

6-1 Abstract

Temporal variations in Fe isotope compositions of the Pacific Ocean over the last 10 million years are inferred from high-resolution analyses of three deep-sea ferromanganese crusts. Here we show that hydrothermal sources are dominant for dissolved Fe in the modern deep Pacific Ocean, because the surfaces of all three Pacific samples exhibit $^{56}Fe/^{54}Fe$ ratios that, consistently, are significantly lower than a NW Atlantic crust reported previously (Zhu *et al.*, 2000b). Comparison of variations in $^{56}Fe/^{54}Fe$ ratios over time for Atlantic and Pacific Fe-Mn crusts demonstrate the isotopic provinciality of Fe in the deep oceans at both the inter- and intra-basin scale. In the Pacific Ocean, both widespread and localised hydrothermal inputs are documented. Although Fe pathways to the central deep Pacific Ocean appear to have remained constant over the past 10 million years, greater variability is observed in the Izu-Bonin back-arc/marginal basin, W. Pacific.

6-2 Introduction

There has been significant interest in the cycling of dissolved Fe in the world's oceans, especially the role that Fe availability plays in controlling phytoplankton growth across large areas of the world's surface ocean, which ultimately may affect draw down of atmospheric CO_2 and, thus, affect global climate cycles (Martin, 1990; Martin *et al.*, 1994; Falkowski, 1997; Boyd *et al.*, 2000). Much attention, therefore, has been paid to the source(s) of surface ocean dissolved Fe, particularly the role of atmospheric input from continental weathering (Jickells and Spokes, 2001; Sarthou *et al.*, 2003). Fewer studies, by contrast, have focused on cycling of dissolved Fe in the deep ocean (Boyle, 1997; Johnson *et al.*, 1997; Wu *et al.*, 2001; Laës *et al.*, 2003), yet upwelling from depth may also represent an important source of surface-ocean dissolved Fe (Coale *et al.*, 1996; Wells *et al.*, 1999; Mackey *et al.*, 2002). Because the residence time of dissolved Fe in seawater is very short (Bruland *et al.*, 1994), it is difficult to identify the Fe cycling pathways based on concentration alone. Iron isotopes fractionate via various processes and therefore hold great promise for tracing

* This chapter is a menuscript for submission as Chu et al. (*in prep.*), The isotopic composition of dissolved Fe in the deep Pacific Ocean (0-10 Ma): sustained influence from seafloor hydrothermal venting

marine Fe biogeochemical cycles (Beard and Johnson, 2004; Johnson *et al.*, 2004). Further, the temporal record of Fe cycling in the oceans may be recorded in Fe-Mn crusts, which due to their slow growth rates may provide insight into Fe cycling over millions of years (Zhu *et al.*, 2000b). We do not expect significant Fe isotope fractionation during hydrogenous accumulation of Fe-Mn crusts because Fe scavenging is efficient and does not involve redox changes (Koschinsky and Halbach, 1995). This should eliminate any transient isotopic fractionations (Johnson *et al.*, 2002; Welch *et al.*, 2003), in contrast to Mo and Tl, whose moderately long (10^4-10^6 yr) residence times (Bruland, 1983) allow significant isotopic contrasts to be maintained between dissolved and solid phases (Rehkämper *et al.*, 2002; Siebert *et al.*, 2003; Barling and Anbar). (A lack of isotopic fractionation upon precipitation has already been observed in submarine hydrothermal systems, where the δ^{56}Fe value of aqueous Fe in end-member vent-fluid is identical to that of both plume-particles precipitated upon mixing with seawater and metalliferous sediments deposited beneath the dispersing hydrothermal plume (Severmann *et al.*, 2004)). To date, only one time-series Fe isotope record is available in the NW Atlantic Ocean (Zhu *et al.*, 2000b) but this cannot provide a complete picture of the isotopic variability in the oceans because the fast reaction rate of dissolved Fe suggests that inter- and even intra-basin differences in Fe isotopic compositions should exist (Beard *et al.*, 2003b). Here, we report the first records for the isotopic composition of dissolved Fe in the deep Pacific Ocean, extending back 5-10 Ma. Our records come from three Fe-Mn crusts, one from the deep Central Pacific Ocean (2600 m water depth, 0-10 Ma) and the other two collected from the Izu-Bonin Arc region of the marginal West Pacific (1860 & 2600 m depth, 0-5 Ma).

6-3 Samples and Methods

Three Fe-Mn crusts (28DSR9 (SC5), D105-5AB (IB1) and D97-1 (IB2)) were taken for the Fe isotope analysis (Fig. 5.1/5.2). The profiles analysed are from the same drilling section as presented in Chapter 5. The chemistry method followed the standard UW-Madison Fe-chemistry as reported by Beard *et al.* (2003a). Samples of ~100 μg total Fe were loaded onto miniaturized Teflon columns filled with a volume of ~400 μl anion-exchange resin (Bio-Rad AG1X4, 200-400 mesh). Impurities were removed by eluting in 7.0 M HCl and the Fe fraction was collected in 0.5 M HCl. All reagents were double distilled. In this study, sample powders from each growth

layers were first digested in 6 M HCl and separated out from undissolved residues by centrifuge. The accuracy of the Fe isotope analyses is demonstrated through tests using artificial Fe-Mn-Co mixtures and Fe of known isotopic compositions, and these tests show that our analytical methods correctly determine the Fe isotope compositions of the crusts (Table 6.1). Artificial Fe-Mn-Co solutions made using Fe:Mn of 3:4 for all solutions, which is the average of the crusts studied, where the Fe used is UW HPS Fe; 15 analyses of the pure HPS Fe standard during the study produced $\delta^{56}Fe$ = 0.49 ±0.06 ‰ and $\delta^{57}Fe$ = 0.74±0.06 ‰ (1SD), which is indistinguishable from the isotopic compositions recovered from the 11 artificial solutions that contained up to 0.5 wt% Co and were passed through the ion-exchange columns up to three times, demonstrating complete purification of Fe from the Co and Mn matrix, and complete recoveries during ion-exchange

Fe isotopic compositions were obtained using a Micromass IsoProbe MC-ICP-MS at Univ. of Wisconsin-Madison. Instrumental mass bias was corrected using a standard-sample bracketing approach. The isobaric interferences, ArN, ArO, and essentially all ArOH species, on the Fe mass spectrum, were completely removed by adding a mixture of hydrogen and argon to the collision cell of the IsoProbe. Two Fe isotope ratios ($^{56}Fe/^{54}Fe$ and $^{57}Fe/^{54}Fe$) were both measured as an internal data quality check. Samples solutions were prepared from 25 ppm Fe stock solutions by the *Ferrozine* method (Stookey, 1970) and in order to avoid concentration-induced fractionation during data acquisition, the concentration of the solutions were controlled at 300 to 500 ppb. All $\delta^{56}Fe$ and $\delta^{57}Fe$ values are normalized to average igneous Fe (the E-M system in eq 6.1), with values of $^{56}Fe/^{54}Fe$ = 0.49 and $^{57}Fe/^{54}Fe$ = 0.73. Three ultra-pure Fe standards were routinely measured *viz.* two internal laboratory standards from Johnson Matthey (labelled J-M Fe and High Purity Standards, HPS Fe) and one from Institute of Reference Materials and Measurements, IRMM-014, which is dissolved from pure Fe metal. The measured Fe isotopic composition of these standards during the course of this study were J-M Fe: $\delta^{56}Fe$ = 0.27 ±0.07 ‰, $\delta^{57}Fe$ = 0.41±0.10 ‰ (1SD, n=49); HPS Fe: $\delta^{56}Fe$ = 0.49 ±0.06 ‰, $\delta^{57}Fe$ = 0.74±0.06 ‰ (1SD, n=15); and IRMM-014: $\delta^{56}Fe$ = -0.10 ±0.07 ‰, $\delta^{57}Fe$ = -0.08±0.13 ‰ (1SD, n=49). Other instrumental descriptions are detailed in Beard *et al.* (2003a).

Table 6.1 Fe isotope of HPS Fe dope synthetic solutions

Synthesis description	Sample notes*	Individual analysis of solution				Grand average incl. replicates			
		δ^{56}Fe	2SE	δ^{57}Fe	2SE	δ^{56}Fe	1SD	δ^{57}Fe	1SD
2 passes									
[Co]=0.1%	2	0.54	0.07	0.85	0.04	0.50	0.05	0.79	0.08
	3	0.47	0.07	0.74	0.04				
3 passes									
[Co]=0.1%	1	0.48	0.06	0.79	0.04	0.48	0.03	0.72	0.06
	2	0.54	0.06	0.71	0.04				
	3	0.47	0.06	0.71	0.05				
	4	0.45	0.06	0.66	0.04				
	5	0.47	0.05	0.72	0.03				
	6	0.47	0.06	0.66	0.03				
	7	0.48	0.06	0.82	0.03				
[Co]=0.3%	8	0.62	0.09	0.86	0.05	0.58	0.06	0.88	0.14
	8	0.51	0.07	0.75	0.04				
	9	0.62	0.10	1.03	0.07				
[Co]=0.5%	10	0.43	0.05	0.63	0.04	0.52	0.07	0.76	0.11
	10	0.61	0.07	0.90	0.03				
	11	0.55	0.07	0.76	0.04	0.52	0.03	0.75	0.02
	11	0.50	0.08	0.73	0.05				
Unprocessed HPS						**0.49**	**0.06**	**0.74**	**0.06**

*Each number indicates measurement from the same column chemistry; repeated number represents an instrumental re-run.

6-4 Results

Fe isotope results are detailed in Table 6.2-6.4 and Figs. 6.1 and 6.2. The overall Fe isotope variation of SC5 over the last 10Ma of this sample has not been large. Excluding the 10.4 Ma layer, which is affected by carbonate fluroapatite diagenetic alteration (see Chapter 2), the average δ^{56}Fe for the 28 layers is –0.41±0.05 (1SD). Except for the oldest part of the IB2 profile the two IB Fe-Mn crusts have lower δ^{56}Fe values than SC5 and exhibit greater variations through time, especially IB2. Average values are as follows: IB1 –0.55±0.06 (from 23 analysed layers) and IB2 –0.60±0.16 (from 31 analysed layers). In IB1, four stepped decreases in δ^{56}Fe are observed at 4.4, 3.2, 1.3-0.6, and 0.4-0 Ma. The variation in IB2 is more dramatic (Fig. 6.3 lower panel) with a strong zig-zag pattern peaking at 4.6 Ma, 3.2 Ma, 1.5 Ma and 0.4 Ma. Significantly from 4.0 Ma to the present, the two IB patterns are strongly coupled although the shifts in IB2 are always more pronounced than IB1.

Table 6.2 Fe isotope time-series for IB1

depth interval	age*		Individual analysis of solution				Grand average incl. replicates			
[mm]	[Ma]		δ^{56}Fe	2SE	δ^{57}Fe	2SE	δ^{56}Fe	1SD	δ^{57}Fe	1SD
IB1 (D105-5AB)										
surface	0.02		-0.59	0.06	-0.87	0.04	-0.61	0.03	-0.90	0.03
			-0.63	0.05	-0.92	0.03				
0.0-0.5	0.05		-0.59	0.05	-0.93	0.04	-0.63	0.05	-0.92	0.02
			-0.67	0.05	-0.90	0.03				
1.0-1.5	0.23		-0.52	0.05	-0.86	0.03				
2.0-2.5	0.42	Aliquot 1	-0.50	0.05	-0.78	0.03	-0.49	0.02	-0.72	0.09
		Aliquot 2	-0.48	0.07	-0.66	0.04				
3.0-3.5	0.6	Aliquot 1	-0.65	0.06	-0.92	0.03	-0.60	0.05	-0.83	0.08
			-0.55	0.07	-0.75	0.04				
		Aliquot 2	-0.60	0.05	-0.81	0.03				
4.0-4.5	0.79		-0.58	0.06	-0.79	0.04				
5.5-6.0	1.06		-0.49	0.07	-0.79	0.04				
6.5-7.0	1.25	Aliquot 1	-0.39	0.05	-0.65	0.03	-0.44	0.07	-0.71	0.08
		Aliquot 2	-0.49	0.06	-0.77	0.04				
7.5-8.0	1.44	Aliquot 1	-0.42	0.06	-0.63	0.04	-0.47	0.05	-0.67	0.10
			-0.46	0.05	-0.60	0.04				
		Aliquot 2	-0.53	0.04	-0.78	0.03				
9.0-9.5	1.71		-0.51	0.06	-0.77	0.05	-0.52	0.02	-0.77	0.00
			-0.54	0.05	-0.78	0.02				
10.0-10.5	1.9		-0.52	0.06	-0.75	0.03				
11.5-12.0	2.18	Aliquot 1	-0.48	0.06	-0.77	0.04	-0.50	0.02	-0.77	0.00
		Aliquot 2	-0.51	0.06	-0.77	0.04				
12.5-13.0	2.36		-0.51	0.05	-0.81	0.02				
13.0-13.5	2.45		-0.57	0.06	-0.84	0.04				
14.0-14.5	2.73		-0.57	0.06	-0.77	0.04	-0.60	0.04	-0.85	0.12
			-0.63	0.07	-0.94	0.04				
15.0-16.0	2.88		-0.53	0.07	-0.83	0.04				
17.0-18.0	3.24		-0.53	0.08	-0.74	0.04	-0.65	0.08	-0.91	0.13
			-0.68	0.05	-0.93	0.04				
			-0.69	0.06	-1.04	0.04				
			-0.71	0.06	-0.95	0.05				
18.0-19.0	3.43		-0.56	0.06	-0.81	0.03	-0.56	0.06	-0.81	0.03
19.0-20.0	3.61		-0.63	0.06	-0.92	0.04	-0.58	0.07	-0.88	0.06
			-0.53	0.07	-0.84	0.04				
21.0-22.0	3.98		-0.53	0.04	-0.83	0.04				
22.1-23.1	4.19	Aliquot 1	-0.57	0.07	-0.87	0.04	-0.56	0.04	-0.82	0.04
			-0.60	0.08	-0.82	0.05				
		Aliquot 2	-0.56	0.07	-0.78	0.05				
			-0.50	0.07	-0.80	0.04				
23.0-24.0	4.37	Aliquot 1	-0.69	0.06	-0.98	0.04	-0.68	0.08	-0.97	0.07
			-0.70	0.05	-0.94	0.04				
		Aliquot 2	-0.57	0.10	-0.89	0.05				
			-0.76	0.06	-1.07	0.04				
24.0-25.0	4.52	Aliquot 1	-0.56	0.07	-0.84	0.04	-0.57	0.01	-0.85	0.02
		Aliquot 2	-0.58	0.05	-0.86	0.04				

Table 6.3 Fe isotope time-series for IB2

depth interval	age*		Individual analysis of solution				Grand average incl. replicates			
[mm]	[Ma]		δ^{56}Fe	2SE	δ^{57}Fe	2SE	δ^{56}Fe	1SD	δ^{57}Fe	1SD
IB2 (D97-1)										
surface	0.01		-0.94	0.05	-1.32	0.03	-0.94	0.00	-1.34	0.03
			-0.94	0.06	-1.37	0.04				
0.0-1.0	0.07		-0.55	0.07	-0.81	0.03	-0.61	0.09	-0.89	0.12
			-0.68	0.05	-0.98	0.03				
1.5-2.0	0.26		-0.45	0.05	-0.66	0.03	-0.49	0.05	-0.71	0.06
			-0.52	0.05	-0.75	0.04				
2.0-2.5	0.34		-0.46	0.06	-0.71	0.04				
2.5-3.0	0.41		-0.47	0.06	-0.69	0.04				
3.0-3.5	0.49		-0.41	0.09	-0.70	0.04	-0.49	0.10	-0.75	0.07
			-0.56	0.05	-0.80	0.03				
3.5-4.0	0.56		-0.48	0.09	-0.74	0.04	-0.46	0.02	-0.75	0.01
			-0.45	0.06	-0.75	0.04				
4.0-4.5	0.63		-0.68	0.06	-1.01	0.04	-0.70	0.03	-1.01	0.00
			-0.71	0.07	-1.01	0.05				
4.5-5.0	0.71	Aliquot 1	-0.74	0.07	-1.16	0.04	-0.77	0.05	-1.18	0.02
			-0.83	0.05	-1.20	0.04				
		Aliguot 2	-0.74	0.05	-1.18	0.03				
5.5-6.0	0.86	Aliquot 1	-0.79	0.05	-1.15	0.04	-0.77	0.03	-1.11	0.03
			-0.77	0.06	-1.10	0.04				
		Aliquot 2	-0.74	0.07	-1.10	0.04				
6.5-7.0	1.01		-0.82	0.06	-1.15	0.03				
7.5-8.0	1.16	Aliquot 1	-0.83	0.05	-1.19	0.04	-0.79	0.03	-1.20	0.00
			-0.78	0.05	-1.20	0.04				
		Aliquot 2	-0.76	0.06	-1.20	0.04				
8.0-8.5	1.23		-0.67	0.06	-1.03	0.04	-0.73	0.08	-1.09	0.08
			-0.79	0.07	-1.15	0.04				
8.5-9.0	1.31		-0.80	0.05	-1.13	0.03				
9.5-10.0	1.46		-0.46	0.07	-0.78	0.04	-0.52	0.05	-0.82	0.04
			-0.57	0.05	-0.81	0.04				
			-0.53	0.05	-0.86	0.03				
10.0-10.5	1.53	Aliquot 1	-0.50	0.07	-0.81	0.04	-0.55	0.07	-0.87	0.10
		Aliquot 2	-0.61	0.07	-0.94	0.04				
11.0-12.0	1.72		-0.68	0.07	-0.99	0.04				
12.0-13.0	1.87		-0.60	0.08	-0.95	0.05	-0.61	0.02	-0.97	0.03
			-0.63	0.06	-0.99	0.04				
13.0-14.0	2.01	Aliquot 1	-0.69	0.05	-1.00	0.03	-0.67	0.06	-1.00	0.03
		Aliquot 2	-0.61	0.07	-0.97	0.04				
			-0.72	0.05	-1.03	0.04				
15.0-16.0	2.31		-0.66	0.04	-1.05	0.05				
17.0-18.0	2.61		-0.75	0.06	-1.10	0.04				
19.0-20.0	2.91	Aliquot 1	-0.65	0.04	-1.02	0.03	-0.67	0.02	-0.99	0.04
		Aliquot 2	-0.68	0.05	-0.96	0.03				
20.0-21.0	3.06		-0.75	0.06	-1.04	0.04				
21.0-22.0	3.21		-0.44	0.04	-0.64	0.02	-0.53	0.07	-0.74	0.09
			-0.57	0.05	-0.79	0.04				
			-0.56	0.06	-0.81	0.04				
22.0-23.0	3.36		-0.53	0.08	-0.76	0.04				
24.0-25.0	3.66		-0.51	0.05	-0.71	0.04				
25.0-26.0	3.81		-0.50	0.06	-0.75	0.04				
26.0-27.0	3.96		-0.47	0.05	-0.72	0.04				
28.0-29.0	4.25		-0.42	0.06	-0.53	0.05	-0.40	0.03	-0.52	0.02
			-0.37	0.07	-0.50	0.04				
29.0-30.0	4.40		-0.32	0.05	-0.45	0.04				
30.0-31.3	4.57	Dissol. 1	-0.22	0.06	-0.34	0.03	-0.26	0.07	-0.37	0.06
			-0.26	0.04	-0.37	0.04				
			-0.36	0.05	-0.46	0.03				
		Dissol. 2	-0.21	0.07	-0.33	0.04				

Table 6.4 Fe isotope time-series for SC5

depth interval	age*		Individual analysis of solution				Grand average incl. replicates			
[mm]	[Ma]		$\delta^{56}Fe$	2SE	$\delta^{57}Fe$	2SE	$\delta^{56}Fe$	1SD	$\delta^{57}Fe$	1SD
SC5 (28DSR9)										
surface	0.03		-0.46	0.08	-0.66	0.03	-0.47	0.01	-0.66	0.01
			-0.48	0.05	-0.67	0.03				
1.0-1.5	0.34	Aliquot 1	-0.38	0.05	-0.64	0.04	-0.43	0.07	-0.65	0.01
		Aliquot 2	-0.48	0.06	-0.66	0.04				
1.5-2.0	0.47	Aliquot 1	-0.45	0.07	-0.77	0.04	-0.44	0.01	-0.70	0.09
		Aliquot 2	-0.43	0.05	-0.64	0.04				
2.6-3.0	0.75		-0.45	0.05	-0.64	0.04	-0.43	0.04	-0.62	0.03
			-0.40	0.06	-0.60	0.04				
4.0-4.5	1.15		-0.46	0.05	-0.74	0.04				
5.5-6.0	1.56		-0.46	0.06	-0.68	0.04				
7.0-7.5	1.96		-0.43	0.06	-0.66	0.03				
8.0-8.5	2.23	Aliquot 1	-0.37	0.07	-0.56	0.04	-0.38	0.06	-0.60	0.05
			-0.44	0.05	-0.66	0.03				
		Aliquot 2	-0.32	0.07	-0.57	0.04				
9.0-9.5	2.50		-0.45	0.07	-0.59	0.04	-0.43	0.03	-0.62	0.04
			-0.41	0.05	-0.65	0.03				
11.0-12.0	3.11	Aliquot 1	-0.38	0.07	-0.54	0.04	-0.35	0.03	-0.51	0.02
			-0.32	0.05	-0.49	0.03				
		Aliquot 2	-0.35	0.06	-0.51	0.03				
12.0-13.0	3.38		-0.41	0.07	-0.58	0.04	-0.44	0.05	-0.61	0.04
			-0.48	0.04	-0.64	0.03				
13.0-14.0	3.65		-0.49	0.06	-0.65	0.03	-0.48	0.01	-0.64	0.02
			-0.47	0.08	-0.63	0.04				
14.0-15.0	3.92		-0.38	0.04	-0.54	0.03	-0.37	0.01	-0.53	0.01
			-0.37	0.07	-0.52	0.04				
16.0-17.0	4.46	Aliquot 1	-0.36	0.05	-0.62	0.03	-0.39	0.02	-0.61	0.03
			-0.39	0.05	-0.63	0.04				
		Aliquot 2	-0.41	0.06	-0.58	0.04				
17.0-18.0	4.73		-0.35	0.04	-0.52	0.03				
18.0-19.0	5.00	Aliquot 1	-0.28	0.06	-0.50	0.04	-0.33	0.08	-0.54	0.06
		Aliquot 2	-0.42	0.03	-0.61	0.03				
			-0.40	0.05	-0.55	0.03				
			-0.38	0.07	-0.59	0.04				
		Dissol. 2	-0.24	0.07	-0.43	0.04				
			-0.27	0.06	-0.54	0.04				
19.0-20.0	5.27		-0.25	0.06	-0.33	0.04	-0.31	0.06	-0.42	0.08
			-0.38	0.07	-0.48	0.05				
			-0.30	0.06	-0.45	0.04				
21.0-22.0	5.81		-0.34	0.04	-0.42	0.03				
23.0-24.0	6.35		-0.43	0.06	-0.60	0.03				
24.0-25.0	6.62		-0.42	0.05	-0.74	0.04	-0.41	0.01	-0.65	0.13
			-0.40	0.06	-0.56	0.07				
26.0-27.0	7.16		-0.45	0.05	-0.62	0.03				
27.0-28.0	7.43		-0.39	0.07	-0.60	0.05	-0.47	0.07	-0.68	0.07
			-0.52	0.06	-0.70	0.03				
			-0.51	0.07	-0.74	0.04				
28.0-29.0	7.70	Aliquot 1	-0.42	0.06	-0.59	0.04	-0.41	0.02	-0.57	0.01
		Aliquot 2	-0.41	0.07	-0.57	0.04				
			-0.39	0.07	-0.56	0.05				
29.0-30.0	7.97		-0.41	0.05	-0.61	0.04				
30.0-31.0	8.24		-0.43	0.06	-0.67	0.04				
32.0-33.0	8.79	Dissol. 1	-0.43	0.07	-0.58	0.04	-0.41	0.01	-0.58	0.01
			-0.40	0.06	-0.59	0.03				
		Dissol. 2	-0.41	0.05	-0.58	0.03				
33.0-34.0	9.05		-0.41	0.06	-0.61	0.04				
36.0-37.0	9.86	Aliquot 1	-0.36	0.06	-0.55	0.04				
		Aliquot 2	-0.25	0.07	-0.38	0.04				

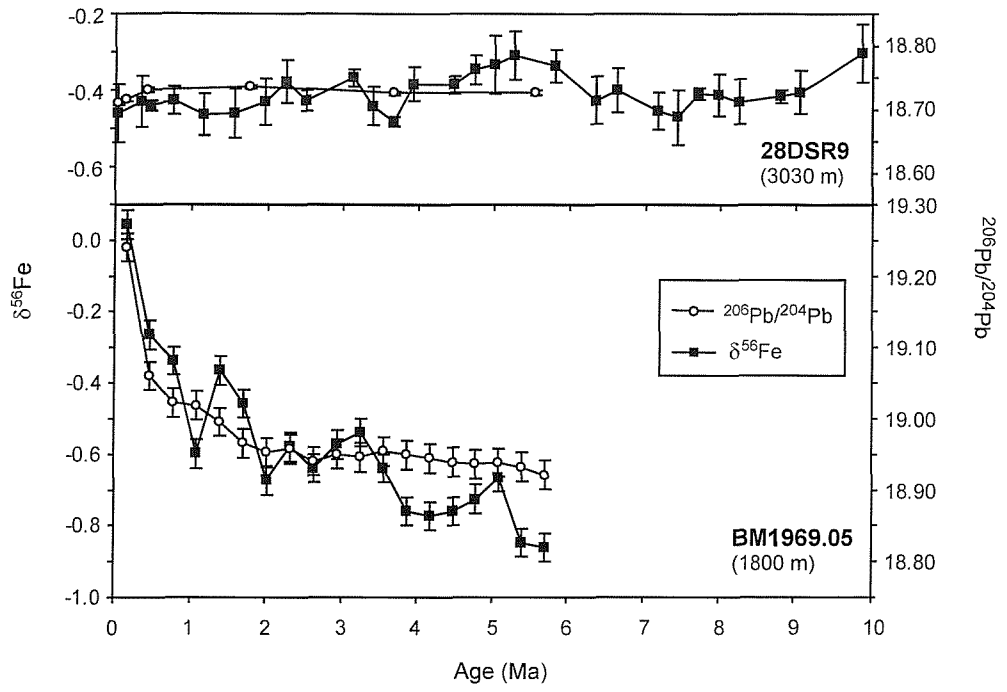

Fig. 6.1 Temporal variations in $\delta^{56}Fe$ values (solid squares) and $^{206}Pb/^{204}Pb$ ratios (open circles) of Central Pacific Fe-Mn crust 28DSR9 (SC5, this study) and N. Atlantic Fe-Mn crust BM1969.05 (Zhu *et al.*, 2000). Ages for individual layers based on $^{10}Be/^{9}Be$ chronology. Error bars for the Pacific crusts of this study are 1SD (external) or 2SE (internal) for $\delta^{56}Fe$ and 2SD (external) for $^{206}Pb/^{204}Pb$. Error bars for the data from Zhu *et al.* (2000) based on their estimated average reproducibility.

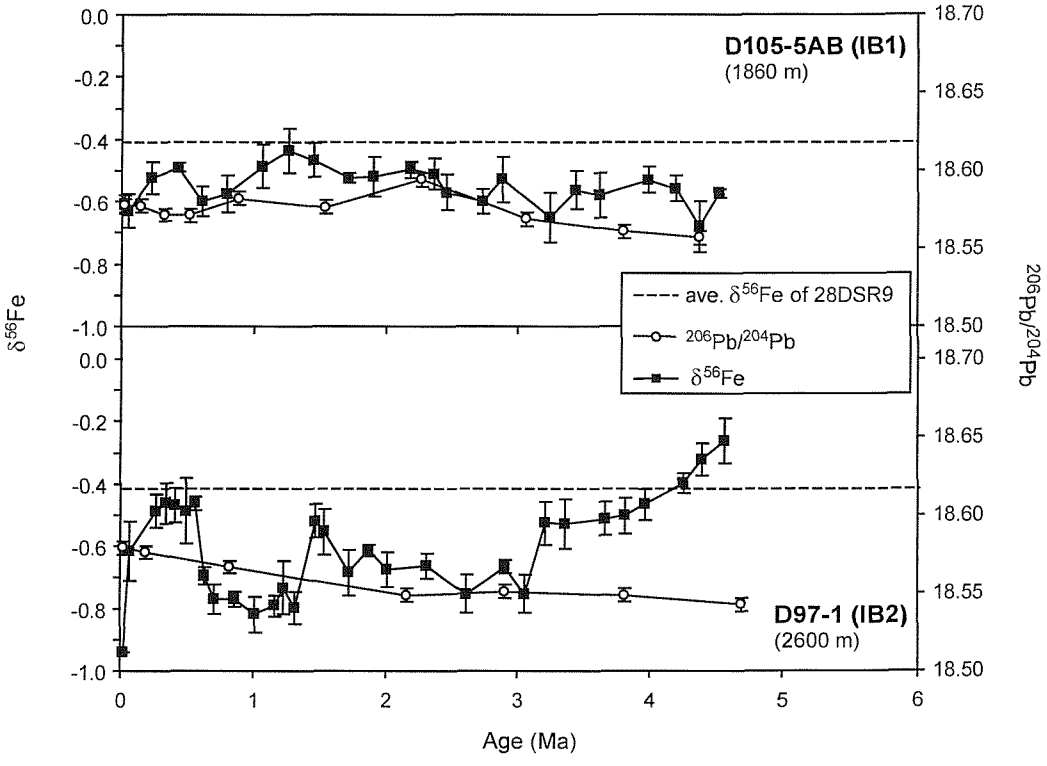

Fig. 6.2 $\delta^{56}Fe$ and $^{206}Pb/^{204}Pb$ variations with time for the two Izu-Bonin back-arc basin Fe-Mn crusts. Average $\delta^{56}Fe$ value for Central Pacific crust 28DSR9 (-0.41±0.05, 1SD), marked as dashed line, and this is taken as representative of the Fe isotope composition of open central Pacific deep water.

6-5 Discussion and Conclusions

The temporal trends in Fe isotope compositions we report from the Pacific Ocean are quite different from those previously measured from the NW Atlantic Ocean (Figs. 6.1 & 6.2). Zhu *et al.* (2000) showed that secular variations in Fe isotope compositions in the NW Atlantic co-varied with Pb isotope ratios over the past 6 Ma and argued that this reflected variations in the Fe and Pb isotope compositions of weathered continental materials. Subsequently, however, Beard *et al.* (2003a) have shown that the Fe isotope composition of terrestrial detrital material is isotopically homogenous; they suggest that a more likely explanation for the rapid increase in δ^{56}Fe values reported by Zhu *et al.* (2000) from 2 Ma to the present lies in changes in the proportions of different sources of Fe during climate change and, specifically, a change in the major source of dissolved Fe to the NW Atlantic from hydrothermal to continental at the onset of continental glaciation. This interpretation is based on the observation that submarine hydrothermal sources have low δ^{56}Fe values as compared to terrestrial (continental or volcanogenic) sources of Fe (Sharma *et al.*, 2001; Beard *et al.*, 2003b; Severmann *et al.*, 2004).

The Fe isotope data for the Pacific Ocean confirm that the Fe isotope composition of seawater between and within the ocean basins is indeed heterogeneous which has also recently been demonstrated from the global distribution of ferromanganese crust surfaces (Figs. 6.1 & 6.2). The observation that the surface δ^{56}Fe value for the Central Pacific crust is more negative than that for the modern NW Atlantic provides strong evidence that there is a significantly larger hydrothermal input of dissolved Fe to central Pacific deep-waters in the present day. This is also consistent with the more "mantle-like" Pb isotope composition of this crust when compared to the NW Atlantic crust (Fig. 6.1). It is important to note, however, that although increased input of volcanogenic material could also account for the observed shift in Pb isotope compositions, the negative δ^{56}Fe values observed here provide unambiguous indications of an increased hydrothermal input. Further, the observation that the δ^{56}Fe values for this crust have remained essentially invariant throughout the past 10 Ma (-0.41±0.05) suggests that the balance of hydrothermal versus terrigenous (δ^{56}Fe = 0) sources of dissolved Fe in this region have remained essentially constant throughout this time. This assertion should not be considered particularly

controversial because hydrothermal fluxes to the deep Pacific Ocean are linked closely to magmatic heat-flux which, in turn, is directly correlated with seafloor spreading rates (Baker *et al.*, 1996), which have not changed significantly since the Cretaceous (Johnson and Pariso, 1993).

Iron isotope variations in the Izu-Bonin (IB) back-arc crusts over the last 5 Ma are different from the Central Pacific Ocean. This contrast is also reflected in the Pb isotope compositions of these crusts, which have lower $^{206}Pb/^{204}Pb$ ratios than those of the central Pacific crust, consistent with input from local volcanic and/or Japan Sea sedimentary material (Hemming and McLennan, 2001; Wang *et al.*, 2004). Because of the overlap in these reservoirs, however, Pb isotope compositions of these crusts do not allow the relative inputs from different potential sources to be discerned. By contrast, both Izu-Bonin crusts have $\delta^{56}Fe$ values that are more negative than those of the Central Pacific crust. Like Central Pacific crust 28DSR9, IB crust D105-5AB (1860 m) exhibits rather constant $\delta^{56}Fe$ values throughout the past 4-5 Ma but with a more negative mean of –0.55±0.06 indicative of a larger contribution of hydrothermal dissolved Fe at this location. Active hydrothermal fields are well known along the Izu-Bonin Arc, including one within 150 km of the site of IB crust D105-5AB (Urabe and Kusakabe, 1990; Tsunogai *et al.*, 1994; Iizasa *et al.*, 1999). It seems likely that systematic exploration along this arc in the future will identify still more abundant activity, as has been demonstrated recently for the Mariana Volcanic Arc (Embley *et al.*, 2004).

The isotopic variations for crust D97-1 (2600 m) are significantly different from those of the other two crusts. $\delta^{56}Fe$ values less than –0.4 are characteristic for this crust throughout the past 4 Ma, and there are significant deviations to even more negative values at 3.1-1.7 Ma ($\delta^{56}Fe$ = -0.69±0.05), at 1.3-0.6 Ma ($\delta^{56}Fe$ = -0.77±0.04), and from 0.2 Ma to present ($\delta^{56}Fe$ as low as –0.9). Although these values are all more negative than the values reported for either Central Pacific crust 28DSR9 or the other IB crust D105-5AB, they exhibit close overlap with the range of the values reported for submarine hydrothermal vent-fluids(Sharma *et al.*, 2001; Beard *et al.*, 2003b; Severmann *et al.*, 2004). $^{206}Pb/^{204}Pb$ ratios in these samples do not correlate with Fe isotope compositions, and, instead, have rather constant ratios that are similar to those observed in crust D105-5AB (Fig. 6.2). This provides the first example of decoupling of Fe and Pb isotope ratios in the oceans. As described above,

by themselves the Pb isotope data do not place constraints on the sources of metals at this location. In contrast, the δ^{56}Fe values for crust D97-1 are indicative of an increased input of hydrothermally-sourced dissolved Fe as compared with both the NW Atlantic and the Central Pacific crusts. Further, the excursions to strongly negative δ^{56}Fe values observed are best explained by discrete episodes of increased hydrothermal input. These periods broadly correlate with two distinct episodes of volcanic activity along the Izu-Bonin Arc, from 2.8 to 1.0 Ma and from 1 Ma to present (Ishizuka *et al.*, 2003b).

Why does crust D105-5AB, which was collected from ca. 1000 m shallower on the seafloor and <100 km farther north along the Izu-Bonin Arc, not record the hydrothermal "episodes" that are seen in the D97-1 crust? One possibility is that highly localized inputs to crust D97-1 reflect the very short length-scales over which hydrothermal effluent is dispersed from any vent site to the surrounding oceans, which may be no greater than 10 km for dissolved Fe in the Pacific Ocean (Field and Sherrell, 2000). Perhaps more important, however, is the depth difference between the two sites. Sill height for across-arc connection with the open Pacific Ocean lies between 1500 m and 2000 m in this region. Strong lateral advection of currents across the top of the Izu-Bonin Arc, therefore, may have led to greater homogenisation of the dissolved Fe-isotope record in shallow crust D105-5AB (1860 m) while deep crust D97-1 (2600 m, more than 500 m below the across-axis sill depth) may have more faithfully recorded input of hydrothermal discharge to the deeper waters of this marginal back-arc basin (Fig. 6.4). Support for a model in which highly negative δ^{56}Fe values reflect pulses of increased hydrothermally-derived Fe comes from correlations of decreasing δ^{56}Fe ratios with increasing Cu, Zn, and V concentrations (Fig. 6.3). Enrichments of these metals are all strongly correlated with particulate, oxidised Fe in submarine hydrothermal systems (Lilley *et al.*, 1995) while these correlations provides direct evidence that their high concentrations indeed represent episodes of increased hydrothermal input.

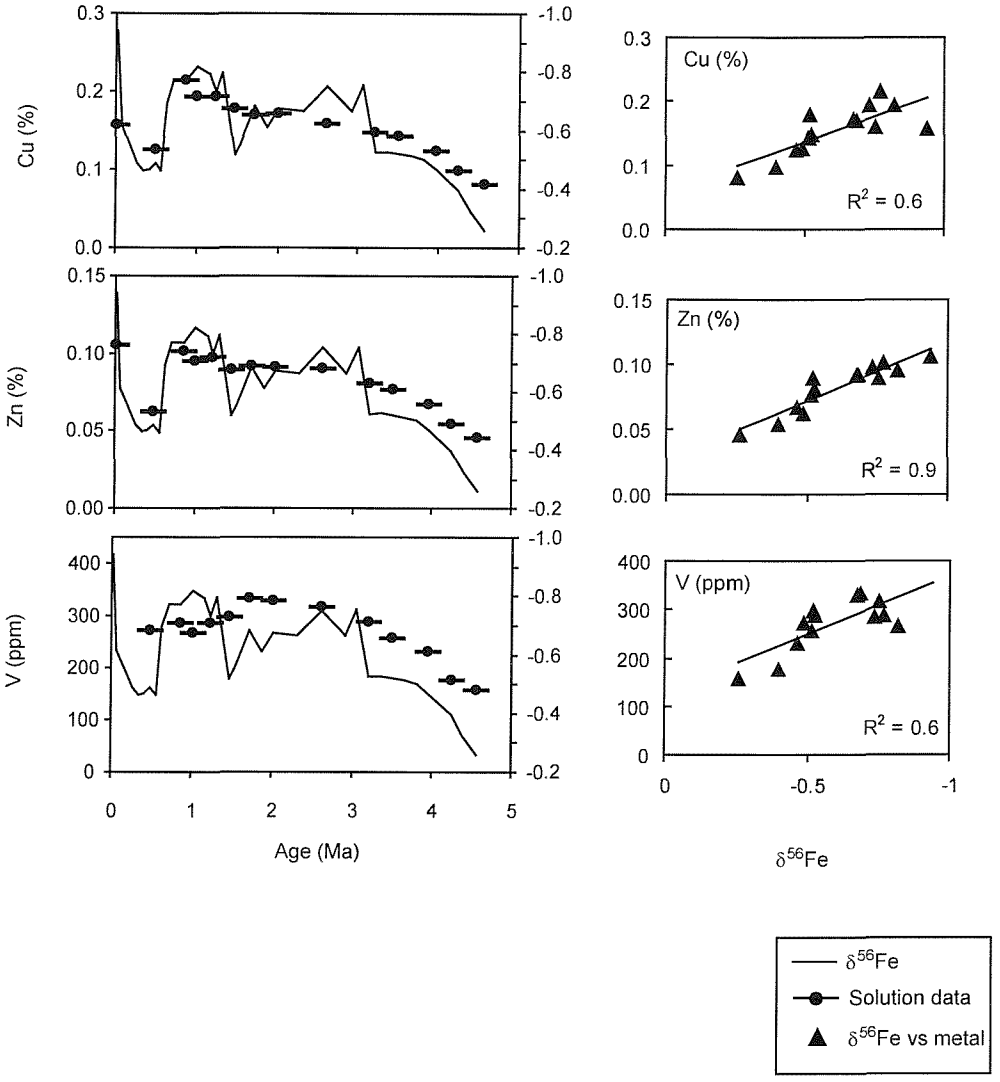

Fig. 6.3 Cu, Zn, and V concentrations versus age (Ma) and their correlations with $\delta^{56}Fe$ for Izu-Bonin Fe-Mn crust D97-1 (IB2). Temporal variations in these metals correlate with Fe isotope compositions for crust D97-1 (solid line in left panel), resulting in good correlations between enrichments in Cu, Zn, and V and progressively more negative $\delta^{56}Fe$ values (right side plots), supporting the interpretations that very low $\delta^{56}Fe$ values record periods of strong hydrothermal fluxes.

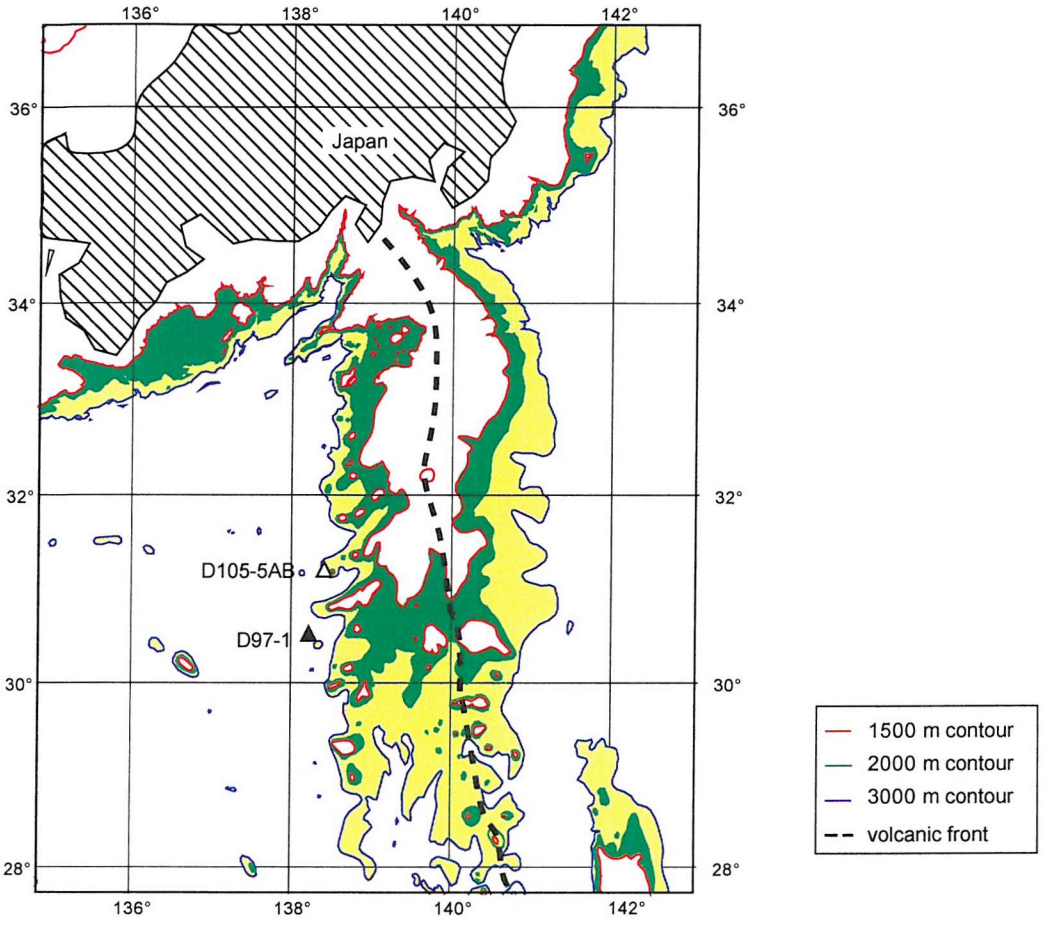

Fig. 6.4 Bathymetric map of Izu-Bonin back-arc basin area. Dashed line represents the modern volcanic front. The current back-arc rift zone lies immediately west. The two Izu-Bonin samples analysed in this study are marked in open and solid triangles, and are situated on the western flanks of current back-arc rift zone. Crust D105-5AB (IB1) was sampled at a depth of 1860 m, and it seems likely that hydrothermal Fe sources would lie in the area marked in green, at depths between ~2000 m and 1500 m. Fe-Mn crust D97-1 (IB2) was sampled at a depth of 2600 m, and hydrothermal sources of Fe are thought to encompass a wider area, as marked in yellow, in addition to the green area.

We demonstrate the highly variability of Fe isotope compositions in the oceans and a stronger hydrothermal input in the Pacific Ocean. It is difficult, at current stage, to encompass the exact range of hydrothermal fluids due to the limited δ^{56}Fe dataset. However, derived from this study, if we assume an end-member vent-fluid composition of δ^{56}Fe = -0.8, ca. 50% of the dissolved Fe content of the deep Pacific Ocean would be derived from submarine hydrothermal activity and this influence (even more pronounced in the Izu-Bonin marginal basin) has been sustained throughout the past 5 to 10 million years. For an ocean volume of ca.700 km^3 and a typical deep-ocean dissolved Fe concentration of 0.2-0.4 nmol/L (Bruland *et al.*, 1994; Wu *et al.*, 2001) an instantaneous standing crop inventory of dissolved Fe in the deep Pacific Ocean can be calculated of $1.4\text{-}2.8\times10^{11}$ moles per year. Assuming a residence time for this dissolved Fe of 70-140 years (Bruland *et al.*, 1994) indicates a removal flux of $1\text{-}4\times10^{9}$ moles per year from the deep Pacific Ocean. At steady state, if 50 % of deep Pacific dissolved Fe is hydrothermally-sourced, a net flux from venting of 0.5 to 2×10^{9} moles per year would be required. The global hydrothermal flux of Fe from vent axial is much greater: 2×10^{11} moles/year (Elderfield and Schultz, 1996). Assuming that hydrothermal flux scales with magmatic accretion and spreading rate, the Pacific Ocean should receive at least 50 % of this global flux (Baker *et al.*, 1996), which, for Fe, equates to ca. 1×10^{11} moles/year. Although the vast majority of this dissolved Fe will be precipitated rapidly as sulfide and/or oxyhydroxide particles in hydrothermal plumes (Mottl and McConachy, 1990; Rudnicki and Elderfield, 1993; Field and Sherrell, 2000), therefore as little as 0.5-2% of the total hydrothermal flux, if stabilised in solution (e.g. by complexation with organic ligands) would be sufficient to contribute 50% of the steady state dissolved Fe flux to the deep Pacific Ocean. These arguments support an early hypothesis (Coale *et al.*, 1996), therefore, that hydrothermal circulation in the deep ocean could indeed act as a significant source of dissolved Fe to the surface ocean, via upwelling.

Chapter 7. Conclusions

7-1 Summary of the thesis

The objective of this thesis is to understand Hf and Fe isotopic systems in their applications to (pale)oceanography with Fe-Mn crusts served as samples for this purpose. In addition to these isotopic systems, Be, Nd, and Pb isotopes as well as a spectrum of major and trace elements were applied for age determination, sample origin and certain source input backgrounds.

First of all, Hf isotope analytical method was established and and a resulting spin-off from this was the determination Yb isobaric interferences on the Hf isotopes. To achieve accurate results it was necessary to revise the accepted isotopic values for Yb and new replacement values are proposed (Chu *et al.*, 2002). Using the new values, it can be demonstrated that Yb and Hf have similar levels of mass bias and that consistent $^{176}Hf/^{177}Hf$ can be achieved following the application of a simple empirical correction.

The selected suite of Fe-Mn crusts from Central and Western Pacific Ocean (Izu-Bonin back-arc basin) have encompassed two different geographic and geological settings. Mineralogical and geochemical data of these samples demonstrate they have a hydrogenetic origin and represent suitable materials for oceanographic studies. The growth rates of the samples were determined by ^{10}Be method for time series studies.

In order to construct a Hf isotope profile in present day Central Pacific seawater column in the continuing absence of direct-measured seawater values, Hf isotope analysese of surface-layers of the Fe-Mn crusts recovered at various depths were measured. The correlation of Nd isotopes (measured on the same material as Hf) with WOCE database-derived 'on-site' hydrological properties demonstrates that this surface-scraping approach is suitable to infer present day seawater properties. Since the Hf isotopic compositions of the water column depth profiles show less variation than Nd when comparing the data with the hydrological properties of nearby sites, this confirms a longer oceanic residence time of Hf than Nd. As a result of this work, estimated Hf isotopic compositions in two water masses (Intermediate Water and Pacific Deep Water) of the Central Pacific are proposed. A weathering input from nearby Papua New Guinea islands to the Central Pacific sites, as suggested by

previous studies (Sholkovitz *et al.*, 1999; Lacan and Jeandel, 2001), is also observed from Nd isotopic composition and REE analyses of this study.

Three Fe-Mn crusts, one from the already well-characterised Central Pacific Ocean and two from a completely novel setting of the Izu-Bonin Back-Arc Basin area, have been investigated in an attempt to decipher secular variations in the radiogenic isotope budgets of the Pacific Ocean. The results from one South Central Pacific Fe-Mn crust agree well with previously published records from North Central Pacific crusts over the period from 5 Ma to the present. Based on their Pb isotopic signatures, two Izu-Bonin back-arc basin samples appear to demonstrate a two-component mixing between aeolian loess input and weathering from volcanic island arcs. A decoupling of Nd from Hf isotope records is observed in both these two crusts at ~4Ma, which could be a direct consequence of localised hydrothermal activity or arc weathering that preferentially impacts the Hf isotopic record over that of Nd in this relatively geographically-confined basin. This is, however, difficult to resolve as the end-members of riverine and hydrothermal Hf isotopic data are still unavailable to date.

At the last part of the thesis, the first high-resolution time series Fe isotopic compositions in the Pacific Ocean were obtatined and the heterogeneous data suggest that Fe has a very short residence time in the ocean. The Fe-isotopic profile from the Central Pacific is distinctly different to those of the arc-associated Izu-Bonin Fe-Mn crusts, suggesting different input sources to these two regions. Work by several groups of laboratories has confirmed the homogeneous nature of δ^{56}Fe values from most terrestrial sources but recent observations by Sharma *et al.* (2001) and Beard *et al.* (2003b) suggest that hydrothermal fluids are characterised by negative values. The δ^{56}Fe values for the back arc samples are hence strongly influenced by hydrothermal inputs.

An additional feature supporting the involvement of hydrothermal solutions is the good correlation between the timing of volcanic activity pulses (based on Ar-Ar ages), and the temporal Fe isotope variations observed in Izu Bonin crusts. This observation suggests that Fe isotopes can be used as a tracer in deciphering past hydrothermal activities.

Another interesting feature of the two Izu Bonin samples is that although the δ^{56}Fe profiles are quite similar in shape they differ in amplitude (IB2>IB1). Clearly the two samples which are only 80 kms apart are recording the same events but one of them (IB2) is much more strongly influenced. It is therefore suggested that two possible factors might have attributed to this. The first is the different water depths of the two samples. Because IB2 occurs at greater depth, it will be more strongly influenced by any hydrothermal activity. Secondly, because IB2 has a faster growth rate, the hydrothermal signature will suffer less dilution or overprint from normal seawater.

In the case of the Central Pacific sample a biogeochemical process is proposed to account for Fe isotope fractionation. This view is based on the observation of the negative correlation between the aeolian input and δ^{56}Fe values in the Central Pacific sample. This will be further discussed in a later section (7-3).

7-2 What controls Hf and Fe isotopic variations in seawater- records from Fe-Mn crusts?

Hf and Fe isotopes were two principal isotopic systems investigated in this study. In the Hf system, weathering and/or hydrothermal inputs were thought to influence the $^{176}Hf/^{177}Hf$ ratios in seawater from Fe-Mn crust records (White *et al.*, 1986; Godfrey *et al.*, 1997; Piotrowski *et al.*, 2000; van de Flierdt *et al.*, 2002). The only Fe isotopic study from a single Fe-Mn crust in the Atlantic Ocean (Zhu *et al.*, 2000b) suggested that weathering style changes induced such variations. However, because most terrestrial sources have a homogeneous Fe isotopic composition (Beard et al. 2003a) this was later modified to a model involving increasing detrital input, which raised the seawater signatures (Beard *et al.*, 2003b). Results from two Izu-Bonin Fe-Mn crusts are used as an example to further these previous discussions.

In Chapter 5, a debate arises concerning whether hydrothermal or weathering caused the decoupling observation in Nd and Hf isotopes at ~ 4 Ma at the Izu-Bonin area. Later, in Chapter 6, it seems that hydrothermal input in this area is an important source for Fe isotope signatures in seawater. Fig. 7.1, combining the results of these two isotopic systems, shows that the radiogenic Hf event does not correspond to the decreasing Fe isotopes trends, as the hydrothermal input indicator, in either of the crusts. The unchanged Fe isotopic profile, at that time, suggests the hydrothermal

activity was not pronounced enough to be recorded in either of the samples. Providing the seawater residence time of Fe is probably more than two orders of magnitude shorter than that of Hf, Fe should be more sensitive to any hydrothermal inputs. In addition to Pb isotope results in favour of a weathering mechanism, it seems therefore less likely that the radiogenic Hf peak was caused by hydrothermal activities.

Contrary to the observation of Zhu *et al.* (2000), there is no correlation between Fe and Pb isotopic compositions in the material investigated in this study. This observation is perhaps more understandable because when on considers the consistent Fe isotopic compositions reported among terrestrial materials (Beard *et al.*, 2003ab) when compared to the significant variations observed in the Pb isotopic composition of continental materials which surround the Atlantic and Pacific Oceans. As such, work on Fe isotopic systems has the potential to identify hydrothermal inputs as opposed to various types of terrestrial input which do not cause fractionation of Fe isotopes. The important point being that hydrothermal input is so far the only negative isotopic value source observed in the modern oceans. Another potential application of Fe isotopes could be for productivity effect (e.g. as described in 6-5-4, this study) but investigations are necessary at this early stage.

It seems, from this study and those based on the literature, that the Hf isotopic system, other than that mechanical weathering can release unradiogenic signatures which will only be significant in the craton-surrounding the Atlantic Ocean, cannot provide much more information than Nd. The main obstacle in this is our poor understanding of the behaviour of Hf in hydrothermal vents and weathering systems. Both end-members therefore need to be resolved before unequivocal interpretations can be made.

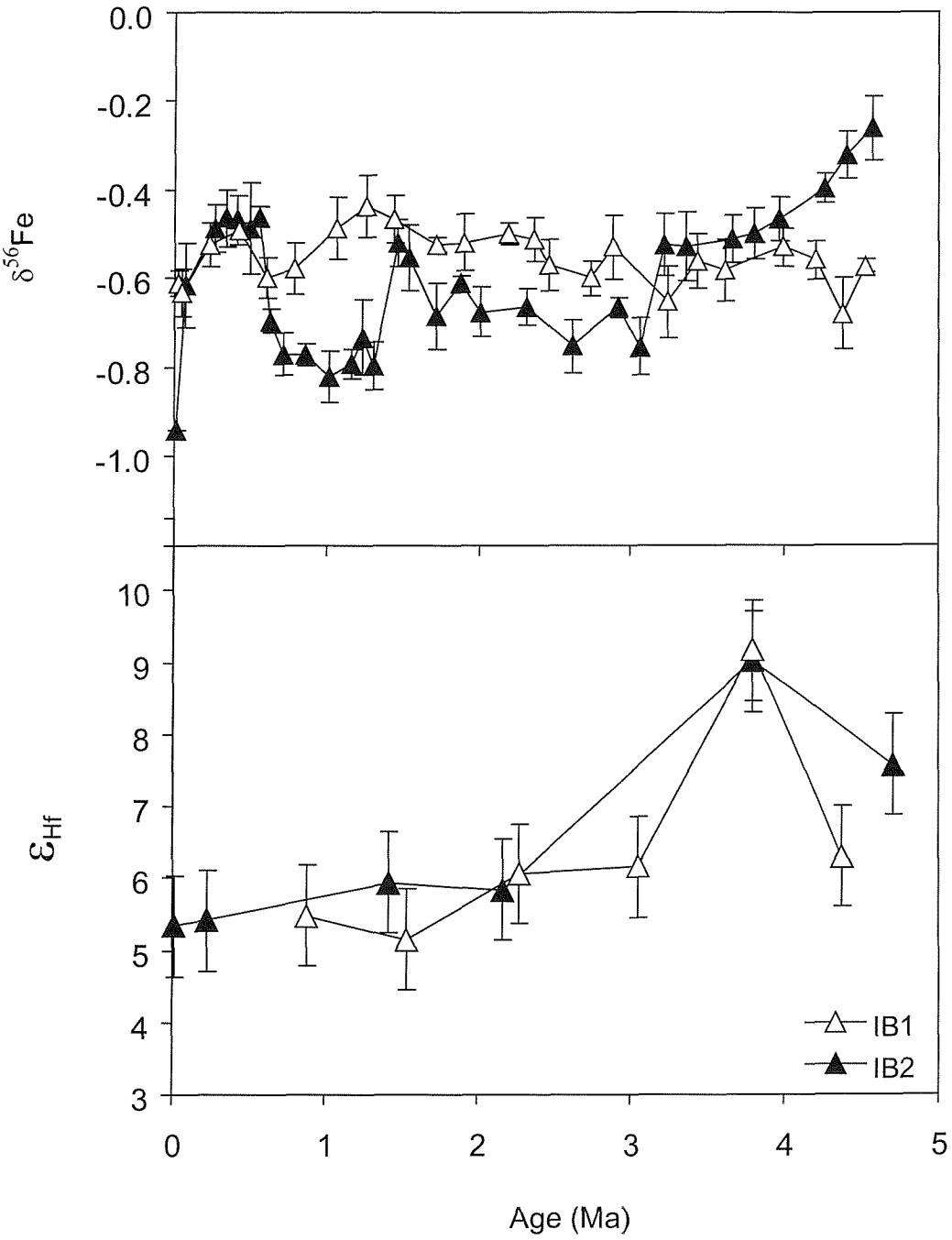

Fig. 7.1 Time series $\delta^{56}Fe$ and ε_{Hf} in IB1&2 (Izu-Bonin Back-Arc Basin). Data from Chapter 5 and 6.

7-3 Further applications and future works

The major conclusion of Hf isotope measuring technique and the related interference corrections (Chapter 3) have been included in a recent review of updated analytical technique in atomic mass spectrometry (Bacon *et al.*, 2003). Moreover, in another recent paper (Segal *et al.*, 2003), the authors follow the discussions of Chu *et al.* (2002) and proposed another technique in determining accurate ytterbium (Yb) isotopic ratios by MC-ICP-MS. A certain discrepancy exhibits (0.1 % with 1 Dalton difference) between the two studies and the causes should be further elucidated. It should be note however, that this compares with a nearly 0.4 % difference reported from previous MC-ICP-MS Yb ratio measurements (Blichert-Toft *et al.*, 1997). It is clear that progress is being made in fundamental isotopic measurement techniques which is essential if we are to see further breakthroughs in the application of isotopic systems.

Before the technique of direct Hf isotope measurements in seawater is available, to further the work of Chapter 4, more analyses from marine precipitates are necessary in order to encompass the entire depths of an ocean basin. These samples could be Fe-Mn crusts with careful surface sampling as in this study or Fe-Mn oxyhydroxide fractions in marine sediments with an appropriate chemistry separating technique. Isotopic studies of the Fe-Mn oxyhydroxide component leached from sedimentary records can potentially provide information on ocean circulation changes, for example, in relation to the Late Quaternary climate (Rutberg *et al.*, 2000; Bayon *et al.*, 2002; Piotrowski *et al.*, 2002). Our understandings in Hf isotopes as a tracer could perhaps be constrained better with more data from its modern day distributions in the ocean.

As being continuously emphasized throughout this thesis, the determination of river Hf isotopic data is very important in the characterisation of any weathering end-member. River water sampling and pre-concentrating techniques have already been established by many studies (Goldstein and Jacobsen, 1987). As a next step we need data from river samples used by Sholkovitz *et al.* (1999) which would provide information on the effects of river water entering the Central Pacific and of course we need similar studies to be made on river water influencing the Western Pacific back arc basins. As well as Hf data on these samples, there needs to be study involving Fe

isotope measurements, in particular for the influence of weathering on Fe isotopic fractionation.

Although this study strongly supports the view that hydrothermal activity affects Fe isotopes, there is little information on its role in Hf isotopic fractionation. The objectives of such a study would be to investigate Hf transport in hydrothermal plumes and its impact on the oceanic Hf budget. This could be achieved, for example, by measuring Hf concentrations in core top metalliferous sediments taken in transects progressively away from the vent site. Such an approach would also require the determination of Hf concentrations in seawater around the vent site and measurements of the associated sulphides and vent fluids.

Finally, an investigation of the biological effect on oceanic Fe isotope fractionation would provide a better understanding to the debate on factors affecting Fe isotopic fractionation (as in 6-5-4). A major difficulty facing this study is the Fe coating formed from the seawater developed on the organism (e.g. the foraminifera) after its death. Because this coating has a much higher Fe content than biological Fe there is a risk of serious contamination which will make the determination of the natural (biological) value more difficult to measure. An alternative approach is through culture experiments with meticulous controls over various kinds of nutrients, and thus the Fe/ nutrient-limitation fractionation discussed previously can therefore be tested.

References

Abouchami W. and Goldstein S. L. (1995) A lead isotope study of Circum-Atlantic manganese nodules. *Geochim. Cosmochim. Acta* **59**, 1809-1820.

Abouchami W., Goldstein S. L., Galer S. J. G., Eisenhauer A., and Mangini A. (1997) Secular changes of lead and neodymium in central Pacific seawater recorded by a Fe-Mn crust. *Geochim. Cosmochim. Acta* **18**, 3957-3974.

Abouchami W., Galer S. J. G., and Koschinsky A. (1999) Pb and Nd isotopes in NE Atlantic Fe-Mn Crusts: Proxies for trace metal paleosources and paleocean circulation. *Geochim. Cosmochim. Acta* **63**(10), 1489-1505.

Adkin J. F. and Boyle E. A. (1997) Changing atmospheric $\Delta^{14}C$ and the record of deep water paleoventilation age. *Paleoceanography* **12**(3), 337-344.

Albarède F. and Goldstein S. L. (1992) World map of Nd isotopes in sea-floor ferromanganese deposits. *Geology* **20**, 761-763.

Albarède F. (1997) Isotopic tracers of past ocean circulation: turning lead to gold. *Science* **277**, 908-909.

Albarède F., Simonetti A., Vervoot J. D., Blichert-Toft J., and Abouchami W. (1998) A Hf-Nd isotopic correlation in ferromanganese nodules. *Geophydical Research Letters* **25**(20), 3895-3898.

Alibo D. S. and Nozaki Y. (1999) Rare earth elements in seawater: Particle association, shale-normalization, and Ce oxidation. *Geochim. Cosmochim. Acta* **63**(3/4), 363-372.

Amakawa H., Ingri J., Masuda A., and Shimizu H. (1991) Isotopic compositions of Ce, Nd and Sr in ferromanganese nodules from the Pacific and Atlantic Oceans, the baltic and Barents Seas, and the Gulf of Bothnia. *Earth Planet. Sci. Lett.* **105**, 554-565.

Amakawa H., Alibo D. S., and Nozaki Y. (2000) Nd isotopic composition and REE pattern in the surface waters of the eastern Indian Ocean and its adjacent seas. *Geochim. Cosmochim. Acta* **64**(10), 1715-1727.

Aplin A. C. (1984) Rare earth element geochemistry of Central Pacific ferromanganese encrustations. *Earth Planet. Sci. Lett.* **71**, 13-22.

Aplin A. C., Michard A., and Albarède F. (1986/1987) $^{143}Nd/^{144}Nd$ in Pacific ferromanganese encrustations and nodules. *Earth Planet. Sci. Lett.* **81**(7-14).

Arnold J. R. (1957) Beryllium-10 produced by cosmic rays. *Science* **124**, 484-485.

Arrhenius G., Mero J., and Korkisch J. (1964) Origin of oceanic manganese materials. *Science* **144**, 170-173.

Bacon J. R., Greenwood J. C., Van Vaeck L., and Williams J. G. (2003) Atomic spectrometry update. Atomic mass spectrometry. *J. Anal. At. Spectrom.* **18**(8), 955-997.

Baker E. T., Chen Y. J., and Morgan J. P. (1996) The relationship between near-axis hydrothermal cooling and the spreading rate of mid-ocean ridges. *Earth and Planetary Science Letters* **142**(1-2), 137-145.

Banakar V. K. and Borole D. V. (1991) Depth profiles of $^{230}Th_{excess}$, transition metals and mineralogy of ferromanganese crusts of the Central Indian basin and implicaiton for palaeoceanographic influence on crust genesis. *Chem. Geol* **94**, 33-44.

Barling J., Arnold G. L., and Anbar A. D. (2001) Natural mass-dependent variations in the isotopic composition of molybdenum. *Earth Planet. Sci. Lett.* **193**, 447-457.

Barling J. and Anbar A. D. (2004) Molybdenum isotope fractionation during adsorption by manganese oxides. *Earth and Planetary Science Letters* **217**(3-4), 315-329.

Barovich K. M., Beard B. L., Cappel J. B., Johnson C. M., Kyser T. K., and Morgan B. E. (1995) A chemical method for hafnium separation from high-Ti whole-rock and zircon samples. *Chem. Geol.* **121**, 303-308.

Barrett T. J., Taylor P. N., and Lugoqski J. (1987) Metalliferous sediments from DSDP Leg 92: The East Pacific Rise transect. *Geochim. Cosmochim. Acta* **51**(9), 2241-2253.

Bau M., Koschinsky A., Dulski P., and Hein J. (1996) Comparison of the partitioning behaviours of yttrium, rare earth elements, and titanium between hydrogenitic marine ferromanganese crusts and seawater. *Geochim. Cosmochim. Acta* **60**(10), 1709-1725.

Bayon G., German C. R., Boella R. M., Milton J. A., Taylor R. N., and Nesbitt R. W. (2002) An improved method for extracting marine sediment fractions and its application to Sr and Nd isotopic analysis. *Chem. Geol.* **187**(3-4), 179-199.

Bayon G., German C. R., Nesbitt R. W., Bertrand P., and Schneider R. R. (2003) Increased input of circumpolar deep water-borne detritus to the glacial SE Atlantic Ocean. *Geochemistry, Geophysics, Geosystems* **4**(3), 2002GC000371.

Beard B. L., Johnson C. M., Skulan J. L., Nealson K. H., Cox L., and Sun H. (2003a) Application of Fe isotopes to tracing the geochemical and biological cycling of Fe. *Chemical Geology* **195**, 87-117.

Beard B. L., Johnson C. M., Von Damm K. L., and Poulson R. L. (2003b) Iron isotope constrains on Fe cycling and mass balance in oxygenated Earth oceans. *Geology* **31**(7), 629-632.

Beard B. L. and Johnson C. M. (2004) Fe isotope variations in the modern and ancient Earth and other planetary bodie. In *Reviews in Mineralogy and Geochemistry: Geochemistry of Non-Traditional Stable Isotopes*, Vol. 55, pp. 319-357.

Belshaw N. S., Freedman P. A., O'Nions R. K., Frank M., and Guo Y. (1998) A new variable dispersion double-focusing plasma mass spectrometer with performance illustrated for Pb isotopes. *Int. J.Mass Spectrom.* **181**, 51-58.

Bertram C. J. and Elderfield H. (1993) The geochemical balance of the rare earth elements and neodymium isotopes in the oceans. *Geochim. Cosmochim. Acta* **57**, 1957-1986.

Bingham F. M. and Talley L. D. (1991) Estimates of Kuroshio transport using an inverse technique. *Deep-Sea Research* **38**(Suppl. 1), S21-43.

Blichert-Toft J., Chauvel C., and Albarède F. (1997) Separation of Hf and Lu for high-precision isotope analysis of rock samples by magnetic sector-multiple collector ICP-MS. *Contrib. Mineral. Petrol.* **127**, 248-260.

Blichert-Toft J. (2001) On the Lu-Hf isotope geochemistry of silicate rock. *Geostand. Newsl.* **25**(1), 41-56.

Bonatti E., Kraemer T., and Rydell H. (1972) Classfication and genesis of submarine iron-manganese deposits. In *Ferromanganese deposits on the ocean floor.* (ed. D. R. Horn), pp. 149-166. National Science Foundation, Washingtion D. C.

Boswell S. M. and Elderfield H. (1988) The determination of zirconium and hafnium in natural waters by isotope dilution mass spectrometry. *Marine Chemistry* **25**, 197-209.

Boyd P. W., Watson A. J., Law C. S., Abraham E. R., Trull T., Murdoch R., Bakker D. C. E., Bowle A. R., Buesseler K. O., Chang H., Matthew C., Croot P., Downing K., Frew R., Gall M., Hadfield M., Hall J., Harvey M., Jameson G., LaRoche J., Liddicoat M., Ling R., Maldonado M. T., McKay R. M., Nodder S., Pickmere S., Pridmore R., Rintoul S., Safi K., Sutton P., Strzepek R., Tanneberger K., Turner S., Waite A., and Zeldis J. (2000) A mesoscale phytoplankton bloom in the polar Southern Ocean stimulated by iron fertilization. *Nature* **407**, 695-702.

Boyle E. A. (1997) What controls dissolved iron concentrations in the world ocean? - a comment. *Marine Chemistry* **57**, 163-167.

Broecker W. S. and Takahashi T. (1980) Hydrography of the Central Atlantic-III, the Nort Atlantic deep-water complex. *Deep-Sea Research* **27A**, 591-613.

Broecker W. S. and Peng T.-H. (1982) *Tracers in the sea.* Eldigio Press.

Broecker W. S. (1991) The great ocean conveyor. *Oceanography* **4**(No. 2), 79-89.

Bruland K. W. (1983) Trace elements in sea-water. In *Chemical Oceanography*, Vol. 8 (ed. J. P. Riley and R. Chester), pp. 157-220. Academic Press Inc.

Bruland K. W., Orians K. J., and Cowen J. P. (1994) Reactive trace metals in the stratified central North Pacific. *Geochim. Cosmochim. Acta* **58**(15), 3171-3182.

Burns R. G. and Burns V. M. (1977) Mineralogy. In *Marine Manganese Deposits* (ed. G. P. Glasby), pp. 185-248. Elsvier Scientific Publishing Company.

Burton K. W., Lee D. C., Christensen J. N., Halliday A. N., and Hein J. R. (1999) Actual timing of neodymium isotopic variations recorded by Fe-Mn crusts in the western North Atlantic. *Earth Planet. Sci. Lett.* **171**, 149-156.

Burton K. W. and Vance D. (2000) Glacial-interglacial variations in the neodymium isotope composition of seawater in the Bay of Bengal recorded by planktonic foraminifera. *Earth Planet. Sci. Lett.* **176**, 425-441.

Cave R. R., Ravizza G., German C. R., Thomson J., and Nesbitt R. W. (2003) Deposition of osmium and other platinum-group elements beneath the ultramafic-hosted Rainbow hydrothermal plume. *Earth Planet. Sci. Lett.* **210**, 65-79.

Chabaux F., Cohen A. S., O'Nions R. K., and Hein J. R. (1995) ^{238}U-^{235}U-^{230}Th chronometry of Fe-Mn crusts: Growth processes and recovery of thorium isotopic ratios of seawater. *Geochim. Cosmochim. Acta* **59**, 633-638.

Chabaux F., O'Nions R. K., Cohen A. S., and Hein J. R. (1997) ^{238}U-^{234}U-^{230}Th disequilibrium in hydrogeneous oceanic Fe-Mn crusts: Palaeoceanographic record or diagenetic alteration? *Geochim. Cosmochim. Acta* **17**, 3619-3632.

Christensen J. N., Halliday A. N., Godfrey L. V., Hein J. R., and Rea D. K. (1997) Climate and ocean dynamics and the lead isotopic records in Pacific ferromanganese crusts. *Science* **277**, 913-918.

Chu N.-C., Taylor R. N., Chavagnac V., Nesbitt R. W., Boella R. M., Milton J. A., German C. R., Bayon G., and Burton K. W. (2002) Hf isotope ratio analysis using multi-collector inductively coupled plasma mass spectrometry: an evaluation of isobaric interference correction. *J. Anal. At. Spectrom.* **17**, 1567-1574.

Chung Y.-C. and Hung G.-W. (2000) Particulate fluxes and transports on the slope between the southern East China Sea and the South Okinawa Trough. *Continental Shelf Research* **20**, 571-597.

Claude-Ivanaj C., Hofmann A. W., Vlastelic I., and Koschinsky A. (2001) Recording changes in ENADW composition over the las 340 ka using high-precision lead isotopes in a Fe-Mn crust. *Earth Planet. Sci. Lett.* **188**, 73-89.

Coale K. H., Fitzwater S. E., Gordon R. M., Johnson K. S., and Barber R. T. (1996) Control of community growth and export production by upwelled iron in the equatorial Pacific Ocean. *Nature* **379**, 621-624.

Corliss J. B., Dymond J., Gordon L. I., Edmond J. M., von Herzen R. P., Ballard R. D., Green K., Williams D., Bainbridge A., Crane K., and van Andel T. H. (1979) Submarine thermal springs on the Galápagos Rift. *Science* **203**(4385), 1073-1083.

Cowen J. P., De Carlo E. H., and McGee D. L. (1993) Calcareous nannofossil biostratigraphic dating of a ferromanganese crust from Schumann Seamount. *Marine Geology* **115**, 289-306.

Cronan D. S. (1967) The distribution of ferromanganese nodule deposits in the north equatorial Pacific. Unpublished Ph.D. thesis., University of London.

Curry W. B. and Lohmann G. P. (1983) Reduced advection into Atlantic ocean deep eastern basins during last glacial maximum. *Nature* **306**, 577-580.

David K., Frank M., O'Nions R. K., Belshaw N. S., Arden J. W., and Hein J. (2001) The Hf isotope composition of global seawater and the evolution of Hf isotopes in the deep Pacific Ocean from Fe-Mn crusts. *Chem. Geol* **178**, 23-42.

de Baar H. J. W., Bacon M. P., Brewer P. G., and Bruland K. W. (1985) Rare earth elements in the Pacific and Atlantic Oceans. *Geochim. Cosmochim. Acta* **49**, 1943-1959.

De Carlo E. H. (1991) Paleoceanographic implications of rare earth element variability within a Fe-Mn crust from the central Pacific Ocean. *Marine Geology* **98**, 449-467.

De Carlo E. H., Wen X. Y., and Cowen J. P. (2000) Rare earth element fractionation in hydrogenitic Fe-Mn crusts: the influence of canrbonate complexation and phosphatization on Sm/Yb ratios. *Marine Authigenesis: from global to microbial., SEPM Special publication* **No. 66**, 271-285.

De La Rocha C. and DePaolo D. J. (2000) Isotopic evidence for variations in the marine calcium cycle over the Cenozoic. *Science* **289**, 1176-1178.

De La Rocha C. L., Brzezinski M. A., DeNiro M. J., and Shemesh A. (1998) Silicon-isotope composition of diatoms as an indicator of past oceanic change. *Nature* **395**, 680-683.

De La Rocha C. L. (2003) Silicon isotope fractionation by marine sponges and reconstruction of the silicon isotope composition of ancient deep water. *Geology* **31**(5), 423-426.

Derry L. A. and France-Lanord C. (1996) Neogene Himalayan weathering history and river $^{87}Sr/^{86}Sr$ impact on the marine Sr record. *Earth Planet. Sci. Lett.* **142**, 59-74.

Dickin A. P. (1997) *Radiogenic isotope geology*. Cambridge University Press.

Dietrich G., Kalle K., Krauss W., and Sielder G. (1980) *General Oceanography: An Introduction*. J. Wiley & Sons.

Duce R. A., Liss P. S., Merrill J. T., Atlas E. L., Buat-Menard P., Hicks B. B., Miller J. M., Prospero J. M., Arimoto R., Church T. M., Ellis W., Galloway J. N., Hansen L., Jickells T. D., Knap A. H., Reinhardt K. H., Schneider B., Soudine A., Tokos J. J., Tsunogai S., Wollast R., and Zhou M. (1991) The atmosphere input of trace species to the world ocean. *Global Biogeochemical Cycles* **5**(3), 193-259.

Duplessy J.-C., Bard E., Labeyrie L., Duprat J., and Moyes J. (1993) Oxygen isotope records and salinity changes in the northeastern Atlantic Ocean during the last 18,000 years. *Paleoceanography* **8**, 341-350.

Edmonds H. N. and German C. R. (2003) Particle geochemistry in the Rainbow hydrothermal plume, Mid-Atlantic Ridge. *Geochim. Cosmochim. Acta.*

Eisenhauer A., Gögen A., Pernicka E., and Mangini A. (1992) Climate influences on the growth rates of Mn crusts during the Late Quaternary. *Earth Planet. Sci. Lett.* **24**, 191-224.

Elderfield H., Hawkesworth C. J., and Greaves M. J. (1981) Rare earth element zonation in Pacific ferromanganese nodules. *Geochim. Cosmochim. Acta* **45**.

Elderfield H. (1988) The oceanic chemistry of the rare-earth elements. *Phil. Trans. R. Soc. Lond. A* **325**, 105-126.

Elderfield H., Upstill-Goddard R., and Sholkovitz E. R. (1990) The rare earth elements in rivers, estuaries, and coastal seas and their significance to the composition of ocean waters. *Geochim. Cosmochim. Acta* **54**, 971-991.

Elderfield H. and Schultz A. (1996) Mid-ocean ridge hydrothermal fluxes and the chemical composition of the ocean. *Ann. Rev. Earth Planet. Sci.* **24**, 191-224.

Embley R., Baker E. T., Chadwick Jr. W. W., Lupton J. E., Resing J. A., Massoth G. J., and Nakamura K. (2004) Explorations of Mariana Arc Volcanoes reveal new hydrothermal systems. *EOS Trans. AGU* **85**(4), 37, 40.

Emiliani C. (1955) Pleistocene temperature. *J. Geol.* **63**, 538-578.

Emiliani C. (1995) Two revolutions in the Earth Sciences. *Terra Nova* **7**(6), 587-597.

Ender R. M., Döbeli M., Suter M., and Synal H.-A. (1997) Accelerator SIMS at PSI/ETH Zurich. *NIM B* **123**, 575-578.

Erel Y., Harlavan Y., and Blum J. D. (1994) Lead isotope systematics of graintoid weathering. *Gemchim. Cosmochim. Acta* **58**, 5299-5306.

Falkowski P. (1997) Evolution of the nitrogen cycle and its influence on the biological sequestration of CO_2 in the ocean. *Nature* **387**(6630), 272-275.

Faure G. (1986) *Principles of Isotope Geology*. John Wiley & Sons.

Field M. P. and Sherrell R. M. (2000) Dissolved and particulate Fe in a hydrothermal plume at 9o45'N, East Pacific Rise: Slow Fe(II) oxidation kinetics in Pacific plumes. *Geochim. Cosmochim. Acta* **64**(4), 619-628.

Frank M. and O'Nions R. K. (1998) Sources of Pb for Indian Ocean ferromanganese crusts: a record of Himalayan erosion? *Earth Planet. Sci. Lett.* **158**, 121-130.

Frank M., O'Nions R. K., Hein J. R., and Banakar V. K. (1999a) 60 Myr records of major elements and Pb-Nd isotopes from hydrogenous ferromanganese crusts: Reconstruction of seawater paleochemistry. *Gemchim. Cosmochim. Acta* **63**, 1689-1708.

Frank M., Reynolds B. C., and O'Nions R. K. (1999b) Nd and Pb isotopes in Atlantic and Pacific water masses before and after closure of the Panama gateway. *Geology* **27**(12), 1147-1150.

Frank M. (2002) Radiogenic isotopes: tracers of past ocean circulation and erosional input. *Reviews of Geophysics* **40**, 10.1029/2000RG000094.

Frank M., Rutgers van der Loeff M. M., Kubik P. K., and Mangini A. (2002a) Quasi-conservative behaviour of ^{10}Be in deep waters of the Weddel Sea and the Atlantic sector of the Antarctic Circumpolar Current. *Earth Planet. Sci. Lett.* **201**, 171-186.

Frank M., Whitely N., Kasten S., Hein J. R., and O'Nions R. K. (2002b) North Atlantic Deep Water export to the Soutern Ocean over the past 14 Myr: Evidence from Nd and Pb isotopes in ferromanganese crusts. *Paleoceanography* **17**(2), 10.1029/2000PA000606.

Fujioka K., Matsuo Y., Nishimura A., Koyama M., and Rodolfo K. S. (1992) Tephras of the Izu-Bonin forearc (Site 787, 792, and 793). In *Proceedings of the Ocean Drilling Program, Scientific Results*, Vol. 126 (ed. B. Taylor and K. Fujioka), pp. 627-651. College Station, TX, USA.

Futa K., Petemenn Z. E., and Hein J. R. (1988) Sr and Nd isotopic variations in ferromanganese crusts from Central Pacific: Implications for age and source provenance. *Geochim. Cosmochim. Acta* **52**, 2229-2233.

Galer S. J. G. and Abouchami W. (1998) Practical application of lead triple spiking for correction of instrumental mass discrimination. *Mineral. Mag.* **62A**, 491-492.

German C. R., Klinkhammer G. P., Edmond J. M., Mitra A., and Elderfield H. (1990) Hydrothermal scavenging of rare-earth elements in the ocean. *Nature* **345**, 516-518.

German C. R., Higgs N. C., Thomson J., Mills R. A., Elderfield H., Blusztajn J., Fleer A. P., and Bacon M. P. (1993) A geochemical study of metalliferous sediment from the TAG hydrothermal mound, 26°08'N, Mid-Atlantic Ridge. *Journal of Geophysical Research* **98**(No. B6), 9683-9692.

German C. R., Bourlès D. L., Brown E. T., Hergt J., Colley S., Higgs N. C., Ludford E. M., Nelsen T. A., Feely R. A., Raisbeck G., and Yiou F. (1997) Hydrothermal scavenging on the Juan de Fuca Ridge: $^{230}Th_{xs}$, ^{10}Be, and REEs in ridge-flank sediments. *Geochim. Cosmochim. Acta* **61**(No. 19), 4067-4078.

German C. R., Hergt J., Palmer M. R., and Edmond J. M. (1999) Geochemistry of a hydrothermal sediment core from the OBS vent-field, 21°N East Pacific Rise. *Chem. Geol* **155**, 65-75.

German C. R., Colley S., Palmer M. R., Khripounoff A., and Klinkhammer G. P. (2002) Hydrothermal plume-particle fluxes at 13°N on the East Pacific Rise. *Deep-Sea Research I* **49**(11), 1921-1940.

German C. R. and Von Damm K. L. (2003) Hydrothermal Process. In *The Ocean and Marine Geochemistry*, Vol. 6 (ed. H. Elderfield). Elsevier.

Gill J. B., Seales C., Thompson P., Hochstaeder A. G., and Dunlap C. (1992) Petrology and geochemistry of Pliocene-Pleistocene volcanic rocks from the Izu Arc, Leg 126. In *Proceedings of the Ocean Drilling Program Scientific Results*, Vol. 126, pp. 383-404.

Gill J. B., Hiscott R. N., and Vidal P. (1994) Turbidite geochemistry and evolution of the Izu-Bonin arc and continents. *Lithos* **33**, 135-168.

Glasby G. P. (2000) Manganese: predominant role of nodules and cursts. In *Marine Geochemistry* (ed. H. D. Schulz and M. Zabel), pp. 335-372. Springer.

Godfrey L. V., Mills R. A., Elderfield H., and Gurvich E. (1994) Lead behavious at the TAG hydrothermal vent field, 26°N, Mid-Atlantic Ridge. *Mar. Chem.* **46**, 237-254.

Godfrey L. V., White W. M., and Salters V. J. M. (1996) Dissolved zirconium an hafnium distributions across a shelf break in the northeastern Atlantic Ocean. *Geochim. Cosmochim. Acta* **60**, 3995-4006.

Godfrey L. V., Lee D. C., Sangrey W. F., Halliday A. N., Salter V. J. M., Hein J. R., and White W. M. (1997) The Hf isotopic composition of ferromanganese nodules and crusts and hydrothermal manganese deposits: Implications for seawater Hf. *Earth Planet. Sci. Lett.* **151**, 91-105.

Godfrey L. V. (2002) Temporal changes in the lead isotopic compsition of read clays: comparison with ferromanganese crust records. *Chem. Geol* **185**, 241-254.

Goldberg E. D., Koide M., Schmitt R. A., and Smith R. H. (1963) Rare earth distribution in the marine environment. *J. Geophys. Res.* **68**, 4209-4217.

Goldstein S. L. and O'Nions R. K. (1981) Nd and Sr isotopic relationships in pelagic clays and ferromanganese deposits. *Nature* **324-327**.

Goldstein S. L. and Jacobsen S. B. (1987) The Nd and Sr isotopic systematics of river-water dissolved material: implications for the sources of Nd and Sr in seawater. *Chem. Geol* **66**, 245-272.

Griffin L., Pearson N. J., Belousova E., Jackson S. E., van Achterbergh E., O'Reilly S. Y., and Shee S. R. (2000) The Hf isotope compositon of cratonic mantle: LAM-MC-ICPMS analysis of zircon megacrysts in kimberlites. *Geochim. Cosmochim. Acta* **64**(1), 133-147.

Halbach P., Hebisch U., and Scherhag C. (1981) Geochemical variations of ferromanganese nodules and crusts from different provinces of the Pacific Ocean and their genetic control. *Chem. Geol.* **34**, 3-17.

Halbach P., Segl M., Puteanus D., and Mangini A. (1983) Relationship between Co fluxes and growth rates in ferromangnanese deposits from Central Pacific seamount areas. *Nature* **304**, 716-719.

Halbach P. E., Sattler C.-D., Teichmann F., and Wahsner M. (1989) Cobalt-rich and platium-bearing manganese crust deposits on seamounts: nature, formation, and metal potential. *Marine Mining* **8**, 23-39.

Harlavan Y., Erel Y., and Blum J. D. (1998) Systematic changes in lead isotopic composition with soil age in glacial granitic terrains. *Geochim. Cosmochim. Acta* **62**, 33-46.

Hein J., Yeh H.-W., Gunn S. H., Sliter W. V., Benninger L. M., and Wang C.-H. (1993) Two major Cenozoic episodes of phosphogenesis recorded in equatorial Pacific seamount deposits. *Paleoceanography* **8**(2), 293-311.

Hein J., Yeh H.-W., Gunn S. H., Gibb A. E., and Wang C.-H. (1994) Composition and origin of hydrothermal ironstones from Central Pacific seamounts. *Geochim. Cosmochim. Acta* **58**, 179-189.

Hein J. R., Koschinsky A., Bau M., Manheim F. T., Kang J.-K., and Roberts L. (2000) Cobalt-rich ferromanganese crusts in the Pacific. In *Handbook of Marine Mineral Deposits* (ed. D. S. Cronan), pp. 239-279. CRC Press.

Hemming S. R. and McLennan S. M. (2001) Pb isotope compositions of modern deep sea turbidites. *Earth Planet. Sci. Lett.* **184**, 489-503.

Henderson G. and Maier-Reimer E. (2002) Advection and removal of ^{210}Pb and stable Pb isotopes in the oceans: A general circulation model study. *Geochim. Cosmochim. Acta* **66**(2), 257-272.

Henderson G. M., Martel D. J., O'Nions R. K., and Shackleton N. J. (1994) Evolution of seawater 87Sr/86Sr over the last 400 ka: The absence of glacial/interglacial cycles. *Earth Planet. Sci. Lett.* **128**, 643-651.

Hirata T. (1996) Lead isotopic analysis of NIST standard reference materials using multiple collector-inductively coupled plasma mass spectrometry coupled with modified external correction method for mass discrimination effect. *Analyst* **121**(10), 1407-1411.

Hiscott R. N. and Gill J. B. (1992) Major and trace element geochemistry of Oligocene to Quaternary volcaniclastic sands and sandstones from the Izu-Bonin Arc. In *Proceedings of the Ocean Drilling Program Scientific Results*, Vol. 126.

Hochstaeder A. G., Gill J. B., and Morris J. D. (1990) Volcanism in the Sumisu Rift, II. Subduction and non-subduction related components. *Earth Planet. Sci. Lett.* **100**, 195-209.

Hochstaeder A. G., Gill J., Peters R., Broughton P., and Holden P. (2001) Across-arc geochemical trends in Izu-Bonin arc: Contributions from the subducting slab. *Geochemistry, Geophysics, Geosystems* **2**, 2000GC000105.

Hodell D. A., Mead G. C., and Mueller P. A. (1990) Variation in the strontium isotopic composition of seawater (8Ma to present): implications for chemical weathering rates and dissolved fluxes to the oceans. *Chem. Geol.* **80**, 291-307.

Hoefs J. (1997) *Stable Isotope Geochemistry*. Springer-Verlag.

Hofmann H. J., Beer J., Bonani G., von Gunten H. R., Raman S., Suter M., Walker R. L., Wolfli W., and Zimmermann D. (1987) ^{10}Be: Half-life and AMS-standards. *Nuclear instruments and methods in physics research* **B29**, 32-36.

Holliger P. and Devillers C. (1981) Contribution à l'étude de la température dans les réacteurs of fossiles d'Oklo Par la measure du rapport isotopique du lutétium. *Earth Planet. Sci. Lett.* **52**, 76-84.

Huh Y., Chan L.-H., and Edmond J. M. (2001) Lithium isotopes as a probe of weathering processes: Orinoco River. *Earth Planet. Sci. Lett.* **194**, 189-199.

Hwang C. and Kao R. (2002) TOPEX/POSEIDON-derived space-time variations of the Kuroshio Current: applications of a gravimetric geoid and wavelet analysis. *Geophys. J. Int.* **151**, 835-847.

Iizasa K., Fiske R. S., Ishizuka O., Yuasa M., Hashimoto J., Ishibashi J., Naka J., Horii Y., Fujiwara Y., Imai A., and Koyama S. (1999) A Kuroko-type polymetallic sulfide deposit in a submarine silicic caldera. *Science* **283**, 975-977.

Ingram B. L., Hein J. R., and Farmer G. L. (1990) Age determinations and growth rates of Pacific ferromanganese deposits using strontium isotopes. *Geochim. Cosmochim. Acta* **54**, 1709-1721.

Ishizuka O., Uto K., Yuasa M., and Hochstaeder A. G. (1998) K-Ar ages from seamount chains in the back-arc region of the Izu-Ogasawara arc. *The Island Arc* **7**, 408-421.

Ishizuka O., Uto K., Yuasa M., and Hochstaeder A. G. (2002a) Volcanism in the earlist stage of back-arc rifting in the Izu-Bonin arc revealed by laser-heating $^{40}Ar/^{39}Ar$ dating. *Journal of Volcanology and Geothermal Research* **120**, 71-85.

Ishizuka O., Yuasa M., and Uto K. (2002b) Evidence of porphyry copper-type hydrothermal activity from a submerged remnant back-arc volcano of the Izu-Bonin arc; implications for the volcanotectonic history of back-arc seamounts. *Earth Planet. Sci. Lett.* **198**, 381-399.

Ishizuka O., Taylor R. N., Milton J. A., and Nesbitt R. W. (2003a) Fluid-mantle interaction in an intra-oceanic arc: constraints from high-precision Pb isotopes. *Earth Planet. Sci. Lett.* **211**(3-4), 221-236.

Ishizuka O., Uto K., and Yuasa M. (2003b) Volcanic history of the back-arc region of the Izu-Bonin (Osagawara) arc. In *Intra-oceanic subduction systems: tectonic and magmatic processes*, Vol. 219 (ed. R. D. Larter and P. T. Leat), pp. 187-205. The Geological Society of London.

Jeandel C. (1993) Concentration and isotopic compositions of Nd in the South Atlantic Ocean. *Earth Planet. Sci. Lett.* **117**, 581-591.

Jeandel C., Bishop J. K., and Zindler A. (1995) Exchange of neodymium and its isotopes between seawater and small and large particles in the Sargasso Sea. *Geochim. Cosmochim. Acta* **59**(3), 535-547.

Jeandel C., Thouron D., and Fieux M. (1998) Concentrations and isotopic compositions of neodymium in the eastern Indian Ocean and Indonesian straits. *Geochim. Cosmochim. Acta* **62**(15), 2597-2607.

Jickells T. D. and Spokes L. J. (2001) Atmospheric Iron inputs to the oceans. In *The Biogeochemistry of Iron in Seawater* (ed. D. R. Turner and K. A. Hunter), pp. 85-121. John Wiley & Sons Ltd.

Johnson C. M., Skulan J. L., Beard B. L., Sun H., Nealson K. H., and Braterman P. S. (2002) Isotopic fractionation between Fe(III) and Fe(II) in aqueous solutions. *Earth Planet. Sci. Lett.* **195**, 141-153.

Johnson C. M., Beard B. L., Roden E. E., Newman D. K., and Nealson K. H. (2004) Isotopic constraints on biogeochemical cycling of Fe. In *Reviews in Mineralogy and Geochemistry: Geochemistry of Non-Traditional Stable Isotopes*, Vol. 55, pp. 359-408.

Johnson H. P. and Pariso J. E. (1993) Variations in oceanic crustal magnetization-systematic changes in the last 160 million years. *journal of Geophysical Research-Solid Earth* **98**(B1), 435-445.

Johnson K. S., Gordon R. M., and Coale K. H. (1997) What controls dissolved iron concentrations in the world ocean? *Marine Chemistry* **57**(3-4), 137-161.

Jones C. E., Halliday A. N., Rea D. K., and Owen R. M. (2000) Eolian input of lead to the North Pacific. *Gemchim. Cosmochim. Acta* **64**(8), 1405-1416.

Joshima M. and Usui A. (1998) Magnetostratigraphy of hysrogenetic manganese crusts from Northwestern Pacific seamounts. *Marine Geology* **146**, 53-62.

Kaiho K. and Saito N. (1994) Oceanic crust production and climate during the last 100 Myr. *Terra Nova* **6**, 376-384.

Kashima M., Imawaki S., Umatani S.-I., Uchida H., Hashibe Y., Ichikawa H., and Fukasawa M. (2003) Geostrophy in the intermediate and deep layers of the Kuroshio and its recirculation regions south of Japan. *Journal of Oceanography* **59**(3), 291-301.

Kempton P. D., Fitton J. G., Saunders A. D., Nowell G. M., Taylor R. N., Hardarson B. S., and Pearson G. (2000) The Iceland plume in space and time: a Sr-Nd-Pb-Hf study of the North Atlantic rifted margin. *Earth Planet. Sci. Lett.* **177**, 255-271.

Klaus A., Taylor B., Moore J. R., MacKay M. E., Brown G. R., Okamura Y., and Murakami F. (1992) Structural and stratigraphic evolution of the Sumisu Rift, Izu-Bonin Arc. In *Proceedings of the Ocean Drilling Program, Scientific Results*, Vol. 126 (ed. B. Taylor and K. Fujioka), pp. 555-573. College Station, TX, USA.

Kleinhanns I. C., Kreissig K., Kamber B. S., Meisel T., Nägler T. F., and Kramers J. D. (2002) Combined chemical separation of Lu, Hf, Sm, Nd, and REEs from a single rock digest: precise and accurate isotope determinations of Lu-Hf and Sm-Nd using multicollector-ICPMS. *Anal. Chem.* **74**(1), 67-73.

Klinkhammer G. P. and Bender M. L. (1980) The distribution of manganese in the Pacific ocean. *Earth Planet. Sci. Lett.* **46**, 361-384.

Klinkhammer G. P., Elderfield H., Edmond J. M., and Mitra A. (1994) Geochemical implications of rare earth element patterns in hydrothermal fluids from mid-ocean ridges. *Geochim. Cosmochim. Acta* **58**(23), 5105-5113.

Koeppenkastrop D. and De Carlo E. H. (1992) Sorption of rare earth elements from seawater onto pure mineral phases: An experimental approach. *Chemical Geology* **95**, 251-263.

Koschinsky A. and Halbach P. (1995) Sequential leaching of marine ferromanganese precipitates: Genetic implications. *Geochim. Cosmochim. Acta* **59**, 5113-5132.

Koschinsky A., Stascheit A., Bau M., and Halbach P. (1997) Effects of phosphatization on the geochemical and mineralogical composition of marine ferromanganese crusts. *Geochim. Cosmochim. Acta* **61**(19), 4079-4094.

Koski R. A., Hein J. R., Bouse R. M., and Sliney R. E. (1985) Composition and origin of ferromanganese crusts from Tonga Platform, Southwest Pacific. In *Geology and offshore resources of Pacific island arcs; Tonga region* (ed. D. W. Scholl and T. L. Vallier), pp. 179-185. Circum-Pac. Counc. Enery and Miner. Resour.

Ku T.-L., Kusakabe M., Measures C. I., Southon J. R., Cusimano G., Vogel J. S., Nelson D. E., and Nakaya S. (1990) Beryllium isotope distribution in the western North Atlantic- a comparison to the Pacific. *Deep-Sea Research* **37**(5), 795-808.

Kumar N., Anderson R. F., Mortlock R. A., Froelich P. N., Kubik P., Dittrich-Hannen B., and Suter M. (1995) Increased biological productivity and export production in the glacial Southern Ocean. *Nature* **378**, 675-680.

Lacan F. and Jeandel C. (2001) Tracing Papua New Guinea imprint on the central Equatorial Pacific Ocean using neodymium isotopic compositions and rare earth element patterns. *Earth Planet. Sci. Lett.* **186**, 497-512.

Laës A., Blain S., Laan P., Achterberg E. P., Sarthou G., and de Baar H. J. W. (2003) Deep dissolved iron profiles in the eastern North Atlantic in relation to water masses. *Geophydical Research Letters* **30**(17), 1902.

Le Fèvre B. and Pin C. (2001) An extraction chromatography method for Hf separation prior to isotopic analysis using multiple collection ICP-Mass Spectrometry. *Anal. Chem.* **73**, 2453-2460.

Lee D.-C., Halliday A. N., Christensen J. N., Burton K. W., Hein J. R., and Godfrey L. V. (1998) High resolution Hf isotope stratigraphy of ferromanganese crusts. *Goldschmidt Conference*, 870-871.

Lee D.-C., Halliday A. N., Hein J. R., Burton K. W., Christensen J. N., and Gunther D. (1999) Hafnium isotope stratigraphy of ferromanganese crust. *Science* **285**, 1052-1054.

Lemarchand D., Gaillardet J., Lewin É., and Allègre C. J. (2000) The influence of rivers on marine boron isotopes and implications for reconstructing past ocean pH. *Nature* **408**, 951-954.

Lilley M. D., Feely R. A., and Trefry J. H. (1995) Chemical and biochemcal transformation in hydrothermal plumes. In *Geophys. Monograph*, Vol. 91, pp. 369-391. Am. Geophys. Union.

Ling H. F., Burton K. W., O'Nions R. K., Kamber B. S., von Blanckenburg F., Gibb A. J., and Hein J. R. (1997) Evolution of Nd and Pb isotopes in Central Pacific seawater from ferromanganese crusts. *Earth Planet. Sci. Lett.* **146**, 1-12.

Longerich H. P., Fryer B. J., and Strong D. F. (1987) Determination of lead isotope ratios by inductively coupled plasma-mass-spectrometry (ICP-MS). *Spectrochim. Acta* **42B**, 39-48.

Luais B., Telouk P., and Albarède F. (1997) Precise and accurate neodymium isotopic measurements by plasma-source mass spectrometry. *Geochim. Cosmochim. Acta* **61**(22), 4847-4854.

Lynn D. C. and Bonatti E. (1965) Mobility of manganese in diagenesis of deep-sea sediments. *Marine Geology* **3**, 457-474.

Mackey D. J., O'Sullivan J. E., and Watson R. J. (2002) Iron in the western Pacific: a riverine or hydrothermal source for iron in the Equatorial Undercurrent? *Deep-Sea Research* **I**(49), 877-893.

Makishima A., Shimizu H., and Masuda A. (1987) Precise measurement of cerium and lanthanum isotope ratios. *Mass. Spectrosc.* **35**, 64-72.

Manheim F. T. (1986) Marine cobalt resources. *Science* **232**, 600-608.

Manheim F. T. and Lane-Bostwick C. M. (1988) Cobalt in ferromanganese crusts as a monitor of hydrothermal discharge on the Pacific sea floor. *Nature* **335**, 59-62.

Maréchal C. N., Telouk P., and Albarède F. (1999) Precise analysis of copper and zinc isotopic compositions by plasma-source mass spectrometry. *Chem. Geol.* **156**, 251-273.

Maréchal C. N., Nicolas E., Douchet C., and Albarède F. (2000) Abundance of zinc isotopes as a marine biogeochemical tracer. *Geochemistry, Geophysics, Geosystems* **1**, paper number 1999GC000029.

Maréchal C. N. and Albarède F. (2002) Ion-exchange fractionation of copper and zinc isotopes. *Geochim. Cosmochim. Acta* **66**(9), 1499-1509.

Martin E. E. and Haley B. A. (2000) Fossil fish teeth as proxies for seawater Sr and Nd isotopes. *Geochim. Cosmochim. Acta* **64**(5), 835-847.

Martin J. H. (1990) Glacial-interglacial CO_2 change: the iron hypothesis. *Paleoceanography* **5**(No.1), 1-13.

Martin J. H., Coale K. H., Johnson K. S., Fitzwater S. E., Gordon R. M., Tanner S. J., Hunter C. N., Elrod V. A., Nowicki J. L., Coley T. L., Barber R. T., Lindley S., Watson A. J., Vanscoy K., Law C. S., Liddicoat M. I., Ling R., Stanton T., Stockel J., Collins C., Anderson A., Bidigare R., Ondrusek M., Latasa M., Millero F. J., Lee K., Yao W., Zhang J. Z., Friedrich G., Sakamoto C., Chavez F., Buck K., Kolber Z., Greene R., Falkowski P., Chisholm S. W., Hoge F., Swift R., Yungel J., Turner S., Nightingale P., Hatton A., Liss P. S., and Tindale N. W. (1994) Test the iron hypothesis in ecosystems of the equatorial Pacific-Ocean. *Nature* **371**, 123-129.

McCulloch M. T., De Laeter J. R., and Rosman K. J. R. (1976) The isotopic composition and elemental abundance of lutetium in meteorites and terrestrial samples and the ^{176}Lu cosmochronometer. *Earth Planet. Sci. Lett.* **28**, 308-322.

McCulloch M. T., Rosman K. J. R., and De Laeter J. R. (1977) The isotopic and elemental abundance of ytterbium in meteorites and terrestrial samples. *Geochim. Cosmochim. Acta* **41**, 1703-1707.

Mchargue L. R. and Damon P. E. (1991) The global beryllium10 cycle. *Reviews of Geophysics* **29**(2), 141-158.

McKelvey B. A. and Orians K. J. (1998) The determination of dissolved zirconium and hafnium from seawater using isotope dilution inductively coupled plasma mass spectrometry. *Marine Chemistry* **60**, 245-255.

Miller S. and Cronan D. S. (1994) Element supply to surface sediments and interrelationships with nodules along the Aitutaki-Jarvis Transect, South Pacific. *Journal of the Geological Society, London* **151**, 403-412.

Mitra A., Elderfield H., and Greaves M. J. (1994) Rare earth elements in submarine hydrothermal fluids and plumes from the Mid-Atlantic Ridge. *Mar. Chem.* **46**, 217-235.

Monaghan M. C., Krishnaswami S., and Turekian K. K. (1985/1986) The global-average production rate of ^{10}Be. *Earth Planet. Sci. Lett.* **76**, 279-287.

Morris J. D. (1991) Applications of cosmogenic Be-10 to problems in the earth sciences. *Ann. Rev. Earth Planet. Sci.* **19**, 313-350.

Mottl M. J. and McConachy T. F. (1990) Chemical processes in buoyant hydrothermal plumes on the East Pacific Rise near 21-degree-N. *Geochim. Cosmochim. Acta* **54**(7), 1911-1927.

Münker C., Weyer S., Scherer E. E., and Mezger K. (2001) Separation of high field strength elements (Nb, Ta, Zr, Hf) and Lu from rock samples fro MC-ICPMS measurements. *Geochemistry, Geophysics, Geosystems* **2**, 2001GC000183.

Nägler T. F., Eisenhauer A., Müller A., Hemleben C., and Kramers J. (2000) The δ^{44}Ca-isotopes: New powerful tool for reconstruction of past sea surface temperatures. *Geochemistry, Geophysics, Geosystems* **1**, 2000GC000091.

Nishimura A., Marsaglia K., Rodolfo K. S., Colella A., Hiscott R. N., Tazaki K., Gill J. B., Janecek T. R., Firth J., Isiminger-Kelso M., Herman Y., Taylor R. N., Taylor B., Fujioka K., and Party L. S. (1991) Pliocene-Quaternary submarine pumice deposits in the Sumisu Rift area, Izu-Bonin Arc. In *Sedimentation in Volcanic Settings* (ed. R. V. Fisher and G. A. Smith), pp. 201-208. SEPM.

Nozaki Y. and Alibo D. S. (2003) Importance of vertical geochemical processes in controlling the oceanic profiles of dissolved rare earth elements in the northeastern Indian Ocean. *Earth Planet. Sci. Lett.* **203**(3-4), 155-172.

Ohta A., Naito K., Okuda Y., and Kawabe I. (1999) Geochemical characteristics of Antarctic deep-sea ferromanganese nodules from highly oxic deep-sea water. *J. Earth Planet. Sci. Nagoya Univ.* **46**, 1-13.

Ohta A. and Kawabe I. (2001) REE (III) adsorption onto Mn dioxide (δ-MnO_2) and Fe oxyhydroxide: Ce(III) oxidation by δ-MnO_2. *Geochim. Cosmochim. Acta* **65**(5), 695-703.

O'Nions R. K., Carter S. R., Cohen R. S., and Evensen N. M. (1978) Pb, Nd and Sr isotopes in oceanic ferromanganese deposits and ocean floor basalts. *Nature* **273**(5662), 435-438.

Oxburgh R. (1998) Variations in the osmium isotope composition of sea water over the past 20,000 years. *Earth Planet. Sci. Lett.* **159**, 183-191.

Oxburgh R. (2001) Residence time of osmium in the oceans. *Geochemistry, Geophysics, Geosystems* **2**, 2000GC000104.

Pagani M., Freeman K. H., and Arthur M. A. (1999) Late Miocene atmospheric CO_2 concentrations and the expansion of C4 grasses. *Science* **285**, 876-879.

Palmer M. R. and Edmond J. M. (1989) The strontium isotope budget of the modern ocean. *Earth Planet. Sci. Lett.* **92**(1), 11-26.

Palmer M. R. and Edmond J. M. (1992) Controls over the strontium isotope composition of river water. *Geochim. Cosmochim. Acta* **56**, 2099-2011.

Palmer M. R. and Pearson P. N. (2003) A 23,000-year record of surface water pH and P_{CO2} in the Western Equatorial Pacific Ocean. *Science* **300**, 480-482.

Patchett P. J. and Tatsumoto M. (1980) A routine high-precision method for Lu-Hf isotope geochemistry and chronology. *Contrib. Mineral. Petrol.* **75**, 263-267.

Patchett P. J. (1983) Importance of the Lu-Hf isotopic system in studies of planetary chronology and chemical evolution. *Geochim. Cosmochim. Acta* **47**, 81-91.

Patchett P. J., White W. M., Feldmann H., Kielinczuk S., and Hofmann A. W. (1984) Hafnium/rare earth element fractionation in the sedimentary system and crustal recyling into the Earth's mantle. *Earth Planet. Sci. Lett.* **69**, 365-378.

Pearce J. A., Kempton P. D., Nowell G. M., and Noble S. R. (1999) Hf-Nd element and isotope prespective on the nature and provenance of mantle and subduction components in Western Pacific arc-basin systems. *Journal of Petrology* **40**(No. 11), 1579-1611.

Pearce N. J. G., Perkins W. T., Westgate J. A., Gorton M. P., Jackson S. E., Neal C. R., and Chenery S. P. (1997) A compilation of new and published major and trace element data for NIST SRM 610 and NIST SRM 612 glass reference materials. *Geostand. Newsl.* **21**, 115-144.

Pearson P. N. and Palmer M. R. (2000) Atmospheric carbon dioxide concentrations over the past 60 million years. *Nature* **406**, 695-699.

Pettke T., Halliday A. N., and Rea D. K. (2002a) Cenozoic evolution of Asian climate and sources of Pacific seawater Pb and Nd derived from eolian dust of sediment core LL44-GPC3. *Paleoceanography* **17**(3), 1-13.

Pettke T., Lee D. C., Halliday A. N., and Rea D. K. (2002b) Radiogenic Hf isotopic compositions of continental eolian dust from Asia, its variability and its implications for seawater Hf. *Earth Planet. Sci. Lett.* **202**, 453-464.

Peucker-Ehrenbrink B. and Ravizza G. (2000) The marine osmium isotope record. *Terra Nova* **12**, 205-219.

Pichat S., Douchet C., and Albarède F. (2003) Zinc isotope variations in deep-sea carbonates from the eastern equatorial Pacific over the last 175ka. *Earth Planet. Sci. Lett.* **210**, 167-178.

Pickard G. L. and Emery W. J. (1990) *Descriptive physical oceanography: an introduction*. Antony Rowe Ltd.

Piepgras D. J., Wasserburg G. J., and Dasch E. J. (1979) The isotopic composition of Nd in different ocean wasses. *Earth Planet. Sci. Lett.* **45**, 223-236.

Piepgras D. J. and Wasserburg G. J. (1982) Isotopic composition of neodymium in waters from the Drake Passage. *Science* **217**(4556), 207-214.

Piepgras D. J. and Wasserburg G. J. (1987) Rare earth element transport in the Western North Atlantic inferred from Nd isotopic observations. *Geochim. Cosmochim. Acta* **51**, 1257-1271.

Piepgras D. J. and Jacobsen S. B. (1988) The isotopic composition of neodymium in the North Pacific. *Geochim. Cosmochim. Acta* **52**, 1373-1381.

Piepgras D. J. and Jacobsen S. B. (1992) The behavior of the rare earth elements in seawater: Precise determination of variations in the North Pacific water column. *Gemchim. Cosmochim. Acta* **56**, 1851-1862.

Piotrowski A. M., Lee D. C., Christensen J. N., Burton K. W., Halliday A. N., Hein J. R., and Günther D. (2000) Changes in erosion and ocean circulation recorded in the isotopic compositions of North Atlantic and Indian Ocean ferromanganese crusts. *Earth Planet. Sci. Lett.* **181**, 315-325.

Piotrowski A. M., Goldstein S. L., and Hemming S. R. (2002) North Atlantic Deep Water strength during the last deglaciation from Nd isotopes. *Geochim. Cosmochim. Acta* **66**, A606.

Puteanus D. and Halbach P. (1988) Correlation of Co concentration and growth rate - a method for age determination of ferromanganese crusts. *Chem. Geol* **69**, 73-85.

Ravelo A. C. and Anderson D. H. (2000) Enhanced circulation during a warm period. *Geophysical Research Letters* **27**(7), 1001-1004.

Ravizza G. and Peucker-Ehrenbrink B. (2003) The marine $^{187}Os/^{188}Os$ record of the Eocene-Oligocene transition: the interplay of weathering and glaciation. *Earth Planet. Sci. Lett.* **210**, 151-165.

Rea D. K. (1994) The paleoclimatic record provided by eolian deposition in the deep sea: the geologic history of wind. *Reviews of Geophysics* **32**(2), 159-195.

Rehkämper M. and Halliday A. N. (1998) Accuracy and long-term reproducibility of lead isotopic measurements by multiple-collector inductively coupled plasma mass spectrometry using an external methods for correction of mass discrimination. *Int. J.Mass Spectrom.* **181**, 123-133.

Rehkämper M., Schönbächler M., and Stirling C. H. (2001) Multiple collector ICP-MS: Introduction to intrumentation, measurement techniques and analytical capabilities. *Geostandards Newsletter* **25**(1), 23-40.

Rehkämper M., Frank M., Hein J., Porcelli D., Halliday A. N., Ingri J., and Liebetrau V. (2002) Thallium isotope variations in seawater and hydrogenetic, diagenetic, and hydrothermal ferromanganese deposits. *Earth Planet. Sci. Lett.* **197**(1-2), 65-81.

Reid J. L. and Lynn R. J. (1971) On the influence of the Norwegian-Greenland and Weddell Seas upon the bottom waters of the Indian and Pacific Oceans. *Deep-Sea Research* **18**, 1063-1088.

Reid J. L. and Lonsdale P. F. (1973) On the flow of water through the Samoan Passage. *Journal of Physical Oceanography* **4**, 58-73.

Reynolds B. C., Frank M., and O'Nions R. K. (1999) Nd- and Pb-isotope time series from Atlantic ferromanganese crusts: implications for changes in provenance and paleocirculation over the last 8 Myr. *Earth Planet. Sci. Lett.* **173**, 381-396.

Reynolds J. H. (1998) Alfred Otto Carl Nier. In *Biographical Memoirs*, Vol. 74, pp. 244-265. National Academies Press.

Richter F. M. and Turekian K. K. (1993) Simple model for the geochemical response of the ocean to climatic and tectonic forcing. *Earth Planet. Sci. Lett.* **199**, 121-131.

Rodolfo K. S., Solidum R. U., Nishimura A., Matsuo Y., and Fujioka K. (1992) Major-oxide stratigraphy of glass shards in volcanic ash layers of the Izu-Bonin arc-backarc sites (sites 788/789 and 790/791). In *Proceedings of the Ocean Drilling*

Program, Scientific Results, Vol. 126 (ed. B. Taylor and K. Fujioka), pp. 505-517. College Station, TX, USA.

Roemmich D. and McCallister T. (1989) Large scale circulation of the North Pacific Ocean. *Prog. Oceanog.* **22**, 171-204.

Rohling E. J. (2000) Paleosalinity: confidence limits and future applications. *Marine Geology* **163**, 1-11.

Roy S. (1981) *Manganese Deposits*. Academic Press.

Rudnicki M. D. and Elderfield H. (1993) A chemical model of the buoyant and neutrally buoyant plume above the TAG vent field, 26 degree N, Mid-Atlantic Ridge. *Geochim. Cosmochim. Acta* **57**(13), 2939-2957.

Russell W. A., Papanastassiou D. A., and Tombrello T. A. (1978) Ca isotope fractionation on the Earth and other solar system materials. *Geochim. Cosmochim. Acta* **42**, 1075-1090.

Rutberg R. L., Hemming S. R., and Goldstein S. L. (2000) Reduced North Atlantic deep water flux to the glacial Southern Ocean inferred from neodymium isotope ratios. *Nature* **405**, 935-938.

Saito N. (1984) Selected data on ion exchange separations in radioanalytical chemistry. *Pure and Applied Chemistry* **56**(No. 4), 523-539.

Sarthou G., Baker A. R., Blain S., Achterberg E. P., Boye M., Bowie A. R., Croot P., Laan P., de Baar H. J. W., Jickells T. D., and Worsfold P. J. (2003) Atmospheric iron deposition and sea-surface dissolved iron concentrations in the eastern Atlantic Ocean. *Deep Sea Research Part I: Oceanographic Research Papers* **50**(10-11), 1339-1352.

Schaule B. K. and Patterson C. C. (1981) Lead concentrations in the northeast Pacific: evidence for global anthropogenic perturbations. *Earth Planet. Sci. Lett.* **54**, 97-116.

Scherer E., Münker C., and Mezger K. (2001) Calibration of the lutetium-hafnium clock. *Science* **293**, 683-687.

Schmitt A.-D., Stille P., and Vennemann T. (2003) Variations of the $^{44}Ca/^{40}Ca$ ratio in seawater during the past 24 million years: Evidence from $\delta^{44}Ca$ and $\delta^{18}O$ values of Miocene phosphates. *Geochim. Cosmochim. Acta* **67**(14), 2607-2614.

Segal I., Halicz L., and Platzner I. T. (2003) Accurate isotope ratio measurements of ytterbium by multiple collection inductively coupled plasma mass spectrometry applying erbium and hafnium in an improved double normalization procedure. *J. Anal. At. Spectrom.* **18**, 1217-1223.

Segl M., Mangini A., Bonani G., Hofmann H. J., Nessi M., Suter M., Wölfli W., Friedrich G., Plüger W. L., Wiechowski A., and Beer J. (1984) ^{10}Be-dating of a manganese crust from Central North Pacific and implication for ocean palaeocirculation. *Nature* **309**, 540-543.

Segl M., Mangini A., Beer J., Bonani G., Suter M., and Wölfli W. (1989) Growth rate variations of manganese bodules and crusts induces by paleoceanographic events. *Paleoceanography* **4**, 511-530.

Severmann S., Johnson C. M., Beard B. L., German C. R., Edmond H. N., Chiba H., and Green D. H. (2004) Origin of the Fe isotope composition of the oceans as inferred

from the Rainbow vent site, Mid-Atlantic Ridge, 36°14'N. *Earth and Plan. Sci. Lett.*, submitted.

Shackleton N. J. and Opdyke N. D. (1973) Oxygen isotope and paleomagnetic stratigraphy of an equatorial Pacific core V28-238: oxygen isotope temperatures and ice volumes on a 10^5 and 10^6 year time scale. *Quat. Res.* **3**, 39-55.

Shallenberger S. B., Hochstaeder A. G., Gill J. B., Ishii T., Morita S., Taira A., and Usui A. (1995) Across-arc volcanic seamount chains and early rifting of the Izu arc: geochemical systematics. *EOS Trans. AGU* **76**, F548.

Sharma M., Polizzotto M., and Anbar A. D. (2001) Iron isotopes in hot springs along the Juan de Fuca Ridge. *Earth Planet. Sci. Lett.* **194**, 39-51.

Sherrell R. M., Field M. P., and Ravizza G. (1999) Uptake and fractionation of rare earth elements on hydrothermal plume praticles at 9°45'N, East Pacific Rise. *Geochim. Cosmochim. Acta* **63**(11/12), 1709-1722.

Shimizu H., Tachikawa K., Masuda A., and Nozaki Y. (1994) Cerium and neodymium isotope ratios and REE patterns in seawater from the North Pacific Ocean. *Geochim. Cosmochim. Acta* **58**, 323-333.

Shinjo R., Woodhead J. D., and Hergt J. (2000) Geochemical variation within the northern Ryukyu Arc: magma source compositions and geodynamic implications. *Contrib. Mineral. Petrol.* **140**, 263-282.

Sholkovitz E. R., Elderfield H., Szymczak R., and Casey K. (1999) Island weathering: river sources of rare earth elements to the Western Pacific Ocean. *Marine Chem.* **68**, 39-57.

Siebert C., Nägler T. F., von Blanckenburg F., and Kramers J. D. (2003) Molybdenum isotope records as a potential new proxy for paleoceanography. *Earth Planet. Sci. Lett.* **211**, 159-171.

Stookey L. C. (1970) Ferrozine-a new spectrophotometric reagent from iron. *Anal. Chem.* **42**, 779-781.

Sun S.-S. (1980) Lead isotopic study of young volcanic rocks from mid-ocean ridges, ocean islands and island arcs. *Philo. Trans. R. Soc. London Ser. A.* **297**(1431), 409-445.

Tachikawa K., Jeandel C., and Roy-Barman M. (1999) A new approach to the Nd residence time in the ocean: the role of atmospheric inputs. *Earth Planet. Sci. Lett.* **170**, 433-446.

Takahashi Y., Shimizu H., Usui A., Kagi H., and Nomura M. (2000) Direct observation of tetravalent cerium in ferromanganese nodules and crusts by X-ray-adsorption near-edge structure (XANES). *Geochim. Cosmochim. Acta* **64**(17), 2929-2935.

Tang T. Y., Tai J. H., and Yang Y. J. (2000) The flow pattern north of Taiwan and the migration of the Kuroshio. *Continental Shelf Research* **20**, 349-371.

Taylor B. (1992) Rifting and the volcanic-tectonic evolution of the Izu-Bonin-Mariana Arc. In *Proceedings of the Ocean Drilling, Scientific Results*, Vol. 126 (ed. B. Taylor and K. Fujioka), pp. 627-651. College Station, TX, USA.

Taylor R. N. and Nesbitt R. W. (1998) Isotopic characteristics of subduction fluids in an intra-oceanic setting, Izu-Bonin Arc, Japan. *Earth Planet. Sci. Lett.* **164**, 79-98.

Taylor R. N., Warneke T., Milton J. A., Croudace I. W., Warwick P. E., and Nesbitt R. W. (2001) Plutonium isotope ratio analysis at femtogram to nanogram levels by multicollector ICP-MS. *J. Anal. At. Spectrom.* **16**, 279-284.

Taylor S. R. and McLennan S. M. (1985) *The continental crust: its composition and evolution.* Blackwell.

Thirlwall M. F. and Walder A. J. (1995) In situ isotope ratio analysis of zircon by inductively coupled plasma multiple collector mass spectrometry. *Chem. Geol.* **122**, 241-247.

Thirlwall M. F. (2000) Inter-laboratory and other errors in Pb isotope analyses investigated using a ^{207}Pb-^{204}Pb double spike. *Chem. Geol.* **163**, 299-322.

Thirlwall M. F. (2001) Inappropriate tail corrections can cause large inaccuracy in isotope ratio analysis by MC-ICP-MS. *J. Anal. At. Spectrom.* **16**(10), 1121-1125.

Toyoda K., Nakamura Y., and Masuda A. (1990) Rare earth elements of Pacific pelagic sediments. *Geochim. Cosmochim. Acta* **54**, 1093-1103.

Tsunogai U., Ishibashi J., Wakita H., Gamo T., Watanabe K., Kajimura T., Kanayama S., and Sakai H. (1994) Peculiar features of Suiyo Seamount hydrothermal fluids, Izu-Bonin Arc: Differences from subaerial volcanism. *Earth and Planetary Science Letters* **126**(4), 289-301.

Tsunogai U., Yoshida N., Ishibashi J., and Gamo T. (2000) Carbon isotopic distribution of methane in deep-sea hydrothermal plume, Myojin Knoll Caldera, Izu-Bonin arc: Implications for microbial methane oxidation in the oceans and applications to heat flux estimation. *Geochim. Cosmochim. Acta* **64**(14), 2439-2452.

Urabe T. and Kusakabe M. (1990) Barite silica chimneys from the Sumisu Rift, Izu-Bonin Arc: possible analog to hematitic chert associated with Kuroko deposits. *Earth Planet. Sci. Lett.* **100**, 283-290.

Urey H. (1947) The thermodynamic properties of isotopic substances. *J. Chem. Soc. (London)*, 562-581.

Usui A., Yuasa M., Ishizuka O., and Hochstaeder A. G. (1996) Hydrogenetic and hydrothermal manganese crusts of the Nishi-Shichito Ridge: R/V *Moana Wave* Cruise MW9507. *Abstr. Jpn. Earth Planet. Sci. Joint Meet., 1995*, 495.

Usui A. and Someya M. (1997) Distribution and composition of marine hydrogenetic and hydrothermal manganese deposits in the northwest Pacific. In *Manganese Mineralization: Geochemistry and Mineralogy of Terrestrial and Marine Deposits*, Vol. No. 119 (ed. K. Nicholson, J. R. Hein, B. Bühn, and S. Dasgupta), pp. 177-198. The Geological Society.

van de Flierdt T., Frank M., Lee D.-C., and Halliday A. N. (2002) Glacial weathering and the hafnium isotope composition of seawater. *Earth Planet. Sci. Lett.* **201**, 639-647.

van de Flierdt T., Frank M., Halliday A. N., Hein J. R., Hattendorf B., Günther D., and Kubik P. K. (2003) Lead isotopes in North Pacific deep water - implications for past changes in input sources and circulation patterns. *Earth Planet. Sci. Lett.* **209**(1-2), 149-164.

Vance D. and Thirlwall M. F. (2002) An assessment of mass discrimination in MC-ICPMS using Nd isotopes. *Chem. Geol* **185**, 227-240.

Vlastélic I., Abouchami W., Galer S. J. G., and Hoffmann E. (2001) Geographic control on Pb isotope distribution and sources in Indian Ocean Fe-Mn deposits. *Geochim. Cosmochim. Acta* **65**(23), 4303-4319.

von Blanckenburg F., O'Nions R. K., Belshaw N. S., Gibb A., and Hein J. R. (1996a) Global distribution of beryllium isotopes in deep ocean water as derived from Fe-Mn crusts. *Earth Planet. Sci. Lett.* **141**, 213-226.

von Blanckenburg F., O'Nions R. K., and Hein J. R. (1996b) Distribution and sources of pre-anthropogenic lead isotopes in deep ocean water from Fe-Mn crusts. *Geochim. Cosmochim. Acta* **60**(24), 4957-4963.

von Blanckenburg F. and Igel H. (1999) Lateral mixing and advection of reactive isotope tracers in ocean basins: observations and mechanisms. *Earth Planet. Sci. Lett.* **169**, 113-128.

von Blanckenburg F. and O'Nions R. K. (1999) Response of beryllium and radiogenic isotope ratios in Northern Atlantic Deep Water to the onset of northern hemisphere glaciation. *Earth Planet. Sci. Lett.* **167**, 175-182.

von Blanckenburg F. and Nägler T. F. (2001) Weathering versus circulation-coutrolled changes in radiogenic isotope tracer composition of the Labrador Sea and Northern Atlantic Deep Water. *Paleoceanography* **16**(4), 424-434.

VonderHaar D. L., McMurtry G. M., and Mahoney J. J. (1988) Chemical and isotopic stratigraphy of a ferromanganese crust from the Hawaiian Archipelago. *EOS Trans. AGU* **69**, 1501.

VonderHaar D. L., Mahoney J. J., and McMurtry G. M. (1995) An evaluation of strontium isotopic dating of ferromanganese oxides in a marine hydrogenous ferromanganese crust. *Geochim. Cosmochim. Acta* **59**(20), 4267-4277.

Walder A. J. and Freedman P. A. (1992) Isotopic ratio measurement using a double focusing magnetic sector amss analyzer with an inductively coupled plasma as an ion source. *J. Anal. At. Spectrom.* **7**, 571-575.

Walder A. J. and Furuta N. (1993) High precision lead isotope ratio measurement by inductively coupled plasma multiple collector mass spectrometry. *Anal. Sci.* **9**, 675-680.

Walder A. J., Platzner A. I., and Freedman P. A. (1993) Isotope ratio measurement of lead, neodymium and neodymium-samarium mixtures, hafnium-lutetium mixtures with a double focusing multiple collector inductively coupled plasma mass spectrometer. *J. Anal. At. Spectrom.* **8**, 19-23.

Walter H. J., Rutgers van der Loeff M. M., and Hoeltzen H. (1997) Enhanced scavenging of ^{231}Pa relative to ^{230}Th in the South Atlantic south of the Polar front: implications for the use of the ^{231}Pa/^{230}Th ratio as a paleoproductivity proxy. *Earth Planet. Sci. Lett.* **149**, 85-100.

Wang K.-L., Chung S.-L., Chen C.-H., and Chen C.-H. (2002) Geochemical constrain on the petrogenesis of high-Mg basaltic andesites from the northern Taiwan volcanic zone and their geodynamic significance. *Chem. Geol.* **182**, 513-528.

Wang K.-L., Chung S.-L., O'Reilly S. Y., Sun S.-S., Shinjo R., and Chen C.-H. (2004) Geochemical constraints for the genesis of post-collisional magmatism and the geodynamic evolution of the northern Taiwan region. *Journal of Petrology* **in press**.

Warren B. A. (1973) Transpacific hydrographic sections of Lats 43°S and 28°S: the SCORPIO expedition, II, Deep water. *Deep-Sea Research* **20**, 209-238.

Wasserburg G. J., Jacobsen S. B., DePaolo D. J., McCulloch M. T., and Wen T. (1981) Precise determination of Sm/Nd ratios, Sm and Nd isotopic abumdances in standard solutions. *Geochim. Cosmochim. Acta* **45**, 2311-2323.

Welch S. A., Beard B. L., Johnson C. M., and Braterman P. S. (2003) Kinetic and equilibrium Fe isotope fractionation between aqueous Fe(II) and Fe(III). *Geochim. Cosmochim. Acta* **67**(22), 4231-4250.

Wells M. L., Vallis G. K., and Silver E. A. (1999) Tectonic processes in Papua New Guinea and past productivity in the eastern equatorial Paicific Ocean. *Nature* **398**(6728), 601-604.

White W. M., Patchett J., and BenOthman D. (1986) Hf isotope ratios of marine sediments and Mn nodules: evidence for a mantle source of Hf in seawater. *Earth Planet. Sci. Lett.* **79**, 46-54.

White W. M., Albarède F., and Telouk P. (2000) High-precision analysis of Pb isotope ratios by multi-collector ICP-MS. *Chem. Geol* **167**, 257-270.

Wong A. P. S., Bindoff N. L., and Church J. A. (1999) Large-scale freshening of intermediate waters in the Pacific and Indian oceans. *Nature* **400**, 440-443.

Wu J., Boyle E., Sunda W., and Wen L.-S. (2001) Soluble and colloidal iron in the Oligotrophic North Atlantic and North Pacific. *Science* **293**(5531), 847-849.

Yu E. F., Francois R., and Bacon M. P. (1996) Similar rates of modern and last-glacial ocean thermocline circulation inferred from radiochemical data. *Nature* **379**, 689-694.

Zhang D., Lee T. N., and Johns W. E. (2001) The Kuroshio east of Taiwan: modes of variability and relationship to interior ocean mesoscale eddies. *Journal of Physical Oceanography* **31**, 1054-1074.

Zhang J. and Nozaki Y. (1996) Rare earth elements and yttrium in seawater: ICP-MS determinations in the East Caroline, Coral Sea, and South Fiji basins of the western South Pacific Ocean. *Geochim. Cosmochim. Acta* **60**, 4631-4644.

Zhu P. and Macdougall J. D. (1998) Calcium isotopes in the marine environment and the oceanic calcium cycle. *Geochim. Cosmochim. Acta* **62**(10), 1691-1698.

Zhu X.-H., Han I.-S., Park J.-H., Ichikawa H., Murakami K., Kaneko A., and Ostrovskii A. (2003) The Northeastward current southeast of Okinawa Island observed during November 2002 to August 2001. *Geophysical Research Letters* **30**(2), 2002GL015867.

Zhu X. K., O'Nions R. K., Guo Y., Belshaw N. S., and Rickard D. (2000a) Determination of natural Cu-isotope variation by plasma-source mass spectrometry: implications for use as geochemical tracers. *Chem. Geol.* **163**, 139-149.

Zhu X. K., O'Nions R. K., Guo Y., and Reynolds B. C. (2000b) Secular variation of iron isotopes in North Atlantic Deep Water. *Science* **287**, 2000-2002.

Zhu X. K., Guo Y., Williams R. J. P., O'Nions R. K., Matthews A., Belshaw N. S., Canters G. W., de Waal E. C., Weser U., Burgess B. K., and Salvato B. (2002) Mass fractionation processes of transition metal isotopes. *Earth Planet. Sci. Lett.* **200**, 47-62.

Appendices

Appendix I Major elements/ mineralogical data

I-1 Major elements of Central Pacific Fe-Mn crusts (from literature)

Table A-1 Major element of the (near) surface Fe-Mn crusts (wt%)

Sample*	ID in this study	Mn	Fe	Co	Ni	Zn	Cu	Pb	Ti	Ca	P	Al	Si
69DSO(1-3mm)	NC4	21.00	14.30	0.65	0.37	0.06	0.07	0.123	0.80	1.96	0.37	0.68	4.70
10DSR(4-3mm)	SC2	17.90	14.30	0.65	0.41	0.05	0.06	0.099	0.83	1.96	0.42	0.80	3.30
5DSR(2-3mm)	SC4	21.00	10.90	0.69	0.52	0.05	0.08	0.100	0.75	1.95	0.28	0.46	2.20
28DSR(2-2mm)	SC5	19.10	13.50	0.54	0.39	0.05	0.05	0.092	0.67	1.90	0.35	0.25	2.20
80DSK(3-3mm)	SC6	20.20	16.10	0.56	0.35	0.06	0.03	0.146	0.69	2.05	0.81	0.33	2.40
59DSR(2-3mm)	SC8	16.70	17.60	0.32	0.27	0.06	0.05	0.091	0.77	1.99	0.45	0.71	3.80

* The samples analysed were not the exact portion of the sample analysed in this study.
Data from Halbach *et al* (1991), Midpac4 Cruise Report, "Geowissenschaftliche Untersuchungen und lagerstattenkundliche Bewertung der Co-Reichen und Pt-haltigen Erzkrustenlagerstatten des zentralen Pazifiks sudlich des Aquators (SO66)", Technische Universitat Clausthal.

Table A-2 Major elements of depth profiles in Fe-Mn crust 28DSR2*

mm	Mn	Fe	Co	Ni	Zn	Cu	Pb	Ti	Ca	P	Al	Si
2	19.1	13.50	0.54	0.39	0.05	0.05	0.09	0.670	1.90	0.35	0.25	2.20
5	19.2	13.70	0.58	0.41	0.05	0.05	0.09	0.790	1.88	0.37	0.33	1.90
8	20.6	12.60	0.68	0.50	0.06	0.08	0.09	0.810	1.93	0.37	0.45	2.30
11	18.3	12.70	0.54	0.46	0.06	0.08	0.09	0.790	1.67	0.26	0.72	3.20
14	22.2	10.20	0.75	0.66	0.07	0.11	0.10	0.860	1.79	0.38	0.41	1.80
18	20.5	12.10	0.58	0.48	0.06	0.10	0.10	1.010	1.80	0.26	0.53	2.30
21	22.6	11.50	0.64	0.60	0.07	0.11	0.10	0.970	1.80	0.24	0.53	3.00
24	22.6	11.50	0.58	0.59	0.08	0.11	0.09	0.950	1.89	0.33	0.49	1.60
28	20.3	12.70	0.52	0.46	0.06	0.11	0.09	1.080	1.76	0.24	0.60	2.10
30	20.8	12.70	0.60	0.45	0.07	0.11	0.10	1.070	1.88	0.25	0.48	1.80
35	18.2	14.60	0.57	0.38	0.07	0.12	0.09	1.370	2.21	0.94	0.75	2.60
37	20.7	12.10	0.82	0.45	0.08	0.13	0.09	1.240	2.18	0.91	0.56	1.80
41	15.9	13.20	0.44	0.48	0.08	0.15	0.06	0.840	4.99	1.57	1.01	3.20
42.5	17.5	12.60	0.50	0.42	0.08	0.13	0.08	1.210	3.46	1.12	0.84	2.60

* Sample 28DSR2 belongs to the same dredges sample 28DSR3/9, equivalent to SC5, of this study.
Data from Halbach *et al* (1991), Midpac4 Cruise Report, "Geowissenschaftliche Untersuchungen und lagerstattenkundliche Bewertung der Co-Reichen und Pt-haltigen Erzkrustenlagerstatten des zentralen Pazifiks sudlich des Aquators (SO66)", Technische Universitat Clausthal.

I-2 Major element and minerological data of Izu-Bonin Fe-Mn crusts

Table A-3 Major elements of depth profiles in Fe-Mn crust D105-5AB* (Usui, unpublished data)

Age (Ma)	Mn	Fe	Na	Mg	Al	P	K	Ca
0.5	13.92	18.4	1.72	0.87	1.07	0.43	0.48	1.70
2	12.06	17.8	1.57	0.80	1.27	0.41	0.51	1.57
4	12.11	17.4	1.76	0.83	1.47	0.34	0.55	1.39
7.5	12.07	16.9	1.59	0.81	1.20	0.34	0.45	1.33
12	12.85	18.0	1.57	0.84	1.20	0.34	0.44	1.38
15	12.95	17.9	1.54	0.78	1.07	0.35	0.38	1.43
17.5	12.45	16.8	1.44	0.76	1.13	0.34	0.38	1.43
20.5	12.12	17.2	1.47	0.87	1.58	0.33	0.39	1.50

* Equivalent to IB1 but different sampling profile.

Age (Ma)	Ti	Co	Ni	Cu	Zn	Pb
0.5	0.41	0.15	0.21	0.02	0.05	0.18
2	0.41	0.14	0.13	0.02	0.04	0.16
4	0.46	0.15	0.19	0.03	0.05	0.16
7.5	0.42	0.16	0.21	0.03	0.05	0.16
12	0.45	0.15	0.19	0.04	0.05	0.16
15	0.49	0.16	0.15	0.03	0.04	0.17
17.5	0.49	0.16	0.15	0.02	0.04	0.16
20.5	0.52	0.13	0.18	0.03	0.05	0.16

Table A-3 Peak heights of XRD results in the depth profiles in D105-5AB* (Usui, unpublished data)

Age (Ma)	Quartz	Plagioclase	Vernadite (Fe-Mn oxides)
0.5	25	3	6
2	39	3	7
4	42	3	7
7.5	33	2	6
12	33	2	6
15	24	10	6
17.5	25	2	6
20.5	31	4	6

I-3 Fe isotope related IB2 XRD data

XRD were carried out on two growth layers of IB2 (at 15-16 mm (2.31 Ma) and 21-22 mm (3.21 Ma)) with the most distinctive $\delta^{56}Fe$. The scaned XRD results show similar pattern demonstrating the consistency of minerology at these two growth layers.

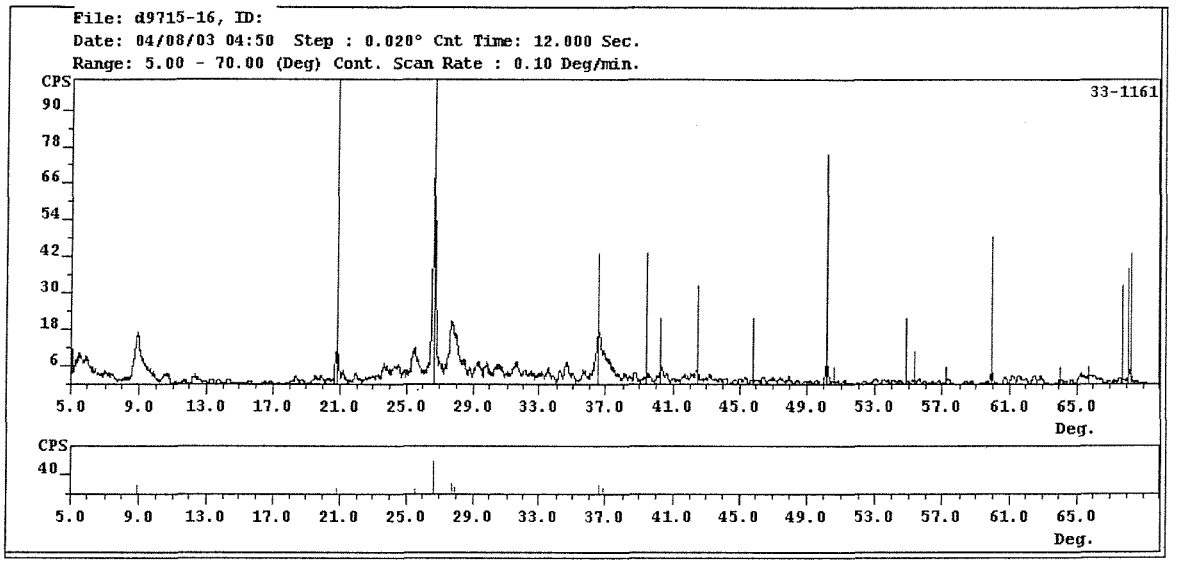

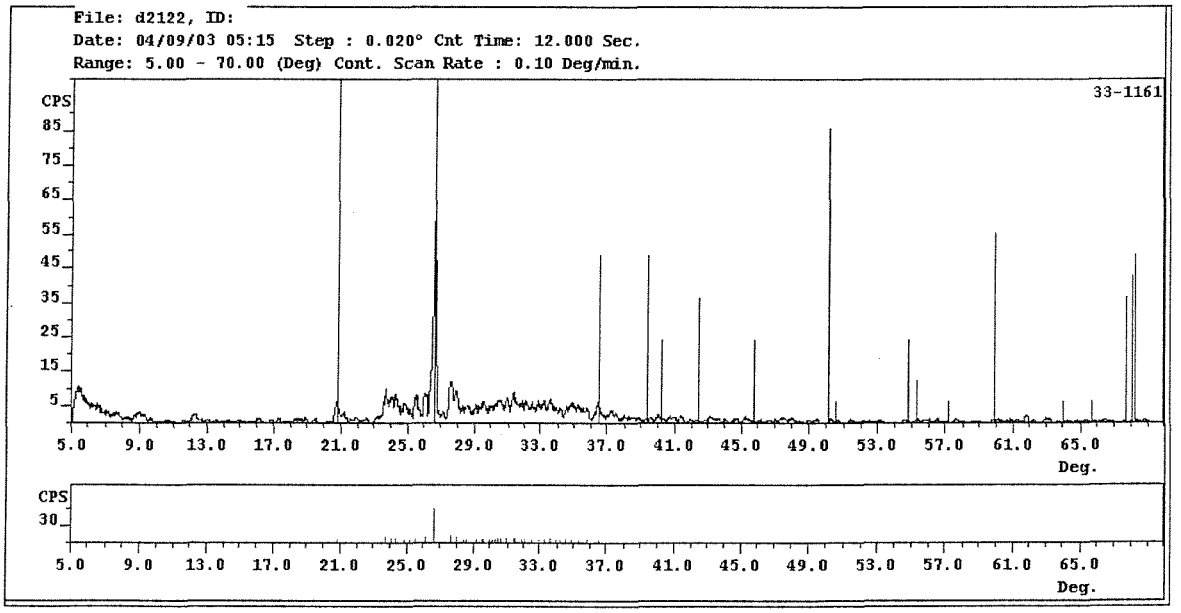

Appendix II Hf Separation Method

This section describes the details of the hafnium chemistry method set up. Column calibration was monitored using the VG Elemental PlasmaQuad PQ2+ Inductively Coupled Plasma Mass Spectrometer in Southampton Oceanography Centre.

II-1 First column

The first column is designed to separate Ti (titanium), Zr (zirconium) and Hf from the sample matrix using anion exchange resin (Bio-Rad AG1×8, 200-400 mesh). These three elements, due to their similar chemical behaviour, will hold onto the ion-exchange site of the resin while others are eluted in a stronger concentration of hydrofluoric acid (hereafter HF). Nearly all elements, except Ti, Zr and Hf, have no absorption under the range of 1M to 24M HF (Saito, 1984).

The column has a reservoir of 10 ml and up to 2 ml resin bed volume with diameter and length of 0.8×4 cm polypropylene material (Bio-Rad). Columns from different manufacturers have also been tested, and it has been shown that exact dimension of the column is not crucial for this stage (Fig. A-1). The Bio-Rad type column was chosen due to their faster throughput of liquids. 1ml of resin is loaded in the column and conditioned with 6ml of 6M HCl and 1M HF mixed acid, 6ml of MQ water and finally 6ml of 4M HF. Samples for first column calibration are rock standards: NIM-G, JG-2, BE-N, and BCR1 (details see, Chu, 2001, MPhil/PhD Transfer Report).

The separation procedure for the 1st column is as follows: (1) loading the sample in 2ml of 4M HF, (2) rinse the column with 1ml of 4M HF, (3) elute with 7ml of 4M HF, and finally (4) collect Ti/Zr/Hf fraction in 8ml of 6M HCl and 1M HF mixed acid, in which the 1 M HF is to keep Hf in solution. The resin of the first column is discarded after each use as resin might degrade with high concentration of HF.

(a) Bio-Rad Column

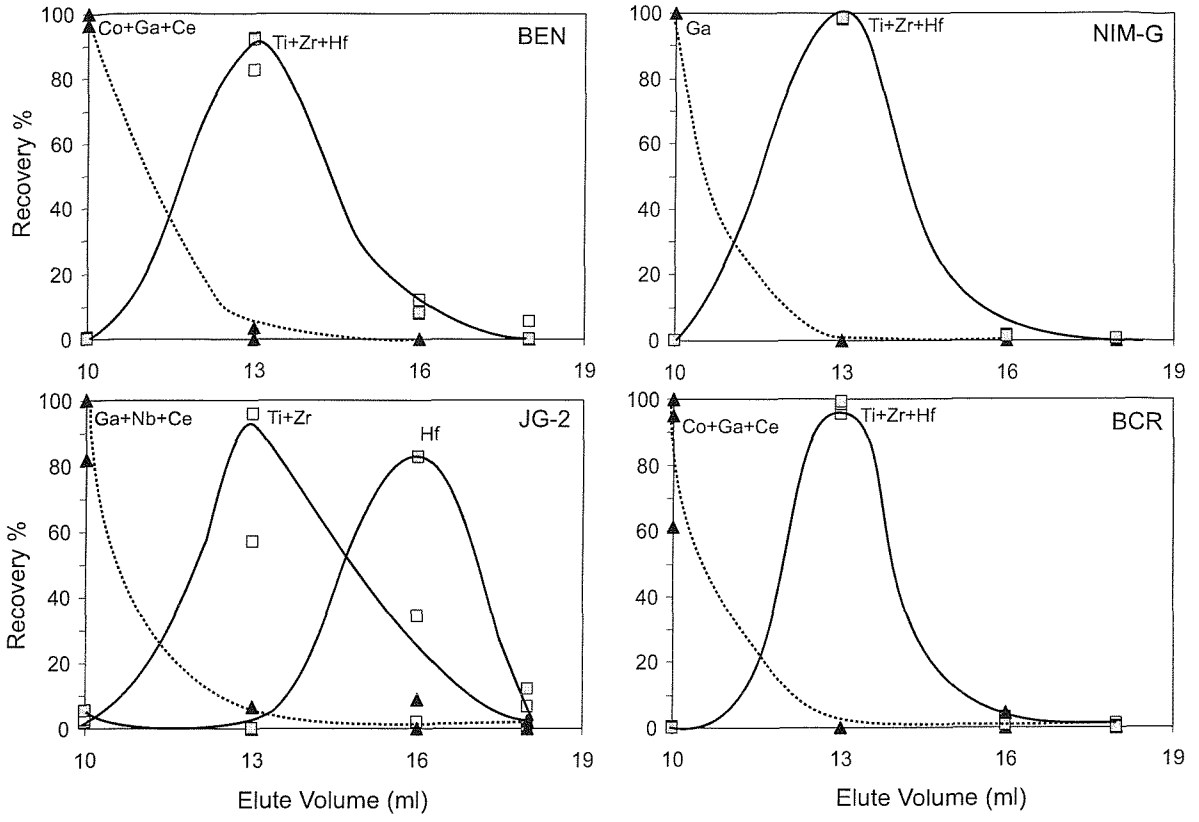

(b) Conical shape Column

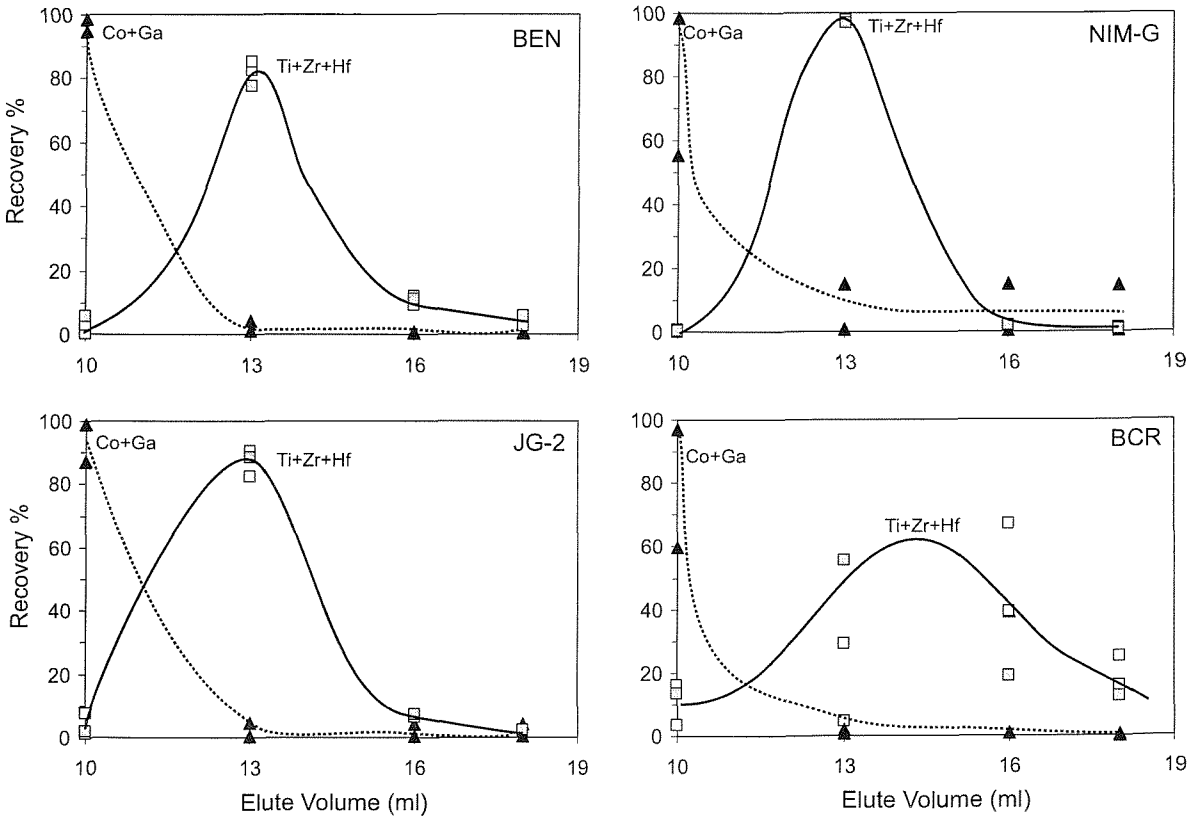

Fig. A-1 First column calibrations for four rock standards. Ti, Zr (both open squares) and Hf (grey square) were eluted in 6M HCl and 1M HF mixed acid in (1) Bio-Rad-made columns and (2) Conical shape columns.

II-2 Second column

Ln resin (Eichrom) is employed in the second column to separate Hf from Ti and part of Zr which will interfere with the ionisation performance during analysis. Two different resin diameters (100-150 μm and 50-100 μm) were tested. Comparing the results, they show a similar level of separation, but the finer one was very time-consuming, it was decided to use the resin with the lager dimension (i.e. 100-150 μm).

The dimension of the 2nd column is 8.3 cm tall, with an internal dimension of 4mm and a reservoir of 6 ml (Savillex®). A total of 0.7 ml Ln resin is loaded in the column and reused, since the concentration of HF at this stage is only about 1M at a maximum and will not cause any degradation to the resin. Two elution schemes were attempted and are discussed below.

(1) Volumetric controlled method

This method is adopted from (Lee *et al.*, 1999), in which the Hf fraction is collected in the exactly titrated 2M HCl and 0.1M HF mixed acid. It is volumetrically controlled: Hf is released in a certain range of the acid during elution. Sample used for this calibration is a Ti/Zr/Hf mixture ([Ti] 10,000 ppm, [Zr] 650 ppm and [Hf] 7.5 ppm), based on the average concentrations of ferromanganese nodules/crusts. The resin is firstly conditioned with 6 ml of 6M HCl and 1M HF followed by 6 ml of 2M HCl and 0.1M HF before loading samples in exactly 1ml of mixed 2M HCl and 1M HF. From the calibration results (Fig. A-2), Ti and Zr are eluted in the first 7 ml and Hf fraction was collected in the next 10 ml. The column is finally washed with 6ml of 6M HCl and 1M HF mixed acid twice and 6M HCl twice.

However, the results of this method did not show a clear separation. Firstly, there were losses of Hf in the beginning of elution and during column cleaning (e.g. the (1) and (2) in Fig. A-2a) because the presence of HF. More significantly, effective separation of Hf for Ti and Zr was not achieved (Fig. A-2b). The recovery of this method obtained from the tests with sample NOD-P, NOD-A and BRR are only about 20-25%.

(a)

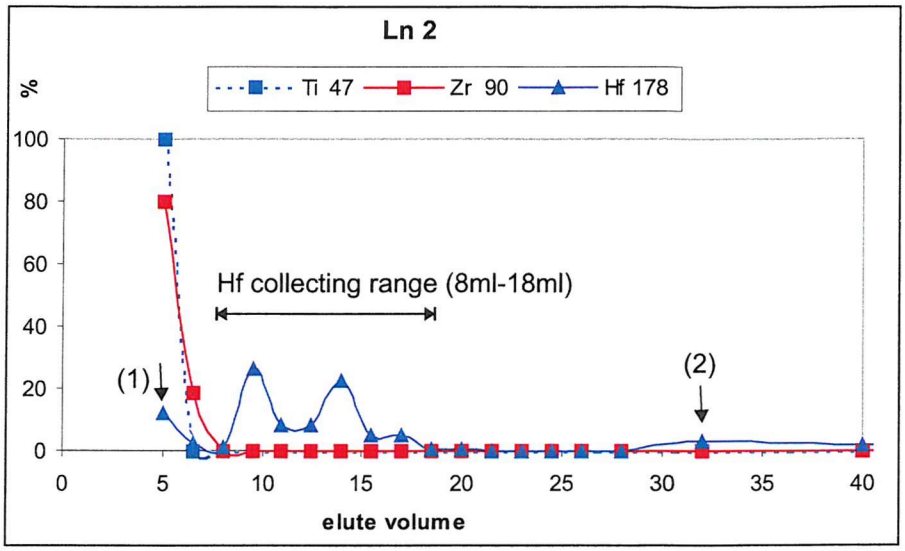

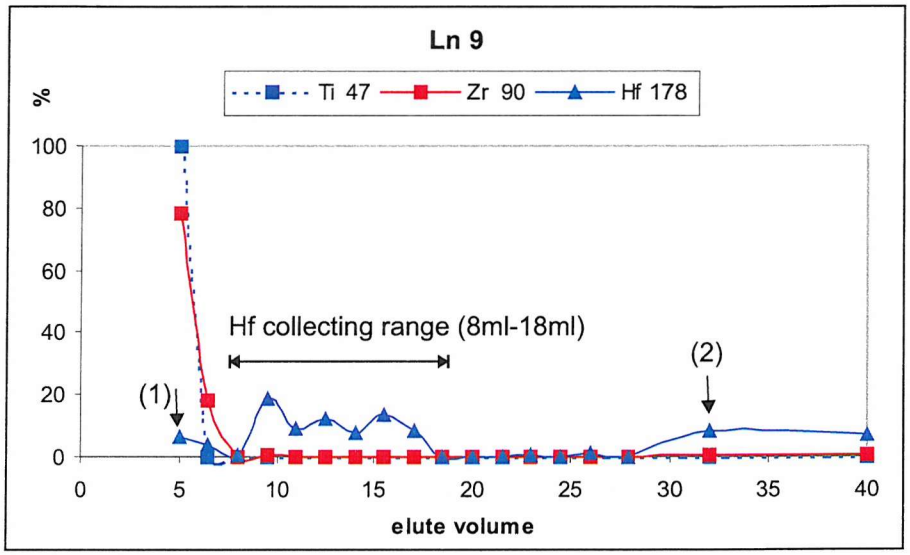

(b)

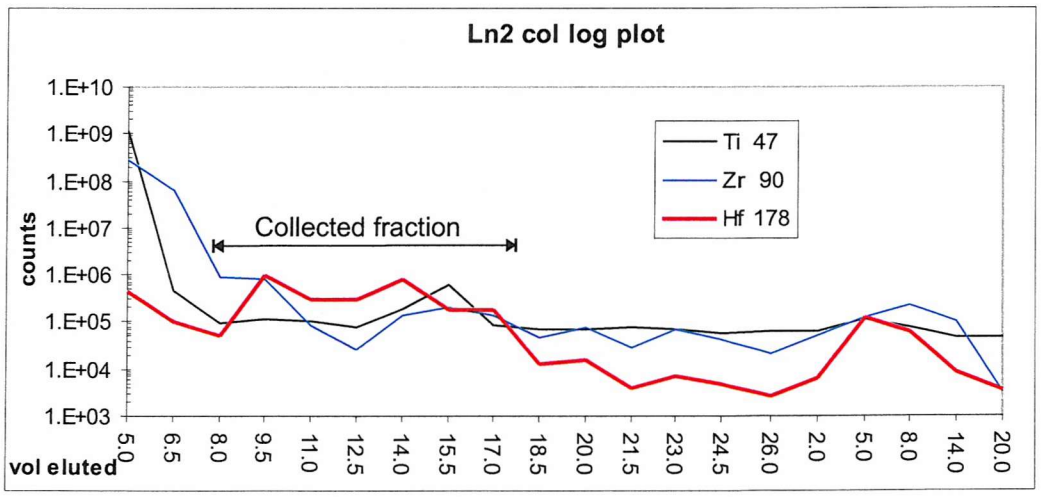

Fig. A-2 (a) Hf 2nd column calibration with volumetric controlled method (two replicates: Ln2 and Ln9). The collecting range is in 2M HCl and 0.1M HF exact titrated mixed acid. Note that there are losses of Hf in the (1) first 5 ml with Ti, Zr fraction and (2) at the elute volume around 32 ml when elute acid is changed for cleaning and contains stronger HF (6M HCl and 1M HF). (b) From this elution scheme, the tail of Ti and Zr are significant to Hf.

(2) Present Method with H_2O_2

An alternative method is adopted under the principle that Hf will only be released with HF acid, whereas Ti, complexed with H_2O_2 (hydrogen peroxide), will be released from the resin with HCl as the yellow-coloured $Ti(O\text{-}O)^{2+}$ (peroxytitanyl) and is also useful in indicating the elution state of Ti from the column.

With the presence of 10% of H_2O_2, nearly all the Ti is eluted in the first 1 ml of 2.2 M HCl (Fig. A-3a). Fig. A-3b&c show that the effectiveness in separating Hf and Ti (160 μg Ti and 150 ng Hf). Improved separation between these two elements is by adding H_2O_2 to both the sample and elution acid (Fig. A-4 a&b) in duplicated experiments. The concentration of H_2O_2 is lowered to 1% in the elute stage to reduce gas bubbles in the resin, which will decrease the flow speed or even stop the flow when the bubble forms across the entire diameter of the column (Barovich *et al.*, 1995). After the H_2O_2 process, 12 ml of 6M HCl is added into the resin to ensure all the REEs (esp Yb, as demonstrated in Chapter 3) have been eluted. Finally, Hf fraction is collected in 6ml of 1M HF. The column is cleaned by 6ml of 6M HCl and 1M HF mixed acid and 6ml of 6M HCl.

The advantage of this method is that it is not necessary to have an exact molarity in the elute acid. Furthermore, the reduced sample amount (100 μl rather than 2 ml) also reduces the matrix profile, which lower both the processing time and the blank. The 2nd columns are stored in weak acid when they are not in use, which is 1M HCl in this case.

All reagents for Hf chemistry are Aristar grade or pure 18 MΩ MQ. The total procedure blank for Hf chemistry is 300 pg.

(a) Ti with H_2O_2

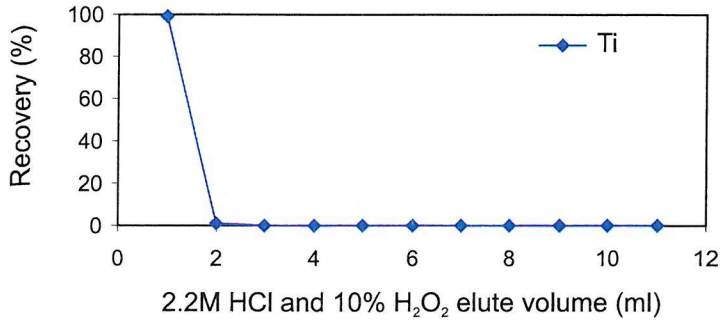

(b) Ti and Hf separtion with H_2O_2

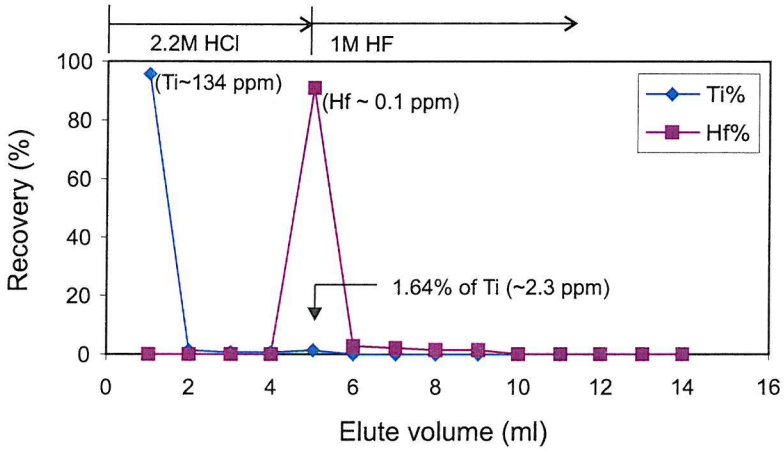

(c) Ti and Hf separtion without H_2O_2

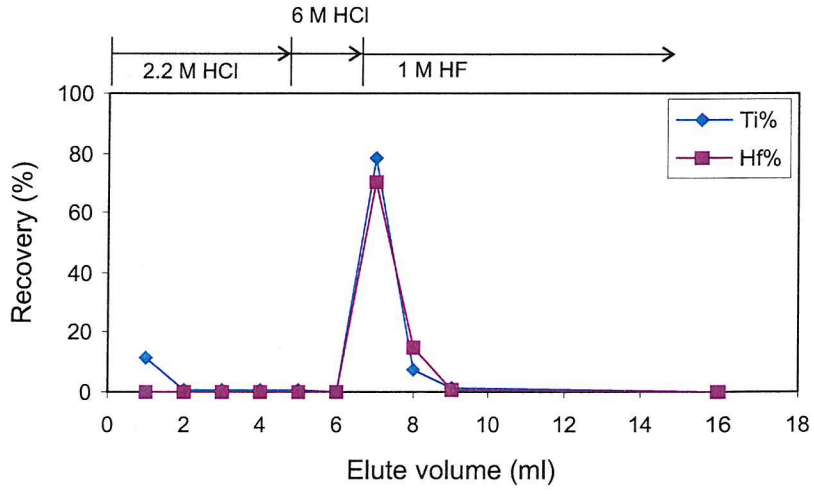

Fig. A-3 H_2O_2 tests. (a) Ti was eluted in the 1ml when H_2O_2 is added in the acid. (b) (c) Elution profiles show that Ti and Hf were hardly separated in this elution scheme without the addition of H_2O_2. Concentration of Ti and Hf in mixed solution are 150 ppm and 0.15ppm respectively.

(a) H_2O_2 in sample only

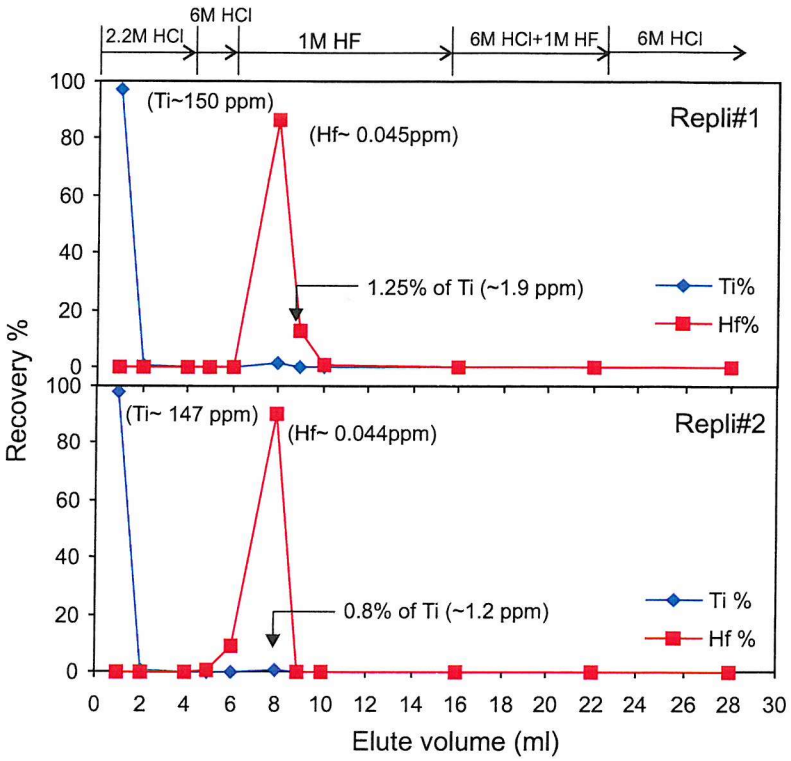

(a) H_2O_2 in sample and first eluent acid

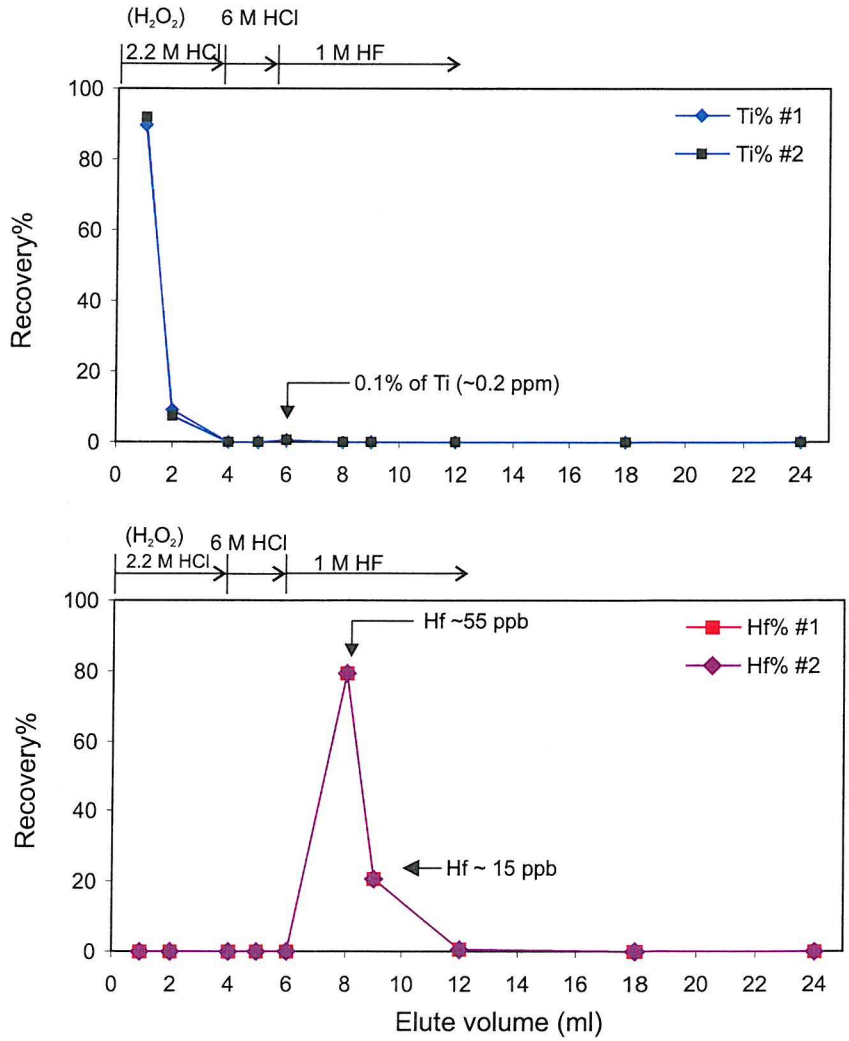

Fig. A-4 Present elution scheme for Hf second column with (a) 10% H_2O_2 added in sample only and (b)H_2O_2 added in both sample fraction (H_2O_2=10%) and eluents (H_2O_2=1%). Concentration for Ti and Hf were 150 and 0.07 ppm.

Appendix III Nd column chemistry and analysis

III-1 REEs Separation

REEs were separated from original solutions with cation exchange resin (~6.5ml, Dowex 50W-X8, 200-400 mesh, H^+ form, Merck Ltd.) in small polypropylene columns (Bio-Rad). Original solution containing about 1μg of Nd was dried and redissolved in 2ml 2.2 M HCl (Aristar).

1) Columns were firstly conditioned by eluting 20 ml of 2.2 M HCl before loading the samples.

2) Wash down the column sides with another 2ml of 2.2 M HCl and allow to run through.

3) Elute the column with 22 ml 2.2 M HCl.

4) REE fraction was collected in a PTFE beaker with 16 ml of 6M HNO_3 (Aristar).

5) Columns were cleaned by eluting 10 ml of 6M HNO_3, followed by 10 ml of 6M HCl, and finally 10 ml of MQ. The columns were stored by topping up with MQ with caps and bottom covers on.

III-2 Nd Separation

Nd was separated from the REEs fractions with HDEHP coated resin (Ln Resin, 100-150 μm, Eichrom Inc.) in glass columns (ID: 6 mm; length: 10 cm with 3 mm med glass frit; 15 ml reservoir). Dried REE fraction was redissolved in 2ml 0.17M HCl.

1) Columns were conditioned by eluting with 10 ml of 0.17M HCl.

2) Samples was loaed onto the column and allow to run through. Another 10 drops of 0.17M HCl were added to wash on the sample.

3) The columns were eluted with 22ml of 0.17M HCl.

4) Nd fractions were collected in 25ml of 0.17M HCl.

5) Columns were washed with 15ml of 6M HCl, followed by 15ml of MQ. The columns were left standing in MQ at the resin level.

III-3 Nd Isotope Analysis

Dried Nd fractions were loaded onto a Ta side filament. This filament is part of a triple set-up (2 Ta at side and 1 Re at centre); all of which should be degassed before loading. Nd isotopes measurements were carried out on a thermal ionisation mass spectrometer (TIMS, VG Sector 54). Standard JNdi-1 throughout the period of analysis are 0.512104±8 (n=21).

Appendix IV Pb column chemistry and analysis

IV-1 Reagent and Labwares

All reagents were distilled (HCl and HNO_3) or high purity quality (HBr). All containers were further cleaned in addition to standard procedures: HNO_3 (concentrated) was filled in cleaned savillex for 3 days before rinsing with 18MΩ MQ. 2ml centrifuge tube were cleaned in 6N HCl and 1N HBr subsequently. Columns were made from 1000 μl pipette tips fitted with previously cleaned frit materials. Columns were reused and cleaned in 6N HCl for a week. Chemistry was carried out in a Clean Laboratory.

IV-2 Pb Separation Chemistry

The Pb column method employed was modified for Fe-Mn crusts from a previously established method (Ishizuka, pers. comm.; Ishizuka *et al.*, 2003). Part of the orginal solutions are dried with about 1 μg of Pb and redissolved in 1ml 1N HBr. 5-6 drops of anion exchange resin (Bio-Rad AG1×8, 200-400 mesh) were put in the columns. Rince the column with 6N HCl, MQ subsequently twice. After conditioning the columns with 0.8ml of 1N HBr, samples were loaded and eluted with 0.8ml 1N HBr three times. Pb fraction was collected in 1.4ml of 6N HCl. The column procedures were repeated once in order to obtain pure Pb fractions. The total procedure blank for Pb chemistry is 300 pg and is insignificant comparing to the sample amount loaded (~1000 ng).

IV-3 MC-ICP-MS (IsoProbe) Measurement

Separated Pb were dissolved in ultra cleaned 2% HNO3. Tl spikes were then added to achieve a concentration of about 2 ppb for correcting mass fractionation. Analytical procedures follow standard Pb measurement scheme (Ishizuka, pers. comm.) including tail correction, on-peak blank subtraction and mass bias corrections.